# *Current* insights into the physiology of the epithelial calcium and magnesium channels

**Cătălin Ninel Topală**

**Cover design: Alex Hariga, Bucharest**

**Printed by PrintPartners Ipskamp, Amsterdam**

**ISBN / EAN: 978-90-9023256-0**

# *Current* insights into the physiology of the epithelial calcium and magnesium channels

Een wetenschappelijke proeve op het gebied van de
Medische Wetenschappen

**Proefschrift**

ter verkrijging van de graad van doctor
aan de Radboud Universiteit Nijmegen
op gezag van de rector magnificus, prof. dr. S.C.J.J. Kortmann,
volgens besluit van het College van Decanen
in het openbaar te verdedigen op donderdag 21 augustus 2008
om 13:30 uur precies

door

**Cătălin Ninel Topală**

geboren op 6 juli 1978
te Giurgiu, Roemenië

**Promotor**:
prof. dr. R.J.M. Bindels

**Copromotor**:
dr. J.G.J. Hoenderop

**Manuscriptcommissie**:
prof. dr. C.C.A. Gielen
prof. dr. B.G.M. Engelen
dr. W.J.J. Scheenen

# *Current* insights into the physiology of the epithelial calcium and magnesium channels

A scientific essay in Medical Sciences

**Doctoral thesis**

to obtain the degree of doctor
from Radboud University Nijmegen
on the authority of Rector Magnificus, prof. dr. S.C.J.J. Kortman,
according to the decision of the Council of Deans
to be defended in public on Thursday 21 August 2008
at 13:30 hours

by

**Cătălin Ninel Topală**

born in Giurgiu, Romania
on the 6-th of July 1978

**Doctoral supervisor**:
prof. dr. R.J.M. Bindels

**Co-supervisor**:
dr. J.G.J. Hoenderop

**Doctoral thesis committee**:
prof. dr. C.C.A. Gielen
prof. dr. B.G.M. Engelen
dr. W.J.J. Scheenen

## Table of Contents

# ***Chapter 1***

## General introduction

**Functional characterization of ion channels**

All living cells are enveloped by a plasma membrane that functions as a barrier between the cell cytoplasm and the surrounding environment. Due to its hydrophobic composition, the plasma membrane is essentially impermeable to ions. Thus, specialized proteins facilitate the flow of ions across the membrane. These proteins can be most broadly categorized as being either transporters or channels.

*Transporters* are proteins that aid movement of electrolytes across membranes without forming a pore (1) and are classically viewed as enzymes whose catalytic cycles involve a selective recognition/binding site of the transported ion(s), conformational changes in the transporter protein itself due to binding of the ion(s) and the coupling of these changes to physical movement of the ion(s) across the membrane. Most transporters, unlike channels, mediate the active transport of certain ions against their electrochemical gradient, ultimately through energy consumption (4-7). However, there are also transporters that transfer ions passively down their electrochemical gradient, e.g. the $Na^+/Ca^{2+}$ exchanger (NCX1), $Na^+/H^+$ exchanger.

*Ion channels* are proteins that facilitate ion diffusion across a membrane by forming a hydrophilic pore (8). Spanning the plasma membrane, ion channels control its permeability to charged molecules. For this purpose, ion channels possess a set of essential properties such as the presence of a hydrophilic pore that connects the intracellular medium with the extracellular medium. This pore provides the route by which diffusion across the plasma membrane can take place. Mainly hydrophilic amino acid residues line the pore. Another important property of ion channels is the existence of a gating mechanism that can close the pore via a change in protein conformation. A range of factors depending on the channel species can initiate this conformational change. Classified by their gating factor, there are three main classes of ion channels:

- Voltage-dependent channels open or close depending on the membrane potential. These channels contain charged amino acid residues that shift position within the protein in response to membrane potential changes, called voltage sensors. Based on structure homology and presumed evolutionary origin with the voltage-gated $K^+$ channels, some members of the Transient Receptor Potential (TRP) superfamily could be included in this category of ion channels (8).
- Ligand-gated channels open or close depending on the binding of an extracellular factor, such as a hormone or a neurotransmitter. Beside the acetylcholine receptor and other channels activated by neurotransmitters, this class could include some members of the TRP family such as TRPV1 (9), activated by capsaicin, and the menthol-activated TRPM8 (10).
- Second messenger-operated channels open or close in response to intracellular factors, such as $Ca^{2+}$ or activated G protein subunits. The members of the TRPC family could be included in this class.

The focus of the present thesis, the epithelial $Ca^{2+}$ and $Mg^{2+}$ channels, form a specific category. These channels open or close (gate) independently of any ligand binding or of voltage changes, since they are constitutively active in physiological states.

These three types of channels species are sometimes referred to as VOCs (voltage-operated channels), ROCs (receptor-operated channels) and SMOCs (second messenger-operated channels), respectively. This classification of ion channels does not exclude inter-associations. For example, some $Ca^{2+}$-activated $K^+$ channels are also voltage-dependent. In addition, modulator mechanisms can influence channel functioning independent of the primary gating factor. Phosphorylation of the protein on the cytosolic side is a common mechanism for fine-tuning the channel activity. Phosphorylation can enhance or reduce channel function, depending on the phosphorylation site and channel type. Another mechanism of controlling ion channels activity is their different expression levels according to the cellular stage. Since ion channels are proteins, they can be subject to varying levels of expression that can modulate channel function over longer time scales.

Most ion channels present a more or less pronounced selective permeability. Ion channels possess selectivity in that their pores are more permeable to some ions than to others. The mechanism of selective permeability is based on a combination of ion size (in its hydrated form) and its charge. Residues in the channel pore lining interact with ions to form a thermodynamic energy barrier that favors the passage of certain ions. Based on their selective permeability, the ion channels could be subdivided in: $Na^+$ selective, $K^+$ selective, $Ca^{2+}$ selective, $Mg^{2+}$ or $Cl^-$ selective channels, and non-selective channels that do not discriminate between their permeants.

The functional characteristics and the molecular mechanism of regulation for ion channels from the TRP superfamily, and in particular, the molecular regulation of the epithelial $Ca^{2+}$ (TRPV5 and TRPV6) and $Mg^{2+}$ channels (TRPM6) are the focus of the present thesis.

**The patch-clamp technique – an ultimate tool in electrophysiology**

From all electrophysiological tools, the patch-clamp technique had the most important role in discovering and describing ion channels properties. In the beginning, ionic currents were recorded by the means of two microelectrodes introduced into large biological samples as the squid giant axons and imposing a certain voltage, with the voltage-clamp method (11). Although very useful for large biological samples, the technique of voltage-clamp (controlling the potential across the plasma membrane) could not be used for smaller samples as the usual mammalian cells. A profound advance in electrophysiology came with the development of the patch-clamp technique in 1976 and its improvement the following years. Erwin Neher and Bert Sakmann recorded ion currents from a tiny area of the plasma membrane (patch) by pressing against it a fire-polished glass pipette. In 1976, the first successful recording of a single-channel current

from the acetylcholine-activated receptor was reported. The main improvement of the technique came in 1981 with development of the “gigaseal” (sealing the pipette to the plasma membrane to resistance in extent of gigaohms) (12).

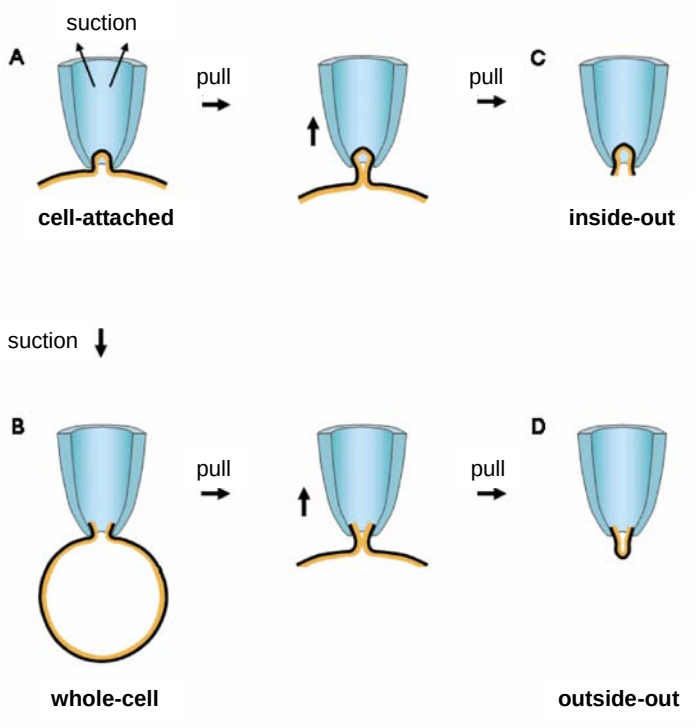


**Figure 1. Configurations of the patch-clamp technique. (A)** Pressing the pipette to the plasma membrane and by applying a slight suction the basic configuration of the patch-clamp technique, cell-attached is achieved. **(B)** By applying a suction pulse, the membrane enclosed by the pipette tip can be ruptured giving access to cell cytoplasm. **(C)** By pulling away the pipette from the cell in the cell-attached configuration the plasma membrane remains sealed to the pipette tip. This maneuver results in the formation of the inside-out configuration (the intracellular side of the membrane faces now the extracellular medium). **(D)** Pulling away the pipette from the cell in the whole-cell configuration results in the coupling of the loose membrane parts forming a vesicle at the pipette tip. In this way the outside-out configuration is achieved

For their discoveries concerning the single-channel recordings in living cells, Erwin Neher and Bert Sakmann received in 1991 the Nobel Prize in Physiology and Medicine.

The gigaseal led to development of four new configurations for recording ion currents **(Figure 1)**. After the pipette is sealed to the plasma membrane, single channel currents can be measured in the *cell-attached* mode **(Figure 1A)**. From the *cell-attached* mode, the patch can be deliberately ruptured by suction with the pipette still sealed to the cell. The resulting configuration is called *whole-cell* **(Figure 1B)**. In this configuration, the content of the pipette solution will diffuse into the cell cytoplasm and allow efficient control of its ionic concentration. The seal achieved in the *cell-attached* mode is so stable, that membrane patch can be pulled off the cell and dipped into a variety of test solutions; this maneuver leads to formation of the *inside-out* configuration **(Figure 1C)**. Finally, pulling the pipette away from the cell, in *whole-cell* mode, results in an *outside-out* patch **(Figure 1D)**. Over the last decades, patch-clamp became the primary technique in membrane biophysics and determined the further development of electrophysiology. Since the pipette solution exchanges molecules with the cytoplasm in the

*whole-cell* mode, this configuration developed into a valuable tool for biological and biochemical studies when is required to introduce ions, metabolites, inhibitors or fluorescent indicators into cells during the recordings. The *whole-cell* configuration enables the measurement of *macroscopic* currents from all ion channels present in the plasma membrane. Thus, measuring this *macroscopic* current can give an estimation of the functioning of all ion channels of one cell. The *macroscopic* currents (*I*) correspond to the formula:

$$I = i * N * P$$

where *i* represents the single-channel current (in pA), *N* is the number of ion channels in the plasma membrane and *P* is the open probability of the channels.

Furthermore, the patch-clamp technique development enabled the stable measurements of real-time activity of single ion channels.

**The Transient Receptor Potential superfamily**

TRP channels were identified in the late 60's in the phototransduction cascade of the fruit fly *Drosophila melanogaster* (13). In wild-type flies, continuous illumination of the eye produced a long lasting depolarization of the photoreceptor cells (13,14). In the *trp* mutant, the initial onset of the response to prolonged illumination was identical to wild-type flies but the depolarization was transiently decaying towards baseline within seconds despite continuous illumination. This results in a functional loss in sensitivity to bright light (15). The *trp* gene was cloned in 1989 (16) and subsequently it was demonstrated that its product, the TRP protein, forms all, or part, of a $Ca^{2+}$-permeable cation channel (17). Following the identification of TRP channels as $Ca^{2+}$-conducting channels in *Drosophila melanogaster*, 28 new genes encoding TRP channels have been cloned from different species and their functions are now beginning to be understood **(Table 1)**.

**Table 1. Functional properties of the mammalian TRP channels.** The table is showing the functional characteristics as activators, blockers or interacting protein partners of the TRP ion channels. (adapted and updated from Clapham (2)).

| TRP | Activators | Inhibitors | Putative Interacting Proteins | Proposed Functions | References |
|---|---|---|---|---|---|
| *TRPC1* | Activation potentiated by PLC pathways | Gd, La | TRPC4, TRPC5, calmodulin, TRPC3, TRPP1, $IP_3Rs$, caveolin-1, PMCA | Homodimer is a supposed stretch-sensitive ion channel; form heteromeric ion channels with TRPC4 or TRPC5 in neurons | (18-20) |

| | | | | | |
|---|---|---|---|---|---|
| *TRPC2* | Pheromone receptor mechanism? | | Calmodulin, $IP_3R$, enkurin, TRPC6 | *TRPC2*$^{-/-}$ mice respond abnormally to urine-based olfactory cues; pheromone sensing | (21-24) |
| *TRPC3* | Diacylglycerol, $[Ca^{2+}]_i$, activation potentiated by PLC pathways | BTP2, flufenamate, Gd, La | TRPC1, calmodulin, $PLC_\beta$, $PLC_\gamma$, $IP_3R$, RyR,SERCA,caveolin-1, αSNAP, NCX1 | Potential role in vasoregulation and airway regulation | (25-27) |
| *TRPC4* | La (100 μM), calmidazolium, activation potentiated by PLC pathways | $[Ca^{2+}]_i$, 2-APB, niflumic acid, DIDS, La (mM) | TRPC1, TRPC5, calmodulin, $PLC_\beta$, NHERF1, $IP_3R$ | *TRPC4*$^{-/-}$ mice have abnormalities in endothelial-based vessel permeability | (28-31) |
| *TRPC5* | La (100 μM), nitric oxide, activation potentiated by PLC pathways | 2-APB, flufenamate, La (mM) | TRPC1, TRPC4, calmodulin, $PLC_\beta$, NHERF1/2, ZO-1, $IP_3R$ | No phenotype yet reported in *TRPC5*$^{-/-}$ mice; potentially regulates growth cones and neurite extension | (32-34) |
| *TRPC6* | Diacylglycerol, $[Ca^{2+}]_i$, 20-HETE, activation potentiated by PLC pathways | 2-APB, amiloride, Cd, La, Gd | Calmodulin, TRPC3, TRPC7, FKBP12 | Missense mutation in human focal segmental vasoregulation in *TRPC6*$^{-/-}$ mice, proposed role in ATII-induced cardiac hypertrophy | (35-38) |
| *TRPC7* | Diacylglycerol, activation potentiated by PLC pathways | $[Ca^{2+}]_i$, flufenamate, La | Calmodulin, TRPC3, TRPC6, FKBP12, MxA, TRPC1 | No phenotype yet reported in *TRPC7*$^{-/-}$ mice; potential role in myocardial apoptosis | (39,40) |
| *TRPV1* | T>~45$^{o}$C, V-dep, $H^+$, activation potentiated by PLC pathways, anandamide, 2-AG, HETE, HPETE, capsaicin, olvanil, resiniferatoxin, arvanil, piperine, OEA, 2-APB, DPDBA, camphor | Capsazepine, RR, acyl-polyamines, camphor desensitizises | Calmodulin, TRPV3, TRPV2, PI3K, snapin, synaptogamin IX, β-tubulin | In *TRPV1*$^{-/-}$ mice decreased response to heat, acid pH; diminished stretch-evoked responses in bladder; upregulated in inflammatory bowel disease, osteoarthritis | (9,41-44) |
| *TRPV2* | T>~53$^{o}$C, neuropeptide head activator, DPBA, 2-APB | RR, La, SKF96365 | TRPV1, RGA | No phenotype yet reported in *TRPV2*$^{-/-}$ mice; role in thermal pain, osmosensing in myocites? | (45-47) |
| *TRPV3* | T>~30$^{o}$C, 2-APB, DPBA, carvacrol, thymol, eugenol, camphor, vanillin, ethyl vanillin, menthol, cinnemaldehyde | RR, La | TRPV1 | *TRPV3*$^{-/-}$ mice have decreased response to heat; potential role in warmth sensing in skin | (46,48-50) |

| | | | | | |
|---|---|---|---|---|---|
| *TRPV4* | Anandamide, arachidonic acid, 5'6'-epoxyeicosatri-enoic acids, 4α-phorbol 12,13 didecanoate, PMA | RR, Gd, La | Calmodulin, Src family kinases, aquaporin 5, pacsin 3 | *TRPV4*$^{-/-}$ mice have impaired pressure and acid sensation, dysregualted ADH; potential role in CNS osmosensing and temperature sensing in skin | (51-56) |
| *TRPV5* | Constitutively active, $PIP_2$ | $[Ca^{2+}]_i$, RR, econazole, Cd>>Gd>La, Mg, Cu, Pb | TRPV6, S100A/annexin, 80K-H, NHERF4, BSPRY, Rab11a | *TRPV5*$^{-/-}$ mice have bone abnormalities; possible role in $Ca^{2+}$ uptake in the kidney, gut | (3,57-60) |
| *TRPV6* | Constitutively active | $[Ca^{2+}]_i$, RR, Cd>>Gd>La, Mg | TRPV5, S100A/annexin | *TRPV6*$^{-/-}$ mice have alopecia, dermatitis and decreased intestinal $Ca^{2+}$ absorption | (59,61,62) |
| *TRPM1* | Not determined | | Not determined | Potential role in melanoma progression | (63) |
| *TRPM2* | Constitutively active, ADP-ribose, cADP-ribose, βNAD, hypo-osmolarity enhances | ADP, N-ACA, econazole, miconazole, clotrimazole, flufenamate | Calmodulin, cADP-ribose hydrolase, Sir2 | Senses oxidant stress in immune cells and glia | (64-67) |
| *TRPM3* | Constitutively active, hypo-osmolarity enhances, sphingolipids, steroids | $[Mg^{2+}]_i$ for TRPM3a1, a2 (9mM); Gd, La | Not determined | Potential role in kidney $Ca^{2+}$ reabsorption | (68-70) |
| *TRPM4* | $[Ca^{2+}]_i$, decavanadate, BTP2, PKC phosphorylation | AMP, ATP, flufenamate, polyamines; La, Gd for TRPM4a; $[ATP]_i$ for TRPM4b | Calmodulin, SUR1 | *TRPM4*$^{-/-}$ mice have enhanced anaphylactic responses; potential role in smooth muscle | (71-74) |
| *TRPM5* | T1R,T2R-$G_{gus}$-$PLC_{\beta 2}$, $[Ca^{2+}]_i$, $PIP_2$, V-dep, heat sensitive | <pH 7.0, spermine | Not determined | *TRPM5*$^{-/-}$ mice do not detect sweet, bitter or umami flavors | (75-78) |
| *TRPM6* | Acid pH, 2-APB | $[Mg^{2+}]_i$, RR | Integral kinase domain, TRPM7, RACK1 | Human *TRPM6* mutations cause hypomagnesemia with secondary hypocalcemia | (79-84) |
| *TRPM7* | Acid pH, $PIP_2$, activation potentiated by PLC pathways | $[Mg^{2+}]_i$, La, $PIP_2$ hydrolysis | Integral kinase domain, $PLC_{\beta 1\text{-}3}$, $PLC_{\gamma 1}$, snapin, TRPM6, myosin IIA heavy chain | Human *TRPM7* variant associated with Guamanian amyotrophic lateral sclerosis and Parkinson dementia; possible mediator of trace metal entry; role in excitotoxic neuron death | (85-91) |

| | | | | | |
|---|---|---|---|---|---|
| *TRPM8* | T<~25$^{o}$C; V-dep, $PIP_2$, menthol, icilin, eucalyptol | BCTC, capsazepine, 2-APB | Not determined | Responds to cold and pain; proposed roles in prostate cancer, activation-induced analgesia | (10,92-94) |
| *TRPA1* | T<~18$^{o}$C, modification of intracellular cysteines by allil isothiocianate, allicin, acrolein, Δ9-THC, carvacrol, icilin, cinnamaldehyde, eugenol, gingerol | RR, amiloride, camphor, menthol, gentamicin, Gd; carvacrol desensitizes | Not determined | *TRPA1*$^{-/-}$ mice have normal hearing; pain defects disputed; responds to pungent natural compounds, environmental irritants, inflammatory peptides | (95-98) |
| *TRPP1* | Also called PC2 or PKD2; mechanical stress, $[Ca^{2+}]_i$? | [Gd, La, Cd, SKF96365, 2-APB]? | PKD1/PKC1, Hax-1, cortactin, Id2, mDia, troponin, tropomyosin, actinin; cadherin via PKD1/PC1 | Mutations in human *TRPP1* cause autosomal dominant polycystic kidney disease; proposed to localize to cilia and be activated by ciliary movement | (99-102) |
| *TRPP2* | Also called PKD2L1; acid, $[Ca^{2+}]_i$? | [Flufenamate, Cd, La]? | PKD1L3 | *TRPP2* is deleted (among other genes) in *krd* mice that have kidney and retinal abnormalities; mice with targeted deletion in taste cells do not respond to sour (acid) stimuli | (101,103-105) |
| *TRPP3* | Also called PKD2L2, $[Ca^{2+}]_i$? | [amiloride, Gd, La, Ni]? | Not determined | Probable function in testis | (106) |
| *TRPML1* | Also called MCOLN1; $[Ca^{2+}]_i$? | [amiloride, Gd, La, Ni]? | Not determined | Mutations in *TRPML1* cause mucolipidosis type IV, a recessive neurodegenerative lysosomal storage disorder | (107,108) |
| *TRPML2* | Also called MCOLN2, not determined | | TRPML3 | Not determined | (108) |
| *TRPML3* | $Na^+$-free extracellular media | $Na^+$ | TRPML1, TRPML2 | +/- Varitint-waddler mice are deaf with vestibular defects | (109,110) |

TRP channels are universal biological sensors that detect changes in the environment. TRP channels gate in response to a multitude of stimuli including cold or hot temperatures, natural chemical compounds (menthol, camphor and “hot pepper”), mechanical stimuli, or changes in the composition of the lipid bilayer. TRP channels are crucially involved in physiological processes, such as photoreception, pheromone sensing, taste perception, thermosensation, pain perception, mechanosensation, perception of pungent compounds (mustard, garlic), renal $Ca^{2+}$/$Mg^{2+}$ handling, smooth muscle tone and blood pressure regulation (9,10,57,81,111-113).

Members of the TRP superfamily of channels share the common features of six transmembrane (TM) domains, with a pore-forming region between TM5 and TM6. Based on amino acid sequence homology, the TRP channel family can be grouped into 6 subfamilies: canonical (TRPC), vanilloid (TRPV), melastatin (TRPM), and the smaller subfamilies anchorin-repeat containing channels (TRPA), polycystins (TRPP) and mucolipins (TRPML).

*TRPC subfamily*

The TRPC subfamily consists of seven channels, named TRPC1-7. From all the TRP channels, this subfamily shares the highest homology with the TRP from *Drosophila melanogaster*. TRPC channels can be subdivided in three groups based on homology: TRPC1-4-5, TRPC3-6-7, and TRPC2 (114). All these channels share a structural feature, a so-called TRP box consisting of an invariant amino acid sequence "*EWKFAR*" located intracellular close to the TM6. Furthermore, these channels contain three to four amino-terminal ankyrin repeats (115). TRPC channels are $Ca^{2+}$ permeable non-selective cation channels with permeability ratios $P_{Ca}/P_{Na}$ varying from ~1 for TRPC4 to ~9 for TRPC5 (28,29,116). In general, TRPC channels open in response to stimulation of receptors that activate different isoforms of phospholipase C (PLC). TRPC3, -6, and -7 are activated by diacylglycerol (DAG), independent of the stimulation of protein kinase C (PKC) (117-120), suggesting that DAG mediates their physiological activation. In contrast, TRPC1, -4, and -5 are completely unresponsive to DAG (19,27,117) and the mechanism via which PLC stimulation leads to channel activation remains controversial. Surprisingly, it was shown that TRPC1 is directly activated by membrane stretch, independent of PLC activity, and that it may be the molecular homologue of the vertebrate stretch-activated cation channel MscCa (19). The TRPC channels are broadly expressed, and a given cell type generally contains multiple TRPC channels (121,122). Further complexity in the functional characterization of TRPC channels arises from the fact that these proteins can form heterotetramers, beside homotetramers. TRPC1 can form heteromers with TRPC4 and TRPC5, and the TRPC subfamilies TRPC4/5, and TRPC3/6/7 can form heteromers among themselves, with current properties significantly different from those of the homotetramers (20,30,123,124).

*TRPV subfamily*

Based on structure and function, the TRPV family comprises four groups of channels: TRPV1/TRPV2, TRPV3, TRPV4 and TRPV5/6. The *Caenorhabditis elegans* Osm-9 (125) and the *Drosophila melanogaster* Nanchung (Nan) are also included in this family (126). The founding member, TRPV1 was identified by expression cloning based on the capacity of hot pepper-derived vanilloid compound capsaicin to induce $Ca^{2+}$ influx within sensory neurons (9). Similar to the TRPC channels, members of the TRPV subfamily have a TRP box close to TM6 and three to six ankyrin repeats in the amino-terminal tail (127-129). TRPV1-4 channels are

non-selective for cations, modestly permeable to $Ca^{2+}$, with permeability ratios ($P_{Ca}/P_{Na}$) between 1 and 10 and can be activated and regulated by temperature. TRPV1 is activated by temperatures above 43°C and in addition, by chemical compounds as 2-aminoethoxydiphenyl borate (2-APB) (46), capsaicin and endogenous cannabinoid receptor ligands like anandamide (41-43).

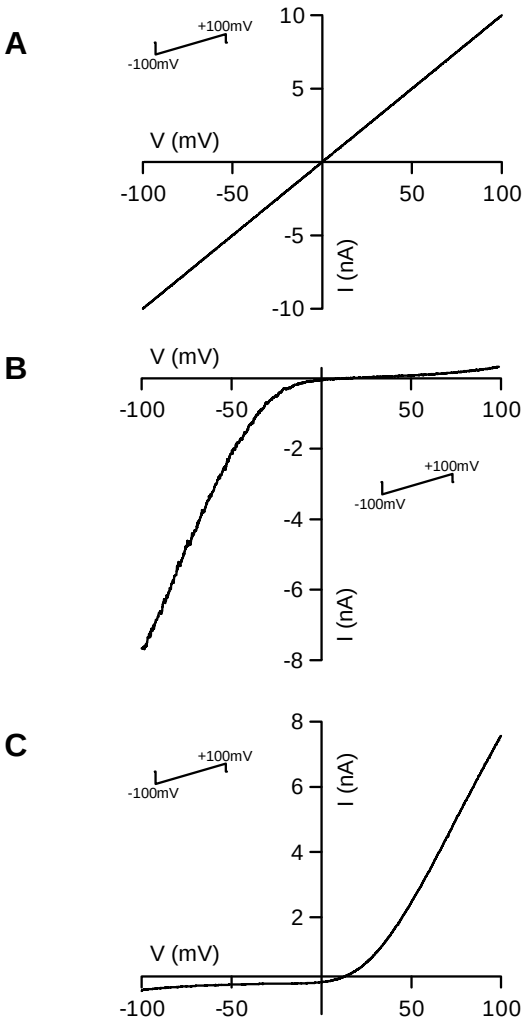


**Figure 2. Typical current-voltage (I-V) relations for TRP channels.** All the traces are obtained by applying a ramp protocol from -100mV to +100mV (inset). **(A)** The linear I-V relation corresponds to a channel that allows both ion influx (inwardly movement of ions) and efflux (outwardly movement of ions) in the same extent. **(B)** The inward rectifying I-V relation corresponds to a channel that allows better ion influx than ion efflux. **(C)** The outward rectifying I-V relations are obtained from channels that allow better efflux of ions compared to ion influx.

When heterologously expressed, TRPV1 channels display an outward rectifying current-voltage relation (I-V) **(Figure 2C)** and an anomalous mole fraction behavior (currents decrease with increasing in the extracellular $Ca^{2+}$ concentration from zero to certain value and then increase) as apparent from linearization of I-V relation in divalent free medium **(Figure 2A)**. TRPV1 currents are activated by pH values in the acid range (below 5.9) (130) and inhibited by phosphatidylinositol-4,5-biphosphate ($PIP_2$) (131). Furthermore, TRPV1 function is regulated by PKC and protein kinase A (PKA) activity via a so far unidentified mechanism. Considering its

expression pattern, TRPV1 is demonstrated to be involved in nociception, hypothermic effects of vanilloid compounds (44), pancreatitis (132) and asthma (133).

TRPV2 shares ~50% sequence homology with TRPV1 and is activated by noxious heat (above 52$^{o}$C) and by 2-APB, rather than capsaicin or acidic pH (46,47,134). TRPV2 channels display a moderately outward rectifying I-V relation upon activation **(Figure 2C)**.

TRPV3 and TRPV4 channels are also temperature-sensitive, but in a lower range: above 31$^{o}$C for TRPV3 (135) and above 25$^{o}$C for TRPV4 (136). TRPV3 channels display an outward rectifying I-V relation **(Figure 2C)** (49), while TRPV4 current show a linear I-V relation **(Figure 2A)** (53). Beside temperature, the activity of TRPV4 channels is enhanced upon hypotonicity (osmotic cell swelling) (137) and similar to TRPV1, their activation is sensitized by PKC (138).

In contrast to the other members of the subfamily, TRPV5 and TRPV6 channels are not activated by temperature changes. These channels, also known as epithelial $Ca^{2+}$ channels, were cloned using expression cloning strategies based on their capacity to mediate sustained $Ca^{2+}$ influx from the renal and intestinal epithelia, respectively (57,61). Opposite to the other subfamily members, TRPV5 and TRPV6 are constitutively active at physiological membrane potentials and intracellular $Ca^{2+}$ concentrations (139). TRPV5 and TRPV6 share 75% homology at the amino acid level with the main sequence differences located in the amino- and carboxyl-terminal tails. Strikingly, several domains in TRPV5 and TRPV6 are conserved within different species including the core structure of the protein consisting of six TM segments and the pore region **(Figure 3A)**. Detailed sequence analysis of TRPV5 and TRPV6 lead to the identification of several putative phosphorylation sites including PKC, PKA, and cGMP-dependent kinase. However, these predicted phosphorylation sites are not conserved in other species or in TRPV6. This is in contrast to the putative PKC phosphorylation sites of which three are conserved within the complete TRPV5 and TRPV6 subfamily **(Figure 3B)**. Despite this, the physiological relevance of the conserved PKC sites is not clear so far. To date, no information is available about the phosphorylation of TRPV5 and TRPV6. In addition, TRPV5 and TRPV6 contain PDZ motifs and ankyrin repeat domains in the amino-terminal region, which are also present in a diverse range of receptors and ion channels including the TRP superfamily. PDZ motifs are recognized by PDZ domains that are modular protein interaction domains playing a role in protein targeting and protein complex assembly. Although binding to carboxyl-terminal motifs appears to be the typical mode of interaction, PDZ domains could also interact with internal motifs that are present in TRPV5 and TRPV6. In general, ankyrins link transporters and cell adhesion molecules to the spectrin-based cytoskeletal elements in specialized membrane domains.

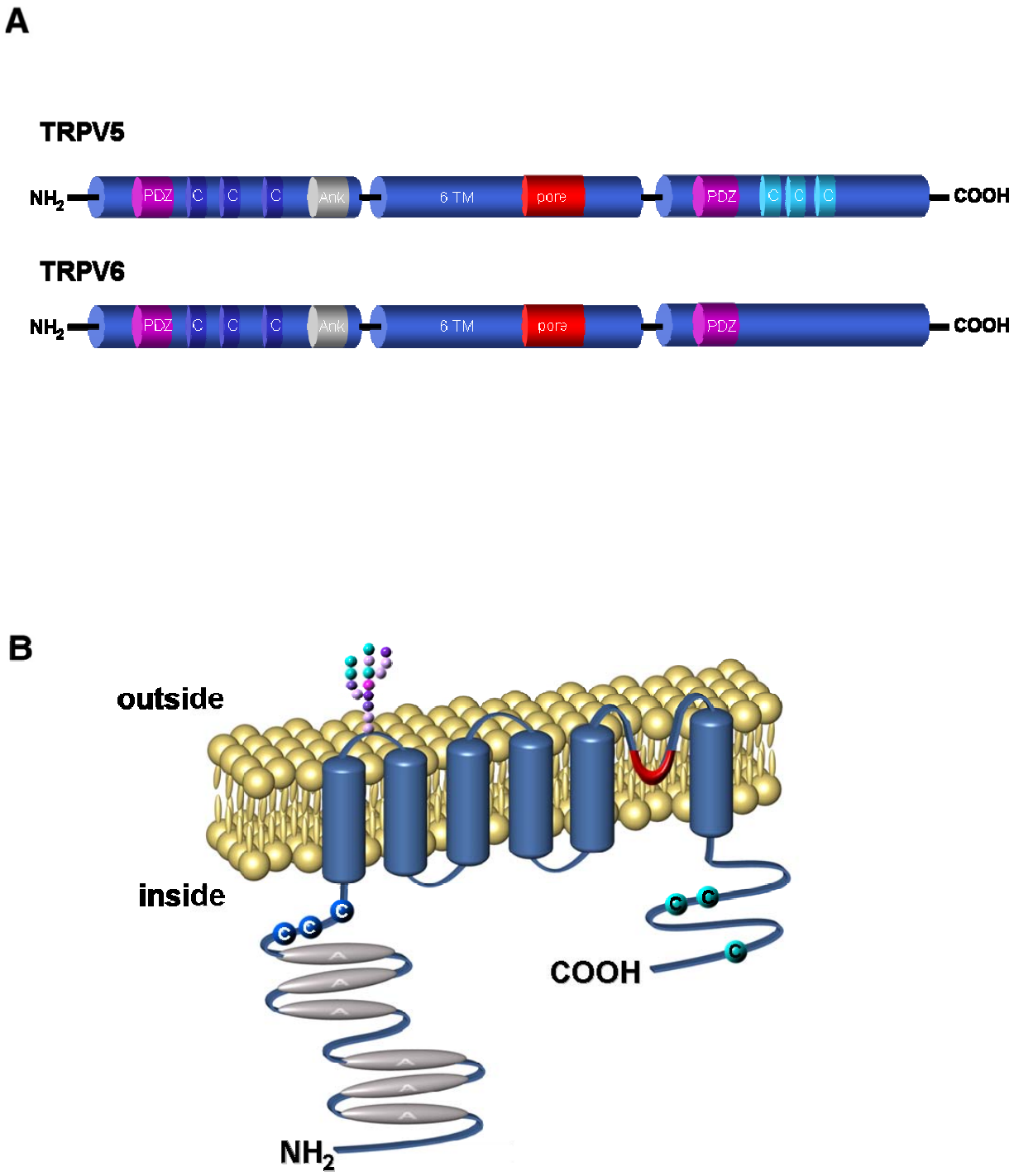


**Figure 3. Structural organization of TRPV5 and TRPV6. (A)** Potential regulatory sites in the amino- and carboxyl-tail of TRPV5 and TRPV6 including ankyrin repeats, PDZ motifs and conserved PKC phosphorylation sites. (modified and updated from Hoenderop *et al* (3)) **(B)** The epithelial $Ca^{2+}$ channels are 730 amino acids long with a predicted molecular mass of ~83 kDa. TRPV5 contains a core domain consisting of six transmembrane (TM) segments. The region between TM1 and TM2 contains an N-glycosylation site. In addition, large cytosolic amino- and carboxyl-terminal domains are present. The amino-terminal domain contains six ankyrin repeats, while conserved PKC phosphorylation sites are present at both termini. Between TM5 and TM6 there is a short hydrophobic stretch predicted to be the pore-forming region of the channel. Inner and outer sides of the plasma membrane are indicated.

When heterologously overexpressed, both channels display inward rectifying I-V relations with almost no outward currents at positive membrane potentials **(Figure 2B)**, and they are highly selective for $Ca^{2+}$ ($P_{Ca}/P_{Na}$ > 100) (140,141). TRPV5 and TRPV6 exhibit a similar ion permeation

sequence for divalent cations ($Ca^{2+}$>$Sr^{2+}$~$Ba^{2+}$>$Mn^{2+}$) (141). Both channels are blocked by extracellular $Mg^{2+}$ and show an anomalous mole fraction behavior (in case of TRPV5 and TRPV6 currents decrease with increasing in the extracellular $Ca^{2+}$ concentration from 0 to 100 µM and then increase) described for L-type voltage-gated $Ca^{2+}$ channels. Similar to the voltage-gated $Ca^{2+}$ channels, the epithelial $Ca^{2+}$ channels allow monovalent cation permeation in the absence of divalent cations, with the permeation sequence of $Na^{+}$>$Li^{+}$>$K^{+}$>$Cs^{+}$>>$NMDG^{+}$ (140,141). Single-channel measurements of TRPV5 $Na^{+}$ currents revealed the same inward rectifying I-V relation as the macroscopic currents. So far, no reliable TRPV5 single-channel measurements could be performed in the presence of extracellular $Ca^{2+}$, since the currents inactivates quickly in the presence of $Ca^{2+}$. Another typical feature of TRPV5 and TRPV6 currents is the inactivation at negative potentials. This inactivation is nearly complete with $Ca^{2+}$ as charge carrier and is delayed when $Ba^{2+}$ substitutes $Ca^{2+}$. Currents of monovalent cations through TRPV5 and TRPV6 do not inactivate.

Although most of the basic electrophysiological properties of TRPV5 and TRPV6 are rather similar, the channels differ in kinetics of $Ca^{2+}$-dependent inactivation, the recovery from inactivation and some pharmacological characteristics. Interestingly, these typical differences could be explained by sequence differences between TRPV5 and TRPV6. While TRPV6 clearly shows a fast component of inactivation, TRPV5 is lacking this: time to 10% inactivation recorded from hyperpolarizing steps to -100 mV is ~125 ms for TRPV5 and just ~40 ms for TRPV6. Fast inactivation is about two fold prolonged when $Ca^{2+}$ is substituted by $Ba^{2+}$ for TRPV5, but ~20 times for TRPV6. Surprisingly, the structural determinants of these differences are not located in either the amino or carboxyl termini, but in the TM2-TM3 intracellular linker. Swapping of the TM2-TM3 linker of TRPV6 to TRPV5 confers the kinetic and permeation phenotype of TRPV6 to TRPV5, whereas swapping of the amino- or carboxyl-terminal is ineffective (142). Some pharmacological properties also discriminate between the epithelial $Ca^{2+}$ channels. Ruthenium red is 100-fold more potent blocker for TRPV5 than for TRPV6 ($IC_{50}$ ~9 µM for TRPV6 but ~90 nM for TRPV5, respectively). TRPV5 is about four times more sensitive to $Cd^{2+}$ block than TRPV6 ($IC_{50}$ ~70 nM for TRPV5 compared to $IC_{50}$ ~260 nM for TRPV6) (143). Significant progress in identification of the molecular determinants of TRP channel pores and understanding of the high selectivity for $Ca^{2+}$ has been particularly achieved for TRPV5 and TRPV6 channels. Structural differences in the channel pore explain the striking permeation differences in the TRPV subfamily.

**Figure 4A** shows an amino acid sequence alignment of the putative pore regions of three mammalian TRPV channels. Based on structural similarity with the selectivity filter of the potassium channel KcsA (signature sequence "*TXXTXGYGD*") (144), the structural determinant of the pore of TRPV1 to TRPV4 channels is the GM(L/M)GD motif (145). Importantly, this motif is missing in TRPV5 and TRPV6. Instead, the molecular determinants of $Ca^{2+}$ selectivity and

permeation of TRPV5 and TRPV6 reside at a single aspartate residue (D542 for TRPV5 and D541 for TRPV6) present in the pore-forming region **(Figure 4A)** (146,147). Neutralization of these residues not only affects the high $Ca^{2+}$ selectivity of TRPV5 and TRPV6, but also abolishes $Mg^{2+}$- and voltage-dependent gating of these channels (147,148). It appears that high $Ca^{2+}$ selectivity of TRPV5 and TRPV6 depends on a ring of four aspartate residues in the channel pore, similar to the ring of four negative residues (aspartate and/or glutamate) in the pore of voltage-gated $Ca^{2+}$ channels **(Figure 4A)**. A detailed analysis of the structure of the TRPV5 and TRPV6 pores has now been published (149,150). To obtain insight in the pore architecture of TRPV6, permeation studies were performed and a pore diameter of ~5.4 Å was estimated. Mutating D541, a residue involved in high-affinity $Ca^{2+}$ binding, altered the apparent pore diameter, indicating that this residue lines the narrowest part of the pore and is part of the selectivity filter (150). Pore lining amino acids were determined by substituted cysteine accessibility method (SCAM). Cysteine residues introduced in a region preceding D542 for TRPV5 and D541 for TRPV6 displayed a cyclic pattern of reactivity to cysteine reacting agents indicative of a pore helix.

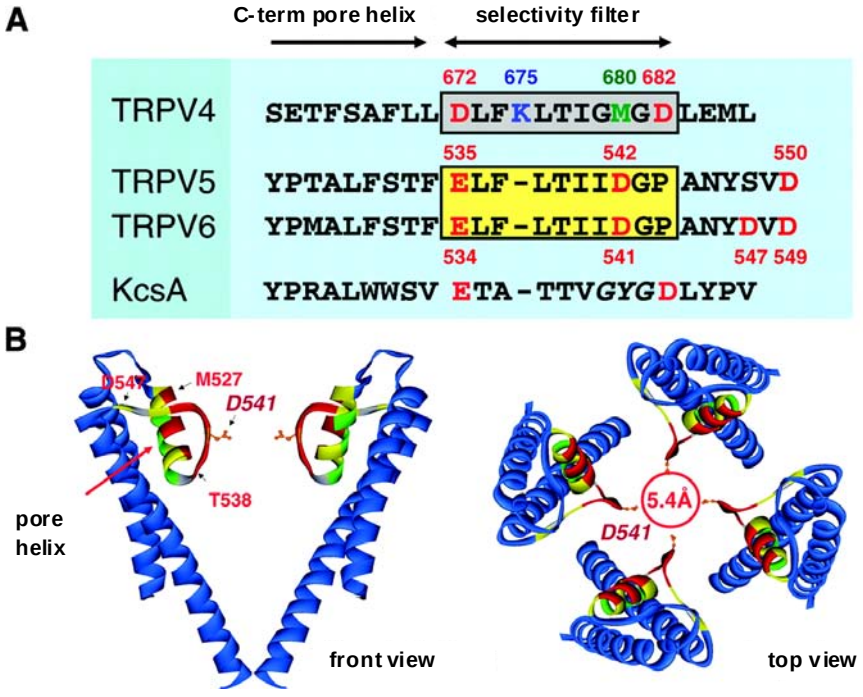


**Figure 4. Structure of the TRPV5 and TRPV6 pores. (A)** Alignment of the pore regions of TRPV4, TRPV5, and TRPV6 with the $K^+$ channel KcsA. The boxed sequences represent the putative selectivity filter of all channels. The amino-terminal part of this pore structure likely represents a putative pore helix. **(B)** Model for the TRPV6 pore region, based on the KcsA structure. Views of the structure are shown, looking sideways at two opposite subunits (left) or looking down from the external solution to the complete homotetrameric channel (right). At the narrowest point, formed by the acidic side chain of D541, the pore has a diameter of 5.4 Å. Blue residues correspond to the residues in TM5 and TM6 (TM1 and TM2 in KcsA), whose accessibility was not tested. Amino acids that were subjected to SCAM analysis (residues P526 to D547) are colored in green, yellow, red, or gray. Residues where cysteine substitution resulted in inactive channels are marked in gray. (figure updated from Hoenderop *et al* (3))

The location of the cation-selective filter was identified at the outer part of the pore helix **(Figure 4B)**. The pattern of covalent modification of cysteines supports a KcsA homology-based three-dimensional model (144). The external vestibule in TRPV5 and TRPV6 may build up the three structural domains consisting of a coiled structure that is connected to a 15-amino acid pore helix followed by the selectivity filter (probably a coiled structure with D542 and D541 as the narrowest part) and another coiled structure before the beginning of TM6 **(Figure 4B)**.

*TRPM subfamily*

TRPM channels show a large variety in cell biological and biophysical properties. The members of this subfamily can be subdivided into three subgroups: TRPM4 and TRPM5 that share significant similarities in both functional and biophysical characteristics; TRPM2, TRPM6 and TRPM7 that are remarkable combinations of ion channels and enzymes; and the remaining channels TRPM1, TRPM3 and TRPM8. In contrast to TRPC and TRPV, TRPM channels do not contain ankyrin repeats within their amino-terminal domain. Alternatively, the amino-terminal part of TRPM proteins, which is considerably longer (by 300–400 amino acids) than the corresponding regions in TRPC and TRPV members, contains a large TRPM homology region. The carboxyl-terminal sequences of TRPM channels are highly variable, thus determining differences in total protein length.

TRPM channels exhibit highly variable permeabilities to $Ca^{2+}$ and $Mg^{2+}$, ranging from $Ca^{2+}$ impermeable (the monovalent cations selective TRPM4 and TRPM5) to $Ca^{2+}$ and $Mg^{2+}$ permeable (TRPM6, TRPM7 and specific splice variants of TRPM3). The gating mechanisms of the TRPM subfamily members are equally varied. TRPM2 is activated by intracellular ADP-ribose, hydrogen peroxide (64,151), and heat (152), whereas reported activation mechanisms for TRPM3 include cell swelling and sphingosine (69). TRPM4 and TRPM5 gate upon an increase in intracellular $Ca^{2+}$ (75,153) and are strongly activated by raising in temperature (154). Finally, TRPM8 is activated upon cooling and by cooling agents such as menthol or icilin (93). So far, functional characterization of TRPM1 has not been reported.

Within the TRPM subfamily, two members, TRPM6 (Chak2) and TRPM7 (ChaK1, TRP-PLIK, LTRPC7), share the unique feature of a kinase domain belonging to the atypical family of α-kinases fused to the ion channel domain **(Figure 5)**. Complete sequence analysis of TRPM6 lead to the identification of several putative phosphorylation sites including PKC and PKA **(Figure 5)**. Additionally, TRPM6 contains PDZ motifs and in the amino- and carboxyl-terminal regions **(Figure 5)**. These putative phosphorylation and protein-protein interaction sites could prove to be important for regulating TRPM6 activity.

The TRPM6 channel conducts mono and divalent cations currents, but at physiological ion concentration and membrane potential, it is an $Mg^{2+}$-selective channel (81). When heterologously expressed, TRPM6 channels display an outward rectifying I-V relation

**(Figure 2C)** with currents reversing ~0 mV (81). TRPM6 currents are activated by a decrease in intracellular $Mg^{2+}$. The analysis of inward and outward currents revealed one interesting feature of TRPM6. Whereas outward currents are mainly carried by monovalent cations, TRPM6 channels preferentially conduct divalent cations in the inward direction, resulting in a high $Ca^{2+}$ and $Mg^{2+}$ (inward) permeability. In the absence of extracellular divalent cations, however, inward currents (carried by monovalent cations) are strongly increased. The resulting linear I-V relation **(Figure 2A)** supports the argument against a voltage-dependent activation of TRPM6. Monovalent cation inward currents were inhibited by 10 µM ruthenium red at negative membrane potentials.

TRPM6 expression pattern is predominantly restricted to intestinal and renal epithelia supporting its proposed role in body $Mg^{2+}$ homeostasis. Recently, it was postulated that TRPM6 requires assembly with TRPM7 to form functional channel complexes in the plasma membrane and that disruption of multimer formation by a mutated TRPM6 variant, TRPM6S141L, results in hypomagnesemia with secondary hypocalcemia (HSH) (82). In this study, TRPM6S141L was not directed to the cell surface by TRPM7 and failed to interact with the co-expressed TRPM7. Remarkably, in contrast to TRPM7, Gudermann and co-workers (82) found that TRPM6 expression in *Xenopus leavis* oocytes and HEK293 cells did not entail significant ion currents. In contrast, we measured significantly larger currents in TRPM6-transfected HEK293 cells compared to control cells (81). An explanation for this discrepancy might be the existence of specific TRPM6 splice variants with different functional properties. Chubanov *et al* (82) demonstrated that 5' rapid amplification of cDNA ends revealed three short alternative 5' exons, called 1A, 1B, and 1C, that were found to be individually spliced onto exon 2, suggesting that the TRPM6 gene harbors a promoter with alternative transcription start sites. These cDNAs have been named accordingly TRPM6a, TRPM6b, and TRPM6c, and additional functional measurements are needed to explain possible biophysical differences.

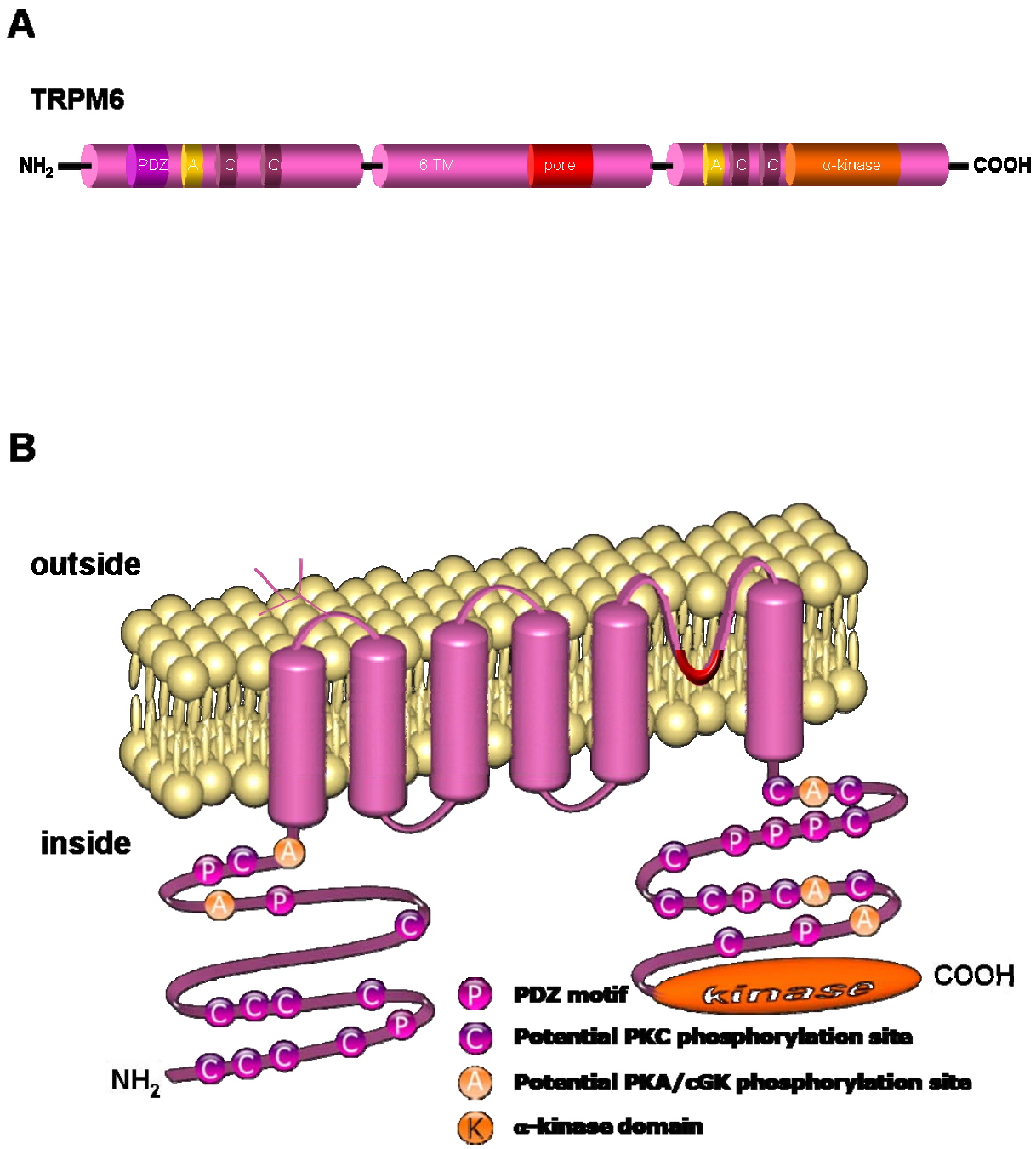


**Figure 5. Structural organization of TRPM6. (A)** Potential regulatory sites in the amino- and carboxyl-tails of TRPM6 including PDZ motifs and conserved PKC and PKA phosphorylation sites. **(B)** TRPM6 is 2022 amino acids long with a predicted molecular mass of ~234 kDa. TRPM6 contains a core domain consisting of six transmembrane (TM) segments. In addition, large cytosolic amino and carboxyl-terminal domains are present. Putative PKC and PKA phosphorylation sites are present at both TRPM6 extremities. Between TM5 and TM6 there is a short hydrophobic stretch predicted to be the pore-forming region of the channel. Inner and outer sides of the plasma membrane are indicated.

Besides showing 50% sequence homology, TRPM7 share many properties with TRPM6. As for TRPM6, the TRPM7 currents are carried by divalent cations and display an outward rectifying I-V relation **(Figure 2C)** (85,86). TRPM7 monovalent cations currents are inhibited by intracellular $Mg^{2+}$ and therefore the I-V relation linearizes in divalent free solutions **(Figure 2A)**. In addition, depletion of intracellular $Mg^{2+}$ (155,156) or Mg-nucleotides (85,157) fully activates TRPM7 by a

mechanism independent of $Mg^{2+}$ permeation block. Besides $Ca^{2+}$ and $Mg^{2+}$, TRPM7 provides a mechanism for entry of trace metal ions as $Ni^{2+}$, $Co^{2+}$, $Mn^{2+}$, and $Zn^{2+}$ (89). Since the cloning of TRPM6 and TRPM7, it has been debated whether the α-kinase domain is involved in the regulation of the channel gating. Initially, it was suggested that TRPM7 gating requires a functional α-kinase domain (86). However, subsequent studies demonstrated that channel gating could be dissociated from the α-kinase activity and TRPM7 autophosphorylation. Furthermore, it has been reported that the α-kinase domain is neither required for the TRPM7 channel activity nor that it contains the internal $Mg^{2+}$ sensing domain (158-160).

*TRPA*

The TRPA family currently comprises one mammalian member, TRPA1, which is expressed in dorsal root ganglion (DRG), trigeminal ganglion (TG) neurons, and in hair cells (95,161,162). TRPA1 exhibits 14 amino-terminal ankyrin repeats (95), an unusual structural feature that may be relevant to the proposed role of the channel as a mechanosensor (162).

*TRPP subfamily*

The TRPP subfamily is heterogeneous and can be divided, based on structures, into PKD1-like (TRPP1-like) and PKD2-like (TRPP2-like) proteins. PKD1-like members comprise TRPP1 (previously termed PKD1), PKDREJ, PKD1L1, PKD1L2, and PKD1L3. TRPP1 consists of 11 transmembrane domains, a very long and complex ~3000 amino acid extracellular domain, and an intracellular carboxyl-terminal domain that interacts with the carboxyl-terminal domain of TRPP2 through a coiled-coil domain. The PKD2-like members structurally resemble other TRP channels in that they are predicted to have intracellular amino- and carboxyl-terminal domains, six TM-spanning domains, and a pore region. The members of this group comprise PKD2 (TRPP2), PKD2L1 (TRPP3), and PKD2L2 (TRPP5). All PKD2-like proteins posses a coiled-coil structure in their carboxyl-terminal domain and form multiprotein/ion channel complexes. Mutations in human *TRPP1* cause autosomal dominant polycystic kidney disease (102).

*TRPML subfamily*

The TRPML family consists of three mammalian members (TRPML1–3) that are relatively small proteins consisting of ~600 amino acid residues. TRPML1 is widely expressed and it appears that resides in late endosomes/lysosomes (163,164). The loop between TM1 and TM2 contains a lipase domain of unknown function, although it may be speculated that this region is enzymatically active, or represents a binding site for lipids that could exert a regulatory influence on TRPML1. Recently, TRPML1 has been described to function as $H^+$ channel determining an $H^+$ leak in lysosomes to prevent excessive acidification in these organelles (165,166). The cellular functions of TRPML2 are presently unknown. TRPML3 is involved in vesicular and

intracellular ion homeostasis in inner ear hair cells and melanocytes (167,168). Gain-of-function mutation in TRPML3 cause cytotoxicity and finally results in the development of the varitint-waddler phenotype in mice (109,110,168).

**Calcium homeostasis**

The maintenance of the extracellular $Ca^{2+}$ concentration is of vital importance for many physiological processes including intracellular signaling, neuronal excitability, muscle contraction and bone formation (3). Disturbed blood $Ca^{2+}$ levels can be associated with serious clinical symptoms ranging from neuromuscular irritability, neuropsychiatric to renal dysfunction and cardiovascular diseases. Therefore, the extracellular $Ca^{2+}$ concentration is regulated by a homeostatic mechanism tightly controlling the concerted actions of intestinal $Ca^{2+}$ absorption, exchange of $Ca^{2+}$ to and from the bone and renal $Ca^{2+}$ reabsorption (3). The main determinants of $Ca^{2+}$ homeostasis are the active form of vitamin D, 1,25-dihydroxyvitamin $D_3$ ($1,25(OH)_2D_3$), the parathyroid hormone (PTH) and calcitonin (169-173). The parathyroid glands play a key role in controlling the $Ca^{2+}$ balance through their capacity to sense small changes in the extracellular $Ca^{2+}$ concentration (174). When the extracellular $Ca^{2+}$ levels drop, PTH is secreted into the blood and acts primarily on kidney and bone. Additionally, PTH stimulates 25-hydroxyvitamin-$D_3$-1α-hydroxylase, the crucial enzyme in the biosynthesis of $1,25(OH)_2D_3$ which controls $Ca^{2+}$ (re)absorption in kidney and intestine. In both organs, $Ca^{2+}$ can cross the epithelial barrier to reach the extracellular fluid via two pathways: paracellular (passive) and transcellular (active) (3). Intestinal $Ca^{2+}$ absorption is a crucial control system in the regulation of $Ca^{2+}$ balance, because it facilitates the entry of dietary $Ca^{2+}$ into the extracellular compartment. Here, $Ca^{2+}$ is absorbed *via* two distinct passive and active mechanisms, with their relative magnitude of importance being set by the dietary $Ca^{2+}$ content. Active transcellular $Ca^{2+}$ absorption is located largely in the duodenum, whereas paracellular $Ca^{2+}$ absorption occurs throughout the entire length of the intestine (175,176). In the kidney, the bulk of filtered $Ca^{2+}$ is reabsorbed through paracellular reabsorption in the proximal tubule, and to a lower degree in the thick ascending loop of Henle (TAL), where it is functionally coupled to $Na^+$ reabsorption (3). The $Na^+$ and water reabsorption in the proximal tubules increases luminal $Ca^{2+}$ concentration, creating a favorable $Ca^{2+}$ concentration gradient resulting in passive diffusion of ~60% of filtered $Ca^{2+}$ through the tight junctions towards the renal interstitium. In TAL, parallel reabsorption of $Na^+$, $K^+$ and $Cl^-$ by the $Na^+$,$K^+$,$2Cl^-$-co-transporter (NKCC2), in combination with $K^+$ recycling through the renal outer medullary $K^+$ channel (ROMK), generates a lumen positive electrochemical gradient to drive the paracellular $Ca^{2+}$ reabsorption in this nephron segment (3). Furthermore, renal active $Ca^{2+}$ reabsorption is limited to the distal convoluted tubules (DCT) and the connecting tubules (CNT) (177). Active renal $Ca^{2+}$ reabsorption is considered to determine the net urinary $Ca^{2+}$ excretion (3).

*Roles of TRPV5 and TRPV5 in active $Ca^{2+}$ transport*

Renal DCT and CNT as well as duodenal epithelial cells are unique in their ability to mediate transcellular $Ca^{2+}$ transport from the luminal to the basolateral compartments, while maintaining their cytosolic $Ca^{2+}$ concentration at low values (3). This transport is a three steps process: (i) $Ca^{2+}$ entry through the apical membrane *via* the specialized epithelial $Ca^{2+}$ channels, TRPV5 and TRPV6, (ii) intracellular buffering and facilitated diffusion of $Ca^{2+}$ bound to $Ca^{2+}$-binding proteins (calbindins). (iii) Subsequently, $Ca^{2+}$ extrusion across the basolateral membranes by the $Na^+/Ca^{2+}$ exchanger subtype 1 (NCX1) and/or by the plasma membrane $Ca^{2+}$ ATPase (PMCA1b) (3). Regulation of $Ca^{2+}$ entry at the apical membranes via TRPV5 and TRPV6 is essential for the active $Ca^{2+}$ process. Therefore, the epithelial $Ca^{2+}$ channels are generally regarded as the gatekeepers of transcellular $Ca^{2+}$ transport (3).

A tight control of the epithelial $Ca^{2+}$ channels activity is important for their function in body $Ca^{2+}$ homeostasis. The regulation of the epithelial $Ca^{2+}$ channels occurs at different levels and involves:

- The long-term transcriptional and translational effects of hormones. TRPV5 and TRPV6 gene expression is regulated by PTH (178) and $1,25(OH)_2D_3$ (179,180).
- The role of regulatory proteins affecting the trafficking of the channels towards and from the plasma membrane. The $Na^+/H^+$ exchanger regulatory factor 4 (NHERF4) (181), Rab11a (182) and “with no lysine” kinase 4 (WNK4) (183) affect trafficking of TRPV5 and TRPV6 proteins to regulate channel activity.
- The contribution of accessory proteins to the regulation of the biophysical properties of the channels directly altering their conformation at the plasma membrane. Modulation of TRPV5 channel activity at the plasma membrane is facilitated by the B-box and SPRY-domain containing protein (BSPRY) (184) and the $Ca^{2+}$-binding protein (calbindin-$D_{28K}$), (185), 80 K-H (186) calmodulin (187,188) .

Whereas the long-term transcriptional and translational regulation of epithelial $Ca^{2+}$ channels by hormones could be systematically studied in mice models, the role of accessory proteins and their molecular mechanisms to regulate channels activity was studied using comprehensive electrophysiological (patch-clamp measurements) and biochemical approaches (binding studies, cell surface biotinylation, *etc*.). Accessory proteins can regulate channel activity either by changing the open probability (gating) of the channel or by modifying channel expression at the plasma membrane (trafficking). The advantage of using the patch-clamp technique was that it enabled us to measure changes in channel gating determined by the action of accessory proteins, while by cell surface biotinylation or by Total Internal Reflection Fluorescence (TIRF) the amount of channels at the plasma membrane could be determined.

**Magnesium homeostasis**

Being the second most abundant intracellular cation, $Mg^{2+}$ plays an important role as co-factor in many enzymatic reactions (189,190). $Mg^{2+}$ homeostasis depends on the balance between intestinal absorption, renal excretion and $Mg^{2+}$ deposit in bone (191). Regulation of body $Mg^{2+}$ balance principally occurs in the kidney where $Mg^{2+}$ excretion tightly matches intestinal $Mg^{2+}$ absorption (192). Around 80% of the total blood $Mg^{2+}$ is filtered in the glomeruli, of which approximately 85% is reabsorbed via passive (paracellular) mechanisms in the proximal tubules and TAL, in a similar manner as $Ca^{2+}$. However, the relative contribution of these nephron segments differs significantly with only ~20% of $Mg^{2+}$ reabsorption taking place in the proximal tubules and the bulk ~70% of filtered $Mg^{2+}$ being reabsorbed in TAL.

*Roles of TRPM6 and TRPM7 in active $Mg^{2+}$ transport*

Active (transcellular) $Mg^{2+}$ transport takes place in DCT, where ~10% of the filtered $Mg^{2+}$ is reabsorbed (190,193). The reabsorption rate in this nephron segment determines the final urinary $Mg^{2+}$ concentration. However, the molecular mechanisms and regulation of $Mg^{2+}$ reabsorption remain largely unknown. Previously, mutations in the $\gamma$ subunit of the basolateral $Na^+,K^+$-ATPase were discovered in patients suffering from autosomal dominant hypomagnesemia (194,195) demonstrating a role of this protein in $Mg^{2+}$ transport. Recently, two groups independently demonstrated that mutations in the gene encoding TRPM6 cause autosomal recessive hypomagnesemia, characterized by disturbed intestinal $Mg^{2+}$ absorption and renal $Mg^{2+}$ wasting (79,80). Subsequently, detailed studies demonstrated that TRPM6 forms $Mg^{2+}$-permeable channels predominantly expressed along the apical membrane of epithelial cells from duodenum and DCT of the kidney (81). Current studies generally acknowledge TRPM6 as the gatekeeper of epithelial $Mg^{2+}$ transport, suggesting a key role in body $Mg^{2+}$ homeostasis, while its closest homologue, TRPM7 plays critical roles in cellular $Mg^{2+}$ homeostasis (159). Dietary $Mg^{2+}$ restriction in mice resulted in hypomagnesemia and renal $Mg^{2+}$ and $Ca^{2+}$ conservation, whereas a $Mg^{2+}$-enriched diet led to increased urinary $Mg^{2+}$ and $Ca^{2+}$ excretion (196). Conversely, $Mg^{2+}$ restriction significantly up-regulated renal TRPM6 mRNA levels, whereas an $Mg^{2+}$ enriched diet increased TRPM6 mRNA expression in colon (196). Dietary $Mg^{2+}$ did not alter TRPM7 mRNA expression in mouse kidney and colon (196), consistent with its role in cellular $Mg^{2+}$ homeostasis.

**Aims and outline of this thesis**

As described in previous paragraphs, the members of the TRPV family of cation channels, TRPV5 and TRPV6, are key players in transepithelial $Ca^{2+}$ transport and thus important factors to modulate body $Ca^{2+}$ balance. Similarly, TRPM6 proteins function as epithelial $Mg^{2+}$ channels contributing to body $Mg^{2+}$ homeostasis. Therefore, the general goal of this thesis was to get

further insight into the physiological and molecular regulation of epithelial $Ca^{2+}$ and $Mg^{2+}$ channels in order to ultimately understand mechanisms of active transport of these divalent cations. To this end, the above-described electrophysiological technique, patch-clamp analysis, was used for functional characterization of different accessory proteins that regulate epithelial $Ca^{2+}$ channels, and to identify the molecular determinants of cation permeation through the epithelial $Mg^{2+}$ channel TRPM6.

In the study described in **chapter 2,** the molecular basis of hypercalciuria observed in tissue kallikrein knockout ($TK^{-/-}$) mice was investigated. The study combined functional and biochemical assays to determine the effect of TK on active $Ca^{2+}$ reabsorption.

The $Ca^{2+}$-sensing receptor (CaSR) is mainly expressed in the chief cell of the parathyroid glands and throughout the whole length of the nephron. CaSR functions as a G-protein coupled receptor and is activated by increased $Ca^{2+}$ concentrations in the blood or extracellular fluids. In the proximal nephron segments, CaSR inhibits passive $Ca^{2+}$ reabsorption. CaSR is also present in the apical membrane of DCT and CNT of the kidney, the primary sites of TRPV5 expression. By the study described in **chapter 3,** a potential role of the CaSR in the DCT and CNT of the kidney was determined using functional assays as patch-clamp recordings and measurements of the intracellular $Ca^{2+}$ concentrations.

FKBP52 is a widely expressed cytosolic enzyme that belongs to the FK506-binding proteins (FKBPs) subfamily of immunophillin proteins. FKBP52 was identified as a candidate to regulate TRPV5 using a microarray to screen for genes that code for proteins involved in $Ca^{2+}$ reabsorption. In the study presented in **chapter 4,** this novel TRPV5 accessory protein, FKBP52, was functionally characterized.

RGS2 is member of the family of proteins that regulate the G protein signaling by enhancing the GTP-ase activity of active Gα subunits. In the study described in **chapter 5**, RGS2 was identified as a novel binding partner of TRPV6 by yeast-two-hybrid screening. The role of the RGS2 protein as putative TRPV6 regulator was further examined using functional and biochemical assays.

Further, the pore permeation properties of the epithelial $Mg^{2+}$ channel TRPM6 were investigate in the study described in **chapter 6**. A combined approach consisting in site-directed mutagenesis and electrophysiological measurements was used to investigate the role of amino acid residues from the putative selectivity filter in the permeation properties of TRPM6.

Finally, the outcome of this thesis and the implications of the described studies in ion channel physiology were discussed and summarized in **chapter 7**.

**REFERENCES**


1. Dubyak, G. R. *Advan. Physiol. Edu.* 28: 143-154, 2004
2. Clapham, D. E. *Cell.* 129: 220, 2007
3. Hoenderop, J. G., Nilius, B., and Bindels, R. J. *Physiol Rev.* 85: 373-422, 2005
4. Toyoshima, C., Nakasako, M., Nomura, H., and Ogawa, H. *Nature.* 405: 647-655, 2000
5. Toyoshima, C., and Nomura, H. *Nature.* 418: 605-611, 2002
6. Toyoshima, C., and Mizutani, T. *Nature.* 430: 529-535, 2004
7. Toyoshima, C., Nomura, H., and Tsuda, T. *Nature.* 432: 361-368, 2004
8. Hille, B. (2001) *Ion Channels of Excitable Membranes*, 3-rd Ed., Sinauer Associates Inc.
9. Caterina, M. J., Schumacher, M. A., Tominaga, M., Rosen, T. A., Levine, J. D., and Julius, D. *Nature.* 389: 816-824, 1997
10. Peier, A. M., Moqrich, A., Hergarden, A. C*., et al. Cell.* 108: 705-715, 2002
11. Hodgkin, A. L., and Huxley, A. F. *J Physiol.* 104: 176-195, 1945
12. Hamill, O. P., Marty, A., Neher, E., Sakmann, B., and Sigworth, F. J. *Pflugers Arch.* 391: 85-100, 1981
13. Cosens, D. J., and Manning, A. *Nature.* 224: 285-287, 1969
14. Pak, W. L., Grossfield, J., and Arnold, K. S. *Nature.* 227: 518-520, 1970
15. Minke, B., Wu, C., and Pak, W. L. *Nature.* 258: 84-87, 1975
16. Montell, C., and Rubin, G. M. *Neuron.* 2: 1313-1323, 1989
17. Hardie, R. C., and Minke, B. *Neuron.* 8: 643-651, 1992
18. Wes, P. D., Chevesich, J., Jeromin, A., Rosenberg, C., Stetten, G., and Montell, C. *Proc Natl Acad Sci U S A.* 92: 9652-9656, 1995
19. Maroto, R., Raso, A., Wood, T. G., Kurosky, A., Martinac, B., and Hamill, O. P. *Nat Cell Biol.* 7: 179-185, 2005
20. Strubing, C., Krapivinsky, G., Krapivinsky, L., and Clapham, D. E. *Neuron.* 29: 645-655, 2001
21. Vannier, B., Peyton, M., Boulay, G*., et al. Proc Natl Acad Sci U S A.* 96: 2060-2064, 1999
22. Lucas, P., Ukhanov, K., Leinders-Zufall, T., and Zufall, F. *Neuron.* 40: 551-561, 2003
23. Liman, E. R., Corey, D. P., and Dulac, C. *Proc Natl Acad Sci U S A.* 96: 5791-5796, 1999
24. Stowers, L., Holy, T. E., Meister, M., Dulac, C., and Koentges, G. *Science.* 295: 1493-1500, 2002
25. Vazquez, G., Wedel, B. J., Kawasaki, B. T., Bird, G. S., and Putney, J. W., Jr. *J Biol Chem.* 279: 40521-40528, 2004
26. Kwan, H. Y., Huang, Y., and Yao, X. *Proc Natl Acad Sci U S A.* 101: 2625-2630, 2004
27. Venkatachalam, K., Zheng, F., and Gill, D. L. *J. Biol. Chem.* 278: 29031-29040, 2003
28. Okada, T., Shimizu, S., Wakamori, M*., et al. J Biol Chem.* 273: 10279-10287, 1998
29. Schaefer, M., Plant, T. D., Obukhov, A. G., Hofmann, T., Gudermann, T., and Schultz, G. *J. Biol. Chem.* 275: 17517-17526, 2000
30. Strubing, C., Krapivinsky, G., Krapivinsky, L., and Clapham, D. E. *J. Biol. Chem.* 278: 39014-39019, 2003
31. Tiruppathi, C., Freichel, M., Vogel, S. M*., et al. Circ Res.* 91: 70-76, 2002
32. Jung, S., Muhle, A., Schaefer, M., Strotmann, R., Schultz, G., and Plant, T. D. *J Biol Chem.* 278: 3562-3571, 2003
33. Greka, A., Navarro, B., Oancea, E., Duggan, A., and Clapham, D. E. *Nat Neurosci.* 6: 837-845, 2003
34. Bezzerides, V. J., Ramsey, I. S., Kotecha, S., Greka, A., and Clapham, D. E. *Nat Cell Biol.* 6: 709-720, 2004
35. Tseng, P. H., Lin, H. P., Hu, H., Wang, C., Zhu, M. X., and Chen, C. S. *Biochemistry.* 43: 11701-11708, 2004
36. Estacion, M., Li, S., Sinkins, W. G*., et al. J Biol Chem.* 279: 22047-22056, 2004
37. Hisatsune, C., Kuroda, Y., Nakamura, K*., et al. J Biol Chem.* 279: 18887-18894, 2004
38. Freichel, M., Vennekens, R., Olausson, J*., et al. J Physiol.* 567: 59-66, 2005

39. Shi, J., Mori, E., Mori, Y.*, et al. J Physiol.* 561: 415-432, 2004
40. Numaga, T., Wakamori, M., and Mori, Y. *Handb Exp Pharmacol.* 143-151, 2007
41. Ahern, G. P. *J Biol Chem.* 278: 30429-30434, 2003
42. Premkumar, L. S., and Ahern, G. P. *Nature.* 408: 985-990, 2000
43. Prescott, E. D., and Julius, D. *Science.* 300: 1284-1288, 2003
44. Caterina, M. J., Leffler, A., Malmberg, A. B.*, et al. Science.* 288: 306-313, 2000
45. Muraki, K., Iwata, Y., Katanosaka, Y.*, et al. Circ Res.* 93: 829-838, 2003
46. Hu, H. Z., Gu, Q., Wang, C.*, et al. J Biol Chem.* 279: 35741-35748, 2004
47. Caterina, M. J., Rosen, T. A., Tominaga, M., Brake, A. J., and Julius, D. *Nature.* 398: 436-441, 1999
48. Chung, M. K., Lee, H., Mizuno, A., Suzuki, M., and Caterina, M. J. *J Neurosci.* 24: 5177-5182, 2004
49. Xu, H., Ramsey, I. S., Kotecha, S. A.*, et al. Nature.* 418: 181-186, 2002
50. Moqrich, A., Hwang, S. W., Earley, T. J.*, et al. Science.* 307: 1468-1472, 2005
51. Vriens, J., Watanabe, H., Janssens, A., Droogmans, G., Voets, T., and Nilius, B. *Proc Natl Acad Sci U S A.* 101: 396-401, 2004
52. Watanabe, H., Davis, J. B., Smart, D.*, et al. J Biol Chem.* 277: 13569-13577, 2002
53. Watanabe, H., Vriens, J., Suh, S. H., Benham, C. D., Droogmans, G., and Nilius, B. *J Biol Chem.* 277: 47044-47051, 2002
54. Watanabe, H., Vriens, J., Prenen, J., Droogmans, G., Voets, T., and Nilius, B. *Nature.* 424: 434-438, 2003
55. Suzuki, M., Mizuno, A., Kodaira, K., and Imai, M. *J Biol Chem.* 278: 22664-22668, 2003
56. Tabuchi, K., Suzuki, M., Mizuno, A., and Hara, A. *Neurosci Lett.* 382: 304-308, 2005
57. Hoenderop, J. G., van der Kemp, A. W., Hartog, A.*, et al. J Biol Chem.* 274: 8375-8378, 1999
58. Chang, Q., Gyftogianni, E., van de Graaf, S. F.*, et al. J Biol Chem.* 279: 54304-54311, 2004
59. van de Graaf, S. F., Hoenderop, J. G., and Bindels, R. J. *Am J Physiol Renal Physiol.* 290: F1295-1302, 2006
60. Hoenderop, J. G., van Leeuwen, J. P., van der Eerden, B. C.*, et al. J Clin Invest.* 112: 1906-1914, 2003
61. Peng, J. B., Chen, X. Z., Berger, U. V.*, et al. J Biol Chem.* 274: 22739-22746, 1999
62. Bianco, S. D., Peng, J. B., Takanaga, H.*, et al. J Bone Miner Res.* 22: 274-285, 2007
63. Duncan, L. M., Deeds, J., Hunter, J.*, et al. Cancer Res.* 58: 1515-1520, 1998
64. Perraud, A. L., Fleig, A., Dunn, C. A.*, et al. Nature.* 411: 595-599, 2001
65. Fonfria, E., Marshall, I. C., Benham, C. D.*, et al. Br J Pharmacol.* 143: 186-192, 2004
66. Kolisek, M., Beck, A., Fleig, A., and Penner, R. *Mol Cell.* 18: 61-69, 2005
67. Sano, Y., Inamura, K., Miyake, A.*, et al. Science.* 293: 1327-1330, 2001
68. Grimm, C., Kraft, R., Sauerbruch, S., Schultz, G., and Harteneck, C. *J Biol Chem.* 278: 21493-21501, 2003
69. Grimm, C., Kraft, R., Schultz, G., and Harteneck, C. *Mol Pharmacol.* 67: 798-805, 2005
70. Oberwinkler, J., Lis, A., Giehl, K. M., Flockerzi, V., and Philipp, S. E. *J Biol Chem.* 280: 22540-22548, 2005
71. Launay, P., Fleig, A., Perraud, A. L., Scharenberg, A. M., Penner, R., and Kinet, J. P. *Cell.* 109: 397-407, 2002
72. Nilius, B., Prenen, J., Janssens, A., Voets, T., and Droogmans, G. *J Physiol.* 560: 753-765, 2004
73. Nilius, B., Prenen, J., Tang, J.*, et al. J Biol Chem.* 280: 6423-6433, 2005
74. Vennekens, R., Olausson, J., Meissner, M.*, et al. Nat Immunol.* 8: 312-320, 2007
75. Hofmann, T., Chubanov, V., Gudermann, T., and Montell, C. *Curr Biol.* 13: 1153-1158, 2003
76. Ullrich, N. D., Voets, T., Prenen, J.*, et al. Cell Calcium.* 37: 267-278, 2005
77. Zhang, Y., Hoon, M. A., Chandrashekar, J.*, et al. Cell.* 112: 293-301, 2003
78. Damak, S., Rong, M., Yasumatsu, K.*, et al. Chem Senses.* 31: 253-264, 2006
79. Walder, R. Y., Landau, D., Meyer, P.*, et al. Nat Genet.* 31: 171-174, 2002

80. Schlingmann, K. P., Weber, S., Peters, M.*, et al. Nat Genet.* 31: 166-170, 2002
81. Voets, T., Nilius, B., Hoefs, S.*, et al. J Biol Chem.* 279: 19-25, 2004
82. Chubanov, V., Waldegger, S., Schnitzler, M. M. y.*, et al. PNAS.* 101: 2894-2899, 2004
83. Li, M., Du, J., Jiang, J.*, et al. J Biol Chem.* 2007
84. Li, M., Jiang, J., and Yue, L. *J Gen Physiol.* 127: 525-537, 2006
85. Nadler, M. J., Hermosura, M. C., Inabe, K.*, et al. Nature.* 411: 590-595, 2001
86. Runnels, L. W., Yue, L., and Clapham, D. E. *Science.* 291: 1043-1047, 2001
87. Kozak, J. A., Matsushita, M., Nairn, A. C., and Cahalan, M. D. *J Gen Physiol.* 126: 499-514, 2005
88. Hermosura, M. C., Nayakanti, H., Dorovkov, M. V.*, et al. Proc Natl Acad Sci U S A.* 102: 11510-11515, 2005
89. Monteilh-Zoller, M. K., Hermosura, M. C., Nadler, M. J., Scharenberg, A. M., Penner, R., and Fleig, A. *J Gen Physiol.* 121: 49-60, 2003
90. Runnels, L. W., Yue, L., and Clapham, D. E. *Nat Cell Biol.* 4: 329-336, 2002
91. Aarts, M., Iihara, K., Wei, W. L.*, et al. Cell.* 115: 863-877, 2003
92. Tsavaler, L., Shapero, M. H., Morkowski, S., and Laus, R. *Cancer Res.* 61: 3760-3769, 2001
93. McKemy, D. D., Neuhausser, W. M., and Julius, D. *Nature.* 416: 52-58, 2002
94. Voets, T., Droogmans, G., Wissenbach, U., Janssens, A., Flockerzi, V., and Nilius, B. *Nature.* 430: 748-754, 2004
95. Story, G. M., Peier, A. M., Reeve, A. J.*, et al. Cell.* 112: 819-829, 2003
96. Jordt, S. E., Bautista, D. M., Chuang, H. H.*, et al. Nature.* 427: 260-265, 2004
97. Bandell, M., Story, G. M., Hwang, S. W.*, et al. Neuron.* 41: 849-857, 2004
98. Kwan, K. Y., Allchorne, A. J., Vollrath, M. A.*, et al. Neuron.* 50: 277-289, 2006
99. Hanaoka, K., Qian, F., Boletta, A.*, et al. Nature.* 408: 990-994, 2000
100. Kim, K., Drummond, I., Ibraghimov-Beskrovnaya, O., Klinger, K., and Arnaout, M. A. *Proc Natl Acad Sci U S A.* 97: 1731-1736, 2000
101. Nauli, S. M., Alenghat, F. J., Luo, Y.*, et al. Nat Genet.* 33: 129-137, 2003
102. Wu, G., D'Agati, V., Cai, Y.*, et al. Cell.* 93: 177-188, 1998
103. Koulen, P., Cai, Y., Geng, L.*, et al. Nat Cell Biol.* 4: 191-197, 2002
104. Nomura, H., Turco, A. E., Pei, Y.*, et al. J Biol Chem.* 273: 25967-25973, 1998
105. Wu, G. *Curr Opin Nephrol Hypertens.* 10: 23-31, 2001
106. Chen, X. Z., Vassilev, P. M., Basora, N.*, et al. Nature.* 401: 383-386, 1999
107. Bach, G. *Pflugers Arch.* 451: 313-317, 2005
108. Song, Y., Dayalu, R., Matthews, S. A., and Scharenberg, A. M. *Euro J Cell Biol.* 85: 1253-1264, 2006
109. Atiba-Davies, M., and Noben-Trauth, K. *Biochim Biophys Acta.* In Press: 2007
110. Kim, H.-J., Li, Q., Tjon-Kon-Sang, S., So, I., Kiselyov, K., and Muallem, S. *J Biol Chem.* C700190200, 2007
111. Walker, R. G., Willingham, A. T., and Zuker, C. S. *Science.* 287: 2229-2234, 2000
112. Liu, D., and Liman, E. R. *Proc Natl Acad Sci U S A.* 100: 15160-15165, 2003
113. Sidi, S., Friedrich, R. W., and Nicolson, T. *Science.* 301: 96-99, 2003
114. Clapham, D. E. *Nature.* 426: 517-524, 2003
115. Pedersen, S. F., Owsianik, G., and Nilius, B. *Cell Calcium.* 38: 233-252, 2005
116. Philipp, S., Cavalie, A., Freichel, M.*, et al. Embo J.* 15: 6166-6171, 1996
117. Hofmann, T., Obukhov, A. G., Schaefer, M., Harteneck, C., Gudermann, T., and Schultz, G. *Nature.* 397: 259-263, 1999
118. Ma, H.-T., Patterson, R. L., Van Rossum, D. B., Birnbaumer, L., Mikoshiba, K., and Gill, D. L. *Science.* 287: 1647-1651, 2000
119. Ma, H.-T., Venkatachalam, K., Parys, J. B., and Gill, D. L. *J. Biol. Chem.* 277: 6915-6922, 2002
120. Venkatachalam, K., van Rossum, D. B., Patterson, R. L., Ma, H. T., and Gill, D. L. *Nat Cell Biol.* 4: E263-E272, 2002
121. Montell, C., Birnbaumer, L., and Flockerzi, V. *Cell.* 108: 595-598, 2002
122. Montell, C. *Sci. STKE.* 2005: re3-, 2005

123. Hofmann, T., Schaefer, M., Schultz, G., and Gudermann, T. *Proc Natl Acad Sci U S A.* 99: 7461-7466, 2002
124. Goel, M., Sinkins, W. G., and Schilling, W. P. *J. Biol. Chem.* 277: 48303-48310, 2002
125. Colbert, H. A., Smith, T. L., and Bargmann, C. I. *J. Neurosci.* 17: 8259-8269, 1997
126. Kim, J., Chung, Y. D., Park, D.-y.*, et al. Nature.* 424: 81-84, 2003
127. Boels, K., Glassmeier, G., Herrmann, D.*, et al. J Cell Sci.* 114: 3599-3606, 2001
128. Iwata, Y., Katanosaka, Y., Arai, Y., Komamura, K., Miyatake, K., and Shigekawa, M. *J. Cell Biol.* 161: 957-967, 2003
129. Kanzaki, M., Zhang, Y. Q., Mashima, H., Li, L., Shibata, H., and Kojima, I. *Nat Cell Biol.* 1: 165-170, 1999
130. Ryu, S., Liu, B., and Qin, F. *J Gen Physiol.* 122: 45-61, 2003
131. Chuang, H. H., Prescott, E. D., Kong, H.*, et al. Nature.* 411: 957-962, 2001
132. Nathan, J. D., Peng, R. Y., Wang, Y., McVey, D. C., Vigna, S. R., and Liddle, R. A. *Am J Physiol Gastrointest Liver Physiol.* 283: G938-946, 2002
133. Hwang, S. W., and Oh, U. *Curr Opin Pharmacol.* 2: 235-242, 2002
134. Jordt, S. E., and Julius, D. *Cell.* 108: 421-430, 2002
135. Peier, A. M., Reeve, A. J., Andersson, D. A.*, et al. Science.* 296: 2046-2049, 2002
136. Guler, A. D., Lee, H., Iida, T., Shimizu, I., Tominaga, M., and Caterina, M. *J Neurosci.* 22: 6408-6414, 2002
137. Liedtke, W., Choe, Y., Marti-Renom, M. A.*, et al. Cell.* 103: 525-535, 2000
138. Gao, X., Wu, L., and O'Neil, R. G. *J Biol Chem.* 278: 27129-27137, 2003
139. Vennekens, R., Prenen, J., Hoenderop, J. G., Bindels, R. J., Droogmans, G., and Nilius, B. *J Physiol.* 530: 183-191, 2001
140. Nilius, B., Vennekens, R., Prenen, J., Hoenderop, J. G., Bindels, R. J., and Droogmans, G. *J Physiol.* 527 Pt 2: 239-248, 2000
141. Vennekens, R., Hoenderop, J. G., Prenen, J.*, et al. J Biol Chem.* 275: 3963-3969, 2000
142. Nilius, B., Prenen, J., Hoenderop, J. G. J.*, et al. J. Biol. Chem.* 277: 30852-30858, 2002
143. Nilius, B., Prenen, J., Vennekens, R., Hoenderop, J. G., Bindels, R. J., and Droogmans, G. *Br J Pharmacol.* 134: 453-462, 2001
144. Doyle, D. A., Cabral, J., atilde*, et al. Science.* 280: 69-77, 1998
145. Voets, T., Prenen, J., Vriens, J.*, et al. J. Biol. Chem.* 277: 33704-33710, 2002
146. Nilius, B., Vennekens, R., Prenen, J., Hoenderop, J. G., Droogmans, G., and Bindels, R. J. *J Biol Chem.* 276: 1020-1025, 2001
147. Voets, T., Janssens, A., Prenen, J., Droogmans, G., and Nilius, B. *J Gen Physiol.* 121: 245-260, 2003
148. Voets, T., Prenen, J., Fleig, A.*, et al. J Biol Chem.* 276: 47767-47770, 2001
149. Dodier, Y., Banderali, U., Klein, H.*, et al. J Biol Chem.* 279: 6853-6862, 2004
150. Voets, T., Janssens, A., Droogmans, G., and Nilius, B. *J Biol Chem.* 279: 15223-15230, 2004
151. Kraft, R., Grimm, C., Grosse, K.*, et al. Am J Physiol Cell Physiol.* 286: C129-137, 2004
152. Togashi, K., Hara, Y., Tominaga, T.*, et al. Embo J.* 25: 1804-1815, 2006
153. Nilius, B., Prenen, J., Droogmans, G.*, et al. J. Biol. Chem.* 278: 30813-30820, 2003
154. Talavera, K., Yasumatsu, K., Voets, T.*, et al. Nature.* 438: 1022-1025, 2005
155. Prakriya, M., and Lewis, R. S. *J Gen Physiol.* 119: 487-507, 2002
156. Kozak, J. A., and Cahalan, M. D. *Biophys J.* 84: 922-927, 2003
157. Demeuse, P., Penner, R., and Fleig, A. *J Gen Physiol.* 127: 421-434, 2006
158. Matsushita, M., Kozak, J. A., Shimizu, Y.*, et al. J Biol Chem.* 280: 20793-20803, 2005
159. Schmitz, C., Perraud, A. L., Johnson, C. O.*, et al. Cell.* 114: 191-200, 2003
160. Clark, K., Langeslag, M., van Leeuwen, B.*, et al. Embo J.* 25: 290-301, 2006
161. Corey, D. P., Garcia-Anoveros, J., Holt, J. R.*, et al. Nature.* 432: 723-730, 2004
162. Nagata, K., Duggan, A., Kumar, G., and Garcia-Anoveros, J. *J. Neurosci.* 25: 4052-4061, 2005
163. LaPlante, J. M., Falardeau, J., Sun, M.*, et al. Febs Letters.* 532: 183-187, 2002
164. LaPlante, J. M., Ye, C. P., Quinn, S. J.*, et al. Biochem Biophys Res Commun.* 322: 1384-1391, 2004

165. Kiselyov, K., Chen, J., Rbaibi, Y.*, et al. J. Biol. Chem.* 280: 43218-43223, 2005
166. Soyombo, A. A., Tjon-Kon-Sang, S., Rbaibi, Y.*, et al. J. Biol. Chem.* 281: 7294-7301, 2006
167. Xu, H., Delling, M., Li, L., Dong, X., and Clapham, D. E. *Proc Natl Acad Sci U S A.* 104: 18321-18326, 2007
168. Di Palma, F., Belyantseva, I. A., Kim, H. J., Vogt, T. F., Kachar, B., and Noben-Trauth, K. *Proc Natl Acad Sci U S A.* 99: 14994-14999, 2002
169. Hoenderop, J. G., Willems, P. H., and Bindels, R. J. *Am J Physiol Renal Physiol.* 278: F352-360, 2000
170. Friedman, P. A., and Gesek, F. A. *Physiol Rev.* 75: 429-471, 1995
171. Friedman, P. A., Coutermarsh, B. A., Kennedy, S. M., and Gesek, F. A. *Endocrinology.* 137: 13-20, 1996
172. Bushinsky, D. A., and Monk, R. D. *Lancet.* 352: 306-311, 1998
173. Brown, A. J., Dusso, A., and Slatopolsky, E. *Am J Physiol.* 277: F157-175, 1999
174. Brown, E. M., and MacLeod, R. J. *Physiol Rev.* 81: 239-297, 2001
175. Bronner, F., Pansu, D., and Stein, W. D. *Am J Physiol.* 250: G561-569, 1986
176. Bronner, F., Pansu, D., and Stein, W. D. *Adv Exp Med Biol.* 208: 227-234, 1986
177. Loffing, J., Loffing-Cueni, D., Valderrabano, V.*, et al. Am J Physiol Renal Physiol.* 281: F1021-1027, 2001
178. van Abel, M., Hoenderop, J. G., van der Kemp, A. W., Friedlaender, M. M., van Leeuwen, J. P., and Bindels, R. J. *Kidney Int.* 68: 1708-1721, 2005
179. Hoenderop, J. G., Muller, D., Van Der Kemp, A. W.*, et al. J Am Soc Nephrol.* 12: 1342-1349, 2001
180. Weber, K., Erben, R. G., Rump, A., and Adamski, J. *Biochem Biophys Res Commun.* 289: 1287-1294, 2001
181. van de Graaf, S. F., Hoenderop, J. G., van der Kemp, A. W., Gisler, S. M., and Bindels, R. J. *Pflugers Arch.* 452: 407-417, 2006
182. van de Graaf, S. F., Chang, Q., Mensenkamp, A. R., Hoenderop, J. G., and Bindels, R. J. *Mol Cell Biol.* 26: 303-312, 2006
183. Jiang, Y., Ferguson, W. B., and Peng, J. B. *Am J Physiol Renal Physiol.* 292: F545-554, 2007
184. van de Graaf, S. F., van der Kemp, A. W., van den Berg, D., van Oorschot, M., Hoenderop, J. G., and Bindels, R. J. *J Am Soc Nephrol.* 17: 26-30, 2006
185. Lambers, T. T., Mahieu, F., Oancea, E.*, et al. Embo J.* 25: 2978-2988, 2006
186. Gkika, D., Mahieu, F., Nilius, B., Hoenderop, J. G., and Bindels, R. J. *J Biol Chem.* 279: 26351-26357, 2004
187. Lambers, T. T., Weidema, A. F., Nilius, B., Hoenderop, J. G., and Bindels, R. J. *J Biol Chem.* 279: 28855-28861, 2004
188. Derler, I., Hofbauer, M., Kahr, H.*, et al. J Physiol.* 577: 31-44, 2006
189. Flatman, P. W. *Annu Rev Physiol.* 53: 259-271, 1991
190. Dai, L. J., Ritchie, G., Kerstan, D., Kang, H. S., Cole, D. E., and Quamme, G. A. *Physiol Rev.* 81: 51-84, 2001
191. Romani, A. *Arch Biochem Biophys.* 458: 90-102, 2007
192. Quamme, G. A. *Kidney Int.* 52: 1180-1195, 1997
193. de Rouffignac, C., and Quamme, G. *Physiol Rev.* 74: 305-322, 1994
194. Meij, I. C., Koenderink, J. B., van Bokhoven, H.*, et al. Nat Genet.* 26: 265-266, 2000
195. Meij, I. C., Koenderink, J. B., De Jong, J. C.*, et al. Ann N Y Acad Sci.* 986: 437-443, 2003
196. Groenestege, W. M., Hoenderop, J. G., van den Heuvel, L., Knoers, N., and Bindels, R. J. *J Am Soc Nephrol.* 17: 1035-1043, 2006

# Chapter 2

## Tissue kallikrein stimulates $Ca^{2+}$ reabsorption via PKC dependent plasma membrane accumulation of TRPV5

Dimitra Gkika[1*], Catalin N. Topala[1*], Qing Chang[1], Nicolas Picard[2], Stéphanie Thébault[1], Pascal Houillier[2], Joost G. Hoenderop[1] and René J. Bindels[1]

[1]Department of Physiology, Nijmegen Centre for Molecular Life Sciences, Radboud University Nijmegen Medical Centre, The Netherlands, [2]INSERM, Unité 652 Institut Fédératif de Recherche 58 and René Descartes University Paris, France

* Contributed equally to this work

*Embo J.* 25: 4707-4716, 2006

**ABSTRACT**

The Transient Receptor Potential Vanilloid 5 (TRPV5) channel determines urinary $Ca^{2+}$ excretion and is therefore critical for $Ca^{2+}$ homeostasis. Interestingly, mice lacking the serine protease tissue kallikrein (TK) exhibit robust hypercalciuria comparable to the $Ca^{2+}$ leak in TRPV5 knockout mice. Here, we delineated the molecular mechanism through which TK stimulates $Ca^{2+}$ reabsorption. Using TRPV5-expressing primary cultures of renal $Ca^{2+}$-transporting epithelial cells, we showed that TK activates $Ca^{2+}$ reabsorption. The stimulatory effect of TK was mimicked by bradykinin (BK) and could be reversed by application of JE049, a BK receptor type 2 antagonist. A cell permeable analog of DAG increased TRPV5 activity within 30 minutes via protein kinase C activation of the channel since mutation of TRPV5 at the putative PKC phosphorylation sites S299 and S654 prevented the stimulatory effect of TK. Cell surface labeling revealed that TK enhances the amount of TRPV5 channels at the plasma membrane by delaying its retrieval. In conclusion, TK stimulates $Ca^{2+}$ reabsorption via the BK-activated PLC/DAG/PKC pathway and the subsequent stabilization of the TRPV5 channel at the plasma membrane.

## INTRODUCTION

The overall $Ca^{2+}$ balance is regulated by a homeostatic mechanism tightly controlling the concerted actions of intestinal $Ca^{2+}$ absorption, exchange of $Ca^{2+}$ from bone and renal $Ca^{2+}$ reabsorption. In kidney, $Ca^{2+}$ can cross the epithelial cells and reach the blood compartment via two pathways: passive (paracellular) and active (transcellular) $Ca^{2+}$ reabsorption. Active $Ca^{2+}$ reabsorption takes place in the distal convoluted (DCT) and the connecting (CNT) tubules (1). Although it accounts only for ~15% of total renal $Ca^{2+}$ reabsorption, it is generally considered the site for fine-tuning of urinary $Ca^{2+}$ excretion. Furthermore, active $Ca^{2+}$ reabsorption is the primary target for regulation by calciotropic hormones, including 1,25-dihydroxyvitamin $D_3$ and parathyroid hormone (PTH), enabling the organism to regulate $Ca^{2+}$ reabsorption to the body's demand.

The Transient Receptor Potential Vanilloid 5 (TRPV5) channel is expressed along the apical membrane of DCT and CNT and represents the rate-limiting step in renal transcellular $Ca^{2+}$ reabsorption (1). Inactivation of TRPV5 in mice ($TRPV5^{-/-}$) abolishes active $Ca^{2+}$ reabsorption in kidney resulting in severe hypercalciuria (2). To compensate this renal $Ca^{2+}$ leak, $TRPV5^{-/-}$ mice exhibit intestinal $Ca^{2+}$ hyperabsorption. In addition, the bone structure of these mice was significantly disturbed as illustrated by a reduced trabecular and cortical bone thickness (2). Hence, these data demonstrate the key function of TRPV5 in active $Ca^{2+}$ reabsorption and its essential role in the body $Ca^{2+}$ homeostasis.

Interestingly, hypercalciuria was recently observed in tissue kallikrein-deficient ($TK^{-/-}$) mice (3). TK is a serine protease produced in CNT (4), where it co-localizes with TRPV5 (2). Proteolytic enzymes such as TK are synthesized as inactive precursors or zymogens, to prevent protein degradation and to enable spatial and temporal regulation of enzymatic activity. The precursor of TK is converted to the mature active form before entering the luminal tubular compartment. Trypsin, plasma kallikrein, plasmin and thermolysin can cleave *in vitro* the TK precursor, but the endogenous activator is still unknown (5). Once activated, TK is excreted and can process low molecular weight kininogen to release kinin which acts through kinin receptors such as the bradykinin (BK) 2 receptor (B2R) (6). Remarkably, recent studies show that TK can directly activate the B2R independently of BK release (7). However, the molecular events that link TK to $Ca^{2+}$ balance are at present unknown.

The aim of this study was, therefore, to elucidate the molecular mechanism of hypercalciuria observed in $TK^{-/-}$ mice. To this end, the relation between TK expression and hypercalciuria was investigated *in vivo* using $TK^{-/-}$ and $TRPV5^{-/-}$ mice. Subsequently, the effect of TK on transcellular $Ca^{2+}$ transport was examined in primary cultures of renal CNT/CCD cells. Finally, the signaling pathway through which TK acts on $Ca^{2+}$ reabsorption and its effect on TRPV5 surface expression was delineated in TRPV5-expressing cells.

## EXPERIMENTAL PROCEDURES

*Animal experiments*

$TK^{-/-}$ mice were produced as previously described (3,8) and fed *ad libitum* two $Na^+$ diets containing 0.3% (w/w) or 3% (w/w) for 14 days. Subsequently, 24 hour urine was collected from $TK^{-/-}$ mice and from their wild-type littermates ($TK^{+/+}$) housed in metabolic cages and blood was obtained by orbital puncture. Measurements of biological parameters in the animals plasma and urine were performed as previously described (3). Urinary $Na^+$, $Ca^{2+}$ and $Mg^{2+}$ excretion was expressed as ratios to urinary creatinine excretion to take into account the variations in urine collection. $TRPV5^{-/-}$ mice were generated as described previously (2). At the age of 4 weeks, mice were fed *ad libitum* two diets containing 0.02% (w/w) or 2% (w/w) $Ca^{2+}$ for 5 weeks and were subsequently placed in metabolic cages. 24 hour urine samples were collected and subjected to TCA precipitation. The animal ethics board of the Radboud University Nijmegen approved all animal experimental procedures.

*Urine protein precipitation by TCA*

10% of the 24 hours urine volume collected of $TRPV5^{-/-}$ mice was centrifuged at 200 *g* for 10 minutes at 4°C to remove cell debris. Proteins in the urine were precipitated using ice-cold TCA (Acros organics, New Jersey, USA). The TCA mixture was centrifuged at 13,000 *g* for 10 minutes at 4°C, and the pellet was subsequently washed with 300 µl acetone. Next, the pellet was air-dried for approximately 3 minutes, dissolved in Laemmli buffer containing 0.1 M DTT and 150 mM Tris (pH 8.8) and analyzed by immunoblot analysis for the expression of TK using a rabbit anti-TK antibody (Calbiochem, San Diego, CA, USA). Immunopositive bands were scanned using an imaging densitometer to determine pixel density (Molecular Analyst Software, BioRad Laboratories, Hercules, CA).

*DNA constructs and cell culture*

The TRPV5 pCINeo/IRES-GFP constructs were generated as described previously (9). Single and combined PKC mutants were generated by alanine substitution of the six putative phosphorylation sites of TRPV5 (S144A, S299A, S316A, S654A, S664A, S698A) using *in vitro* mutagenesis (QuickChange Site-Directed Mutagenesis kit, Stratagene, La Jolla, CA, USA). The B2R pcDNA3 was a kind gift from Prof G. Erdös, MD (Department of Pharmacology, University of Illinois, Chicago, USA). HEK293 cells were transfected at 70% of confluency using polyethylenimine (Polysciences, Inc., Warrington, USA) or Lipofectamin 2000 (Invitrogen Life Technologies, Breda, The Netherlands). After 48-60 hours, cells were used for $^{45}Ca^{2+}$ uptake assays, patch-clamp and/or biotinylation experiments. Prior to the assays, cells were incubated for 1 hour in serum-free medium containing the particular compound.

*Transcellular $Ca^{2+}$ transport in renal primary cultures*

CNT/CCD tubules were immunodissected from kidney cortex of New Zeeland White rabbits (~0.5 kg) using antibody R2G9 and then placed in primary culture on permeable filters (0.33 $cm^2$; Costar, Cambridge, MA, USA) as described before (10). At confluence, monolayers were used for the transepithelial $Ca^{2+}$ transport assay as previously described (10). Transepithelial potential difference and resistance were checked before and after transport measurement to confirm the integrity of the monolayer.

*$^{45}Ca^{2+}$ uptake assay*

HEK293 cells were transfected with TRPV5 pCINeo/IRES-GFP or pCINeo/IRES-GFP cDNA. $Ca^{2+}$ uptake was determined in uptake medium (110 mM NaCl, 5 mM KCl, 1.2 mM $MgCl_2$, 0.1 mM $CaCl_2$, 10 mM Na-acetate, 2 mM $NaH_2PO_4$, 20 mM HEPES-Tris, pH 7.4 supplemented with 10 µM felodipine, 10 µM methoxy-verapamil, 1 mM $BaCl_2$ and 1 µCi/ml $^{45}CaCl_2$) for 10 minutes at room temperature (20–25°C). Each well was washed extensively with stop buffer (110 mM NaCl, 5 mM KCl, 1.2 mM $MgCl_2$, 0.5 mM $CaCl_2$, 1.5 mM $LaCl_3$, 10 mM Na-acetate, 20 mM HEPES-Tris, pH 7.4) at 4 °C, incubated with 0.05% (w/v) SDS and the lysates were counted for radioactivity using liquid scintillation.

*Electrophysiology and solutions*

Patch-clamp experiments were performed as described previously (11) in the tight seal whole-cell configuration at room temperature using an EPC-9 patch-clamp amplifier computer controlled by the Pulse software (HEKA Elektronik, Lambrecht, Germany). Two voltage protocols were used: a ramp, to establish the I-V relation in nominally DVF or in 10 mM $Ca^{2+}$-containing extracellular solutions and a hyperpolarizing step protocol to measure the $Ca^{2+}$-dependent inactivation. $Na^+$ current densities were calculated from the current at -80 mV during the ramp protocols, while the and $Ca^{2+}$ currents were calculated from the current at -80 mV during the ramp protocols or from $Ca^{2+}$ peak values were extracted from the current at -100 mV during the step protocol. The analysis and display of patch-clamp data were performed using Igor Pro software (WaveMetrics, Lake Oswego, USA).

*Cell surface labeling with biotin*

HEK293 cells were transfected with 15 µg HA-TRPV5, TRPV5-S299A or TRPV5- S654A pCINeo/IRES-GFP or pCINeo/IRES-GFP in poly-L-lysine (Sigma, St Louis, MO, USA) coated 10 cm dishes. 48 hours after transfection, cells were incubated for 1 hour with 100 nM TK and 1 µM JE049. The biotinylation assay was performed, cells were homogenized in 1 ml lysis buffer as described previously (12) using the NHS-LC-LC-biotin (Pierce, Etten-Leur, The Netherlands). Finally, biotinylated proteins were precipitated using neutravidin-agarose beads (Pierce, Etten-

Leur, The Netherlands). TRPV5 expression was analyzed by immunoblot for the precipitates (plasma membrane fraction) and for the total cell lysates using the guinea pig anti-TRPV5 antibody (13). For the half-life assay, the biotinylation assay was pursued as described above. For time point 0 hours, cells were collected from plates and lysed, immediately after biotinylation. Other plates of cells were further cultured after biotinylation for 1, 3, 6 or 12 hours, then washed once with ice-cold PBS (pH 7.4), and subsequently homogenized in lysis buffer. All samples were processed as described above.

*Compounds*

TK, BK, PMA and OAG were purchased from Sigma (St Louis, MO, USA). U73122 and U73343 were purchased from Upjohn Laboratories (Kalamazoo, MI, USA). JE049, formerly known as icatibant or HOE140, was a kind gift of Dr. J. Pünter (Aventis Pharma Deutschland GmbH, Frankfurt, Germany).

*Statistical analysis*

In all experiments, the data is expressed as mean ± SEM. Overall statistical significance was determined by analysis of variance (ANOVA). In case of significance, differences between the means of two groups were analyzed by unpaired *t*-test, while multiple comparisons between groups were performed by Bonferroni post-hoc tests. $P < 0.05$ were considered significant. The statistical analyses were performed using the SPSS software (SPSS Inc, Chicago, Il, USA).

**RESULTS**

*TK expression levels inversely correlate with urinary $Ca^{2+}$ excretion*

The relation between urinary TK expression and urinary $Ca^{2+}$ excretion was investigated by using wild-type ($TK^{+/+}$) and $TK^{-/-}$ mice fed a 0.3% (w/w) (normal) and 3% (w/w) (high) $Na^+$ diet. Urinary $Ca^{2+}$ excretion was significantly increased in $TK^{+/+}$ mice on high $Na^+$ diet compared to mice on normal diet ($P < 0.05$, n = 12 mice) **(Figure 1A)**.

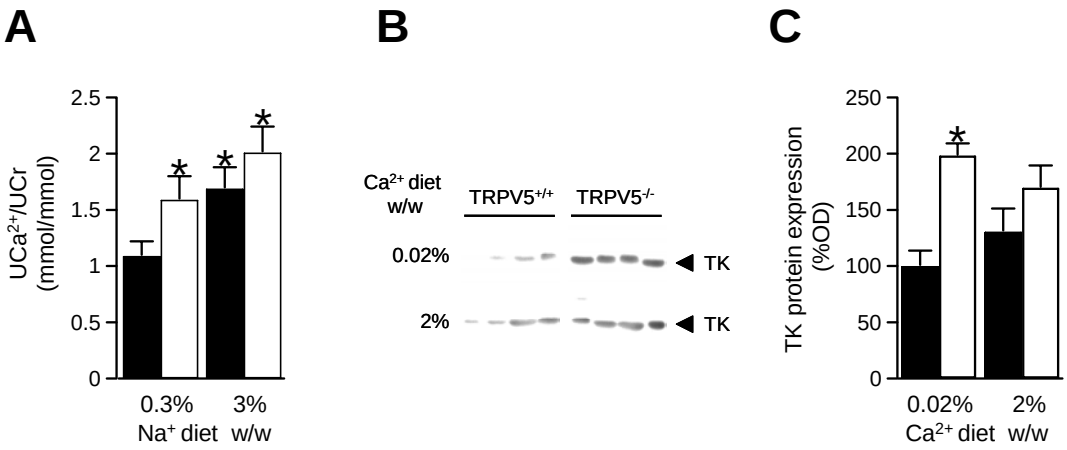


**Figure 1. TK expression in relation to $Ca^{2+}$ excretion. (A)** 24 hour $Ca^{2+}$ excretion normalized for creatinine excretion ($UCa^{2+}$/UCr) in wild-type ($TK^{+/+}$, closed bars) and knockout ($TK^{-/-}$, open bars) mice fed a 0.3% (w/w) or 3% (w/w) $Na^+$ diet. Data are expressed as means ± SEM (n = 12 mice). *$P < 0.05$ versus $TK^{+/+}$ mice on 0.3% (w/w) diet. **(B)** Immunoblotting of urinary TK in wild-type ($TRPV5^{+/+}$) and knockout ($TRPV5^{-/-}$) mice fed a 0.02 % or a 2% (w/w) $Ca^{2+}$ diet. Each lane represents the protein TCA-precipitate of 24 hours urine from one individual mouse. **(C)** The intensity of the immunopositive bands was quantified by densitometry and TK expression was depicted as a percent ratio to $TRPV5^{+/+}$ mice (closed bars) fed with 0.02% (w/w) $Ca^{2+}$ diet. Data are expressed as means ± SEM (n = 4 mice). *$P < 0.05$ versus $TRPV5^{+/+}$ mice on the same diet.

Conversely, $Ca^{2+}$ excretion in $TK^{-/-}$ mice on normal $Na^+$ diet was significantly higher (140 ± 13%) than in $TK^{+/+}$ mice ($P < 0.05$, n = 12 mice), but remained constant on a high $Na^+$ diet ($P > 0.2$, n = 12 mice) **(Figure 1A)**. On the high $Na^+$ diet there was no significant difference in urinary $Ca^{2+}$ excretion between $TK^{+/+}$ and $TK^{-/-}$ mice. Body weight, food intake, urinary creatinine as well as plasma values of $Ca^{2+}$, creatinine and protein concentrations did not differ between mice genotypes on either diet **(Table 1)**.

| | 0.3% (w/w) $Na^+$ | | 3% (w/w) $Na^+$ | |
|---|---|---|---|---|
| | $TK^{+/+}$ | $TK^{-/-}$ | $TK^{+/+}$ | $TK^{-/-}$ |
| Weight (g) | 23.8 ± 1.0 | 24.5 ± 0.8 | 24.6 ± 1.0 | 23.8 ± 0.4 |
| Food intake (g/24 h) | 2.68 ± 0.64 | 2.09 ± 0.5 | 1.91 ± 0.32 | 2.18 ± 0.34 |
| ***Plasma values*** | | | | |
| Total $Ca^{2+}$ (mM) | 2.05 ± 0.06 | 1.96 ± 0.07 | 2.01 ± 0.08 | 2.07 ± 0.08 |
| Creatinine (µM) | 10.5 ± 1.0 | 9.3 ± 0.9 | 9.5 ± 2.1 | 9.0 ± 2.2 |
| Protein (g/L) | 46.3 ± 0.9 | 44.9 ± 0.9 | 49.3 ± 1.0 | 44.8 ± 1.0 |
| ***Urine values*** | | | | |
| Volume (ml/24 h) | 1.47 ± 0.20 | 1.36 ± 0.26 | 3.47 ± 0.89* | 2.18 ± 0.34 |
| Creatinine excretion (µmol/24 h) | 4.94 ± 0.42 | 4.56 ± 0.37 | 4.79 ± 0.39 | 4.71 ± 0.38 |
| $UNa^+/UCr$ (mmol/mmol) | 39.6 ± 2.5 | 33.9 ± 2.4 | 292.5 ± 38.3* | 223.2 ± 23.8* |

**Table 1. Phenotypic characterization of $TK^{+/+}$ and $TK^{-/-}$ mice on 0.3% (w/w) and 3% (w/w) $Na^+$ diets.** *$P$ < 0.05 versus same genotype on 0.3% (w/w) Na diet (n = 12 mice).

*TK is up-regulated in $TRPV5^{-/-}$ mice*

The amount of TK excreted in the urine was determined by trichloroacetic acid (TCA) protein precipitation of 24 hours urine collected from wild-type ($TRPV5^{+/+}$) and $TRPV5^{-/-}$ mice fed either a 0.02% (w/w) (low) or a 2% (w/w) (high) $Ca^{2+}$ diet. Immunoblot analysis of the TCA-precipitate showed the specific TK band migrating at ~40 kDa **(Figure 1B)**. Semi-quantitative densitometry of the TK corresponding protein band demonstrated that urinary TK excretion increased in $TRPV5^{-/-}$ mice compared to $TRPV5^{+/+}$ littermates on low $Ca^{2+}$ diet, whereas the high $Ca^{2+}$ diet did not affect TK excretion between $TRPV5^{-/-}$ and $TRPV5^{+/+}$ genotypes **(Figure 1C)**.

*TK stimulates $Ca^{2+}$ transport in renal primary cell cultures*

The effect of TK on transcellular $Ca^{2+}$ transport was evaluated in primary cultures of renal CNT/CCD cells. Application of 100 nM TK to the apical side of the monolayer significantly stimulated $Ca^{2+}$ transport compared to non-treated monolayers, while no effect was observed when TK was added to the basolateral side only **(Figure 2A)**. Importantly, apical addition of TRPV5 channel blocker ruthenium red (10 µM) completely inhibited baseline $Ca^{2+}$ transport and

abrogated the stimulatory effect of TK on transepithelial $Ca^{2+}$ transport **(Figure 2A)**. TK action was mimicked by apical addition of 100 nM trypsin, which like TK displays serine protease activity, **(Figure 2B)** as well as 1 µM BK **(Figure 2C)**. Interestingly, the stimulatory effect on $Ca^{2+}$ reabsorption of both BK and TK was inhibited by apical application of 1 µM JE049, a B2R antagonist **(Figure 2C)**. Basolateral treatment of trypsin, BK or JE049 did not affect transcellular $Ca^{2+}$ transport across the monolayer (data not shown).

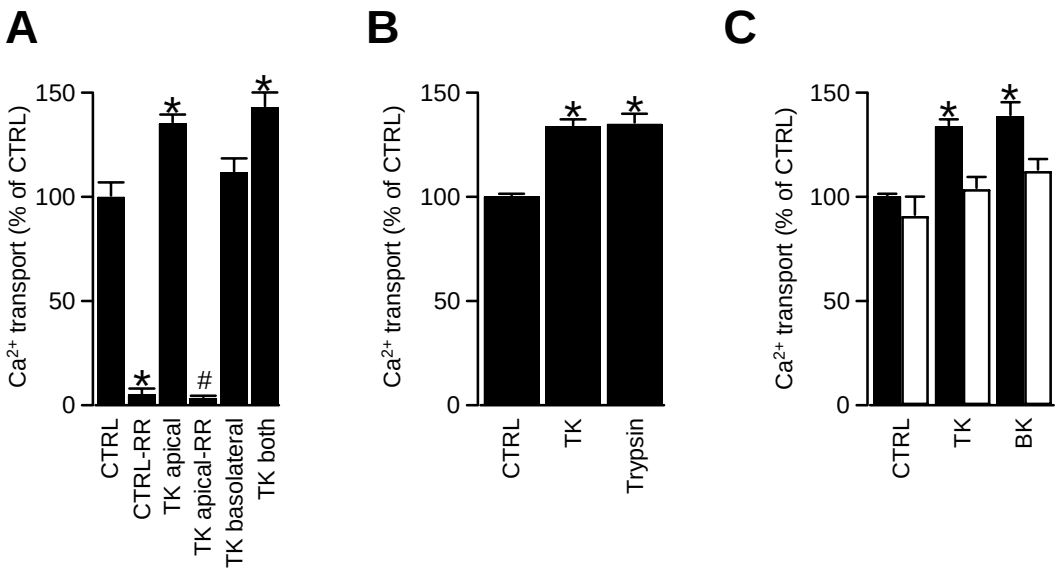


**Figure 2. Stimulatory effect of TK on active $Ca^{2+}$ reabsorption. (A)** Monolayers of rabbit primary cultures of CNT/CCD cells were incubated with 100 nM TK for 90 minutes at the apical, basolateral or both sides. Some monolayers were incubated for 90 minutes in the presence of the TRPV5 blocker ruthenium red (RR, 10 µM, apical side) in the presence or absence of TK (100 nM, apical side). Vehicle-treated cells were used as control (CTRL) and net apical to basolateral $Ca^{2+}$ transport was measured. Data are expressed as means ± SEM. (n = 6 wells). *$P$ < 0.05 versus CTRL, $^{\#}P$ < 0.05 versus TK-treated. **(B)** Primary cells were treated apically with 100 nM trypsin or 100 nM TK. **(C)** 1 µM BK and 100 nM TK were applied at the apical side of the monolayers in the presence (open bars) or absence (closed bars) of 1 µM JE049, a B2R antagonist. In all experiments vehicle-treated cells were used as control (CTRL) and net apical to basolateral $Ca^{2+}$ transport was measured. Data are expressed as means ± SEM (n = 4 wells). *$P$ < 0.05 versus CTRL.

*TK enhances TRPV5 channel activity*

The stimulatory effect of TK on $Ca^{2+}$ transport was further examined in TRPV5-transfected Human Embryonic Kidney (HEK) 293 cells. Incubation of these cells with TK concentrations ranging from 0.05 to 5,000 nM enhanced $^{45}Ca^{2+}$ influx in a dose-dependent manner with a maximal stimulation at 500 nM and an $EC_{50}$ of 6.00 ± 0.04 nM **(Figure 3A)** whereas no effect was observed in mock-transfected cells (data not shown). Further, TK action on TRPV5 channel activity was investigated by the whole-cell patch-clamp technique in TRPV5-expressing HEK293 cells. Pre-incubation with 100 nM TK increased the inward $Ca^{2+}$ current in response to the step protocol, but the $Ca^{2+}$-dependent inactivation of the TRPV5 currents remained unchanged **(Figure 3B)**.

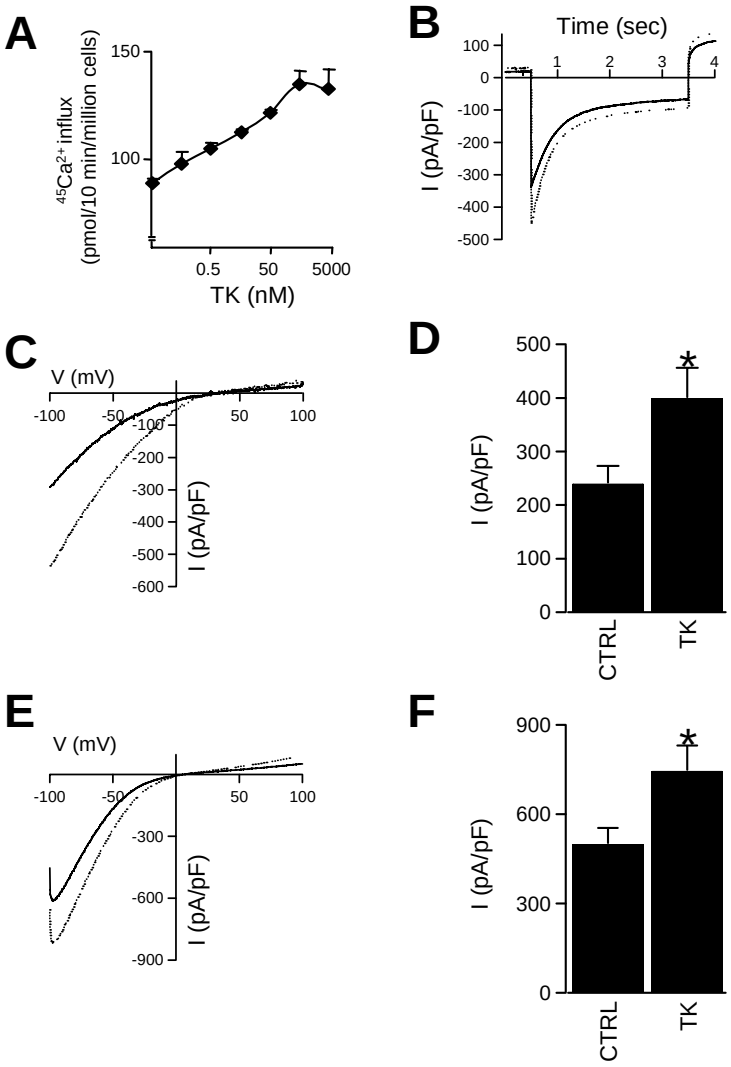


**Figure 3. Effect of TK on TRPV5-transfected HEK293 cells. (A)** HEK293 cells were transfected with TRPV5 and treated for 1 hour with TK in concentrations ranging from 0.05 to 5,000 nM and finally $^{45}Ca^{2+}$ uptake was measured. Values are expressed as means ± SEM (n = 6 wells). **(B)** Averaged $Ca^{2+}$ currents measured with 10 mM $Ca^{2+}$ in the extracellular solution during a 3 seconds step to -100 mV from a holding potential of +70 mV in TRPV5-transfected HEK293 cells treated (dotted trace) or non-treated (solid trace) with 100 nM TK. **(C)** Current-voltage relations measured from 450 milliseconds voltage ramps in 10 mM $Ca^{2+}$-containing extracellular solution from non-treated CTRL (solid trace) or TK treated (dotted trace) TRPV5-expressing HEK293 cells. **(D)** Average density of the $Ca^{2+}$ current measured as in **(C)**, was 400 ± 56 pA/pF (n = 15 cells) for TK treated cells compared to 240 ± 33 pA/pF (n = 15 cells) for CTRL cells. **(E)** Current-voltage relations measured from 450 milliseconds voltage ramps in nominally DVF solution in TRPV5-transfected HEK293 cells treated (dotted trace) or non-treated (solid trace) with TK. **(F)** Average $Na^{+}$ current density at -80 mV in nominally DVF solution were 745 ± 85 pA/pF (n = 15 cells) for TK treated cells compared to 500 ± 55 pA/pF for CTRL cells (n = 15 cells). *$P$ < 0.05 versus CTRL.

The current-voltage (I-V) relation of the currents in response to a voltage ramp did not change after pre-incubation with 100 nM TK **(Figure 3C)**, but the inward $Ca^{2+}$ current at -80 mV increased by 167 ± 14% compared to non-treated, control (CTRL) cells ($P$ < 0.05, n = 15 cells) as depicted in **Figure 3D**.

Likewise, in divalent free (DVF) solution a significant increase of 149 ± 17% in $Na^{+}$ inward currents at -80 mV ($P$ < 0.05, n = 15 cells) was observed, while the I-V relation remained unchanged **(Figure 3E,F)**.

*TK increases TRPV5-mediated currents via the B2R*

Since BK mimicked the TK action on $Ca^{2+}$ transport in primary cultures of CNT/CCD cells, the effect of BK on TRPV5-expressing HEK293 cells was further studied. First, the expression of B2R in HEK293 cells was confirmed by immunoblot analysis. B2R-transfected HEK293 cells were used as a positive control. In both mock and B2R-transfected HEK293 cells, B2R was detected as a single immunopositive band of ~69 kDa **(Figure 4A)**, confirming the presence of endogenous B2R in this cell line. Subsequently, TRPV5-transfected HEK293 cells were incubated for 1 hour with 1 µM BK and functionally characterized by patch-clamp measurements in comparison to non-treated (CTRL) cells. Interestingly, BK treatment resulted in a significant increase of 150 ± 18% in both $Ca^{2+}$ **(Figure 4D)** and $Na^{+}$ **(Figure 4F)** currents ($P < 0.05$, n = 12 cells) compared to CTRL cells, without affecting the $Ca^{2+}$-dependent inactivation **(Figure 4B)** or the I-V relations of the currents **(Figure 4C,E)**. Because the different treatments of TRPV5-expressing HEK293 cells affected both $Ca^{2+}$ and $Na^{+}$ current amplitudes leaving unaffected the other current properties, only the $Ca^{2+}$ currents are now depicted to demonstrate the effect of particular compounds. Incubation of TRPV5-transfected cells with 1 µM JE049 reversed the stimulatory effect of TK on TRPV5-mediated currents. The $Ca^{2+}$-dependent inactivation of $Ca^{2+}$ currents remained unchanged for cells treated with TK or TK and JE049 **(Figure 4G)**. $Ca^{2+}$ current amplitudes measured from the step protocol were significantly lower, 285 ± 50 pA/pF, for the JE049-treated cells ($P < 0.05$, n = 11 cells) compared to TK-treated cells **(Figure 4H)**.

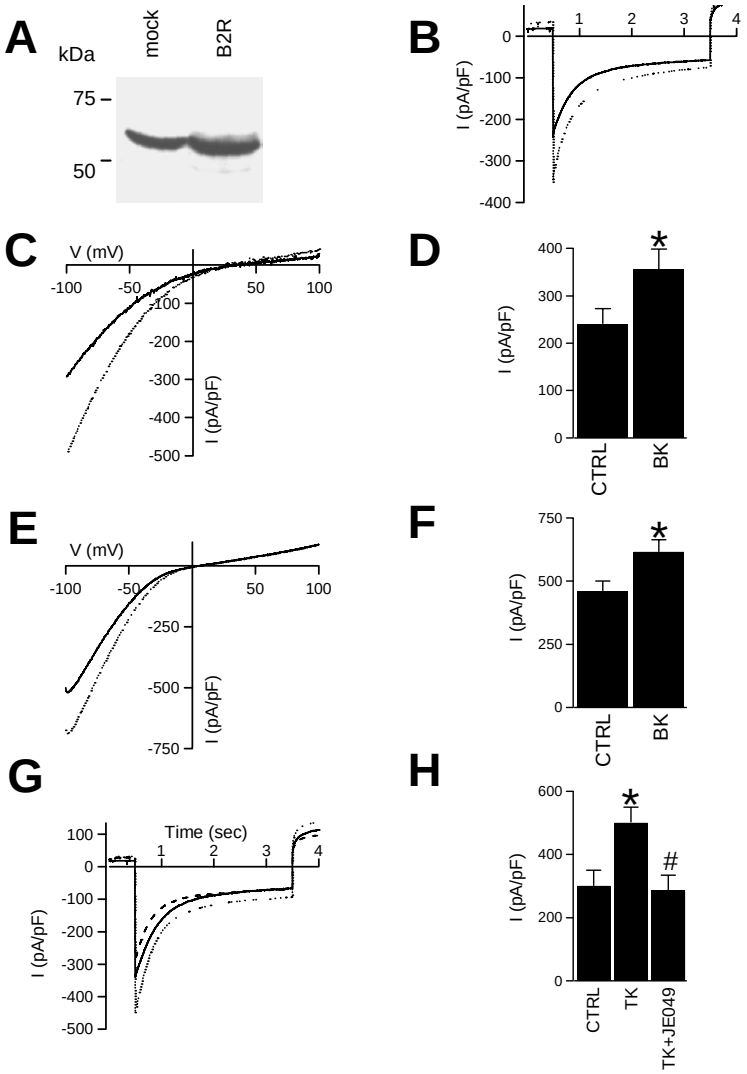


**Figure 4. TK stimulation of TRPV5 activity is mediated by B2R. (A)** B2R transfected and mock cells were lysed and calibrated for equally protein loading on gel. Immunoblot analysis of the samples shows the B2R expression. **(B)** Inward $Ca^{2+}$ currents in TRPV5-transfected HEK293 cells treated (dotted trace) or non-treated (solid trace) with 1 µM BK for 1 hour measured with the step protocol as in **Figure 3B**. **(C)** Current-voltage relations measured from 450 milliseconds voltage ramps in 10 mM $Ca^{2+}$-containing extracellular solution from non-treated CTRL (solid trace) or BK (dotted trace) treated TRPV5-expressing HEK293 cells. **(D)** Amplitude of $Ca^{2+}$ current for BK treated cells was 363 ± 45 pA/pF and for control cells 240 ± 30 pA/pF (n = 12 cells for each condition). **(E)** Current-voltage relations measured from voltage ramps in nominally DVF extracellular solution from non-treated CTRL (solid trace) and BK (dotted trace) treated TRPV5-expressing HEK293 cells. **(F)** Average $Na^{+}$ current for cells treated with BK was 615 ± 49 pA/pF and for CTRL cells 460 ± 46 pA/pF. **(G)** Inward $Ca^{2+}$ currents measured with 10 mM $Ca^{2+}$ in the extracellular solution during the voltage step to -100 mV of control non-treated cells (solid trace), cells treated with TK (dotted trace), and cells treated with both TK and 1 µM of the B2R antagonist JE049 (dashed trace). Inactivation of currents remained unchanged. **(H)** Average peak $Ca^{2+}$ current of cells treated with TK and JE049 was 285 ± 45 pA/pF and for CTRL cells 300 ± 50 pA/pF compared to 500 ± 55 pA/pF measured from TK treated cells. $^{*}P < 0.05$ versus CTRL. $^{\#}P < 0.05$ versus TK treated cells.

*TK stimulates TRPV5-mediated currents via the PLC-dependent PKC pathway*

To elucidate in detail the mechanism through which TK enhances TRPV5 activity, the following strategies were followed. First, pre-treatment with 10 µM of the PLC inhibitor U73122 for 10 minutes abolished the TK stimulatory effect on TRPV5-mediated $Ca^{2+}$ currents, whereas 10 µM of its inactive analogue U73343 had no effect ($P < 0.05$, n = 10 cells) **(Figure 5A)**. Then, TRPV5-transfected cells were incubated for 1 hour with 10 µM 1-oleoyl-acetyl-sn-glycerol (OAG), a synthetic DAG analogue. OAG mimicked the stimulatory effect of TK on TRPV5-

mediated $Ca^{2+}$ currents ($P < 0.05$, n = 10 cells) **(Figure 5B)**. The stimulatory effect of OAG was observed within 30 minutes after addition **(Figure 5C)**. Next, the effect of TK on the sextuple PKC phosphorylation-deficient mutant was tested. In HEK293 cells expressing this mutant, the stimulatory effect of TK was abolished **(Figure 5D)**.

Subsequently, the PKC phosphorylation sites were individually mutated into an alanine residue. TK increased $Ca^{2+}$ currents of all single PKC mutants, except of S299A and S654A ($P < 0.05$, n = 12 cells) **(Figure 5E)**. Furthermore, to determine which PKC isoforms are involved in this process, cells were incubated for 24 hours with 1 µM of phorbol ester (phorbol 12-myristate 13-acetate-PMA) to down-regulate the PMA-sensitive PKC isoforms expressed in HEK293 cells as previously described (14). Then, these PMA-pretreated cells were treated as aforementioned with 100 nM TK for 1 hour. TK was still able to significantly increase (164 ± 14% of control, $P < 0.05$, n = 14 cells) the TRPV5-mediated $Ca^{2+}$ currents **(Figure 5F)**. Vehicle-incubated (NT) cells were used as control for the effect of PMA on TRPV5 currents and PMA incubation left TRPV5-mediated currents unaffected.

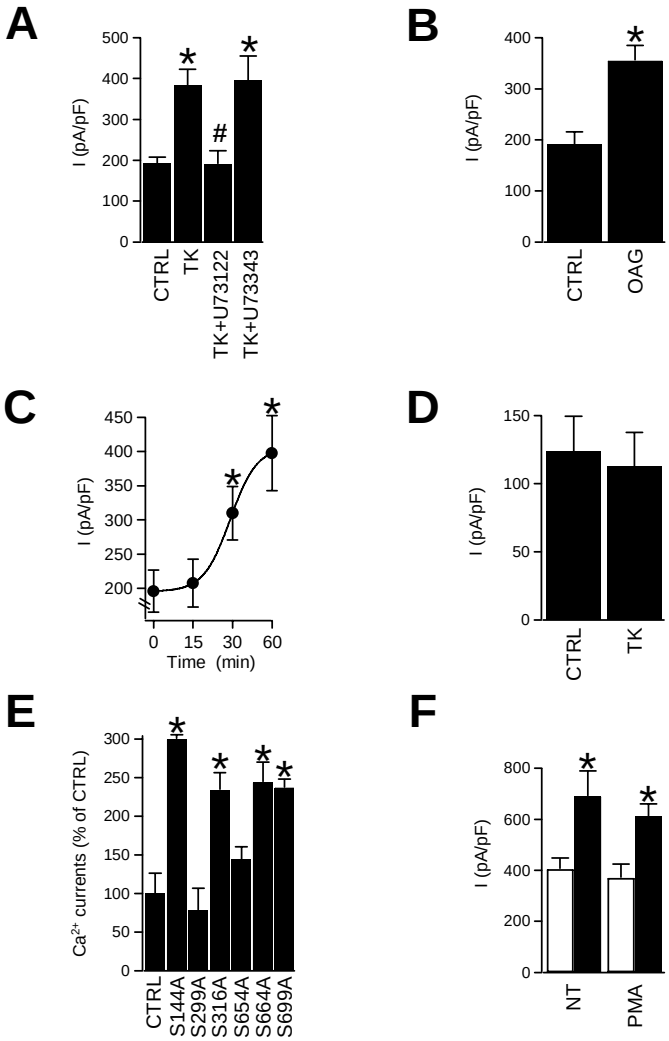


**Figure 5. TK action is mediated by the DAG/PKC-dependent PLC signaling pathway.** TRPV5 expressing cells were incubated for 1 hour with 100 nM TK and subsequently treated as described below. **(A)** 10 minutes incubation with 10 µM of the PLC inhibitor U73122 reverted the average $Ca^{2+}$ currents amplitude of the TK treated cells to values similar to CTRL cells, contrary to its inactive form U73343 which let the TK effect unaltered (n = 10 cells). **(B)** $Ca^{2+}$ current of cells pre-treated for 1 hour with 10 µM OAG $Ca^{2+}$ currents was 355 ± 30 pA/pF and for CTRL cells 191 ± 25 pA/pF. **(C)** Time-course of TRPV5 currents stimulation by OAG. Points represent $Ca^{2+}$ peak current measured at -100 mV using the step protocol from cells pre-treated with 10 µM OAG for 15, 30 and 60 minutes or non-treated cells. **P* < 0.05 versus non-treated cells at 0 min. **(D)** Average $Ca^{2+}$ currents for cells expressing TRPV5 mutated for all its six PKC phosphorylation sites were 123 ± 36 pA/pF and TK treated cells were 113 ± 25 pA/pF (n = 10 cells for each condition). **(E)** Point mutation of the PKC phosphorylation sites S299 and S654 did not affect $Ca^{2+}$ currents in comparison with the other four PKC mutants upon TK treatment. Data are expressed as percentage of $Ca^{2+}$ currents measured of cells expressing PKC-TRPV5 point mutants treated with 100 nM TK normalized to non-treated CTRL cells (n = 12 cells for each mutant). **(F)** 24 hours incubation with 1 µM PMA was used to down-regulate the PMA-sensitive PKC isoforms in TRPV5-transfected cells. In both cases, non-treated (NT), or 24 hours incubation with PMA, TK (black bars) was still able to significantly increase TRPV5-mediated $Ca^{2+}$ currents compared to control cells (white bars) (n = 14 cells for each condition) **P* < 0.05 versus CTRL cells.

Subsequently, the possible involvement of other G-protein coupled receptors in addition to B2R was investigated. To this end, purinergic receptors were activated by the addition of extracellular ATP (1 mM for 1 hour) to TRPV5-expressing HEK293 cells. Indeed, as shown in the **Figure 6**, ATP treatment enhanced the inward $Ca^{2+}$ currents in these cells, while leaving the I-V relation and $Ca^{2+}$-dependent inactivation unchanged. Moreover, after pre-treatment with the

B2R antagonist JE049, ATP was still able to stimulate the TRPV5 currents, indirectly demonstrating the specificity of TK stimulation via the B2R.

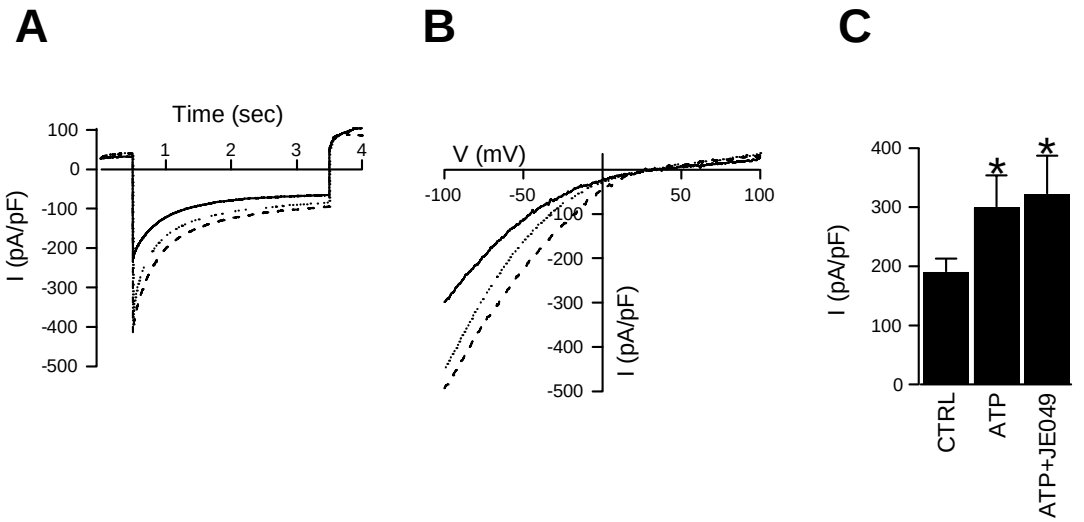


**Figure 6. B2R confers specificity to TK-dependent stimulation of TRPV5 activity. (A)** Averaged $Ca^{2+}$ currents measured with 10 mM $Ca^{2+}$ in the extracellular solution during a 3 seconds step to -100 mV from a holding potential of +70 mV in TRPV5-transfected HEK293 cells treated with 1 mM ATP (dotted trace), treated with 1 mM ATP and 1 µM of the B2R antagonist JE049 (dashed line) or non-treated CTRL (solid trace). **(B)** Current-voltage relationships measured from 450 milliseconds voltage ramps in 10 mM $Ca^{2+}$-containing solution in TRPV5-transfected HEK293 cells treated with ATP (dotted trace), treated with ATP and JE049 (dashed trace) or non-treated (solid trace) with ATP. **(C)** Average density of the $Ca^{2+}$ peak current measured as in **(B)**, was 300 ± 54 pA/pF for ATP treated cells and 322 ± 65 pA/pF for ATP and JE049, compared to 190 ± 23 pA/pF (n = 15 cells) for CTRL cells. **P* < 0.05 versus CTRL.

*TK increases cell surface expression of TRPV5 by delaying channel retrieval*

The effect of TK on the amount of TRPV5 channel expressed at the plasma membrane was investigated in HEK293 cells. TRPV5-transfected cells were incubated with 100 nM TK alone or in combination with 1 µM JE049 for 1 hour and then subjected to cell surface biotinylation. Biotinylated cell lysates were precipitated with neutravidin-agarose beads and immunoblotted for TRPV5. Mock-transfected and non-biotin-treated cells were used as negative controls. TK treatment enhanced TRPV5 expression in the biotinylated fraction, whereas JE049 abolished this effect **(Figure 7A, left panel)**. Importantly, TRPV5 was equally expressed in total cell lysates of all tested conditions **(Figure 7A, right panel)**. The observed increase in cell surface expression of TRPV5 by TK could be due to either an enhanced trafficking from the Golgi apparatus to the cell surface or a reduction in channel retrieval from the plasma membrane. The kinetics of cell-surface retrieval was measured in HEK293 cells using half-life cell-surface biotinylation. After a 2 hours TK treatment, the retrieval of TRPV5 channel from the plasma membrane was decreased by 71, 46, and 17% ($P < 0.05$, n = 3 blots) at the time points of 1, 3 and 6 hours, respectively **(Figure 7B)**. TRPV5 expression in total cell lysates was identical in all tested conditions **(Figure 7C)**. These results suggested that TK increases cell surface expression of TRPV5 by delaying channel retrieval from the plasma membrane.

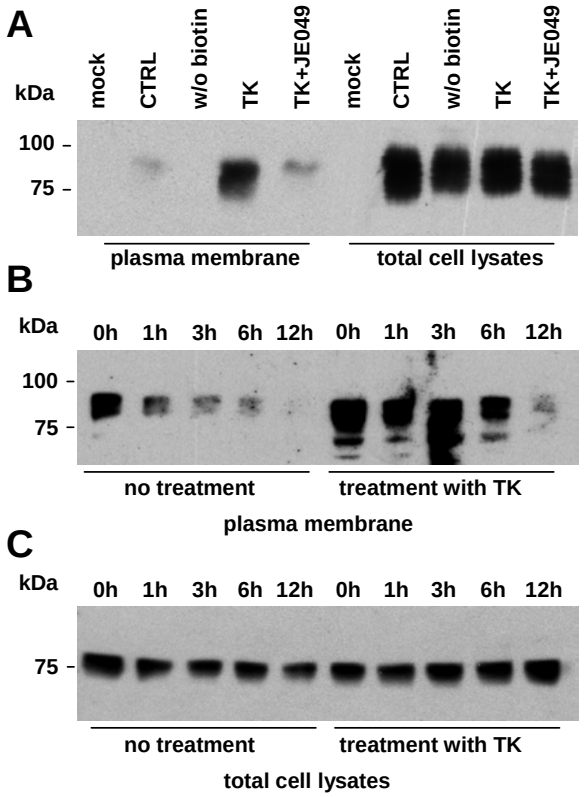


**Figure 7. TK affects the plasma membrane expression of TRPV5. (A)** TRPV5-transfected HEK293 cells were treated with 100 nM TK with or without 1 µM JE049. Cells were subjected to cell surface biotinylation and after lysis precipitated with neutravidin-agarose beads. TRPV5 expression was analyzed by immunoblot for the plasma membrane fraction (left panel) and for the total cell lysates (right panel). As negative controls, mock cells were used and biotin was omitted in the procedure. **(B)** and **(C)** TK treated or non-treated TRPV5-transfected cells were subjected to biotinylation. Cells were immediately homogenized (time point 0), or further cultured for 1, 3, 6, 12 hours. Subsequently, the cells were lysed, following immunoprecipitation with neutravidin-agarose beads and TRPV5 expression of plasma membrane **(B)** and total lysates **(C)** was visualized by immunoblot analysis.

*TRPV5 PKC mutants S299A and S654A are insensitive to TK treatment*

The effect of TK on the TRPV5 PKC mutants S299A and S654A was investigated in HEK293 cells by half-life analysis. $TRPV5^{+/+}$, S299A and S654A transfected cells were incubated with or without 100 nM TK for 1 hour and then the kinetics of cell-surface retrieval was measured in HEK293 cells using half-life cell-surface biotinylation. Without an hour TK treatment **(Figure 8A)**, the plasma membrane expression of $TRPV5^{+/+}$, S299A and S654A was decreased at the similar extent at the time points of 1, 3, 6 and 12 hours. Interestingly, with an hour TK treatment **(Figure 8B)**, the retrieval of TRPV5 channel from the plasma membrane was decreased, but S299A and S654A were not. $TRPV5^{+/+}$, S299A and S654A expression in total cell lysates was identical in all tested conditions. These results suggested that the TK effect of delaying channel retrieval from the plasma membrane is abolished in TRPV5 PKC mutants S299A and S654A.

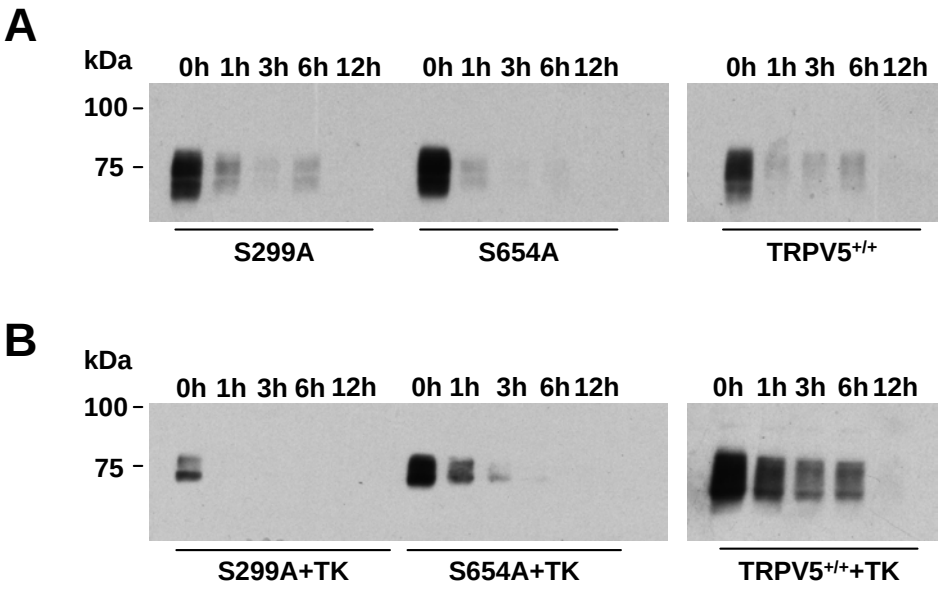


**Figure 8. TK does not affect the plasma membrane expression of TRPV5 PKC mutants S299A and S654A.** TRPV5$^{+/+}$, S299A and S654A-transfected HEK293 cells were treated for 1 hour without **(A)** or with **(B)** 100 nM TK. Subsequently, cells were subjected to cell-surface biotinylation and then homogenized at 0, 1, 3, 6, 12 hours after biotinylation. Subsequently, Cells were immediately homogenized (time point 0), or further cultured for 1, 3, 6, 12 hours. Subsequently, the cells were lysed, following immunoprecipitation with neutravidin-agarose beads and TRPV5 expression of plasma membrane was visualized by immunoblot analysis. The expression of TRPV5 in the cell lysates was similar in the various conditions (data not shown).

**DISCUSSION**

The present study showed that extracellular TK stimulates TRPV5-mediated $Ca^{2+}$ reabsorption by activating the B2R and subsequently the DAG/PKC pathway resulting in the stabilization of TRPV5 channels at the cell surface. This conclusion is based on the following experimental observations: (i) Urinary $Ca^{2+}$ excretion in mice is inversely related to the expression of TK; (ii) TK stimulates $Ca^{2+}$ reabsorption in primary cultures of renal CNT/CCD cells, which can be blocked by the B2R antagonist JE049; (iii) the stimulatory effect of TK is mediated by the PLC/DAG-pathway and requires the two conserved PKC sites S299 and S654 in TRPV5; (iv) TK enhances $Ca^{2+}$ transport by increasing TRPV5 abundance at the plasma membrane.

TK stimulated TRPV5-mediated $Ca^{2+}$ transport via the B2R receptor. The physiological relevance of this latter finding is substantiated by the co-localization of B2R with TK (15) and TRPV5 (2) in DCT and CNT. B2R belongs to the seven-transmembrane domain G protein-coupled receptor superfamily (16) and signals via $G\alpha_q$ protein with consequent activation of PLC. PLC catalyzes the hydrolysis of phosphatidylinositol-4,5-biphosphate ($PIP_2$) in inositol trisphosphate ($IP_3$) and DAG (17). Commonly, $IP_3$ releases $Ca^{2+}$ from the endoplasmic reticulum stores, while DAG activates PKC (17). Certainly, our results show that TRPV5 activation requires $PIP_2$ breakdown following B2R stimulation and relies on DAG as a down-stream effector. Subsequently, DAG increases TRPV5 activity via PKC phosphorylation of the channel since potential PKC phosphorylation deficient mutants of TRPV5 at positions S299 and S654 lack the TK effect. This is the first study demonstrating that TRPV5 is activated through its PKC phosphorylation sites. Among the six predicted phosphorylation sites in the TRPV5 sequence, two serines, S299 and S654 are critical for TRPV5 activation by TK. Importantly, TRPV5 closest homologue, TRPV6, did not respond to TK (data not shown). Since the second serine (S654) is not conserved in TRPV6, both serines are apparently critical for stimulation of TRPV5 by TK. In addition, 24 hours pre-incubation with PMA down-regulates α, β, and ε isoforms of PKC, but not PKC ζ (18). This latter PKC isoform is presumably involved in TK increase of TRPV5 currents since the stimulatory effect of PKC was similar in PMA-pretreated and control cells. Interestingly, stimulation of active $Ca^{2+}$ transport in primary cultures of renal CNT/CCD also involves PMA-insensitive PKC isotypes (19) among which the isotype PKC ζ can be activated by B2R (20). However, B2R knockout mice ($B2R^{-/-}$) mice showed no change in urine $Ca^{2+}$ excretion (3), in contrast with $TK^{-/-}$ mice, suggesting that compensation mechanisms could mask the TK effect on $Ca^{2+}$ balance in these knockout mice. For instance, it has been shown that in these knockout mice a compensatory induction of the B1 receptor occurs which could theoretically be a new target for TK. Alternatively, TK exerts its *in vivo* effect via a mechanism independent of B2R.

Previous studies showed that different signaling molecules of the PLC pathway activate TRP channels. For example, the three canonical TRP members TRPC3, 6 and 7 are characterized

by their sensitivity to DAG (21). Alternatively, the vanilloid and melastatine members of TRP family, TRPV1 (22), TRPV5 (23), TRPM4 (24), TRPM5 (25), TRPM7 (26) and TRPM8 (27) can be directly regulated by $PIP_2$. Thus, *in vivo* TRPV5 activation by $PIP_2$ (23) or DAG/PKC could adjust TRPV5 activity in response to physiological fluctuations. In addition, $Ca^{2+}$ entering the cell through TRPV5 could prevent the electrostatic interaction between the negatively charged $PIP_2$ and the channel by screening the negative charge on the lipid head group, as proposed for $Mg^{2+}$ and TRPM7 (28).

Stimulation of $Ca^{2+}$ transport through TRPV5 upon TK action could be the result of an increase in either open probability of the channel or in expression of TRPV5 at the plasma membrane. Surface biotinylation analysis showed that TK increases the amount of TRPV5 channels at the plasma membrane. Thus, PKC activation of TRPV5 following the TK application would regulate the balance between constitutive exocytosis and endocytosis in favor of the former leading to the accumulation of TRPV5 at the cell surface. Similarly, the epidermal growth factor prevents the internalization of plasma membrane TRPC3 (29). The role of the cytoskeleton in this translocation process is at present unknown. It is possible that PKC-dependent phosphorylation of TRPV5 leads to activation of motor proteins that transport the channels towards the plasma membrane. This process could involve the FKBP52 protein, characterized previously as a TRPV5 regulatory protein (30), since FKBP52 is known to interact with the motor protein dynein (31,32). Interestingly, TRPM7 associates to the actomyosin cytoskeleton upon BK stimulation regulating cell adhesion (33). Interestingly, the protein synaptotagmin has been proposed to regulate the exocytosis of TRPC5, in part because of their co-localization (34). However, the cytoskeletal elements and the motor proteins participating in the incorporation of TRPV5 in the plasma membrane remain to be determined. Furthermore, accumulation of channels at the cell surface can also occur by increased incorporation into the plasma membrane. Indeed, PKC potentiation of TRPV1 promotes the recruitment of a channel vesicular pool to the cell surface (35). This exocytosis process of TRPV1 is dependent on the soluble N-ethylmaleimide-sensitive-factor attachment proteins receptor (SNARE) (35), known to act as membrane recognition molecules and acceptors for vesicle trafficking, docking and fusion (36). It would be interesting to investigate the role of similar scaffold proteins in the assembly of TRPV5 and PKC upon TK treatment, considering that such signaling pathways are currently indicated to function in spatially distinct microdomains (37). For instance, the A-kinase-anchoring protein, AKAP, has been described to coordinate the subcellular localization of second messenger-regulated enzymes, such as PKC in order to modulate the activity of $K^+$ channel, KCNQ/M, upon agonist stimulation via Gq-coupled pathway (38).

The aforementioned data are in support of plasma membrane recycling of TRPV5 protein as mechanism of channel regulation. A tight control of TRPV5 activity is of primordial importance for body $Ca^{2+}$ homeostasis, since TRPV5 constitutes the fine-tuned $Ca^{2+}$ entry step in active

$Ca^{2+}$ reabsorption (1). Besides the hormonal regulation of TRPV5, accessory proteins play a role in modulating channel trafficking and activity (9,39). Together with a recent report on the β-glucuronidase klotho (12), our study introduces a new mechanism of TRPV5 regulation which is based on extracellular enzymatic activation. TK and klotho co-localize with TRPV5 in the distal part of the nephron where they activate the channel from the luminal side. A comparable enzymatic regulation is described for the epithelial $Na^+$ channel, ENaC, present in CNT, by the channel activating proteases, CAP-1, CAP-2 and CAP-3 (40). Unlike the protease CAP and the β-glucuronidase klotho, TK stimulates TRPV5 indirectly via activation of B2R that then induces a redistribution of TRPV5 channels towards the plasma membrane. On the contrary, CAPs which are membrane-bound serine proteases, act directly on the channel gating by enhancing the open probability of ENaC (41) to stimulate epithelial $Na^+$ absorption. Likewise, klotho directly activates TRPV5 by enzymatic modification of the N-glycan to stabilize TRPV5 channels in the plasma membrane (12).

Interestingly, we showed that an increase in $Na^+$ supply induced a $Ca^{2+}$ wasting in wild-type mice. It is well know that a high $Na^+$ diet increases the plasma volume that triggers the renin-angiotensin-aldosterone system (42). These hormones will act as a negative feedback response lower the reabsorption of $Na^+$ and consequently $Ca^{2+}$ in the proximal tubules. Ultimately, this will increase the urinary excretion of $Ca^{2+}$. The anticipated calciuria was not observed in $TK^{-/-}$ mice, possibly these mice cannot further increase their urinary $Ca^{2+}$ excretion. In addition, the rates of urinary $Ca^{2+}$ excretion in wild-type and TK-null mice were similar on a high $Na^+$ diet, whereas they markedly differed on a normal $Na^+$ diet. This strongly supports the fact that TK participates in the renal response to a high $Na^+$ diet and to the attendant decrease in urinary $Ca^{2+}$ reabsorption.

Here, we demonstrated that TK displays autocrine or paracrine stimulation of active $Ca^{2+}$ reabsorption in a dose-dependent manner. As shown in the mice models, reduction in TK expression increases urinary $Ca^{2+}$ excretion as reflecting of impaired tubular $Ca^{2+}$ reabsorption. Conversely, genetic ablation of TRPV5 doubled the renal expression of TK possibly to counterbalance the $Ca^{2+}$ wasting observed in the $TRPV5^{-/-}$ mice by maximally stimulating the process of $Ca^{2+}$ reabsorption. Indeed, an increase in dietary $Ca^{2+}$ intake as an alternative maneuver to offset the renal $Ca^{2+}$ loss in $TRPV5^{-/-}$ mice prevented the compensatory increase in TK expression. These results underline the role of TK during $Ca^{2+}$ restriction. It is, therefore, interesting to study the $Ca^{2+}$ excretion in humans with a genetically reduced TK activity. In this respect, a loss-of-function polymorphism of the TK gene in which the active-site arginine at position 53 is changed into a histidine (R53H), reduces by 50-60% TK activity is interesting (43). Partial genetic deficiency in TK activity of the R53H subjects is associated with a form of arterial dysfunction (44). TK is well known as a vasodilator factor of renal cortical blood vessels through BK production, while abnormalities of TK levels has long been documented in the pathogenesis

of hypertension (45). It is therefore tempting to speculate that TK stimulation of TRPV5-mediated $Ca^{2+}$ reabsorption plays a role in TK hypotensive action, since urinary $Ca^{2+}$ leak has been correlated with higher baseline systolic and diastolic blood pressures (46).

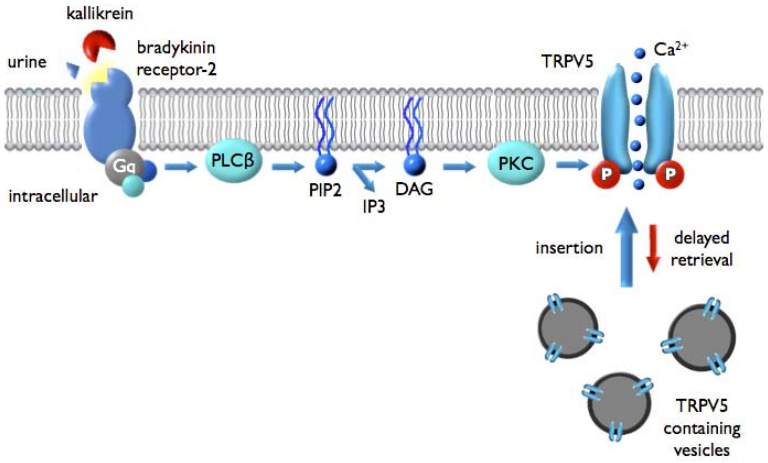


**Figure 9. Schematic diagram of TK stimulatory effect on TRPV5.** TK activates the B2R and subsequently PLC, leading to the hydrolysis of PIP2 in IP3 and DAG. DAG induces subsequently the phosphorylation of TRPV5 through PKC-dependent mechanism with consequent stabilization of TRPV5 channel in the plasma membrane. The increased number of channels at the plasma membrane is the result of delayed channel retrieval ensuing enhanced $Ca^{2+}$ transport through TRPV5.

In conclusion, our data demonstrated that TK reduces urinary $Ca^{2+}$ excretion by an autocrine and paracrine stimulation of TRPV5-mediated $Ca^{2+}$ reabsorption explaining the hypercalciuria in $TK^{-/-}$ mice. **Figure 9** illustrates the molecular pathway linking TK to stimulation of TRPV5, as elucidated in the present study. TK activates B2R and through the PLC derived-messenger DAG initiates the phosphorylation of the TRPV5 PKC sites S299 and S654. Subsequently, $Ca^{2+}$ influx through TRPV5 is enhanced by the accumulation and stabilization of the channel at the plasma membrane. Thus, TK-directed translocation of TRPV5 channels constitutes a mechanism by which renal cells can fine-tune $Ca^{2+}$ reabsorption.


## ACKNOWLEDGMENTS

We thank Mrs. A. van der Kemp, Mr. D. van den Berg and Mr. R. Janssen for expert technical assistance. This work was supported by the Dutch Organization of Scientific Research (Zon-Mw 016.006.001, Zon-Mw 902.18.298, NWO-ALW 810.38.004, NWO-ALW 805.09.042), Dutch Kidney Foundation (C03.6017), the European Molecular Biology Organization (long-term fellowship ALTF 727-2005) and the Human Frontiers Science Program (RGP0032/2004).

## REFERENCES


1. Hoenderop, J. G., Nilius, B., and Bindels, R. J. *Physiol Rev.* 85: 373-422, 2005
2. Hoenderop, J. G., van Leeuwen, J. P., van der Eerden, B. C.*, et al. J Clin Invest.* 112: 1906-1914, 2003
3. Picard, N., Van Abel, M., Campone, C.*, et al. J Am Soc Nephrol.* 16: 3602-3610, 2005
4. Figueroa, C. D., MacIver, A. G., Mackenzie, J. C., and Bhoola, K. D. *Histochemistry.* 89: 437-442, 1988
5. Margolius, H. S. *Hypertension.* 26: 221-229, 1995
6. Bhoola, K. D., Figueroa, C. D., and Worthy, K. *Pharmacol Rev.* 44: 1-80, 1992
7. Hecquet, C., Tan, F., Marcic, B. M., and Erdos, E. G. *Mol Pharmacol.* 58: 828-836, 2000
8. Meneton, P., Bloch-Faure, M., Hagege, A. A.*, et al. Proc Natl Acad Sci U S A.* 98: 2634-2639, 2001
9. van de Graaf, S. F., Hoenderop, J. G., Gkika, D.*, et al. Embo J.* 22: 1478-1487, 2003
10. Bindels, R. J., Hartog, A., Timmermans, J., and Van Os, C. H. *Am J Physiol.* 261: F799-807, 1991
11. Vennekens, R., Hoenderop, J. G., Prenen, J.*, et al. J Biol Chem.* 275: 3963-3969, 2000
12. Chang, Q., Hoefs, S., van der Kemp, A. W., Topala, C. N., Bindels, R. J., and Hoenderop, J. G. *Science.* 310: 490-493, 2005
13. Hoenderop, J. G., Hartog, A., Stuiver, M., Doucet, A., Willems, P. H., and Bindels, R. J. *J Am Soc Nephrol.* 11: 1171-1178, 2000
14. Camden, J. M., Schrader, A. M., Camden, R. E.*, et al. J. Biol. Chem.* 280: 18696-18702, 2005
15. Figueroa, C. D., Gonzalez, C. B., Grigoriev, S.*, et al. J Histochem Cytochem.* 43: 137-148, 1995
16. Hess, J. F., Borkowski, J. A., Young, G. S., Strader, C. D., and Ransom, R. W. *Biochem Biophys Res Commun.* 184: 260-268, 1992
17. Blaukat, A. *Andrologia.* 35: 17-23, 2003
18. Frecker, H., Munk, S., Wang, H., and Whiteside, C. *Am J Physiol Renal Physiol.* 289: F1078-1087, 2005
19. Hoenderop, J. G., De Pont, J. J., Bindels, R. J., and Willems, P. H. *Kidney Int.* 55: 225-233, 1999
20. Christopher, J., Velarde, V., Zhang, D., Mayfield, D., Mayfield, R. K., and Jaffa, A. A. *Am J Physiol Heart Circ Physiol.* 280: H1537-1546, 2001
21. Hofmann, T., Obukhov, A. G., Schaefer, M., Harteneck, C., Gudermann, T., and Schultz, G. *Nature.* 397: 259-263, 1999
22. Chuang, H. H., Prescott, E. D., Kong, H.*, et al. Nature.* 411: 957-962, 2001
23. Lee, J., Cha, S. K., Sun, T. J., and Huang, C. L. *J Gen Physiol.* 126: 439-451, 2005
24. Nilius, B., Mahieu, F., Prenen, J.*, et al. Embo J.* 25: 467-478, 2006
25. Liu, D., and Liman, E. R. *Proc Natl Acad Sci U S A.* 100: 15160-15165, 2003
26. Runnels, L. W., Yue, L., and Clapham, D. E. *Nat Cell Biol.* 4: 329-336, 2002
27. Liu, B., and Qin, F. *J Neurosci.* 25: 1674-1681, 2005
28. Kozak, J. A., and Cahalan, M. D. *Biophys J.* 84: 922-927, 2003
29. Smyth, J. T., Lemonnier, L., Vazquez, G., Bird, G. S., and Putney, J. W., Jr. *J Biol Chem.* 281: 11712-11720, 2006
30. Gkika, D., Topala, C. N., Hoenderop, J. G., and Bindels, R. J. *Am J Physiol Renal Physiol.* 290: F1253-1259, 2006
31. Czar, M. J., Lyons, R. H., Welsh, M. J., Renoir, J. M., and Pratt, W. B. *Mol Endocrinol.* 9: 1549-1560, 1995
32. Silverstein, A. M., Galigniana, M. D., Kanelakis, K. C., Radanyi, C., Renoir, J. M., and Pratt, W. B. *J Biol Chem.* 274: 36980-36986, 1999
33. Clark, K., Langeslag, M., van Leeuwen, B.*, et al. Embo J.* 25: 290-301, 2006
34. Strubing, C., Krapivinsky, G., Krapivinsky, L., and Clapham, D. E. *Neuron.* 29: 645-655, 2001

35. Morenilla-Palao, C., Planells-Cases, R., Garcia-Sanz, N., and Ferrer-Montiel, A. *J Biol Chem.* 279: 25665-25672, 2004
36. Duman, J. G., and Forte, J. G. *Am J Physiol Cell Physiol.* 285: C237-249, 2003
37. Ambudkar, I. S. *Trends Pharmacol Sci.* 27: 25-32, 2006
38. Hoshi, N., Langeberg, L. K., and Scott, J. D. *Nat Cell Biol.* 7: 1066-1073, 2005
39. Gkika, D., Mahieu, F., Nilius, B., Hoenderop, J. G., and Bindels, R. J. *J Biol Chem.* 279: 26351-26357, 2004
40. Rossier, B. C. *Proc Am Thorac Soc.* 1: 4-9, 2004
41. Vuagniaux, G., Vallet, V., Jaeger, N. F., Hummler, E., and Rossier, B. C. *J Gen Physiol.* 120: 191-201, 2002
42. Nijenhuis, T., Vallon, V., van der Kemp, A. W., Loffing, J., Hoenderop, J. G., and Bindels, R. J. *J Clin Invest.* 115: 1651-1658, 2005
43. Slim, R., Torremocha, F., Moreau, T.*, et al. J Am Soc Nephrol.* 13: 968-976, 2002
44. Azizi, M., Boutouyrie, P., Bissery, A.*, et al. J Clin Invest.* 115: 780-787, 2005
45. Chao, J., and Chao, L. *Exp Physiol.* 90: 291-298, 2005
46. McCarron, D. A., and Reusser, M. E. *J Am Coll Nutr.* 18: 398S-405S, 1999

# ***Chapter 3***

## The $Ca^{2+}$-sensing receptor stimulates TRPV5 activity

Catalin N. Topala[1], Joost P. Schoeber[1], Daniela Riccardi[2],
Joost G. Hoenderop[1] and René J. Bindels[1]

[1]Department of Physiology, Nijmegen Centre for Molecular Life Sciences, Radboud University Nijmegen Medical Centre, The Netherlands, [2]Cardiff School of Biosciences, University of Cardiff, United Kingdom

Manuscript in preparation

**ABSTRACT**

The role of the $Ca^{2+}$-sensing receptor (CaSR) in the parathyroid glands has been thoroughly studied in recent years and its central function in $Ca^{2+}$ homeostasis is now well established. Moreover, the CaSR is expressed in kidney, where it modulates divalent mineral excretion and urinary concentrating ability particularly in the proximal nephron segments. However, in distal convoluted tubules (DCT) and connecting tubules (CNT) of the kidney, the role of CaSR is not yet understood. Here, the $Ca^{2+}$-selective Transient Receptor Potential Vanilloid subtype 5 channel (TRPV5) is a key player in renal active $Ca^{2+}$ reabsorption, forming the apical entry gate in the $Ca^{2+}$-transporting cells. Using patch-clamp measurements, determinations of the relative intracellular $Ca^{2+}$ concentrations and cell surface biotinylation, we demonstrated that CaSR activation leads to elevated TRPV5-mediated currents when co-expressed in Human Embryonic Kidney (HEK293) cells. CaSR stimulation by neomycin (200 µM) initiated a down-stream signaling cascade that activated phorbol 12-myristate 13-acetate (PMA)-insensitive protein kinase C (PKC) isoforms which in turn increased the TRPV5 channel activity. Detailed analysis of TRPV5 amino acid sequence revealed the existence of six putative PKC phosphorylation sites. Only inactivation of the putative PKC phosphorylation sites at positions S299 and S654 in TRPV5 prevented the effect of CaSR activation, proving that these two amino acid residues are essential for the observed effect. Preliminary results from cell surface biotinylation assays suggested that CaSR activation increases the plasma membrane localization of TRPV5 channels. Interestingly, the activity of the TRPV5 closest homologue, TRPV6, was not affected upon CaSR activation. In conclusion, activation of the CaSR stimulated TRPV5-mediated $Ca^{2+}$ transport via the PMA-insensitive PKC isoforms pathway possibly due to a subsequent increase in cell surface availability of the TRPV5 protein.

## INTRODUCTION

The cloning of an extracellular $Ca^{2+}$-sensing receptor (CaSR) from parathyroid (1), kidney (2) and other cell types (3-5) has clarified the mechanisms through which $Ca^{2+}$ exerts its direct actions on various cells and tissues. In the parathyroid glands, the CaSR mediates the inhibitory effect of elevated blood ionized $Ca^{2+}$ concentrations on parathyroid hormone (PTH) secretion. As a G protein-coupled receptor (GPCR), CaSR determines intracellular signaling cascades, which result in low-frequency oscillations in cytosolic $Ca^{2+}$ concentration. Oscillations in cytosolic $Ca^{2+}$ concentration determine reductions in the secretion of PTH. In addition to its primary effect of reducing PTH secretion, CaSR activation could influence the expression of the PTH gene (6) and parathyroid cell proliferation (7). CaSR expressed in the parathyroid glands plays a central role in overall body $Ca^{2+}$ homeostasis, directly controlling the blood release of PTH, body's main calciotropic hormone.

Beside its main expression site in the chief cells of the parathyroid glands, the CaSR is also expressed in the kidney. Here, the CaSR protein expression is prominently observed in proximal tubules, thick ascending limbs (TAL) of the Henle's loop, and cortical collecting tubules (8). Notably, the membrane domain at which the CaSR is detected differs between different segments of the nephron. In proximal tubules, the CaSR is expressed in apical brush-border membranes. In contrast, in TAL the CaSR is found on the basolateral site (8,9). In cortical and inner medullar collecting ducts the CaSR is localized on the apical plasma membrane (8,10,11). Together with the expression pattern, the function of CaSR in the respective nephron segments was thoroughly investigated. In TAL, where it is expressed at the basolateral membrane, CaSR inhibits $Ca^{2+}$ reabsorption that is driven by the lumen-positive, transepithelial potential gradient. This electrical gradient is generated by the apical $Na^+$-$K^+$-$2Cl^-$ co-transporter (NKCC2) combined with the recycling of $K^+$ into the tubular lumen *via* the renal outer medulla $K^+$ channel (ROMK1). CaSR activation reduces NKCC2 activity by lowering the cAMP levels (12) and inhibits ROMK1 by stimulating the production of arachidonic acid (13,14). Although the role of the CaSR in TAL was clearly demonstrated, the functional importance of the apical localization of CaSR in distal convoluted tubules (DCT) and connecting tubules (CNT), where active $Ca^{2+}$ reabsorption takes place (15), remains elusive. DCT and CNT (15) account for ~15% of total renal $Ca^{2+}$ reabsorption and are generally considered the fine-tuning sites of urinary $Ca^{2+}$ excretion. Here, the Transient Receptor Potential Vanilloid subtype 5 (TRPV5) channel is the gatekeeper for active $Ca^{2+}$ reabsorption (16,17). TRPV5 proteins form tetrameric channel complexes (18), remarkable selective for $Ca^{2+}$ ($P_{Ca}/P_{Na}$ ~100) (19). TRPV5-mediated currents exhibit an inward-rectifying signature of their current-voltage (I-V) relations (19).

Until now, the physiological relevance of the co-localization of TRPV5 with CaSR in DCT and CNT is unclear. The aim of the present study was, therefore, to investigate the functional link between the CaSR and TRPV5 in the kidney. To this end, the putative role of the CaSR in

regulating TRPV5 function was assessed using a combined approach including intracellular $Ca^{2+}$ measurements, patch-clamp measurements and TRPV5 cell surface protein labeling.

## EXPERIMENTAL PROCEDURES

*DNA constructs and cell culture*

The rabbit TRPV5pCINeo/IRES-GFP and mouse TRPV6pCINeo/IRES-GFP vectors were generated as described previously (20,21). Single and combined protein kinase C (PKC) TRPV5 mutants were generated by alanine substitution of the six putative phosphorylation sites (S144A, S299A, S316A, S654A, S664A, S698A) using *in vitro* mutagenesis (Quick-Change Site-Directed Mutagenesis kit, Stratagene, La Jolla, CA, USA). The amino-terminally GFP-tagged human CaSR in the pcDNA3.1 vector was generated as described previously (22). Human embryonic kidney (HEK293) cells were grown in DMEM (BioWhittaker, Walkersville, MD, USA) containing 10% (v/v) fetal calf serum, 2 mM L-glutamine, and 10 µg/ml Ciproxin at 37°C in a humidity-controlled incubator with 5% (v/v) $CO_2$. Cells were transiently transfected at 70% of confluence using polyethylenimine (Polysciences, Inc., Warrington, PA, USA) and Lipofectamin 2000 (Invitrogen Life Technologies, Breda, The Netherlands) according to manufacturer's protocols (23). After 24-48 hours, cells were used for patch-clamp and/or biotinylation experiments. Prior to the assays, cells were incubated for 1 hour in serum-free DMEM containing neomycin, or L-phenylalanine (L-Phe) (Sigma, St Louis, MO, USA). To down-regulate the phorbol 12-myristate 13-acetate (PMA)-sensitive PKC isoforms (24) cells were incubated overnight with PMA.

*Fura-2 measurements*

Intracellular $Ca^{2+}$ concentration measurements were performed as described previously (25,26). Shortly, HEK293 cells co-transfected with CaSR and TRPV5 or empty vector were loaded for 20 minutes with 3 µM Fura-2 AM (Invitrogen, Leiden, The Netherlands) in the presence of 100 nM pluronic (Invitrogen, Leiden, The Netherlands) and 500 µM probenecid (Sigma, St Louis, MO, USA) in DMEM and incubated at 37°C before starting the measurements. Since the phenol red in DMEM interferes with the Fura-2 measurements, the experiments were performed in HEPES/Tris buffer (in mM: 132.6 NaCl, 5.8 glucose, 10 HEPES, 4.2 KCl, and 1 $MgCl_2$, 1.2 $CaCl_2$ pH = 7.4 with TRIS) supplemented with 500 µM probenecid. At the specified time-points, neomycin was added from a stock solution to reach a concentration of 200 µM in the recording chamber. The Fura-2 dye was excited alternatively 340 at 380 nm using a monochromator (Polychrome IV; TILL Photonics, Gräfelfing, Germany). Fluorescence emission light was directed by a 560DRLP dichroic mirror (Omega Optical, Brattleboro, VT, USA) through a 565ALP emission filter (Omega) on a CoolSNAP HQ monochrome charge coupled device (CCD) camera (Roper Scientific, Vianen, The Netherlands). All hardware was controlled by Metafluor 6.0 software (Universal Imaging, Downingtown, PA, USA).

*Electrophysiology and solutions*

Patch-clamp experiments were performed as described previously (19) in the tight seal whole-cell configuration at room temperature using an EPC-9 patch-clamp amplifier computer controlled by the Pulse software (HEKA Elektronik, Lambrecht, Germany). Two voltage protocols were used: a ramp from -100 to +100 mV with a holding potential of +20 mV, to establish the current-voltage (I-V) relation in nominally DVF or in 10 mM $Ca^{2+}$-containing extracellular solutions, and a hyperpolarizing step protocol to -100 mV to measure the $Ca^{2+}$-dependent inactivation. $Na^{+}$ current densities were calculated from the current at -80 mV during the ramp protocols while the $Ca^{2+}$ currents values were extracted from the peak current at –100 mV during the step protocol. The analysis and display of patch-clamp data were performed using Igor Pro software (WaveMetrics, Lake Oswego, OR, USA).

*Cell surface labeling with biotin*

HEK293 cells seeded on poly-L-lysine (Sigma, St Louis, MO, USA) coated 10 cm dishes were co-transfected with an empty vector or with CaSR-eGFP pcDNA3.1 and TRPV5pCINeo/IRES-GFP. At 48 hours after transfection, cells were incubated for 1 hour with 200 µM neomycin. The biotinylation assay was performed using NHS-LC-LC-biotin (Pierce, Etten-Leur, The Netherlands) and cells were homogenized in 1 ml lysis buffer as described previously (27). Finally, biotinylated proteins were precipitated using neutravidin-agarose beads (Pierce, Etten-Leur, The Netherlands) and TRPV5 expression was analyzed by immunoblotting using the guinea-pig anti-TRPV5 antibody (16).

*Statistical analysis*

In all experiments, the data are expressed as mean ± SEM. Overall statistical significance was determined by analysis of variance (ANOVA). In case of significance, differences between the means of two groups were analyzed by unpaired Student's *t*-test, while multiple comparisons between groups were performed by Bonferroni *post hoc* tests. $P < 0.05$ was considered as significant.

## RESULTS

*CaSR activation stimulates TRPV5 activity*

The potential role of CaSR co-localization with TRPV5 at the apical membrane of the DCT and CNT cells (8,10) was first investigated by measurements of the intracellular $Ca^{2+}$ concentration performed using the $Ca^{2+}$-sensing dye Fura-2. Neomycin (200 µM) was used to activate the CaSR co-transfected in HEK293 cells with TRPV5 or with an empty vector. CaSR stimulation by neomycin increased significantly ($P < 0.05$) intracellular $Ca^{2+}$ concentrations of the cells co-transfected with CaSR and the empty vector (140 ± 4%) and of the cells co-transfected with CaSR and TRPV5 (138 ± 3%), as shown in **Figure 1A**. The non-transfected control cells did not show an increase in the intracellular $Ca^{2+}$ concentration upon neomycin application **(Figure 1A)**. To address the effect of CaSR stimulation on TRPV5-mediated currents, HEK293 cells co-transfected with CaSR and TRPV5 were incubated for 1 hour with neomycin (200 µM) or L-phenylalanine (L-Phe) (3.5 mM) to activate CaSR and functionally characterized by patch-clamp measurements in comparison to non-treated control cells. Interestingly, the amplitude of the inward-rectifying $Na^+$ currents measured at -80 mV from the treated cells **(Figure 1B,C)** was significantly increased ($P < 0.05$) compared to non-treated control cells, as depicted in **Figure 1C**, while the current-voltage relation (I-V) of the currents remained unaffected. Pre-incubation with both neomycin and L-Phe increased the inward $Ca^{2+}$ currents elicited by the step protocol, without affecting the $Ca^{2+}$-dependent inactivation of the TRPV5 currents **(Figure 1D,E)**.

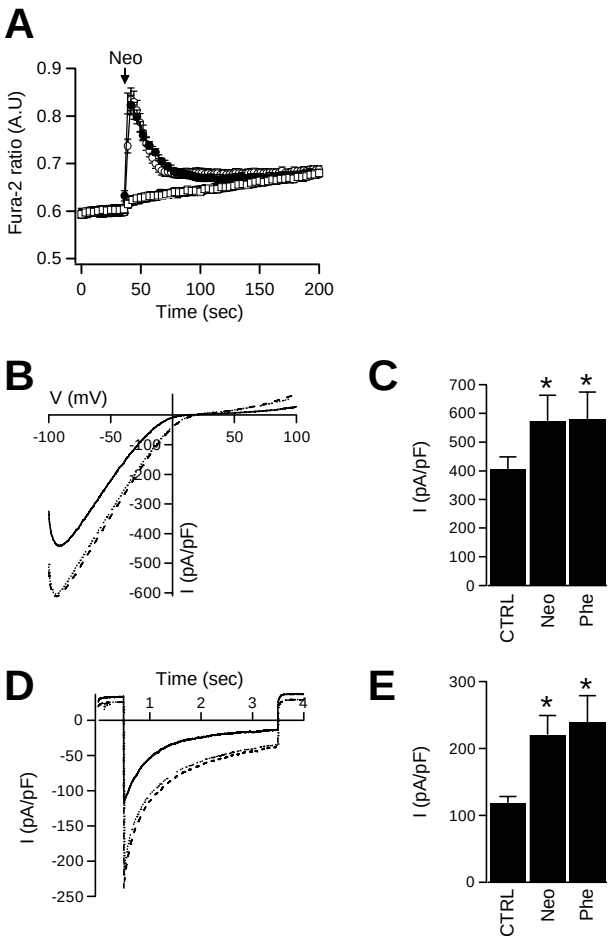


**Figure 1. Functional correlation between CaSR and TRPV5 co-expressed in HEK293 cells. (A)** Ratiometric Fura-2 measurements from cells co-transfected with CaSR and TRPV5 (filled circles) or CaSR and an empty vector (empty circles) or not-transfected cells (squares) stimulated with neomycin at the time point indicated by the arrow. **(B)** I-V relations measured using voltage ramps in divalent-free (DVF) extracellular solution from HEK293 cells co-transfected with CaSR and TRPV5, incubated (dotted trace) with neomycin, with L-Phe (dashed trace) or non-treated (solid trace). **(C)** Average $Na^+$ currents density at -80mV in DVF solution were 575 ± 80 pA/pF (n = 12 cells) and 580 ± 95 pA/pF (n = 8 cells) for cells treated with neomycin, respective with L-Phe, compared to 405 ± 40 pA/pF for control (CTRL) non-treated cells (n = 10 cells) **(D)** Average $Ca^{2+}$ currents measured with 10 mM $Ca^{2+}$ in the extracellular solution using the step protocol from CaSR and TRPV5 co-transfected HEK293 cells treated (dotted trace), treated with L-Phe (dashed trace) or non-treated (solid trace) with neomycin **(E)** Average density of the $Ca^{2+}$ peak current measured as in **(D)**, was 220 ± 25 pA/pF (n = 12 cells) for neomycin treated cells and 239 ± 40 pA/pF (n = 8 cells) compared to 118 ± 10 pA/pF (n = 10 cells) for CTRL cells. **P* < 0.05 *versus* CTRL cells.

The specificity of the effect of CaSR activation on TRPV5-mediated currents was investigated using HEK293 cells transfected with TRPV5 alone. When the cells were incubated with 200 µM neomycin for 1 hour, the I-V relation **(Figure 2A)** and the amplitude at -80 mV **(Figure 2B)** of TRPV5-mediated $Na^+$ currents remained identical to those of non-treated control cells. Moreover, $Ca^{2+}$-dependent inactivation and the peak value of the TRPV5-mediated inward $Ca^{2+}$ currents recorded from the neomycin-stimulated cells were similar to $Ca^{2+}$ currents measured in control cells **(Figure 2C,D)**.

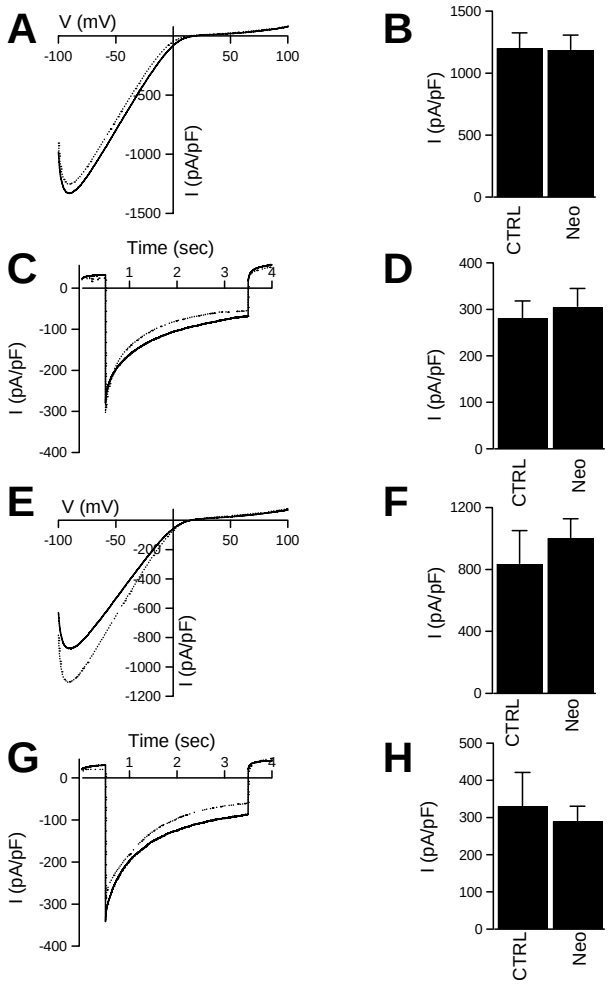


**Figure 2. CaSR activation is required to increase TRPV5-mediated currents. (A)** I-V relations measured using voltage ramps in DVF extracellular solution from TRPV5-transfected HEK293 cells treated (dotted trace) or non-treated (solid trace) with neomycin. **(B)** Average $Na^+$ currents density at -80 mV in DVF solution were 1185 ± 125 pA/pF (n = 8 cells) for neomycin treated cells compared to 1200 ± 125 pA/pF for CTRL cells (n = 6 cells). **(C)** Average $Ca^{2+}$ currents measured with 10 mM $Ca^{2+}$ in the extracellular solution using the step protocol from TRPV5-transfected HEK293 cells treated (dotted trace) or non-treated (solid trace) with neomycin **(D)** Average density of the $Ca^{2+}$ peak current measured as in **(C)** was 305 ± 40 pA/pF (n = 8 cells) for neomycin treated cells compared to 280 ± 38 pA/pF (n=6 cells) for CTRL cells. **(E)** I-V relations measured using voltage ramps in DVF extracellular solution from HEK293 cells co-transfected with the dominant negative mutant of CaSR (R185Q) together with TRPV5 treated (dotted trace) or non-treated (solid trace) with neomycin. **(F)** Average $Na^+$ currents densities at -80 mV in DVF solution were 1000 ± 130 pA/pF (n = 8 cells) for neomycin treated cells compared to 840 ± 215 pA/pF for CTRL cells (n = 5 cells). **(G)** Average $Ca^{2+}$ currents measured with 10 mM $Ca^{2+}$ in the extracellular solution using the step protocol from HEK293 cells co-transfected with CaSR-R185Q and TRPV5 treated (dotted trace) or non-treated (solid trace) with neomycin. **(H)** Average density of the $Ca^{2+}$ peak current measured as in **(G)**, was 290 ± 40 pA/pF (n = 8 cells) for neomycin treated cells compared to 330 ± 90 pA/pF (n = 5 cells) for CTRL cells.

The role of CaSR activation in the subsequent increased TRPV5 activity, was studied using a dominant-negative mutant of the CaSR, CaSR-R185Q (28,29) co-transfected with TRPV5 in HEK293 cells. The I-V relation **(Figure 2E,F)** and the amplitude at -80 mV of TRPV5-mediated $Na^+$ currents measured from the neomycin-incubated cells were not different compared to currents measured from non-treated control cells. The $Ca^{2+}$-dependent inactivation **(Figure 2G)** as well as the peak value **(Figure 2H)** of the inward $Ca^{2+}$ currents also remained unaffected after neomycin stimulation compared to non-treated control cells.

To determine the specificity of the effect of CaSR on TRPV5-mediated currents, TRPV6, the closest relative of TRPV5, was co-transfected with CaSR in HEK293 cells.

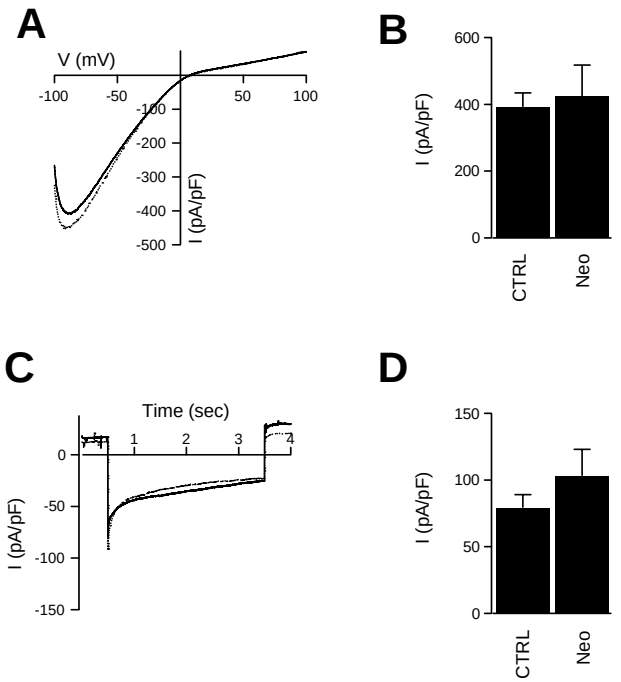


**Figure 3. TRPV6 activity is unaffected upon CaSR activation. (A)** I-V relations measured using voltage ramps in DVF extracellular solution from HEK293 cells co-transfected with CaSR and TRPV6, treated (dotted trace) or non-treated (solid trace) with neomycin. **(B)** Average $Na^+$ currents density at -80 mV in DVF solution were 423 ± 115 pA/pF (n = 8 cells) for neomycin treated cells compared to 391 ± 42 pA/pF for CTRL cells (n = 13 cells). **(C)** Average $Ca^{2+}$ currents measured with 10 mM $Ca^{2+}$ in the extracellular solution using the step protocol from HEK293 cells co-transfected with CaSR and TRPV6, treated (dotted trace) or non-treated (solid trace) with neomycin. **(D)** Average density of the $Ca^{2+}$ peak current measured as in (*C*) was 102 ± 29 pA/pF (n = 8 cells) for neomycin treated cells compared to 80 ± 10 pA/pF (n = 6 cells) for CTRL cells.

After stimulation of CaSR with neomycin, the TRPV6-mediated inward $Na^+$ currents recorded with the ramp protocol showed no difference in I-V relation **(Figure 3A)** or amplitude at -80 mV **(Figure 3B)** compared to non-treated control cells. $Ca^{2+}$-dependent inactivation of the TRPV6 currents **(Figure 3C)** and the peak $Ca^{2+}$ current recorded with the step protocol from neomycin-treated were comparable to non-treated control cells **(Figure 3D)**.

*The role of PKC in the effect of CaSR activation on TRPV5 currents*

To elucidate the molecular mechanism down stream of CaSR activation in enhanced TRPV5 activity consequent to CaSR activation, a sextuple PKC phosphorylation deficient mutant with all the six computer-predicted PKC phosphorylation sites in TRPV5 changed to alanines (23), was co-transfected with the CaSR in HEK293 cells. Subsequent to neomycin incubation, the inward rectification of the I-V relation **(Figure 4A)** as well as the amplitude at -80 mV of the $Na^+$ currents were similar to non-treated control cells **(Figure 4B)**. The peak value and the $Ca^{2+}$-dependent inactivation of the inward $Ca^{2+}$ currents were unaffected by neomycin incubation compared to non-treated control cells **(Figure 4C,D)**. Subsequently, the putative PKC phosphorylation sites were individually mutated into an alanine residue. Neomycin increased

$Ca^{2+}$ currents of all single PKC mutants except of S299A and S654A ($P < 0.05$, n = 12 cells for each condition, **Figure 4E**).

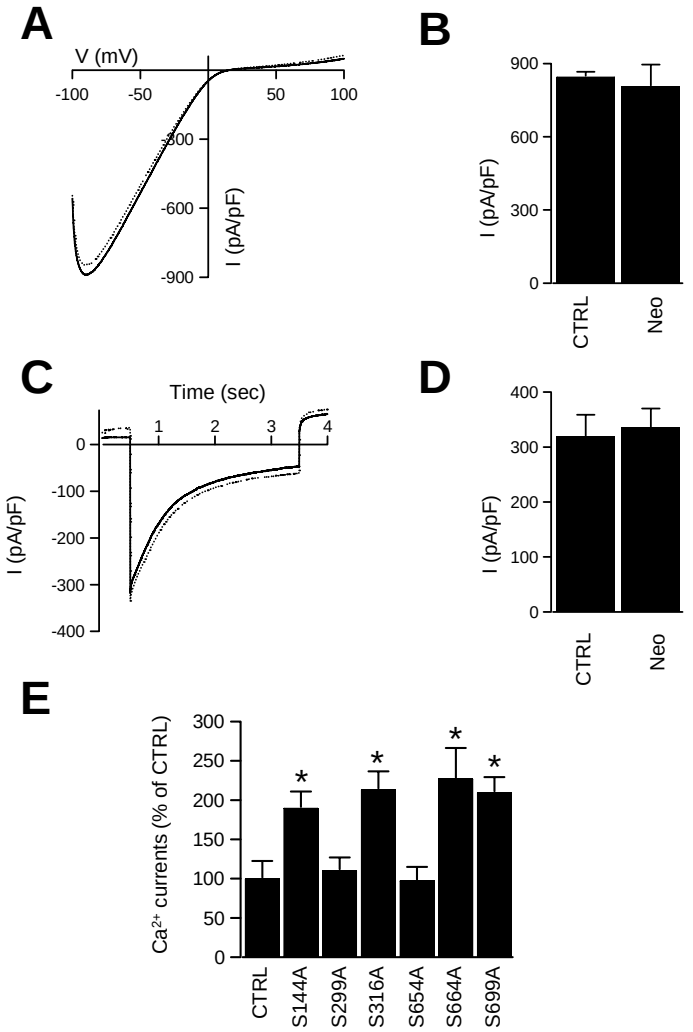


**Figure 4. The effect of CaSR activation on TRPV5-mediated currents involves the PKC signaling pathway.** **(A)** I-V relations measured using voltage ramps in DVF extracellular solution from HEK293 cells co-transfected with CaSR and TRPV5 mutated for all its six PKC phosphorylation sites and treated (dotted trace) or non-treated (solid trace) with neomycin. **(B)** Average $Na^+$ currents densities at -80 mV in DVF solution were 806 ± 90 pA/pF (n = 10 cells) for neomycin treated cells compared to 846 ± 90 pA/pF for CTRL cells (n = 5 cells). **(C)** Average $Ca^{2+}$ currents measured with 10 mM $Ca^{2+}$ in the extracellular solution using the step protocol from HEK293 cells co-transfected with CaSR and TRPV5, treated (dotted trace) or non-treated (solid trace) with neomycin. **(D)** Average density of the $Ca^{2+}$ peak current measured as in **(C)**, was 335 ± 35 pA/pF (n = 10 cells) for neomycin treated cells compared to 319 ± 40 pA/pF (n = 5 cells) for CTRL cells. **(E)** Point mutation of the PKC phosphorylation sites S299 and S654 did not affect $Ca^{2+}$ currents in comparison with the other four PKC mutants upon CaSR stimulation with neomycin. Data are expressed as percentage of $Ca^{2+}$ currents measured from neomycin treated cells transfected with the indicated point mutants of TRPV5, normalized to non-treated CTRL cells (n = 12 cells for each mutant). *$P < 0.05$ versus CTRL cells.

Furthermore, to determine which of the PKC isoforms was involved in the increased TRPV5-mediated currents consequent to CaSR activation, HEK293 cells were incubated overnight with 1 µM of phorbol ester (phorbol 12-myristate 13-acetate (PMA) to down-regulate the PMA-sensitive PKC isoforms) (24). Then, the PMA-pretreated cells were incubated with 200 µM neomycin for 1 hour. CaSR activation increased ($P < 0.05$, n = 10-17 cells for each condition) the TRPV5-mediated $Na^+$ **(Figure 5B)** and $Ca^{2+}$ currents **(Figure 5D)** versus non-treated control

cells. The I-V relations **(Figure 5A)** and the $Ca^{2+}$-dependent inactivation **(Figure 5C)** remained identical to control cells. Overnight incubation with PMA (1 µM) had no effect on control TRPV5-mediated currents (as previously shown (23)).

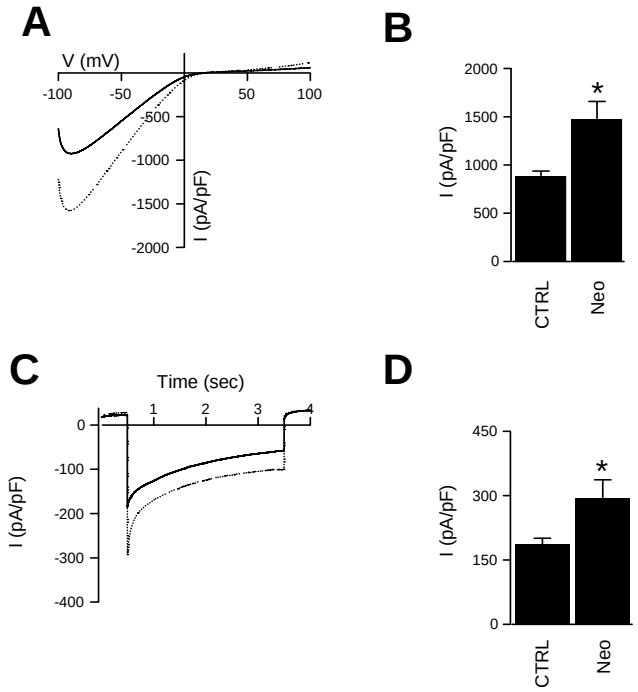


**Figure 5. TRPV5 activity is stimulated by a PMA-sensitive PKC isoforms downstream of CaSR activation.** 24 hours incubation with 1 µM PMA was used to down-regulate the PMA-sensitive PKC isoforms in cells co-transfected with CaSR and TRPV5. **(A)** I-V relations measured using voltage ramps in DVF extracellular solution from cells co-transfected with CaSR and TRPV6, treated (dotted trace) or non-treated (solid trace) with neomycin. **(B)** Stimulation of CaSR with neomycin significantly increased TRPV5-mediated $Na^{+}$ currents (881 ± 56 pA/pF) compared to CTRL cells (1477 ± 180 pA/pF) (n = 10-17 cells for each condition) **(C)** Averaged $Ca^{2+}$ currents measured with 10 mM $Ca^{2+}$ in the extracellular solution using the step protocol from HEK293 cells co-transfected with CaSR and TRPV5, treated (dotted trace) or non-treated (solid trace) with neomycin. **(D)** Stimulation of CaSR with neomycin significantly increased TRPV5-mediated $Ca^{2+}$ currents (186 ± 14 pA/pF) measured as in **(C)** compared to CTRL cells (294 ± 40 pA/pF) (n = 10-17 cells for each condition). *$P$ < 0.05 versus CTRL cells.

*CaSR activation increases cell surface expression of TRPV5*

To address the effect of CaSR activation on the amount of TRPV5 channels expressed at the plasma membrane, cell surface biotinylation assays were performed using HEK293 cells. Cells co-transfected with CaSR and TRPV5, and the cells transfected with the empty vector (mock) were incubated with 200 µM neomycin for 1 hour and then subjected to cell surface biotinylation. Biotinylated cell lysates were precipitated with neutravidin-agarose beads and immunoblotted for TRPV5. Mock cells and the cells not treated with biotin were used as negative controls. Importantly, TRPV5 was equally expressed in total cell lysates of all tested conditions **(Figure 6, upper panel)**. Preliminary results indicated that stimulation of CaSR by neomycin enhances TRPV5 expression in the biotinylated fraction **(Figure 6, lower panel)**.

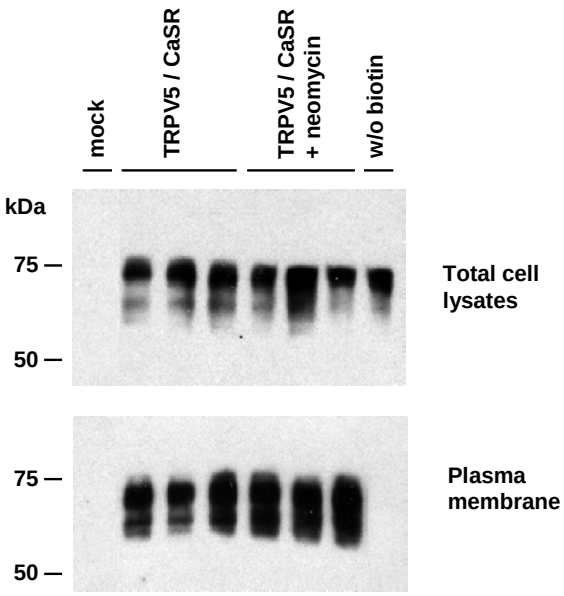


**Figure 6. CaSR activation likely increases the plasma membrane localization of TRPV5.** HEK293 cells co-transfected with CaSR and TRPV5 were treated with 200 µM neomycin for 1 hour, or left untreated. Cells were subjected to cell surface biotinylation and after lysis precipitated with neutravidin-agarose beads. TRPV5 expression was analyzed by immunoblotting for the total cell lysates (*upper panel*) and for the plasma membrane fraction (*lower panel*). As negative controls, cells transfected with the empty vector (mock) were used and biotin was omitted in the procedure.

**DISCUSSION**

The present study demonstrated that activation of CaSR stimulates TRPV5 activity. This conclusion is based on the following experimental data: First, both $Ca^{2+}$ and $Na^{+}$ TRPV5-mediated currents were stimulated after CaSR activation by neomycin or L-Phe. Second, CaSR stimulation influences specifically TRPV5, since the currents of its closest relative, TRPV6, were unaffected after CaSR activation. Moreover, obstruction of the CaSR signaling pathway using a dominant negative mutant of CaSR normalized the amplitudes of TRPV5-mediated currents to their standard values. Third, the stimulatory effect of CaSR activation on TRPV5-mediated currents was mediated via the PKC pathway and requires two conserved PKC phosphorylation sites, S299 and S654, in TRPV5. Fourth, CaSR activation likely increases TRPV5 channel abundance at the plasma membrane.

To date, the expression pattern of the CaSR in the kidney is under extended investigation. CaSR was shown to be expressed essentially throughout the whole nephron with highest levels in the proximal segments. In TAL, where it is expressed at the basolateral membrane, CaSR inhibits the passive $Ca^{2+}$ reabsorption by reducing the negative potential that drives this process (9,30). In contrast to TAL, where the role of CaSR was thoroughly studied, the role of CaSR in DCT and CNT remained elusive. Here, $Ca^{2+}$ reabsorption occurs against a concentration gradient *via* an active mechanism in which TRPV5 plays a crucial role. We demonstrated by *in vitro* functional analysis that stimulation of the CaSR enhances TRPV5 activity. This effect can account for a distinct role of CaSR in DCT and CNT, compared to the TAL, stimulating active $Ca^{2+}$ reabsorption while it inhibits passive $Ca^{2+}$ reabsorption. The site of CaSR expression in the nephron segments, apical or basolateral can be determined by its physiological functions in the respective segments. In the proximal segments CaSR senses $Ca^{2+}$ concentrations in the blood controlling $Ca^{2+}$ passive reabsorption, while in the DCT and CNT, CaSR is activated by increased $Ca^{2+}$ levels in the pro-urine. Elevated levels of $Ca^{2+}$ in the pro-urine may stimulate the apical CaSR in DCT and CNT and increase here the active $Ca^{2+}$ reabsorption. This process suggests novel local feedback regulatory mechanisms in DCT and CNT activated by $Ca^{2+}$ levels in the pro-urine, beside the hormonal regulation that responds to $Ca^{2+}$ concentration in the blood. This mechanism could minimize the $Ca^{2+}$ loss *via* the urine by stimulating active $Ca^{2+}$ reabsorption. We have previously shown that activation of another GPCR, the bradykinin receptor subtype 2, by tissue kallikrein (TK) increases TRPV5-mediated $Ca^{2+}$ reabsorption (23). TK acts from the tubular compartment to regulate active $Ca^{2+}$ reabsorption, supporting our hypothesis on the existence of local regulatory mechanisms in DCT and CNT for efficient control of $Ca^{2+}$ balance.

CaSR is functionally linked to a multitude of G-proteins isoforms and signal transduction pathways from $G_i$ to $G_s$ and $G_q$ expressed in the parathyroid chief cells (31). In overexpression systems it was demonstrated that CaSR functionally couples to $G_i$ isoforms inhibiting the

adenylate cyclase to reduce cAMP production (32), and with $G_q$ isoforms to stimulate the phospholipase C pathway (33). The present study, demonstrated that CaSR activation initiates signaling pathways that activate PKC isoforms, which in turn determine the increase in TRPV5 activity. In addition, by using an overnight incubation with PMA to down-regulate α, β and ε isoforms of PKC, but not PKC ζ (24), we imply that a PMA-insensitive isoform of PKC is responsible for the enhanced TRPV5 currents upon CaSR activation. This latter PKC isoform is presumably involved in the increase of TRPV5 currents since this stimulatory effect was similar in PMA-incubated and control cells. Interestingly, in primary cultures of rabbit kidney connecting and cortical collecting tubules, stimulation of active $Ca^{2+}$ transport also involves PMA-insensitive PKC isoforms (34). Moreover, our study delineated the conserved residues S299 and S654 as the PKC phosphorylation sites involved in this effect. Importantly, the activity of TRPV6, the closest homologue of TRPV5, was not affected subsequent to CaSR activation. Since the serine residue S654 is not conserved in TRPV6, it appears that both serines are apparently critical for the increase in TRPV5 activity upon CaSR activation. The absence of this serine residue in TRPV6 may explain its insensitivity to neomycin activation of CaSR. Interestingly, TRPV6 activity was also unaffected by TK (23) that activates another GPCR. Beside this, both CaSR activation and TK manifest their effect on the same PKC phosphorylation sites and both increase TRPV5 plasma membrane localization suggesting a common mechanism down-stream of GPCR regulating TRPV5 functioning.

Stimulation of TRPV5-mediated currents upon CaSR activation could be the result of an increase in either open probability of the channel or in expression of TRPV5 proteins at the plasma membrane. Preliminary data from surface biotinylation analysis suggested that activation of the CaSR might increase the amount of TRPV5 channels at the plasma membrane Thus, PKC phosphorylation of TRPV5, following the stimulation of CaSR could regulate the balance between constitutive exocytosis and endocytosis in favor of the first leading to the accumulation of TRPV5 at the cell surface. Interestingly, Colley and colleagues (35) demonstrated that a member of the Shaker family of $K^+$ channels, the voltage-gated $K^+$ channel Kv1.3, is regulated upon phosphorylation by the neurotrophin B receptor kinase. Pulse-chase experiments showed an increased half-life residence time of these channels at the cell surface. The plasma membrane abundance of Kv1.3 was enhanced after phosphorylation, as a consequence of their retention at the plasma membrane. The mechanism for the increase of TRPV5 activity upon CaSR stimulation involves the activation of a signaling pathway that initiates the PKC-dependent phosphorylation of two serine residues in its sequence. PKC phosphorylation of these amino acid residues, S299 and S654, following the CaSR activation could increase the accumulation of TRPV5 at the cell surface. Still, the exact molecular mechanism of this process is presently unknown. It is possible that PKC-dependent phosphorylation of TRPV5 leads to activation of motor proteins that transport the channels to

the plasma membrane. Interestingly, depolymerization of filamentous actin increased functional expression of $Ca^{2+}$-activated $K^+$ channels in neurons (36). Nevertheless, the motor proteins participating in the incorporation of TRPV5 in the plasma membrane remain to be identified. Moreover, presumably accumulation of channels at the cell surface can occur by increased incorporation into the plasma membrane of newly synthesized channels. Supporting this hypothesis, PKC activation delivers newly formed *N*-methyl-D-aspartate channels to the plasma membrane through increased exocytosis (37). On the other hand, the suggested increase in the number of channels present at the cell surface could be the consequence of diminished retrieval of the proteins from the plasma membrane. In accordance with this premise, we demonstrated that TK enhances the amount of TRPV5 channels at the plasma membrane by delaying their retrieval (23). Supporting this finding, a recent study by Cha and colleagues (38) showed that TRPV5 accumulation at the plasma membrane is determined by a decrease in the caveolin-dependent endocytosis of the channels, consecutive to PKC activation. However, exactly which of these events determines the suggested increase of TRPV5 expression at the plasma membrane upon CaSR activation, explaining its enhanced channel activity, remains to be investigated.

In conclusion, we postulate a role for the CaSR apical expressed in DCT and CNT of the kidney, the main expression sites of TRPV5. These results attest the existence of local feedback mechanisms that could rapidly adapt renal $Ca^{2+}$ reabsorption to increased $Ca^{2+}$ levels in the pro-urine independently from hormonal regulation.

**ACKNOWLEDGMENTS**

We thank Mr. D. van den Berg and Mr. R. Janssen for expert technical assistance. This work was supported by the Netherlands Organization for Scientific Research (ZonMw 016.006.001, NWO-ALW 814.02.001), the Dutch Kidney Foundation (C03.6017), and by the European Science Foundation (EURYI award to JH).

**REFERENCES**


1. Brown, E. M., Gamba, G., Riccardi, D.*, et al. Nature.* 366: 575-580, 1993
2. Riccardi, D., Park, J., Lee, W. S., Gamba, G., Brown, E. M., and Hebert, S. C. *Proc Natl Acad Sci U S A.* 92: 131-135, 1995
3. Ruat, M., Molliver, M. E., Snowman, A. M., and Snyder, S. H. *Proc Natl Acad Sci U S A.* 92: 3161-3165, 1995
4. Yamaguchi, T., Kifor, O., Chattopadhyay, N., Bai, M., and Brown, E. M. *J Bone Miner Res.* 13: 1390-1397, 1998
5. Chattopadhyay, N., Cheng, I., Rogers, K.*, et al. Am J Physiol.* 274: G122-130, 1998
6. Levi, R., Ben-Dov, I. Z., Lavi-Moshayoff, V.*, et al. J Am Soc Nephrol.* 17: 107-112, 2006
7. Wada, M., Furuya, Y., Sakiyama, J.*, et al. J Clin Invest.* 100: 2977-2983, 1997
8. Riccardi, D., Hall, A. E., Chattopadhyay, N., Xu, J. Z., Brown, E. M., and Hebert, S. C. *Am J Physiol.* 274: F611-622, 1998
9. Riccardi, D., Lee, W. S., Lee, K., Segre, G. V., Brown, E. M., and Hebert, S. C. *Am J Physiol.* 271: F951-956, 1996
10. Sands, J. M., Naruse, M., Baum, M.*, et al. J Clin Invest.* 99: 1399-1405, 1997
11. Butters, R. R., Jr., Chattopadhyay, N., Nielsen, P.*, et al. J Bone Miner Res.* 12: 568-579, 1997
12. Hebert, S. C., Brown, E. M., and Harris, H. W. *J Exp Biol.* 200: 295-302, 1997
13. Wang, W., Lu, M., Balazy, M., and Hebert, S. C. *Am J Physiol.* 273: F421-429, 1997
14. Wang, W. H., Lu, M., and Hebert, S. C. *Am J Physiol.* 271: C103-111, 1996
15. Hoenderop, J. G., Nilius, B., and Bindels, R. J. *Physiol Rev.* 85: 373-422, 2005
16. Hoenderop, J. G., Hartog, A., Stuiver, M., Doucet, A., Willems, P. H., and Bindels, R. J. *J Am Soc Nephrol.* 11: 1171-1178, 2000
17. Hoenderop, J. G., van der Kemp, A. W., Hartog, A.*, et al. J Biol Chem.* 274: 8375-8378, 1999
18. Hoenderop, J. G., Voets, T., Hoefs, S.*, et al. Embo J.* 22: 776-785, 2003
19. Vennekens, R., Hoenderop, J. G., Prenen, J.*, et al. J Biol Chem.* 275: 3963-3969, 2000
20. van de Graaf, S. F., Hoenderop, J. G., Gkika, D.*, et al. Embo J.* 22: 1478-1487, 2003
21. Hoenderop, J. G., Vennekens, R., Muller, D.*, et al. J Physiol.* 537: 747-761, 2001
22. Garrett, J. E., Capuano, I. V., Hammerland, L. G.*, et al. J. Biol. Chem.* 270: 12919-12925, 1995
23. Gkika, D., Topala, C. N., Chang, Q.*, et al. Embo J.* 25: 4707-4716, 2006
24. Camden, J. M., Schrader, A. M., Camden, R. E.*, et al. J Biol Chem.* 280: 18696-18702, 2005
25. Visch, H. J., Koopman, W. J., Zeegers, D.*, et al. Am J Physiol Cell Physiol.* 291: C308-316, 2006
26. Robben, J. H., Sze, M., Knoers, N. V., and Deen, P. M. *Mol Biol Cell.* 17: 379-386, 2006
27. Chang, Q., Hoefs, S., van der Kemp, A. W., Topala, C. N., Bindels, R. J., and Hoenderop, J. G. *Science.* 310: 490-493, 2005
28. Bai, M., Pearce, S. H. S., Kifor, O.*, et al. J. Clin. Invest.* 99: 88-96, 1997
29. Bai, M., Quinn, S., Trivedi, S.*, et al. J Biol Chem.* 271: 19537-19545, 1996
30. Hebert, S. C., Brown, E. M., and Harris, H. W. *J Exp Biol.* 200: 295-302, 1997
31. Varrault, A., Pena, M. S., Goldsmith, P. K., Mithal, A., Brown, E. M., and Spiegel, A. M. *Endocrinology.* 136: 4390-4396, 1995
32. Quitterer, U., Hoffmann, M., Freichel, M., and Lohse, M. J. *J. Biol. Chem.* 276: 6763-6769, 2001
33. Kifor, O., Diaz, R., Butters, R., and Brown, E. M. *J Bone Miner Res.* 12: 715-725, 1997
34. Hoenderop, J. G., De Pont, J. J., Bindels, R. J., and Willems, P. H. *Kidney Int.* 55: 225-233, 1999
35. Colley, B. S., Biju, K. C., Visegrady, A., Campbell, S., and Fadool, D. A. *Neuroscience.* 144: 531-546, 2007
36. Chae, K.-S., and Dryer, S. E. *J Neurochem.* 94: 367-379, 2005
37. Lan, J.-y., Skeberdis, V. A., Jover, T.*, et al. Nat Neurosci.* 4: 382-390, 2001

38. Cha, S.-K., Wu, T., and Huang, C.-L. *Am J Physiol Renal Physiol.* in press, 2008

# ***Chapter 4***

## The immunophilin FKBP52 inhibits the activity of the epithelial $Ca^{2+}$ channel TRPV5

Dimitra Gkika, Catalin N. Topala, Joost G. Hoenderop and René J. Bindels

Department of Physiology, Nijmegen Centre for Molecular Life Sciences, Radboud University Nijmegen Medical Centre, Netherlands

*Am J Physiol Renal Physiol*. 290: 1253-1259, 2006

**ABSTRACT**

In kidney, the epithelial $Ca^{2+}$ channel TRPV5 constitutes the apical entry pathway in the process of active $Ca^{2+}$ reabsorption. The regulation of $Ca^{2+}$ influx through TRPV5 is of crucial importance, since it determines the final amount of $Ca^{2+}$ excreted in the urine. The present study identifies FKBP52 as an auxiliary protein of TRPV5, inhibiting the channel activity. FKBP52 shows specific interaction with TRPV5 and both proteins co-localize in the distal part of the nephron. On the functional level, FKBP52 decreases $Ca^{2+}$ influx through TRPV5 as demonstrated in radioactive $^{45}Ca^{2+}$ uptake measurements and electrophysiological studies on TRPV5-overexpressing human embryonic kidney 293 cells. On the other hand, gene-silencing of FKBP52 or administration of the FKBP52 blocker, FK506, enhances $Ca^{2+}$ influx through TRPV5. The inhibitory action of FKBP52 on TRPV5 activity is blunted by mutation of its peptidyl-propyl cis-trans isomerase domain, showing that the FKBP52 catalytic property is critical for channel activity. In conclusion, these results suggest that FKBP52 plays an important role in the regulation of TRPV5 and thus in the process of $Ca^{2+}$ reabsorption.

## INTRODUCTION

FKBP52 (also designed as FKBP59, p59 or Hsp56) is a widely expressed cytosolic enzyme that belongs to the FK506-binding proteins (FKBPs) subfamily of immunophillin proteins (1-3). FKBPs are characterized by their ability to catalyze the cis-trans isomerization of cis-peptidyl-propyl bonds, as well as by their strong affinity to the immunosuppressive drug FK506 (2). The peptidyl-propyl cis-trans isomerase (PPIase) activity of FKBP52 plays an important role in diverse cellular processes and in particular in the translocation of steroid receptors to the nucleus through dynein association (4,5). Besides its function as a chaperone, FKBP52 is involved in ion regulation such as $Cu^{2+}$ efflux (6), while its *Drosophila melanogaster* homologue inhibits $Ca^{2+}$ influx through association with the transient receptor potential (TRP) channel, TRPL (7,8). Concerning the mammalian TRP channels, it was recently demonstrated that FKBP52 associates with TRPC1, -C4, -C5 orthologues (7,8), while there is no functional data addressing the effect of FKBP52 on these channels.

In kidney, the TRP channel TRPV5 mediates $Ca^{2+}$ reabsorption in the distal part of the nephron and determines the final amount of $Ca^{2+}$ excreted in the urine (9,10). Therefore, a tight control of TRPV5 expression, trafficking to the plasma membrane and/or gating of the channel is important for the amount of reabsorbed $Ca^{2+}$ in the kidney (11). There is growing interest in the identification of accessory proteins regulating TRPV5 activity. The S100A10-annexin 2 complex modulates TRPV5 trafficking towards the plasma membrane by direct association to the carboxyl-terminal tail of the channel (12). On the other hand, the 80K-H protein binds to the channel and acts as a $Ca^{2+}$ sensor that facilitates $Ca^{2+}$ influx through the TRPV5 channel (13).

The aim of the present study was to assess whether FKBP52 is a regulator of TRPV5. To this end, we demonstrated by immunohistochemical, biochemical and functional analysis that FKBP52 inhibits TRPV5-mediated $Ca^{2+}$ influx via its PPIase activity.

## EXPERIMENTAL PROCEDURES

*DNA constructs and cRNA synthesis*

TRPV5 constructs were generated as described previously (12). FKBP52 was cloned in a pCMV-Sport6 vector (clone IRAKp961i125Q2) by the RZPD (Deutsches Ressourcenzentrum fuer Genomforschung, Berlin, Germany) and then subcloned into the pCINeo/IRES-GFP (14), pGEX6p-2 (Amersham Pharmacia Biotech AB, Uppsala, Sweden) and the pT7Ts (15) vectors. The FD67DV mutant of FKBP52 was generated by *in vitro* mutagenesis (QuickChange site-directed Mutagenesis kit, Stratagene, La Jolla, California) with the primer set 5'-CTAGATGGCACAAAGGATGTCTCCAGTCTGGACCGC-3', 5'-GCGGTCCAGACTGGAGACATCCTTTGTGCCATCTAG-3' (the underlined sequence shows the mutated codons). All constructs were verified by sequence analysis. pT7Ts constructs were linearized and cRNA was synthesized *in vitro* using T7 RNA polymerase as described previously (16).

*Experimental animals*

Young adult male Wistar rats were randomly assigned to either the control group animals receiving vehicle only (n = 5), or FK506 (n = 5) (17). TRPV5 knockout ($TRPV5^{-/-}$) mice were generated as described previously (10). Kidney cortex was sampled and immediately frozen in liquid nitrogen. Subsequently, samples were stored at -80°C until further processing. The animals were kept in a light- and temperature-controlled room with *ad libitum* access to standard pelleted diet and water. The animal ethics board of the Radboud University Nijmegen approved all experimental procedures.

*Real-time quantitative PCR*

FKBP52 mRNA expression level was quantified by real-time quantitative PCR in a mouse cDNA panel including kidney, brain, heart, muscle, duodenum, jejunum, ileum, cecum, colon, bone and in renal tissue from control and FK506 treated rats. Total RNA was isolated using TRIzol (GIBCO, Life Technologies, Breda, The Netherlands) from which 2 µg were subjected to reverse transcription using Moloney murine leukemia virus reverse transcriptase. The following primers were used: the forward 5'-GAGTGGACATCAGCCCCAA-3' and the reverse 5'-TGTGCCTGTACCCTCTCTCTTG-3'. The probe (5'-CAGGACGAGGGCGTGCTCAAGGT-3') was labeled with the reporter dye 6-carboxyfluorescein (5'-end) and the quencher dye 6-carboxytetramethylrhodamine (3'-end) (Biolegio, Malden, The Netherlands). The mRNA expression level of hypoxanthine-guanine phosphoribosyl transferase (HPRT) was used as an internal control.

*Immunohistochemistry*

Immunohistochemistry was performed as previously described (18). Briefly, rabbit kidney PLP-treated sections were incubated for 16 hours at 4 ºC with guinea pig anti-TRPV5 (18) and mouse anti-FKBP52 antibodies (Stressgen, Victoria, Canada). To visualize the proteins corresponding secondary Alexa 488/594-conjugated antibodies (Molecular Probes, Eugene, USA) were used.

*Trypan-blue exclusion assay*

Cell suspension was mixed with an equal volume of 0.4% (w/v) isotonic trypan-blue solution. Total number of non-viable cells was counted after 2 minutes in a Fuchs-Rosenthal haemocytometer using a light microscope.

*Co-immunoprecipitation*

HEK293 cells were transfected with pCINeo/TRPV5-IRES-GFP and lysed after 48 hours in sucrose buffer containing 20 mM Hepes/Tris pH 7.4, 5 mM EDTA, 135 mM NaCl, 0.3% (v/v) NP-40, and 10% (w/v) sucrose. Lysates were centrifuged at 13,000 *g* for 1 hour and the protein concentration of the supernatants was determined with the BioRad protein assay (BioRad laboratories GmbH, München). Equal amounts of the lysates were incubated with guinea pig anti-TRPV5 antibody immobilized on protein A-agarose beads (Kem-En-Tec A/S, Kopenhagen, Denmark) for 16 hours at 4 °C. After three washing steps with sucrose buffer, immunoprecipitated proteins were eluted with SDS-PAGE loading buffer, separated on 12% (w/v) SDS-PAGE gels. TRPV5 and FKBP52 protein expression was detected by immunoblotting using guinea pig anti-TRPV5 (18) and mouse anti-FKBP52 (Stressgen, Victoria, Canada) respectively.

*Immunoblot analysis*

Cells were lysed in sucrose buffer containing 20 mM Hepes/Tris pH 7.4, 5 mM EDTA, 135 mM NaCl, 0.3% (v/v) NP-40, and 10% (w/v) sucrose and were centrifuged at 13,000 *g* for 1 hour. After the determination of the supernatants protein concentration, equal amounts of the lysates were subjected to SDS-PAGE electrophoresis (10-12% w/v). Immunoblots were incubated overnight at 4°C with primary antibodies including mouse anti-FKBP52 (Stressgen, Victoria, Canada), goat anti-FKBP52 (Santa Cruz Biotechnology, California, USA) and guinea pig anti-TRPV5 in 1% (w/v) non-fat dry milk. After washing, immunoblots were incubated at room temperature with the corresponding secondary antibody IgG peroxidase sheep anti-mouse (Jackson ImmunoResearch Laboratories, West Grove, USA), rabbit anti-goat (DakoCytomation, Denmark) or anti-guinea pig (Sigma, St Louis, MO, USA) respectively. The specificity of the two commercial FKBP52 antibodies was confirmed by immunoblot analysis (data not shown). Both

antibodies recognized an abundant band of ~60 kDa, while the polyclonal antibody (Santa Cruz Biotechnology, California, USA) displayed an additional but weak band (lower than 25 kDa) that could be FKBP12 as suggested previously (7). Importantly, monoclonal antibody (Stressgen, Victoria, Canada), that only recognized the single band, was used in immunohistochemistry, immunoprecipitation and siRNA assays.

*GST-fusion proteins and pull-down assay*

pGEX6p-2 constructs were transformed in *Escherichia coli* BL21 and GST-fusion proteins were expressed and purified according to the manufacturer's protocol (Amersham Pharmacia Biotech AB, Uppsala, Sweden). GST-fused TRPV5 N- and C-terminal tails constructs were generated as described previously (12). [$^{35}$S]methionine-labeled TRPV5 or FKBP52, was prepared using the reticulocyte lysate system in the presence of canine microsomal membranes (Promega) and added to GST, GST-fused FKBP52 or GST-fused TRPV5 N- and C-terminal tails fusion proteins immobilized on glutathion-Sepharose 4B beads (Amersham Pharmacia Biotech AB, Uppsala, Sweden) in PBS containing 0.3% (v/v) Triton X-100. After 2 hours incubation at room temperature, the beads were washed extensively and bound proteins were eluted with SDS-PAGE loading buffer, separated on 10% (w/v) SDS-PAGE gels and visualized by autoradiography.

*Small interference (si) RNA*

The mammalian expression vector, pSUPER (19) was used for expression of siRNA in Human Embryonic Kidney (HEK) 293 cells. The gene-specific insert specifies a 19-nucleotide sequence 5'-GAGAGAGGGCACAGGTACA-3' corresponding to nucleotides 114-133 downstream of the transcription start site of human FKBP52, which was separated by a 9-nucleotide non-complementary spacer (5'-TTCAAAGA-3') from the reverse complement of the 19-nucleotide sequence. HEK293 cells were co-transfected with pSUPER-FKBP52 and pCINeo/IRES GFP-TRPV5 or empty pCINeo/IRES-GFP while the pSUPER-luciferase construct was used as a control. The gene-specific insert for luciferase specifies the 19-nucleotide sequence 5'-CTTACGCTGAGTACTTCGA-3'. Three days after transfection cells were sorted for GFP expression by flow cytometry (FACS) using an Epics Elite flow cytometer (Coulter, Miami, FL, USA). The GFP-positive cells were used for the functional analysis. One day later measured for their functional activity using the $^{45}Ca^{2+}$ uptake assay. FKBP52 protein expression was detected by immunoblotting using the mouse anti-FKBP52 (Stressgen, Victoria, Canada).

*$^{45}Ca^{2+}$ uptake assay*

HEK293 cells were transfected with pCINeo/TRPV5-IRES-GFP or co-transfected with pCINeo/TRPV5-IRES-GFP and wild-type or mutated FKBP52 constructs. $Ca^{2+}$ uptake was

determined two days after transfection whereas co-transfected cells were first sorted for GFP by FACS. For the assays where FK506 was used, TRPV5-transfected cells were incubated overnight with 10, 100, and 1000 nM of FK506 (Fujisawa Pharmaceutical Co., Osaka, Japan). $Ca^{2+}$ uptake was determined by incubation in uptake medium (110 mM NaCl, 5 mM KCl, 1.2 mM $MgCl_2$, 0.1 mM $CaCl_2$, 10 mM Na-acetate, 2 mM $NaH_2PO_4$, 20 mM HEPES/Tris, pH 7.4 supplemented with 10 µM felodipine, 10 µM methoxy-verapamil and 1 mM $BaCl_2$) for 10 minutes at room temperature. Radioactive $Ca^{2+}$ (1 µCi/ml $^{45}CaCl_2$) was applied to the cells. Each well was washed extensively in stop buffer (110 mM NaCl, 5 mM KCl, 1.2 mM $MgCl_2$, 0.5 mM $CaCl_2$, 1.5 mM $LaCl_3$, 10 mM Na-acetate, 20 mM HEPES/Tris, pH 7.4) at 4°C, incubated with 0.05% (w/v) SDS, and counted for radioactivity using liquid scintillation.

*Electrophysiology and solutions*

Patch-clamp experiments were performed in the tight-seal whole-cell configuration at room temperature (20–25°C) using an EPC-9 patch-clamp amplifier controlled by the Pulse software (HEKA Electronics, Lambrecht, Germany). Patch pipettes had resistances between 3 and 5 MΩ after filling with the standard intracellular solution. Cells were held at +20 mV, and voltage ramps of 450 milliseconds duration ranging from -100 to +100 mV were applied every 5 seconds. Cell capacitance and access resistance were monitored continuously using the automatic capacitance compensation of the Pulse software. Current densities were obtained by dividing the current amplitude measured at -80 mV by the cell capacitance. $Ca^{2+}$-dependent inactivation was studied using a 3 seconds voltage step to –100 mV from a holding potential of +70 mV. The inactivation rate was assessed by the time for 10% decay of the current. The standard extracellular solution (Krebs) contained 150 mM NaCl, 6 mM CsCl, 1 mM $MgCl_2$, 10 mM HEPES/NaOH, pH 7.4 and 10 mM glucose. The concentration of $Ca^{2+}$ ranged between 1 and 10 mM. Divalent free (DVF) solutions did not contain added divalent cations, whereas trace amounts of divalent cations were removed with 100 µM EDTA. The standard internal (pipette) solution contained 20 mM CsCl, 100 mM Cs-aspartate, 1 mM $MgCl_2$, 4 mM $Na_2ATP$, 10 mM BAPTA, 10 mM HEPES/CsOH, pH 7.2. Cells were kept in a nominal $Ca^{2+}$-free medium to prevent $Ca^{2+}$ overload and exposed for a maximum of 5 minutes to a Krebs solution containing 1.5 mM $Ca^{2+}$ before sealing the patch pipette to the cell.

*Transcellular $Ca^{2+}$ transport in primary culture of rabbit kidney connecting tubule and cortical collecting duct*

Rabbit kidney connecting tubules (CNT) and cortical collecting ducts (CCD) were immunodissected from kidney cortex of New Zeeland White rabbits (~0.5 kg) using antibody R2G9 and then placed in primary culture on permeable filters (0.33 $cm^2$; Costar, Cambridge, MA, USA) as described previously in detail (20). At confluence, monolayers of rabbit CNT/CCD

cells growing on permeable filters were incubated overnight with 10, 100 and 1000 nM of FK506 at the apical and the basolateral side. The next day filters were washed twice and preincubated in PSS buffer containing 140 mM NaCl, 2 mM KCl, 1 mM $K_2HPO_4$, 1 mM $MgCl_2$, 1 mM $CaCl_2$, 5 mM glucose, 5 mM L-alanine, 5 µM indomethacin, 10 mM Hepes/Tris, pH 7.4, for 15 minutes at 37°C. Subsequently, the filters were incubated in PSS (100 µl to apical and 600 µl to basolateral compartment). After 90 minutes transepithelial $Ca^{2+}$ transport was measured by using a colorimetric assay kit as described (20). Transepithelial potential difference and resistance were checked before and after transport measurement to confirm cell confluence and integrity of the monolayer.

*Statistical analysis*

Values are expressed as mean ± SEM. Overall statistical significance was determined by analysis of variance (ANOVA). In case of significance, differences between the means of two groups were analyzed by unpaired t-test, while multiple comparisons between groups were performed by Bonferroni posthoc tests. *P* values < 0.05 were considered significant. The statistical analyses were performed using the SPSS software (SPSS Inc, Chicago, Illinois, USA).

## RESULTS

*FKBP52 tissue distribution and localization*

FKBP52 expression was investigated at the mRNA level by quantitative real time PCR analysis, showing a higher abundance in kidney and heart in comparison to other tissues **(Figure 1A)**.

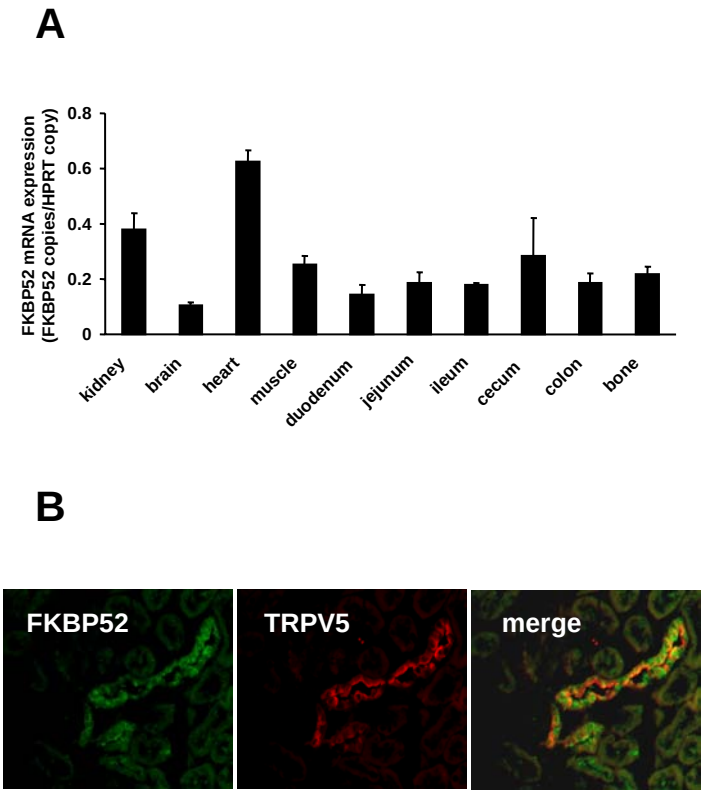


**Figure 1. Expression profile and localization of FKBP52. (A)** RNA was extracted from mouse tissues and after reverse transcription, the relative FKBP52 expression was determined by real time PCR analysis. FKBP52 mRNA expression was normalized for the respective HPRT values. **(B)** Immunohistochemical localization of FKBP52 (green) and TRPV5 (red) in rabbit kidney sections. In the merged picture the partial co-localization of the two proteins is depicted in yellow.

Subsequently, the localization of FKBP52 was analyzed in kidney. Immunohistochemical staining of rabbit kidney sections showed partial co-localization of FKBP52 with TRPV5 in DCT and CNT, nephron segments known to be responsible for active transepithelial $Ca^{2+}$ transport **(Figure 1B)**.

*Interaction of FKBP52 with TRPV5*

In order to assess the FKBP52 interaction with TRPV5, HEK293 cells were transfected with TRPV5 or the empty vector and cell lysates were subsequently subjected to immunoprecipitation using the TRPV5 antibody. The endogenous FKBP52 was co-immunoprecipitated with TRPV5 from these cells lysates, as represented by the immunopositive band of ~59 kDa **(Figure 2A)**. The expression of both proteins in the cell lysates was also verified as shown in the two upper panels.

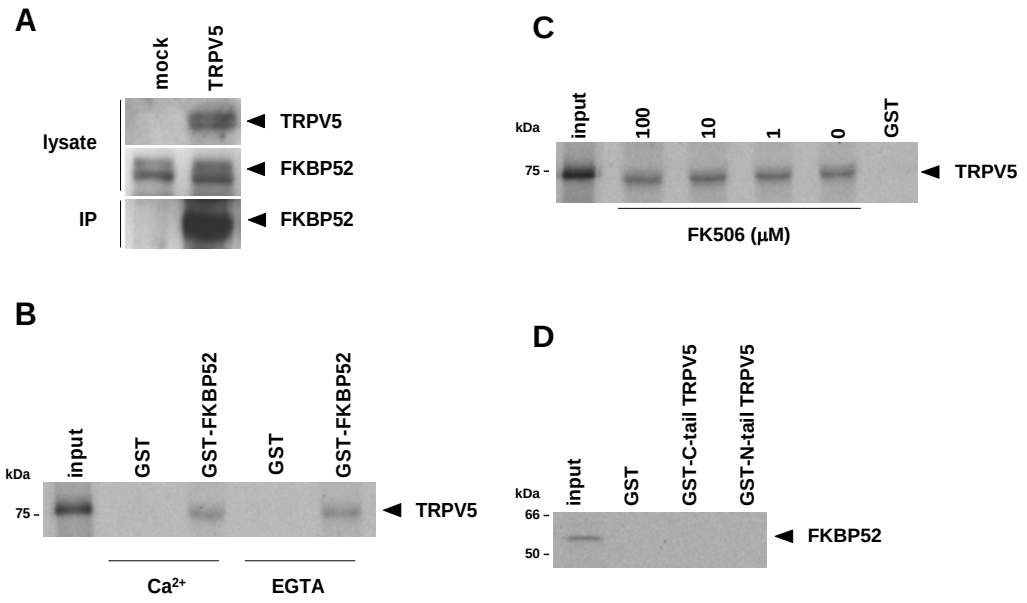


**Figure 2. FKBP52 binds the TRPV5 channel. (A)** Interaction of FKBP52 with TRPV5 as demonstrated by co-immunoprecipitation in HEK293 cells transfected with TRPV5 or mock. Equal amount of cell lysates were subjected to immunoprecipitation using the TRPV5 antibody and co-immunoprecipitation of the endogenous FKBP52 was detected by immunoblot analysis using the FKBP52 antibody (IP). Total lysates were analyzed for TRPV5 and FKBP52 protein expression (lysates). **(B)** Direct interaction of FKBP52 and TRPV5 was confirmed by GST-pull down assay. *In vitro* translated [$^{35}$S]methionine-TRPV5 associated with the GST-fused FKBP52 in the presence (1 mM $CaCl_2$) and the absence (10 mM EGTA/ no $CaCl_2$ added) of $Ca^{2+}$. **(C)** Binding of GST-fused FKBP52 was not altered by the addition of FK506. **(D)** GST-fused TRPV5 N- and C-terminal tails were incubated with *in vitro* translated [$^{35}$S]methionine-FKBP52 demonstrating no binding of FKBP52.

The interaction between FKBP52 and TRPV5 was further substantiated using GST pull-down assays. FKBP52 was expressed as a GST-fusion protein and analyzed for its interaction with the *in vitro* translated full-length $^{35}$S-methionine-TRPV5 in the presence (1 mM $CaCl_2$) or absence of $Ca^{2+}$ (10 mM EGTA) and with different concentrations of FK506. FKBP52 bound to TRPV5 in a $Ca^{2+}$ **(Figure 2B)** and FK506 **(Figure 2C)** independent manner. No interaction was observed with GST alone indicating the specificity of the interaction. To determine the role of TRPV5 tails in the binding with FKBP52, the GST-fused N- and C-terminal tails of TRPV5 were analyzed for their interaction with the *in vitro* translated FKBP52. Both tails did not interact with FKBP52 **(Figure 2D)**.

*Effect of FKBP52 knock-down on $Ca^{2+}$ influx*

The role of FKBP52 in $Ca^{2+}$ influx through TRPV5 was investigated using the pSUPER siRNA system. HEK293 cells were co-transfected with the pSUPER-FKBP52 (siFKBP52) and TRPV5. The pSUPER-luciferase (siLuc) construct was used as a negative control for the suppression of FKBP52, and the empty vector (mock) as a control for TRPV5 transfection.

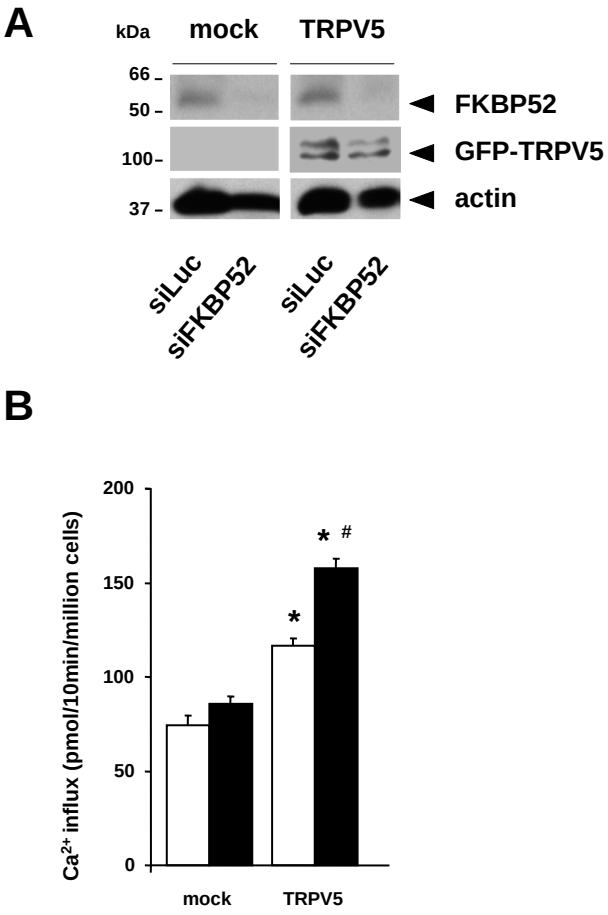


**Figure 3. Enhancement of TRPV5 activity by siRNA-mediated gene-silencing of FKBP52.** HEK293 cells were co-transfected with the pSUPER-FKBP52 (siFKBP52) construct together with TRPV5 or the empty vector (mock). The pSUPER-Luciferase (siLuc) construct was used as a control for the specificity of FKBP52 gene-silencing. **(A)** Immunoblot analysis for FKBP52 on lysates from co-transfected HEK293 cells demonstrated suppression of the FKBP52 protein. TRPV5 expression was not altered by the FKBP52 protein suppression. **(B)** $^{45}Ca^{2+}$ uptake was measured in HEK293 cells as shown in **Figure 3A**. Cells co-transfected with the siFKBP52 and TRPV5 showed an increased $^{45}Ca^{2+}$ influx compared to siLuc/TRPV5-transfected cells. The closed bars represent cells transfected with siFKBP52, while the open bars are used for the siRNA control, siLuc. Values are expressed as means ± SEM. (n = 4). *$P$ < 0.01 significantly different from the respectively mock-transfected cells. $^{\#}P$ < 0.02 significantly different from siLuc TRPV5-transfected cells.

Application of FKBP52 siRNA significantly reduced FKBP52 protein expression, whereas no effect was observed in the siLuc-transfected cells demonstrating the specificity of the FKBP52 gene-silencing **(Figure 3A)**. $^{45}Ca^{2+}$ uptake assay was performed to determine the effect of FKBP52 suppression on TRPV5 activity. Expression of siFKBP52 (closed bars) enhanced $^{45}Ca^{2+}$ influx through TRPV5, whereas no effect was observed for the siRNA control, siLuc (open bars), or the mock-transfected cells **(Figure 3B)**.

*Modulation of TRPV5 currents by FKBP52*

To study whether FKBP52 affects TRPV5 channel kinetics, HEK293 cells were co-transfected with TRPV5 and FKBP52 and analyzed by the whole-cell patch-clamp technique. Both the $Ca^{2+}$ and $Na^{+}$ currents were significantly inhibited by FKBP52 over-expression **(Figure 4)**. Measurements in nominally DVF solution (100 µM EDTA) revealed that the current-voltage

relation of currents remained unchanged **(Figure 4A)**, whereas a significant reduction in macroscopic currents was observed **(Figure 4B)**. Application of a hyperpolarizing voltage step to -100 mV from a holding potential of +70 mV showed a decreased $Ca^{2+}$ peak current, whereas no significant differences were observed on the $Ca^{2+}$-dependent inactivation (a hallmark of the channel) (**Figure 4*C,D***).

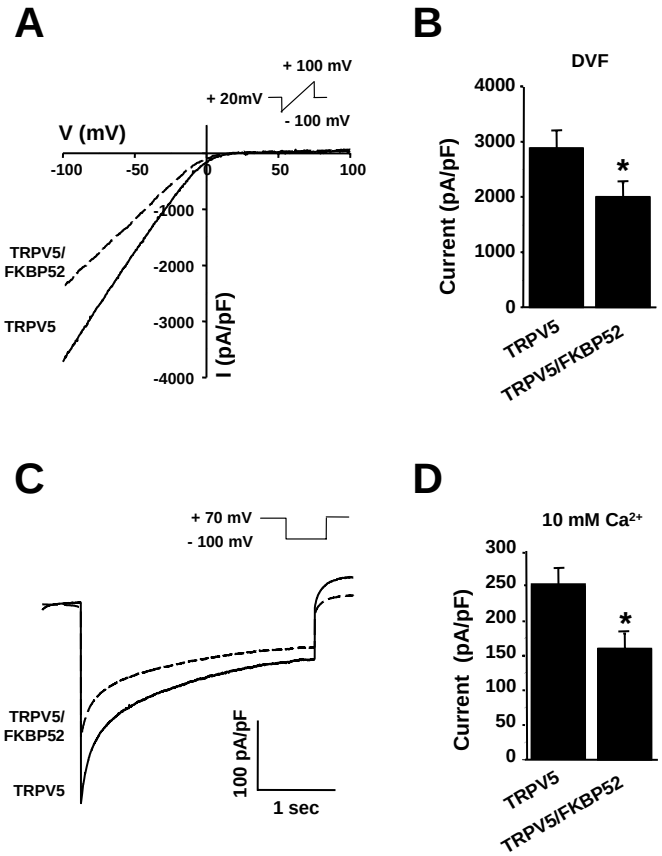


**Figure 4. Inhibition of TRPV5 activity by FKBP52 over-expression.** HEK293 cells were co-transfected with TRPV5 and FKBP52, or/and empty vector, and were analyzed by patch-clamp. **(A)** Current-voltage relations measured from 450 milliseconds voltage ramps in nominally DVF solution in HEK293 cells over-expressing either TRPV5 and empty vector or TRPV5 in combination with FKBP52. **(B)** Average current densities at -80 mV in nominally DVF solution for cells co-expressing either TRPV5 and empty vector or TRPV5 in combination with FKBP52. Cells co-transfected with TRPV5 and FKBP52 displayed significantly decreased $Na^{+}$ currents at -80 mV (1997 ± 260 pA/pF versus 2882 ± 325 pA/pF (n = 20)). ($P < 0.001$ versus TRPV5 control currents). **(C)** Inward $Ca^{2+}$ currents measured with 10 mM extracellular $Ca^{2+}$ during a 3 seconds step to -100 mV from a holding potential of +70 mV. **(D)** Average peak current density during a voltage step to -100 mV in 10 mM $Ca^{2+}$. Cells co-transfected with TRPV5 and FKBP52 displayed significantly decreased $Ca^{2+}$ peak current 160 ± 22 versus 250 ± 25 pA/pF (n = 20). *$P < 0.005$, versus TRPV5 control currents.

Inactivation of TRPV5 $Ca^{2+}$ currents at negative membrane potentials was assessed by comparing the time of 10% inactivation in cells co-expressing TRPV5 and FKBP52. Time of 10% inactivation was not significantly different for $Ca^{2+}$ currents in cells co-expressing FKBP52 and TRPV5 compared to cells expressing TRPV5 only (32 ± 12 milliseconds, n = 20 versus 38 ± 5 milliseconds, n = 15, respectively, $P > 0.05$).

*Role of the FKBP52 PPIase activity in TRPV5-mediated $Ca^{2+}$ influx*

The enzymatic activity of FKBP52 was abolished by double mutation of two highly conserved amino acidic residues (FD67DV mutant) as described previously (21). The FD67DV mutant and wild-type FKBP52 were co-transfected in HEK293 cells with TRPV5 and functionally analyzed using the $^{45}Ca^{2+}$ uptake assay. The FD67DV mutant reverted the inhibitory effect of FKBP52 on TRPV5-mediated $Ca^{2+}$ influx **(Figure 5A)**. Immunoblot analysis of the cell lysates demonstrated that both FKBP52 wild-type and the mutant FD67DV are equally expressed and do not interfere with the TRPV5 expression **(Figure 5B)**.

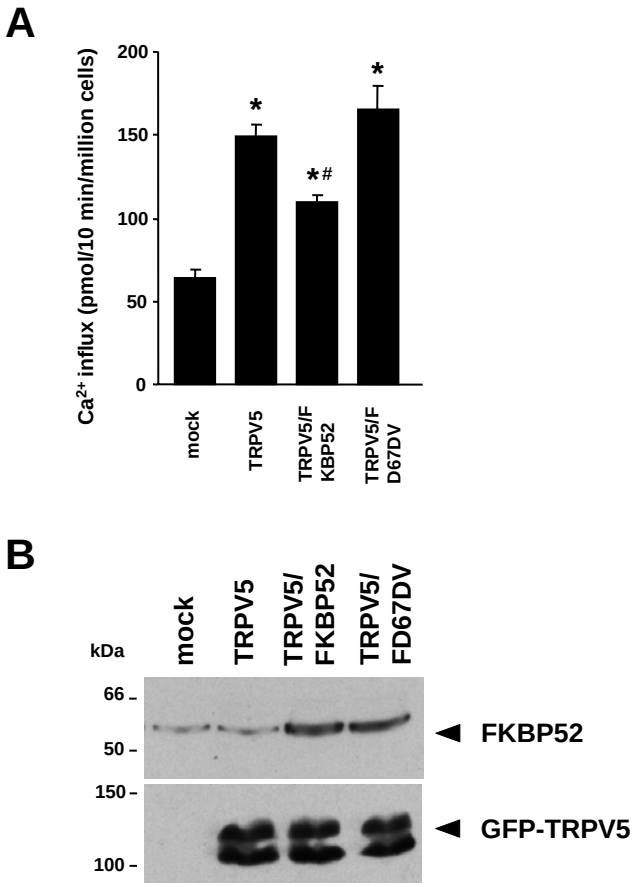


**Figure 5. FKBP52 inhibitory effect on $^{45}Ca^{2+}$ influx through TRPV5 depends on the PPIase activity of FKBP52. (A)** HEK293 cells were co-transfected with TRPV5 and the empty vector (TRPV5), or the FKBP52 construct (FKBP52/TRPV5) or the catalytic inactive FKBP52 mutant (FD67DV/TRPV5). The inhibitory effect of FKBP52 on TRPV5-mediated $^{45}Ca^{2+}$ influx was abolished by FD67DV. Data are expressed as means ± SEM. (n = 5). $^{*}P < 0.01$ significantly different from mock-transfected cells. $^{\#}P < 0.02$ significantly different from TRPV5-transfected cells. **(B)** Immunoblot analysis for FKBP52 was performed on the lysates of HEK293 cells co-transfected with TRPV5 and the empty vector (TRPV5), or the FKBP52 construct (FKBP52/TRPV5) or the catalytic inactive FKBP52 mutant (FD67DV/TRPV5) that were applied in the functional assay in **(A)**. The results demonstrated equal expression of wild-type and mutated FKBP52 and immunostaining for TRPV5 showed equal expression of the channel.

*Effect of FK506 on TRPV5 activity*

The immunosuppressant FK506, known to bind and inhibit FKBP52 enzymatic activity, was assessed for its effect on TRPV5-mediated $Ca^{2+}$ influx. First, the dose-dependent relationship of FK506 was determined in HEK293 cells demonstrating that overnight incubation with high

concentrations (in the range of 10 nM to 100 µM) diminishes the cell viability **(Figure 6A)**. Then, HEK293 cells transiently transfected with TRPV5 were incubated overnight with 10 nM of FK506 and tested for their $^{45}Ca^{2+}$ uptake. Incubation with FK506 resulted in significantly increased $^{45}Ca^{2+}$ influx in TRPV5-transfected cells **(Figure 6B)**. To further substantiate this effect, FK506 action was evaluated in kidney primary cultures. The primary cultures of rabbit CNT/CCD cells form confluent monolayers that exhibit many characteristics of the original polarized epithelia, including a PTH- and vitamin D-stimulated transepithelial $Ca^{2+}$ transport (20). Overnight incubation of 10 nM FK506 significantly stimulated transcellular $Ca^{2+}$ transport in these primary kidney cells **(Figure 6C)**.

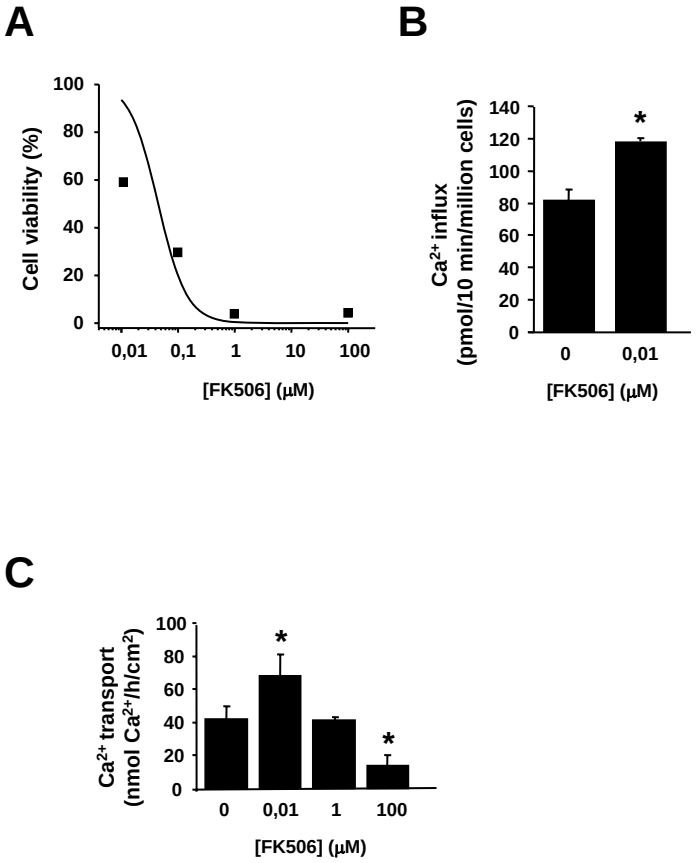


**Figure 6. FK506 stimulatory effect on $Ca^{2+}$ influx of TRPV5-expressing HEK293 and primary CNT/CCD cells. (A)** HEK293 cells were incubated overnight with FK506 at a concentration between 0 to 100 µM. The effect of FK506 on cell viability was counted by the trypan-blue exclusion assay. **(B)** TRPV5-transfected HEK293 cells were incubated overnight with 0 or 10 nM FK506. $^{45}Ca^{2+}$ uptake measurements showed a stimulatory effect of FK506 on $^{45}Ca^{2+}$ influx. **(C)** TRPV5-expressing monolayers of rabbit CNT/CCD primary cell cultures were incubated overnight with FK506 at a concentration of 0 to 100 µM. 10 nM of FK506 showed increased $Ca^{2+}$ transport upon FK506 treatment whereas higher concentrations disturbed the cell monolayer resulting in reduced $Ca^{2+}$ transport. Data are expressed as means ± SEM. (n = 4). *$P$ < 0.01 versus control cells.

Measurements of the transepithelial resistance across the cell monolayer showed that higher concentrations (1 µM and 100 µM) of FK506 disturbed the integrity of the confluent cell monolayer.

*Regulation of FKBP52 in kidney*

To estimate the putative effect of FK506 on FKBP52 transcription, renal mRNA expression was determined by quantitative real time PCR in rats treated with FK506 (1 mg/day) or vehicle for seven days. The results demonstrated that FK506 has no significant effect on FKBP52 mRNA expression compared to control (0.32 ± 0.03 versus 0.28 ± 0.02 copies FKBP52/HPRT). In addition, the FKBP52 protein expression was measured in renal total lysates from TRPV5$^{-/-}$ mice. Immunoblot analysis for FKBP52 showed a 63 ± 11% decrease in TRPV5$^{-/-}$ mice compared to their wild-type littermates **(Figure 7)**.

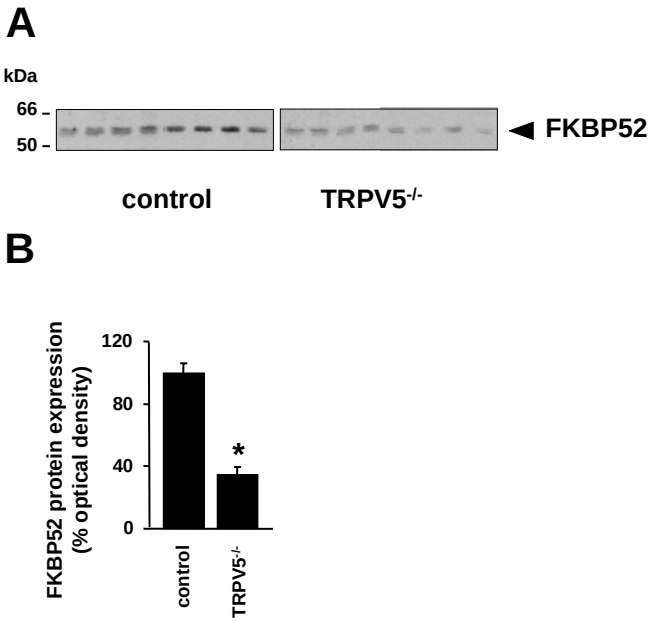


**Figure 7. Regulation of FKBP52 expression. (A)** Immunoblotting of FKBP52 in total kidney homogenates of TRPV5$^{-/-}$ and wild-type littermates. 10 µg of total protein was loaded per lane and each lane represents the renal homogenate from an individual mouse. **(B)** The intensity of the immunopositive bands were quantified by densitometry. FKBP52 expression is depicted as a percent ratio to wild-type mice. Data are expressed as means ± SEM. **P* < 0.05 versus wild-type mice.

**DISCUSSION**

The present study demonstrated that FKBP52 binds and co-localizes with the epithelial $Ca^{2+}$ channel TRPV5 in the distal part of the nephron. FKBP52 reduced TRPV5 activity as indicated by the functional analysis using FKBP52 siRNA and co-expression studies in HEK293 cells. This inhibitory action was reverted by abrogation of the PPIase activity in FKBP52, as well as by administration of the FKBP52 blocker, FK506. Our findings suggest that the immunophilin FKBP52 is a TRPV5 auxiliary protein regulating channel activity.

FKBP52 transcription was strongly stimulated by two majors regulators of the $Ca^{2+}$ homeostasis: vitamin $D_3$ and dietary $Ca^{2+}$ (22), in line with the regulation observed for TRPV5 (23). We showed here that renal FKBP52 expression is diminished in TRPV5$^{-/-}$ mice further supporting a functional coupling between both proteins.

Indeed, knockdown of the FKBP52 protein expression by siRNA gene silencing, as well as inhibition of FKBP52 enzymatic activity by binding to FK506, increased $Ca^{2+}$ influx through TRPV5. In addition, expression of the FKBP52 protein reduced TRPV5-mediated $Ca^{2+}$ and $Na^{+}$ currents, suggesting that FKBP52 decreases the number of functional channels at the plasma membrane. In this regulatory process, it seems that the enzymatic activity of FKBP52 plays a critical role, since inactivation of FKBP52 PPIase activity abolished its effect on TRPV5 activity. FKBP52 ability to modify its substrates by catalyzing the cis-trans isomerization of proline residues is often a rate-limiting step in protein folding (24). Moreover, it is possible that FKBP52 operates through multiple targets to regulate the function of the channel, considering that it contains putative ATP, GTP and calmodulin binding sites (25,26).

Consistent with our findings on the FKBP52 inhibitory role in TRPV5 $Ca^{2+}$ influx, is a previous study that identified the FKBP52 *Drosophila melanogaster* homologue, FKBP59, as a physiological regulator of TRPL channel activity (7). FKBP59 interacts directly with the highly conserved TRPL sequence $^{701}$LPPPFNVLP$^{709}$ and inhibits $Ca^{2+}$ influx. In *Drosophila melanogaster* (7) as well as in mammals (8) the proline residue of the first LP-motif, located next to mouth of the channel pore, plays a crucial role in this association. Conspicuously, TRPV5 contains such an LP motif next to the pore region at the amino acidic position 551-552, where the FKBP52 binding site is located. The FK506 drug has been shown to mimic the LP-dipeptide (27) and to disrupt the FKBP52 interaction with TRPCs (8). However, FK506 did not interrupt the FKBP52-TRPV5 association suggesting an alternative mechanism. This would mean that FK506 binds TRPV5 and modulates its activity without displacing the association of FKBP52, similar to the mechanism previously described for the regulation of the *Drosophila melanogaster* homologues FKBP59 and TRPL (7). The physiological relevance of the latter hypothesis needs further confirmation since it is based on *in vitro* experiments.

FKBP52 is expressed along the apical region of DCT and CNT tubules together with TRPV5. In addition, FKBP52 is also localized in the cytosol. This finding together with the stimulatory effect

of FK506 drug on $Ca^{2+}$ influx observed in primary CNT/CCD renal cells further substantiated the physiological relevance of FKBP52 in active transepithelial $Ca^{2+}$ transport. Our results imply that while high concentrations of FK506 are toxic for the cells, submicromolar concentrations (10 nM) stimulate transcellular $Ca^{2+}$ transport. This dose-dependent effect could explain the nephrotoxicity observed in patients treated with the immunosuppressive drug FK506 (28,29). On the other hand, it has been previously demonstrated that the hypercalciuric effect of FK506 is mediated through the decreased expression of calbindin-$D_{28K}$ (30) and TRPV5 (17). Contrary to the reduction in TRPV5 expression upon FK506 administration, we showed that FKBP52 expression is not altered under the same conditions. To this regard, the reduction of the TRPV5/FKBP52 ratio is reminiscent of transient expression in HEK293 cells where an excess of FKBP52 inhibits TRPV5-mediated $Ca^{2+}$ influx. Certainly, given the complexity of the *in vivo* situation, the FK506-induced hypercalciuria awaits further investigation particularly concerning the putative role of other FKBP proteins.

In conclusion, FKBP52 participates in active transepithelial $Ca^{2+}$ transport along the distal part of the nephron by reducing TRPV5 activity. This inhibitory effect on TRPV5 is mediated by the enzymatic PPIase activity of FKBP52 and is reverted by FK506 administration.

**ACKNOWLEDGMENTS**

We thank Dr. R. Agami (Division of Tumor Biology, Netherlands Cancer Institute, Amsterdam, Netherlands) for kindly providing the pSuper vector and Mrs. A. van der Kemp for expert technical assistance, as well as Mr. R. Woestenenk and Mrs. G. Vierwinden for performing the FACS sorting and analysis. This work was supported by the Dutch Organization of Scientific Research (Zon-Mw 016.006.001, Zon-Mw 902.18.298, NWO-ALW 810.38.004, NWO-ALW 805.09.042) and Human Frontiers Science Program (RGP0032/2004).

**REFERENCES**


1. Gothel, S. F., and Marahiel, M. A. *Cell Mol Life Sci.* 55: 423-436, 1999
2. Ivery, M. T. *Med Res Rev.* 20: 452-484, 2000
3. Ruff, V. A., Yem, A. W., Munns, P. L.*, et al. J Biol Chem.* 267: 21285-21288, 1992
4. Galigniana, M. D., Radanyi, C., Renoir, J. M., Housley, P. R., and Pratt, W. B. *J Biol Chem.* 276: 14884-14889, 2001
5. Silverstein, A. M., Galigniana, M. D., Kanelakis, K. C., Radanyi, C., Renoir, J. M., and Pratt, W. B. *J Biol Chem.* 274: 36980-36986, 1999
6. Sanokawa-Akakura, R., Dai, H., Akakura, S.*, et al. J Biol Chem.* 279: 27845-27848, 2004
7. Goel, M., Garcia, R., Estacion, M., and Schilling, W. P. *J Biol Chem.* 276: 38762-38773, 2001
8. Sinkins, W. G., Goel, M., Estacion, M., and Schilling, W. P. *J Biol Chem.* 279: 34521-34529, 2004
9. Hoenderop, J. G., van der Kemp, A. W., Hartog, A.*, et al. J Biol Chem.* 274: 8375-8378, 1999
10. Hoenderop, J. G., van Leeuwen, J. P., van der Eerden, B. C.*, et al. J Clin Invest.* 112: 1906-1914, 2003
11. Gkika, D., Hoenderop, J. G., and Bindels, R. J. *J Med Sci.* 24: 291–299, 2004
12. van de Graaf, S. F., Hoenderop, J. G., Gkika, D.*, et al. EMBO J.* 22: 1478-1487, 2003
13. Gkika, D., Mahieu, F., Nilius, B., Hoenderop, J. G., and Bindels, R. J. *J Biol Chem.* 279: 26351-26357, 2004
14. Trouet, D., Nilius, B., Voets, T., Droogmans, G., and Eggermont, J. *Pflugers Arch.* 434: 632-638, 1997
15. Krieg, P. A., and Melton, D. A. *Nucleic Acids Res.* 12: 7057-7070, 1984
16. Hoenderop, J. G., van der Kemp, A. W., Hartog, A., van Os, C. H., Willems, P. H., and Bindels, R. J. *Biochem Biophys Res Commun.* 261: 488-492, 1999
17. Nijenhuis, T., Hoenderop, J. G., and Bindels, R. J. *J Am Soc Nephrol.* 15: 549-557, 2004
18. Hoenderop, J. G., Hartog, A., Stuiver, M., Doucet, A., Willems, P. H., and Bindels, R. J. *J Am Soc Nephrol.* 11: 1171-1178, 2000
19. Brummelkamp, T. R., Bernards, R., and Agami, R. *Science.* 296: 550-553, 2002
20. Bindels, R. J., Hartog, A., Timmermans, J., and Van Os, C. H. *Am J Physiol.* 261: F799-807, 1991
21. Riggs, D. L., Roberts, P. J., Chirillo, S. C.*, et al. EMBO J.* 22: 1158-1167, 2003
22. Hoenderop, J. G., Chon, H., Gkika, D.*, et al. Kidney Int.* 65: 531-539, 2004
23. Hoenderop, J. G., Dardenne, O., Van Abel, M.*, et al. FASEB J.* 16: 1398-1406, 2002
24. Schiene, C., and Fischer, G. *Curr Opin Struct Biol.* 10: 40-45, 2000
25. Callebaut, I., Renoir, J. M., Lebeau, M. C.*, et al. Proc Natl Acad Sci U S A.* 89: 6270-6274, 1992
26. Le Bihan, S., Renoir, J. M., Radanyi, C.*, et al. Biochem Biophys Res Commun.* 195: 600-607, 1993
27. Rosen, M. K., Standaert, R. F., Galat, A., Nakatsuka, M., and Schreiber, S. L. *Science.* 248: 863-866, 1990
28. Allison, A. C. *Ann N Y Acad Sci.* 696: xi-xx, 1993
29. Andoh, T. F., Burdmann, E. A., Fransechini, N., Houghton, D. C., and Bennett, W. M. *Kidney Int.* 50: 1110-1117, 1996
30. Aicher, L., Meier, G., Norcross, A. J.*, et al. Biochem Pharmacol.* 53: 723-731, 1997

# ***Chapter 5***

## RGS2 inhibits the epithelial $Ca^{2+}$ channel TRPV6

Joost P. Schoeber[1], Catalin N. Topala[1], Xinhua Wang[2], Shmuel Muallem[2], Tim T. Lambers[1], Robin J. Diepens[1], Joost G. Hoenderop[1] and René J. Bindels[1]

[1]Department of Physiology, Nijmegen Centre for Molecular Life Sciences, Radboud University Nijmegen Medical Centre, The Netherlands, [2]Department of Physiology, University of Texas Southwestern Medical Center Dallas, Dallas, USA

*J Biol Chem.* 281: 29669-29674, 2006

**ABSTRACT**

The epithelial $Ca^{2+}$ channels TRPV5 and TRPV6 constitute the apical $Ca^{2+}$ entry pathway in the process of active $Ca^{2+}$ (re)absorption. By yeast-two-hybrid and GST pull-down analysis we identified RGS2 as a novel TRPV6-associated protein. RGS proteins determine the inactivation kinetics of heterotrimeric G protein-coupled receptor (GPCR) signaling by regulating the GTP-ase activity of $G_\alpha$ subunits. Here we demonstrate that TRPV6 interacts with the N-terminal domain of RGS2 in a $Ca^{2+}$-independent fashion and that over-expression of RGS2 reduces the $Na^+$ and $Ca^{2+}$ current of TRPV6 but not those of TRPV5-transfected HEK293 cells. In contrast, over-expression of the deletion mutant ΔN-RGS2, lacking the N-terminal domain of RGS2, in TRPV6-expressing HEK293 cells did not show this inhibition. Furthermore, cell surface biotinylation indicated that the inhibitory effect of RGS2 on TRPV6 activity is not mediated by differences in trafficking or retrieval of TRPV6 from the plasma membrane. This effect probably results from the direct interaction between RGS2 and TRPV6, affecting the gating properties of the channel. Finally, the scaffolding protein spinophilin (SPL), shown to recruit RGS2 and regulate GPCR-signaling via $G_\alpha$, did not affect RGS2 binding and electrophysiological properties of TRPV6, indicating a GPCR-independent mechanism of TRPV6 regulation by RGS2.

## INTRODUCTION

The Transient Receptor Potential (TRP) superfamily includes more than 30 different proteins, all of which are considered to form subunits of cation channels (1-5). Based on sequence homology, the TRP family can be divided in seven main subfamilies: the TRPC ('Canonical') family, the TRPV ('Vanilloid') family, the TRPM ('Melastatin') family, the TRPP ('Polycystin') family, the TRPML ('Mucolipin') family, the TRPA ('Ankyrin') family, and the TRPN ('NOMPC') family. TRPV6 is the most $Ca^{2+}$ selective ion channel in the TRP superfamily with a $Ca^{2+}$ selectivity of more than 100 times over monovalent cations (6,7).

Recently, the electrophysiological properties of TRPV6 have been studied extensively. When measured in heterologous expression systems, TRPV6 displays characteristic inward rectifying currents carried by $Ca^{2+}$ or monovalent cations when $Ca^{2+}$ is omitted from the extracellular solution. These inward currents are blocked by $Mg^{2+}$ in a voltage-dependent manner (8), that is removed upon neutralization of a single negatively charged amino acid residue - $D^{541}$ - within the pore region. The pore diameter of TRPV6 was recently estimated at 5.4 Å by cystein scanning experiments (9). Together with its closest relative, TRPV5, TRPV6 shares a common feature that is the $Ca^{2+}$-dependent inactivation of the currents.

TRPV6 is predominantly expressed in placenta, pancreas, small intestine, and colon (6,10-12). In these tissues TRPV6 plays a major role in $Ca^{2+}$ transport (reviewed in (13,14).

To date, screening and domain-mapping of the carboxyl-terminus of TRPV6 has revealed proteins associating with TRPV6 and subsequently the regulatory functions of these interacting proteins have been studied; *e.g.* Rab11a, NHERF4, S100A10 (15-17). In contrast, little is known about the molecular mechanisms involved in regulation of the channel via its intracellular N-terminal domain. At present, six ankyrin repeats have been predicted in this region (18). Ankyrin repeats have been shown to act as a scaffold in molecular recognition to mediate protein-protein interactions (19). These, or other regions in the N-terminal domain of TRPV6, may bind regulatory proteins interacting in pathways that mediate the $Ca^{2+}$-transporting activity of the channel.

The aim of this study was to identify regulatory proteins that interact with the N-terminal domain of TRPV6. To this end, we identified RGS2 as a novel binding partner of TRPV6 by yeast-two-hybrid screening. RGS2 is a member of the RGS family of proteins that are able to terminate signaling of heterotrimeric G protein-coupled receptors (GPCRs) by enhancing the GTP-ase activity of active $G_\alpha$ subunits (20). To date, over 20 different RGS proteins have been identified, and their effector functions extend beyond negative regulation of GPCR signaling. RGS proteins can act as effector antagonists, binding to either the effector protein or the $G_\alpha$ subunit to prevent an operative physical interaction. They have also been shown to interact with a wide variety of auxiliary proteins, such as CaM, spinophilin (SPL) and 14-3-3 protein, which can influence their subcellular localization, stability and function (21). In this respect, the finding of RGS2 as a

protein interacting with TRPV6 may lead to altered channel activity by disturbances in protein trafficking or a direct effect at the cell surface. The putative role of RGS2 in active $Ca^{2+}$ absorption was established by a comprehensive approach including pull-down assays, electrophysiological analysis and cell-surface expression of RGS2 interacting with TRPV6.

## EXPERIMENTAL PROCEDURES

*Constructs and cRNA synthesis*

The TRPV6, TRPV6 N-tail, and TRPV5 constructs were generated in pGEX 6p-2 and pCINeo/IRES-GFP vectors as described previously (22). The coding sequence of wild-type RGS2 protein was amplified from total mouse kidney cDNA material using primers with a HA tag included and cloned into the PT7Ts vector as BglII – SpeI fragment, and subsequently into the pCINeo/IRES-GFP vector as an NheI – XhoI fragment. RGS2 and ΔN-RGS2 (deletion of the N-terminal domain of RGS2: amino acids 1-82) were subcloned from the PT7Ts vector without the HA-tag to the pGEX 6p-2 (Amersham Biosciences, Piscataway, NJ, USA) vector using forward and reverse primers containing BamH I and XhoI restriction sites respectively. pT7Ts constructs were linearized, and cRNA was synthesized *in vitro* as described previously (16). In pCINeo/IRES-GFP, ΔN-RGS2 was obtained by *in vitro* mutagenesis of wild-type RGS2. All constructs were verified by sequence analysis. Rat-SPL (in pCMV-myc) and human-RGS2 (in pGex-KG) constructs were described previously (23).

*Yeast-two-hybrid system*

Yeast-two-hybrid experiments were performed as described previously (16). In short, the N-tail of mouse TRPV6 was cloned in the pAS-1 yeast cloning and expression vector. Using this vector, the yeast strain Y153 was transformed to Trp prototrophy. Subsequently, yeast was transformed with a mouse kidney cDNA library (Clontech, Palo Alto, CA, USA) present in the pACT2 vector, containing a leucine selection marker. Yeast cells were plated on Trp-Leu-His selective medium containing 25 mM 3-aminotriazole. Positive colonies were assayed for β-galactosidase activity. Subsequently, yeast DNA of positive colonies was isolated and prey plasmids were rescued by electroporation into KC8-cells. Results were confirmed using purified library plasmids and a negative control was performed by replacing the pAS-1 containing the N-tail of mouse TRPV6 with the pAS-1 containing the N-tail of rat γ-subunit of the epithelial $Na^+$ channel (ENaC).

*Reverse Transcriptase (RT)-PCR analysis*

Total RNA was isolated from different mouse tissues using TRIzol and subjected to reverse transcription as described (24). For RGS2 RT-PCR, the oligonucleotide primer sequences were as follows: forward primer with BglII restriction site 5'-GAAGATCTGCCACCATGCAAAGTGCCAGTTCCTG-3' and reverse with SpeI restriction site 5'-GGACTAGTTCATGTAGCATGGGGCTCCG-3'; β-actin forward 5'-ACGATTTCCCTCTCAGCTGTG-3', reverse 5'-GTATGCCTCTGGTCGTACCAC-3'. For SPL the following primers were used: forward primer 5'-CTTAGGAACACCAAAGGCC-3', and reverse

primer 5'-GTAGTCCTTGATGAGACGC-3'. PCR fragments were analyzed by electrophoresis on 1% (w/v) agarose.

*Pull-down assays*

RGS2 pGex-KG and HA-RGS2, HA-ΔN-RGS2 and empty pGex 6p-2 constructs were transformed in *Escherichia coli* BL21 and glutathione *S*-transferase (GST) fusion proteins were expressed and purified according to the manufacturer's protocol (Amersham Biosciences, Piscataway, NJ, USA). [$^{35}$S]Methionine-labeled TRPV6 N-tail was prepared using a reticulocyte lysate system (Promega, Madison, WI, USA) and analyzed for pull-down with GST, GST-HA-RGS2 or GST-HA-ΔN-RGS2 fusion proteins immobilized on glutathione-Sepharose 4B beads (Amersham Biosciences, Piscataway, NJ) as described previously (16). After extensive washing, bound proteins were subjected to sodium dodecyl sulfate-polyacrylamide gel electrophoresis (SDS-PAGE), and visualized by Coomassie staining and autoradiography. For pull-down with hRGS2; TRPV6/mock, SPL/mock, and TRPV6/SPL were transiently transfected in human embryonic kidney 293 (HEK293) cells and after 72 hours extracts from lyzed cells were adjusted to equal input concentrations and analyzed for pull-down with GST or GST-hRGS2 fusion proteins immobilized on gluthatione-Sepharose 4B beads. The beads were washed extensively and pulled proteins were analyzed by SDS-PAGE and immunoblotting.

*Electrophysiology and solutions*

The full-length cDNAs encoding TRPV5, TRPV6, RGS2, and ΔN-RGS2 were transiently transfected in HEK293 cells and patch-clamp experiments were performed in the tight-seal whole-cell configuration at room temperature using an EPC-9 patch-clamp amplifier controlled by the Pulse software (HEKA Elektronik, Lambrecht, Germany), as described previously (25). Cells were held at +20 mV, and voltage ramps of 450 milliseconds, ranging from -100 to +100 mV, were applied every 5 seconds. Cell capacitance and access resistance were monitored continuously using the automatic capacitance compensation of the Pulse software. $Na^+$ current densities were obtained by dividing the current amplitude measured at -80 mV during the ramp protocols by the cell capacitance. $Ca^{2+}$-dependent inactivation was studied using a 3 seconds voltage step to -100 mV from a holding potential of +70 mV. From this step protocol, $Ca^{2+}$ peak values were extracted by dividing the current at -100 mV by the cell capacitance. The standard extracellular solution (Krebs) contained: 150 mM NaCl, 6 mM CsCl, 1 mM $MgCl_2$, 10 mM HEPES/NaOH, and 10 mM glucose, pH 7.4. The concentration of $Ca^{2+}$ ranged between 1 and 10 mM. Divalent free (DVF) solutions did not contain added divalent cations, whereas trace amounts of divalent cations were removed with 100 µM EDTA. The standard internal (pipette) solution contained: 20 mM CsCl, 100 mM Cs-aspartate, 1 mM $MgCl_2$, 4 mM $Na_2ATP$, 10 mM BAPTA, 10 mM HEPES/CsOH, pH 7.2. Cells were kept in a nominal $Ca^{2+}$-free medium to

prevent $Ca^{2+}$ overload and exposed for a maximum of 5 minutes to a Krebs solution containing 1.5 mM $Ca^{2+}$ before sealing the patch pipette to the cell. The analysis and display of patch-clamp data were performed using Igor Pro software (WaveMetrics, Lake Oswego, USA).

*Biotinylation*

TRPV6, HA-RGS2 and empty pCINeo/IRES-GFP constructs were transfected transiently in HEK293 cells and subjected to cell surface biotinylation as described previously (26). Biotinylated proteins were eluted with SDS-PAGE loading buffer, separated on 10% (w/v) SDS-PAGE gel, and analyzed by immunoblotting with rabbit antiserum against TRPV6 (1:2000) (11).

*Statistical Analysis*

In all experiments, the data are expressed as mean ± SEM. Overall statistical significance was determined by analysis of variance. In case of significance ($P < 0.05$), individual groups were compared using a Student's *t* test.

## RESULTS

*Identification of RGS2 as a TRPV6-associated protein*

To identify proteins that interact with TRPV6, the N-terminal tail of TRPV6 was used to screen a library of mouse kidney cDNA by the yeast-two-hybrid technique. RGS2 was identified as a positive clone and belongs to the R4 subfamily of Regulator of G-protein Signaling proteins (27). To confirm the interaction, the full-length cDNA sequence of RGS2 was re-analyzed in a yeast-two-hybrid with the N-tail of TRPV6 as bait. The γ-subunit of the epithelial $Na^+$ channel (γENaC) was used as a negative control. TRPV6 and RGS2 displayed a strong interaction whereas TRPV6 and γENaC did not interact (data not shown).

*The RGS2 gene is ubiquitously expressed*

The expression of RGS2 in different mouse tissues was analyzed by RT-PCR. RGS2 was detected ubiquitously **(Figure 1, upper panel)**. All tissues expressed β-actin that was used as a positive control to confirm the integrity of the cDNAs **(Figure 1, lower panel)**. As negative controls, the primer sets for RGS2 and β-actin were screened in the absence of cDNA (depicted as $H_2O$ samples in **Figure 1**).

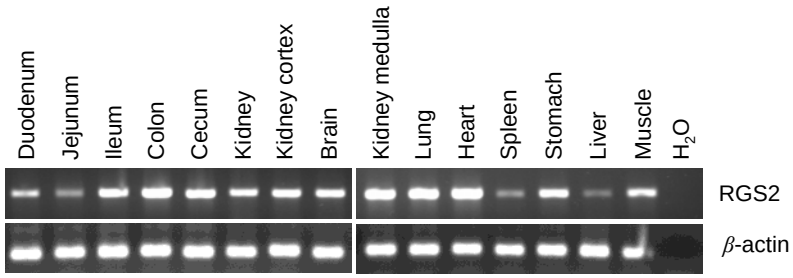


**Figure 1. Tissue distribution of RGS2.** RNA was extracted from different mouse tissues and RGS2 expression was determined by RT-PCR. The RGS2 specific band was amplified from all the indicated tissues (*upper panel*). As a control, β-actin was amplified to ensure the integrity of the cDNAs (*lower panel*).

*TRPV6 interacts with the N-terminal domain of RGS2*

The interaction between TRPV6 and the binding domain of RGS2 was further established using GST pull-down assays. To this end, RGS2 and ΔN-RGS2 were expressed as GST fusion proteins immobilized on gluthatione sepharose 4B beads. Subsequently, these fusion proteins were tested for their interaction with *in vitro* translated [$^{35}$S]methionine-labeled N-tail of TRPV6 in the presence or absence of 1 mM $Ca^{2+}$. As shown in **Figure 2**, the N-tail of TRPV6 associated with GST-fused RGS2 in a $Ca^{2+}$-independent fashion whereas no binding between the N-tail of TRPV6 and GST-fused ΔN-RGS2 or GST alone was observed, neither in the presence nor absence of $Ca^{2+}$.

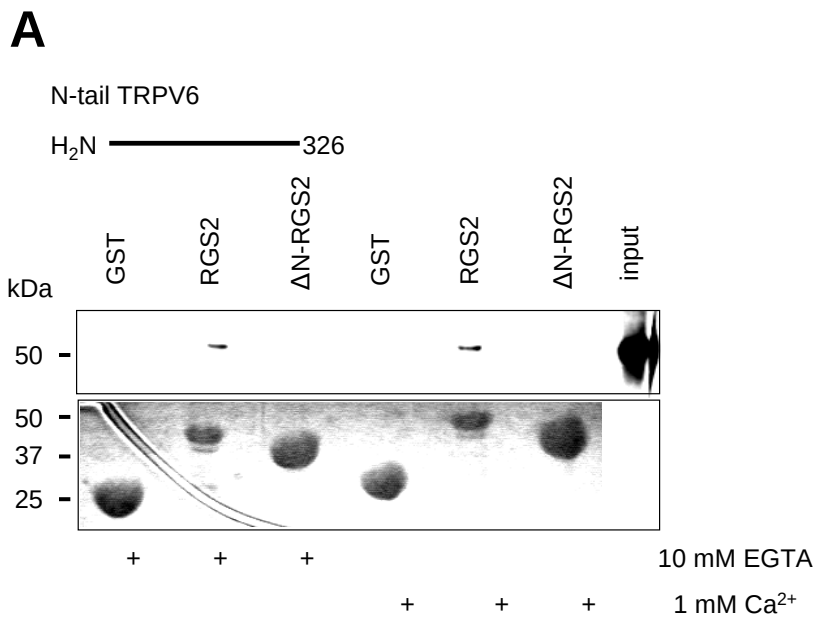


**Figure 2. Interaction of TRPV6 and RGS2.** [$^{35}$S]Methionine labeled TRPV6 N-tail was incubated with GST, GST/RGS2 or GST/ΔN-RGS2 immobilized on glutathione-sepharose 4B beads, either in the presence (1 mM $Ca^{2+}$) or absence (10 mM EGTA) of $Ca^{2+}$. TRPV6 N-tail interacted with RGS2 whereas no binding with GST/ΔN-RGS2 or GST alone was observed.

*RGS2 inhibits specifically TRPV6 activity*

To study the functional effect of RGS2 binding to TRPV6 the electrophysiological properties of the TRPV6 channel were investigated in the presence of RGS2. Steeply inward rectifying currents carried by $Na^+$ could be measured in HEK293 cells co-expressing TRPV6 and empty vector (mock) and in cells expressing both TRPV6 and RGS2 **(Figure 3A,B**). The current carried by $Na^+$ was significantly reduced in cells expressing both TRPV6 and RGS2 (**Figure 3B,C,** n = 15 cells, $P < 0.001$).

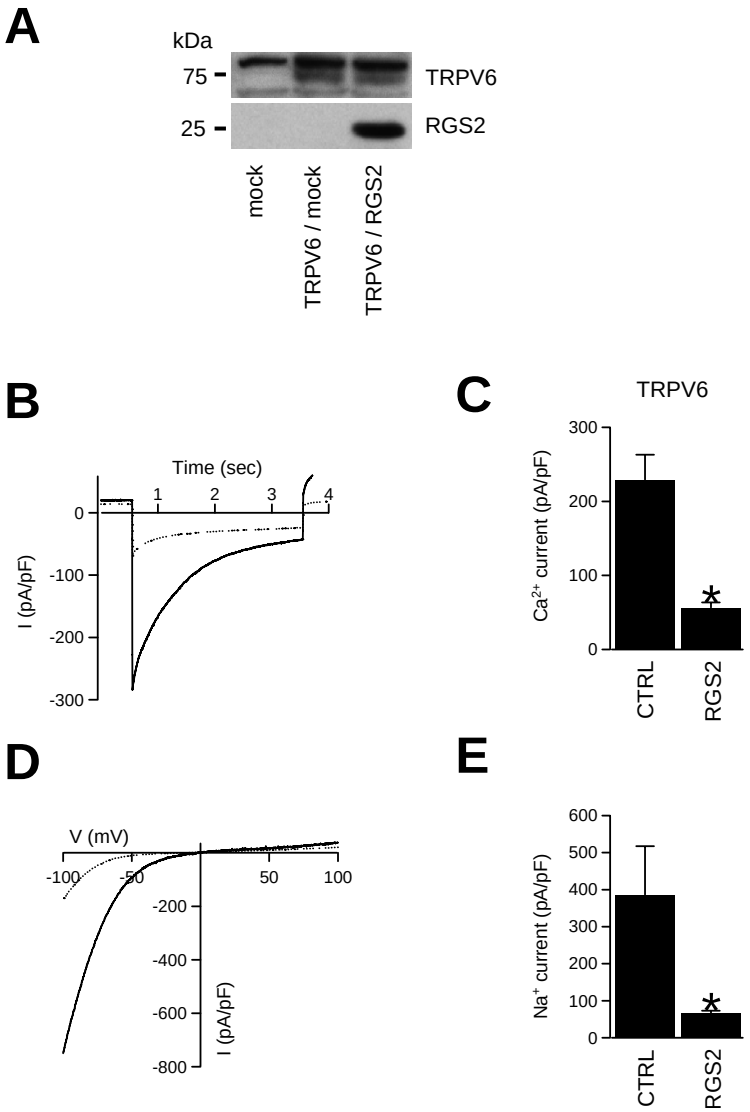


**Figure 3. Inhibition of TRPV6-induced $Na^+$ and $Ca^{2+}$ currents by RGS2.** HEK293 cells were transiently transfected with TRPV6/mock (CTRL) or TRPV6/RGS2 and subsequently analyzed by immunoblotting **(A)** and by whole-cell patch-clamp. **(B)** Current-voltage (I-V) relations measured from ramp protocol in nominally DVF solution from CTRL (solid trace) or TRPV6/RGS2-transfected cells (dotted trace). The I-V curve shows inward rectification typical for TRPV6 (solid trace), which is not changed by co-expressing RGS2 (dotted trace). **(C)** Average $Na^+$ current density at -80 mV in nominally DVF solution was 384 ± 133 pA/pF for CTRL cells compared to 65 ± 8 pA/pF for TRPV6/RGS2 co-expressing cells (n = 15 cells for each condition). **(D)** Averaged $Ca^{2+}$ currents measured with 10 mM $Ca^{2+}$ in the extracellular solution using the step protocol in CTRL cells (solid trace) and TRPV6/RGS2 co-expressing cells (dotted trace). **(E)** Average density of the $Ca^{2+}$ peak current measured as in **(D)** was 228 ± 35 pA/pF for CTRL compared to 56 ± 8 pA/pF for cells co-transfected with TRPV6 and RGS2 (n = 15 cells for each condition). * indicates significant difference ($P < 0.001$).

Likewise, RGS2 co-expression significantly reduced the $Ca^{2+}$ current in response to a hyperpolarizing voltage step in TRPV6-expressing cells (**Figure 3D,E**, n = 15 cells, $P < 0.001$), while the $Ca^{2+}$-dependent inactivation of the currents remained unchanged. In addition, the inhibitory effect of RGS2 on TRPV6-mediated $Na^+$ and $Ca^{2+}$ currents was studied for its closest relative, TRPV5, during identical experimental conditions. In contrast to TRPV6, RGS2 had no significant effect on $Na^+$ and $Ca^{2+}$ currents recorded from TRPV5-expressing HEK293 cells **(Figure 4)**.

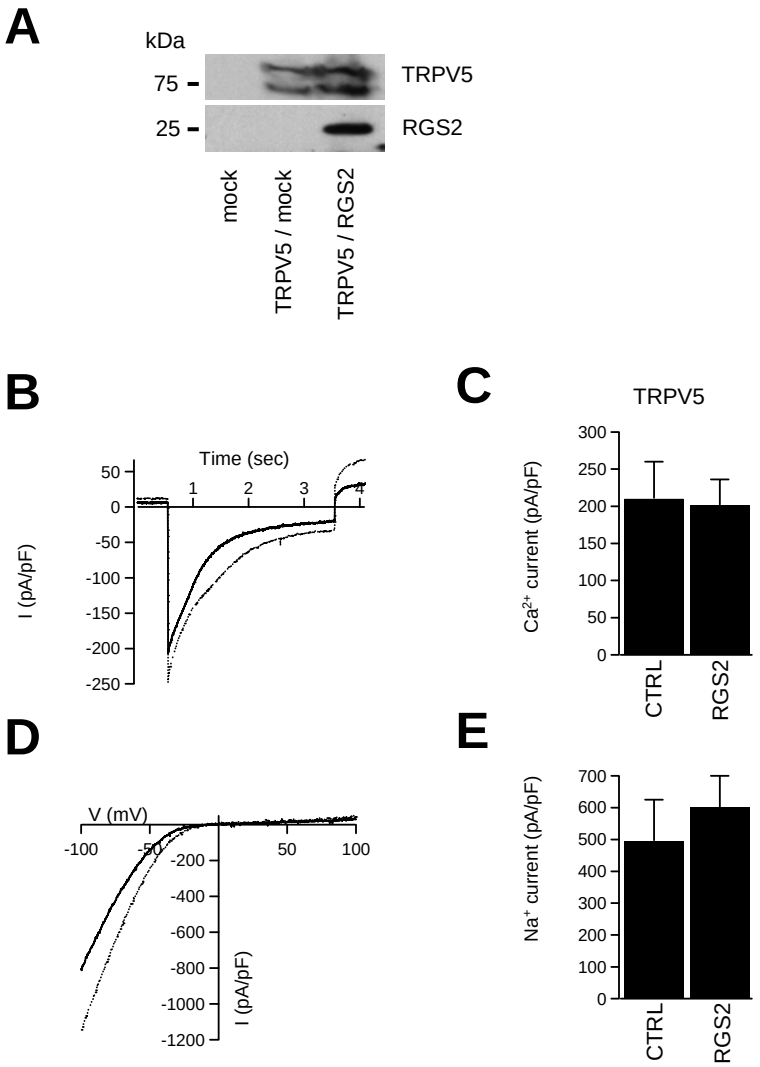


**Figure 4. Activity of TRPV5 is not affected by co-expressing RGS2.** HEK293 cells were transiently transfected with TRPV5/mock (CTRL) or TRPV5/RGS2 and analyzed using immunoblotting **(A)** and by whole-cell patch-clamp. **(B)** I-V relations measured from ramp protocol in nominally DVF solution in CTRL (solid trace) or TRPV5/RGS2-transfected cells (dotted trace). **(C)** Average $Na^+$ current density at -80 mV in nominally DVF solution was 495 ± 130 pA/pF for CTRL cells compared to 600 ± 100 pA/pF for TRPV5/RGS2 co-expressing cells (n = 15 cells for each condition). **(D)** Averaged $Ca^{2+}$ currents measured with 10 mM $Ca^{2+}$ in the extracellular solution using the step protocol in CTRL cells (solid trace) and TRPV5/RGS2-expressing cells (dotted trace). **(E)** Average density of the $Ca^{2+}$ peak current measured as in **(D)**, was 210 ± 50 pA/pF for CTRL compared to 201 ± 35 pA/pF for cells co-transfected with TRPV5 and RGS2 (n = 15 cells for each condition).

*TRPV6 activity is inhibited by the N-terminal domain of RGS2*

To test the physiological significance of the N-terminal domain of RGS2 on TRPV6 activity, the electrophysiological properties of TRPV6-mediated currents in HEK293 cells co-expressing either RGS2 or ΔN-RGS2 were determined. Inward rectifying currents carried by $Na^+$ could be measured in HEK293 cells co-transfected with TRPV6 and ΔN-RGS2 or RGS2, or with TRPV6 and mock **(Figure 5A,B)**. The $Na^+$ currents were significantly reduced in cells co-expressing TRPV6 with RGS2 whereas cells co-expressing ΔN-RGS2 and TRPV6 did not show this reduction (**Figure 5B,C**, n = 10 cells, $P < 0.001$). Likewise, RGS2 significantly reduced the $Ca^{2+}$ current in response to a hyperpolarizing voltage step in TRPV6-expressing cells (**Figure 5D,E**,

n = 10 cells, *P* < 0.001) whereas co-expression of ΔN-RGS2 with TRPV6 had no effect on the TRPV6-mediated current amplitude.

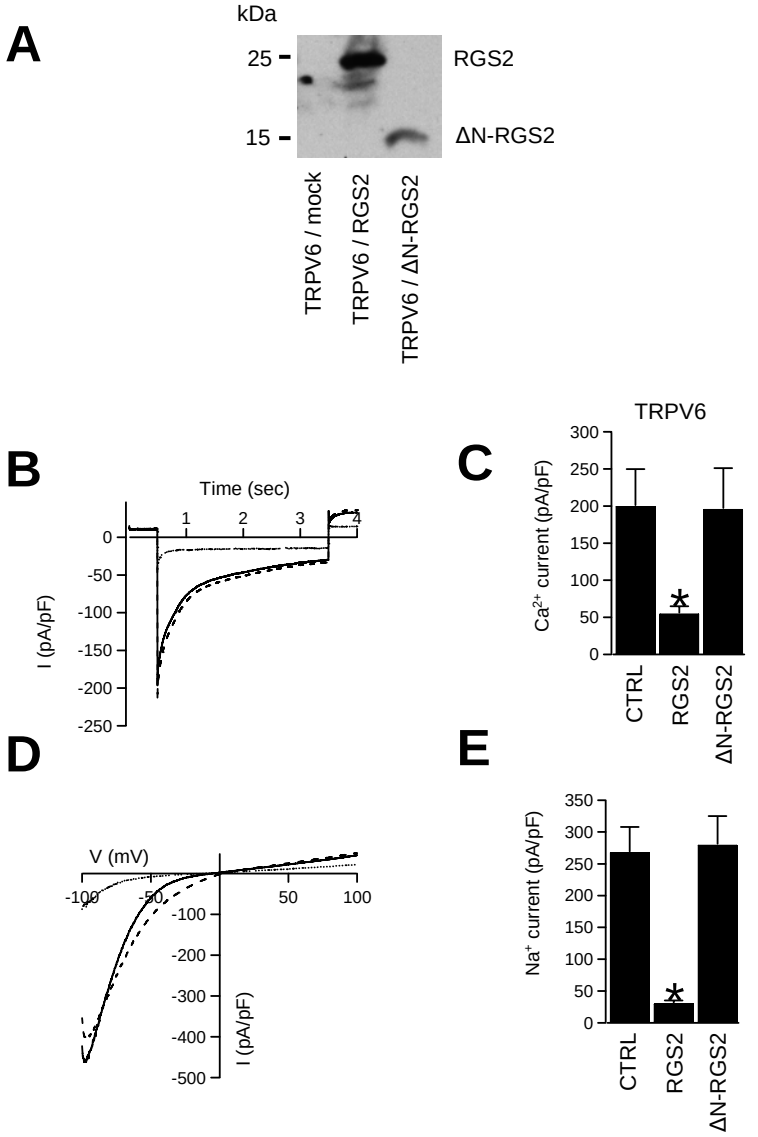


**Figure 5. Inhibition of TRPV6-mediated $Na^+$ and $Ca^{2+}$ currents by RGS2, but not ΔN-RGS2.** HEK293 cells were transiently transfected with TRPV6/mock (CTRL) or TRPV6 and RGS2 or ΔN-RGS2 and analyzed using immunoblotting **(A)** and by whole-cell patch-clamp. **(B)** I-V relations measured from ramp protocol in nominally DVF solution from CTRL (solid trace), TRPV6/RGS2-transfected cells (dotted trace) and TRPV6/ΔN-RGS2-transefected cells (dashed trace). **(C)** Average $Na^+$ current density at -80 mV in nominally DVF solution was 268 ± 40 pA/pF for CTRL, 30 ± 5 pA/pF for cells transfected with TRPV6 and RGS2 and 280 ± 45 pA/pF for TRPV6/ΔN-RGS2-transfected cells (n = 10 cells for each condition). **(D)** Averaged $Ca^{2+}$ currents measured with 10 mM $Ca^{2+}$ in the extracellular solution using the step protocol in CTRL cells (solid trace), TRPV6/RGS2-expressing cells (dotted trace) and TRPV6/ΔN-RGS2 co-expressing cells (dashed trace). **(E)** Average density of the $Ca^{2+}$ peak current measured as in **(D)**, was 200 ± 50 pA/pF for CTRL, 55 ± 10 pA/pF for TRPV6/RGS2 co-expressing cells and 196 ± 55 pA/pF for TRPV6/ΔN-RGS2 co-expressing cells (n = 10 cells for each condition). * indicates significant difference (*P* < 0.001).

*RGS2 does not affect TRPV6 abundance at the plasma membrane*

To investigate whether RGS2 influences trafficking of TRPV6, cell surface expression of TRPV6 in HEK293 cells co-expressing RGS2 and TRPV6 was examined using Sulfo-NHS-LC-LC-Biotin. TRPV6 was detected in total cell lysates of TRPV6-expressing cells as well as in the biotinylated plasma membrane fractions of TRPV6 and TRPV6/RGS2 co-expressing cells

**(Figure 6)**. TRPV6 expression in the biotinylated membrane fraction was not significantly altered by co-expression of RGS2.

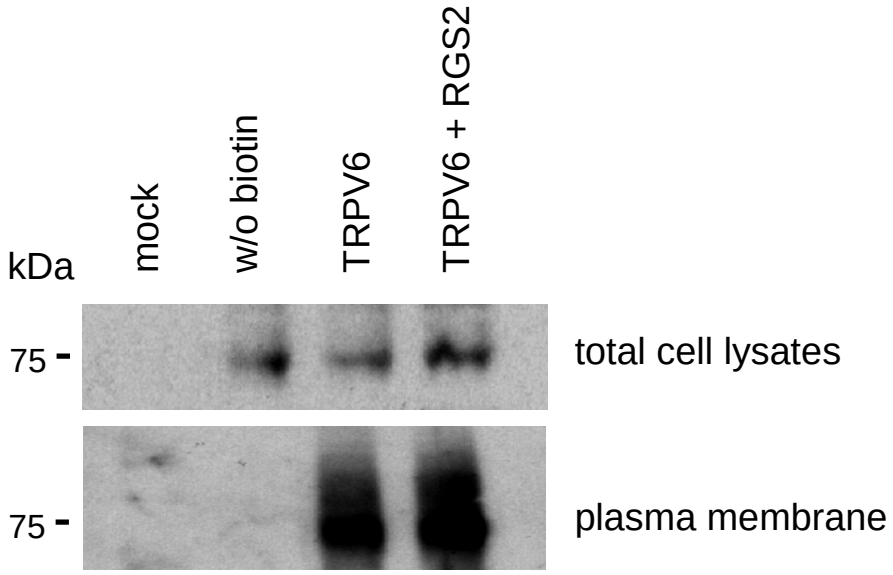


**Figure 6. Cell-surface expression of TRPV6.** HEK293 cells were transfected with TRPV6 ± RGS2. The extracellular parts of the proteins were biotinylated, precipitated with neutravidin beads, and immunoblotted for TRPV6. Samples of the lysed cells ("total cell lysates", **left panel**) were immunoblotted in parallel to visualize the amount of expressed proteins. Both TRPV6 alone and TRPV6 with RGS2-transfected cells showed cell surface expression, whereas mock-transfected cells did not ("plasma membrane", **right panel**).

*TRPV6 is independently regulated from the scaffolding protein SPL*

The effect of SPL on the interaction of RGS2 with TRPV6 was investigated by GST pull-down assay. Total cell lysates of HEK293 cells transiently transfected with TRPV6, SPL, or TRPV6 and SPL, were prepared and equal amounts of protein were analyzed for the interaction with RGS2. As indicated in **Figure 7**, TRPV6 associated with RGS2 both in the presence or absence of SPL.

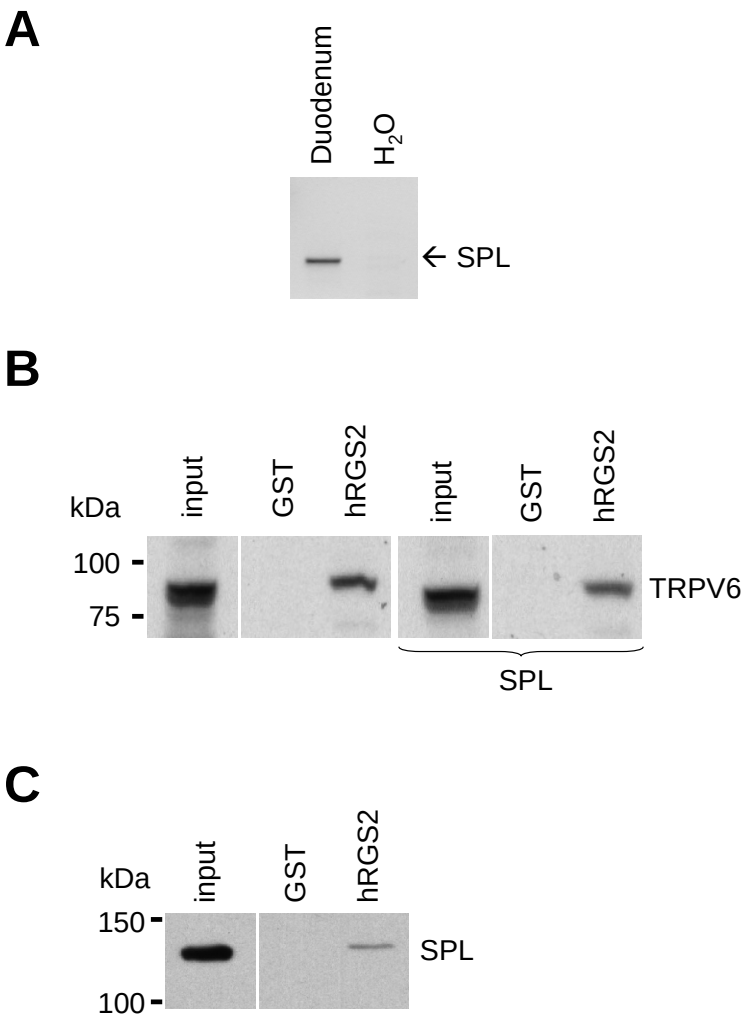


**Figure 7. Effect of SPL on the interaction of RGS2 and TRPV6.** Extracts from HEK293 cells transfected with TRPV6 and SPL were used for pull-down assay with GST or GST fused to RGS2. Pulled proteins were analyzed for TRPV6 **(top panel)** and SPL **(lower panel)** expression by immunoblotting.

Next, the electrophysiological properties of TRPV6-mediated currents were examined by whole cell patch-clamp in HEK293 cells co-expressing TRPV6 and SPL or TRPV6 and mock. Co-expression of SPL and TRPV6 had no significant effect either on $Na^+$ or $Ca^{2+}$ currents (n = 12 cells for each condition) as depicted in **Figure 8**.

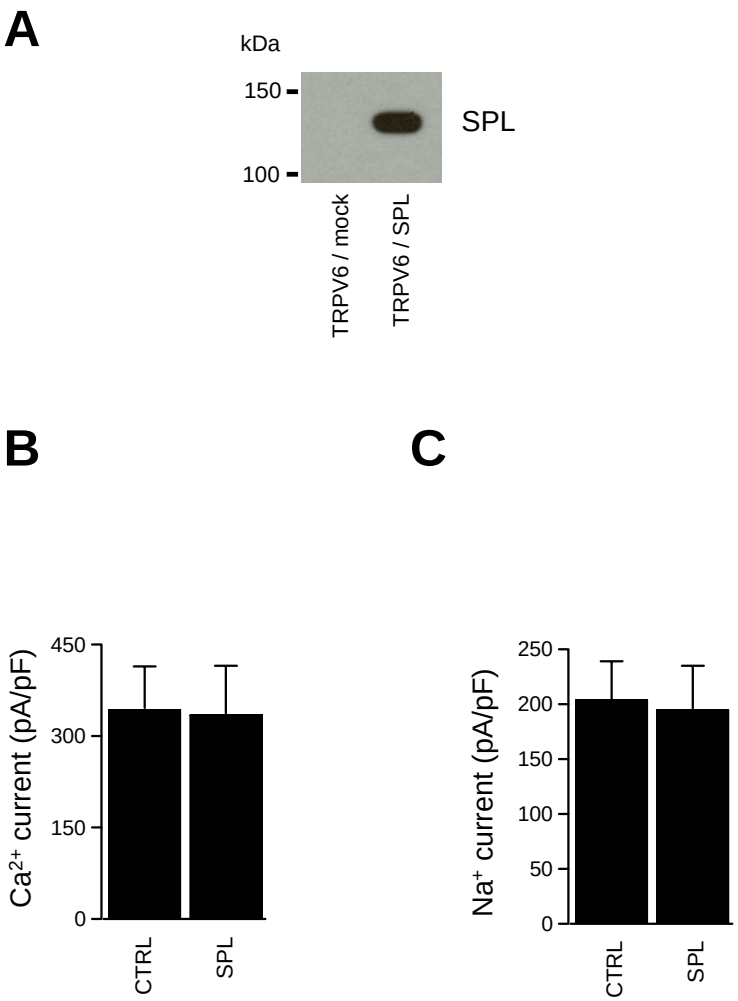


**Figure 8. Activity of TRPV6 is not affected by SPL.** HEK293 cells were transiently transfected with TRPV6/mock (CTRL) or TRPV6/SPL and analyzed by immunoblotting and by whole-cell patch clamp. Average $Na^+$ current density measured at -80 mV from the ramp protocol was 344 ± 70 pA/pF for CTRL and 335 ± 80 pA/pF for TRPV6/SPL co-expressing cells and average density of the $Ca^{2+}$ peak current measured from the step protocol was 204 ± 35 pA/pF for CTRL and 195 ± 40 pA/pF for TRPV6/SPL co-expressing cells (n = 12 cells for each condition).

**DISCUSSION**

The present study demonstrates a novel regulatory function of RGS2 by direct inhibition of TRPV6 channel activity at the plasma membrane. This conclusion is based on the following experimental data. First, interaction of RGS2 with TRPV6 specifically inhibits both $Na^+$ and $Ca^{2+}$ currents through TRPV6 whereas no effect on TRPV5 activity was observed. Second, deletion of the N-terminal domain of RGS2 disrupts the binding with TRPV6 and restores the original electrophysiological properties of the channel. Third, RGS2 expression does not interfere with TRPV6 trafficking from and towards the plasma membrane (to mediate its inhibitory effect on channel activity). Fourth, the multi-domain scaffolding protein SPL does not affect binding and electrophysiological properties of TRPV6 in the presence of RGS2. Therefore, our data indicate that TRPV6 activity is regulated by RGS2 without the involvement of GPCR signaling.

We showed that the N-terminal tail of RGS2 is essential for the interaction with and the activity of TRPV6. The N-terminal domain has already been described to be an important regulatory site for RGS2. Together with the "RGS-box" domain, it is necessary for its effector protein interactions, *e.g.* GPCRs and/or auxiliary proteins such as SPL (23,28,29). In addition, the membrane targeting sequence has also been predicted in this domain (30,31).

Patch-clamp analysis of HEK293 cells transfected with TRPV6 or TRPV5 revealed that specifically TRPV6 activity is inhibited by co-expression of RGS2. Interestingly, an analogous inhibitory mechanism has only been found for CaM and TRPV6 (32). Since both $Na^+$ and $Ca^{2+}$ currents through TRPV6 were inhibited by RGS2, and thus affecting not specifically the $Ca^{2+}$ conductance of the channel, we expected a disturbed TRPV6 trafficking towards the cell surface. In contrast, cell surface biotinylation in TRPV6-expressing HEK293 cells demonstrated that RGS2 does not affect channel expression in the biotinylated fractions. Therefore, the inhibitory effect of RGS2 is presumably mediated directly at the plasma membrane.

RGS2 needs to be recruited towards the cell surface in order to affect the gating properties of TRPV6. Roy and co-workers (33) showed that G proteins recruit RGS proteins towards the plasma membrane. In their study, the abundance of RGS2 and RGS4 proteins at the plasma membrane was enhanced when the number of G proteins was increased or when they interacted with their GPCR. Also SPL has been shown to be involved in RGS protein recruitment (23). Investigating the role of SPL provided us with additional evidence for a direct effect of RGS2 on TRPV6 activity. Wang and co-workers (23) showed that SPL is a scavenger of RGS2 which forms a SPL-RGS2 protein complex that regulates $Ca^{2+}$ signaling by binding the third intracellular domain of GPCRs. In their study, the binding of RGS2 with the α-adrenergic receptor (AR) was investigated by GST pull-down analysis. The interaction between RGS2 and the AR was significantly increased in the presence of SPL. Furthermore, they observed that the inhibitory effect of RGS2 on $Ca^{2+}$-activated $Cl^-$ currents in parotid duct cells was increased in the presence of SPL. For this reason, we anticipated that SPL could increase the inhibitory effect of

endogenously present RGS2 on TRPV6 activity in HEK293 cells when acting via a $G\alpha_q$-coupled GPCR. RGS2 expression was confirmed in HEK293 cells by RT-PCR (data not shown). First, it was demonstrated that SPL does not change TRPV6 expression **(Figure 7, top panel)**. Second, TRPV6-mediated $Na^+$ and $Ca^{2+}$ currents were not affected by SPL as well **(Figure 8)**. Therefore, we conclude that the inhibitory effect of RGS2 on TRPV6 activity is independently regulated of a GPCR, but is rather mediated by direct interaction of RGS2 and TRPV6.

In conclusion, we have identified RGS2 as a novel regulatory protein specifically inhibiting the activity of the epithelial $Ca^{2+}$ channel TRPV6. Our findings may provide insight in the direct regulation of different TRP channels by interacted proteins at the plasma membrane.

**ACKNOWLEDGEMENTS**

We thank Dr. K.M. Druey (Molecular Signal Transduction Section, Laboratory of Allergic Diseases, National Institute of Allergy and Infectious Diseases, National Institutes of Health, Bethesda, Maryland 20892) for kindly providing the RGS2 antibody and J.A. Janssen for excellent technical assistance. This work was supported by the Dutch Organization of Scientific Research (NWO-ALW 814.02.001 and Zon-MW 016.006.001).

**REFERENCES**


1. Birnbaumer, L., Yildirim, E., and Abramowitz, J. *Cell Calcium.* 33: 419-432, 2003
2. Clapham, D. E. *Nature.* 426: 517-524, 2003
3. Montell, C. *Cell Calcium.* 33: 409-417, 2003
4. Putney, J. W., Jr. *Cell Calcium.* 34: 339-344, 2003
5. Montell, C., Birnbaumer, L., and Flockerzi, V. *Cell.* 108: 595-598, 2002
6. Hoenderop, J. G., Vennekens, R., Muller, D.*, et al. J Physiol.* 537: 747-761, 2001
7. Pedersen, S. F., Owsianik, G., and Nilius, B. *Cell Calcium.* 38: 233-252, 2005
8. Voets, T., Janssens, A., Prenen, J., Droogmans, G., and Nilius, B. *J Gen Physiol.* 121: 245-260, 2003
9. Voets, T., Janssens, A., Droogmans, G., and Nilius, B. *J Biol Chem.* 279: 15223-15230, 2004
10. Peng, J. B., Chen, X. Z., Berger, U. V.*, et al. J Biol Chem.* 274: 22739-22746, 1999
11. Nijenhuis, T., Hoenderop, J. G., van der Kemp, A. W., and Bindels, R. J. *J Am Soc Nephrol.* 14: 2731-2740, 2003
12. Wissenbach, U., Niemeyer, B. A., Fixemer, T.*, et al. J Biol Chem.* 276: 19461-19468, 2001
13. den Dekker, E., Hoenderop, J. G., Nilius, B., and Bindels, R. J. *Cell Calcium.* 33: 497-507, 2003
14. Hoenderop, J. G., Nilius, B., and Bindels, R. J. *Physiol Rev.* 85: 373-422, 2005
15. van de Graaf, S. F., Chang, Q., Mensenkamp, A. R., Hoenderop, J. G., and Bindels, R. J. *Mol Cell Biol.* 26: 303-312, 2006
16. Van de Graaf, S. F., Hoenderop, J. G., Gkika, D.*, et al. EMBO J.* 22: 1478-1487, 2003
17. van de Graaf, S. F., Hoenderop, J. G., van der Kemp, A. W., Gisler, S. M., and Bindels, R. J. *Pflugers Arch.* 452: 407-417, 2006
18. Erler, I., Hirnet, D., Wissenbach, U., Flockerzi, V., and Niemeyer, B. A. *J Biol Chem.* 279: 34456-34463, 2004
19. Mosavi, L. K., Cammett, T. J., Desrosiers, D. C., and Peng, Z. Y. *Protein Sci.* 13: 1435-1448, 2004
20. De Vries, L., Zheng, B., Fischer, T., Elenko, E., and Farquhar, M. G. *Annu Rev Pharmacol Toxicol.* 40: 235-271, 2000
21. Abramow-Newerly, M., Roy, A. A., Nunn, C., and Chidiac, P. *Cell Signal.* 18: 579-591, 2006
22. Nilius, B., Prenen, J., Hoenderop, J. G.*, et al. J Biol Chem.* 277: 30852-30858, 2002
23. Wang, X., Zeng, W., Soyombo, A. A.*, et al. Nat Cell Biol.* 7: 405-411, 2005
24. Van Abel, M., Hoenderop, J. G., Dardenne, O.*, et al. J Am Soc Nephrol.* 13: 2102-2109, 2002
25. Vennekens, R., Hoenderop, J. G., Prenen, J.*, et al. J Biol Chem.* 275: 3963-3969, 2000
26. Chang, Q., Hoefs, S., van der Kemp, A. W., Topala, C. N., Bindels, R. J., and Hoenderop, J. G. *Science.* 310: 490-493, 2005
27. Ross, E. M., and Wilkie, T. M. *Annu Rev Biochem.* 69: 795-827, 2000
28. Bernstein, L. S., Ramineni, S., Hague, C.*, et al. J Biol Chem.* 279: 21248-21256, 2004
29. Hague, C., Bernstein, L. S., Ramineni, S., Chen, Z., Minneman, K. P., and Hepler, J. R. *J Biol Chem.* 280: 27289-27295, 2005
30. Heximer, S. P., Lim, H., Bernard, J. L., and Blumer, K. J. *J Biol Chem.* 276: 14195-14203, 2001
31. Kehrl, J. H., and Sinnarajah, S. *Int J Biochem Cell Biol.* 34: 432-438, 2002
32. Lambers, T. T., Weidema, A. F., Nilius, B., Hoenderop, J. G., and Bindels, R. J. *J Biol Chem.* 279: 28855-28861, 2004
33. Roy, A. A., Lemberg, K. E., and Chidiac, P. *Mol Pharmacol.* 64: 587-593, 2003

# ***Chapter 6***

## Molecular determinants of permeation through the cation channel TRPM6

Catalin N. Topala[1], Wouter Tiel Groenestege[1], Stéphanie Thebault[1], Dennis van den Berg[1], Bernd Nilius[2], Joost G. Hoenderop[1] and René J. Bindels[1]

[1]Department of Physiology, Nijmegen Centre for Molecular Life Sciences, Radboud University Nijmegen Medical Centre, The Netherlands, [2]Department of Physiology, Campus Gasthuisberg, Catholic University Leuven, Belgium

*Cell Calcium.* 41: 513-523, 2007

**ABSTRACT**

TRPM6 and its closest relative TRPM7 are members of the Transient Receptor Potential Melastatin (TRPM) subfamily of cation channels and are known to be $Mg^{2+}$ permeable. By aligning the sequence of the putative TRPM6 pore with the pore sequences of the other subfamily members, we located in the loop between the $5^{th}$ and the $6^{th}$ transmembrane domain, a stretch of amino acids residues, $^{1028}$GEIDVC$^{1033}$, as the potential selectivity filter. Two negatively charged residues, $E^{1024}$ (conserved in TRPM6, TRPM7, TRPM1 and TRPM3) and $D^{1031}$ (conserved along the entire TRPM subfamily), were identified as important determinants of cation permeation through TRPM6, because neutralization of both residues into an alanine resulted in non-functional channels. Neutralization of $E^{1029}$ (conserved in TRPM6, TRPM7, TRPM4 and TRPM5) resulted in channels with increased conductance for $Ba^{2+}$ and $Zn^{2+}$, decreased ruthenium red sensitivity and larger pore diameter compared to wild-type TRPM6. Changing the residue $I^{1030}$ into methionine, resulted in channels with lower conductance for $Ni^{2+}$, decreased sensitivity to ruthenium red block and reduced pore diameter. Thus, these data demonstrate that amino acid residues $E^{1024}$, $I^{1030}$ and $D^{1031}$ are important for channel function and that subtle amino acid variation in the pore region accounts for TRPM6 permeation properties.

## INTRODUCTION

Beside being the most abundant intracellular cation after $K^+$, $Mg^{2+}$ is an important cofactor for many biological processes, such as protein synthesis, nucleic acid stability and neuromuscular excitability (1,2). $Mg^{2+}$ homeostasis involves the kidney as the primary regulatory site, the intestine as the absorption place, while the bone is the storage location (3). Transcellular $Mg^{2+}$ transport in renal and intestinal epithelia is of vital importance for overall $Mg^{2+}$ homeostasis. There is both a passive (paracellular) and an active (transcellular) mechanism for $Mg^{2+}$ (re)absorption in renal and intestine epithelia (2). However, the molecular mechanism of transcellular $Mg^{2+}$ transport is not fully understood. Recently, investigations in consanguineous families suffering from hypomagnesemia with secondary hypocalcemia (HSH) have identified mutations in the gene encoding the Transient Receptor Potential Melastatin 6 (TRPM6) protein as the cause of the disease (4,5). It was demonstrated that TRPM6 functions as a molecular determinant of transcellular $Mg^{2+}$ transport in renal and intestinal epithelia (6).

TRPM6 shares with its closest relative TRPM7 approximately 50% sequence homology at the amino acid level (6). Whereas TRPM7 appears to be ubiquitously expressed, TRPM6 expression is restricted to kidney and intestine (6), where it plays an important role in $Mg^{2+}$ (re)absorption (6). Consistent with a role in $Mg^{2+}$ homeostasis, we demonstrated recently that dietary $Mg^{2+}$ restriction upregulates TRPM6 expression in mice kidney, while a $Mg^{2+}$-enriched diet increases TRPM6 expression in colon (7). These diets did not affect TRPM7 expression levels in kidney and colon. Atypically for other ion channels, TRPM6 and TRPM7 contain a serine/threonine protein kinase domain at the C-terminus resembling that of elongation factor 2 (eEF-2) kinase and other α-kinases. The kinase function in channel regulation remains elusive (4,8-12).

Recently, we have functionally characterized TRPM6 using electrophysiological analysis (6). This protein forms constitutively active divalent selective cation channels, with a higher affinity for $Mg^{2+}$ than for $Ca^{2+}$ at physiological membrane potentials and divalent concentrations. TRPM6 becomes permeable to monovalent cations when all divalent cations are omitted from the extracellular solution. Despite this initial characterization of TRPM6, the molecular determinants of its $Mg^{2+}$ permeability remain unknown. Moreover, in a recent paper, Li *et al* described in detail the functional differences in divalent ion permeability between homomeric TRPM6, homomeric TRPM7 and heteromeric TRPM6/TRPM7 channel complexes demonstrating unequivocally that TRPM6 can form by itself functional channels without TRPM7 co-expression (13). The study also demonstrated that TRPM6 displays single channel conductance that is 2- and 1.5-fold bigger than TRPM7 and TRPM6/TRPM7 complexes.

To date there is limited knowledge about the structures of TRP channels pores and even less is known about TRPM channels pores. In a recent study Owsianik *et al* summarized the current knowledge about permeation and selectivity of TRP channels (14). They propose and describe

a general approach as a toolkit for characterizing the permeation and selectivity of ion channels. The aim of the present study was to identify the amino acid stretch responsible for $Mg^{2+}$ permeation of TRPM6. To this end, a combined approach consisting in site-directed mutagenesis and electrophysiological measurements was used to investigate the role of amino acid residues from the putative selectivity filter in the permeation properties of TRPM6. Our data indicate that a short amino acid stretch of the pore region, $^{1028}$GEIDVC$^{1033}$, determines the TRPM6 conductance properties and its sensitivity to the channel pore blocker, the hexavalent cation ruthenium red.

## EXPERIMENTAL PROCEDURES

*Molecular biology*

The full-length open reading frame from N-terminally HA-tagged human (h)TRPM6 was cloned as a *Bcl*I - *BspE*I fragment in the pCINeo/IRES-GFP vector (6). This bicistronic expression vector, pCINeo/IRES-GFP/HA-hTRPM6, was used to co-express hTRPM6 and enhanced GFP in Human Embryonic Kidney cells (HEK293). Mutagenesis of the amino acids $E^{1024}$, $E^{1029}$, $I^{1030}$, $D^{1031}$, $V^{1032}$ and of the TRPM6-TRPM4 and TRPM6-TRPV6 chimeric constructs was performed using QuickChange™ site-directed mutagenesis (Stratagene, La Jolla, USA). The sequence of each mutant was verified by sequence analysis of the corresponding cDNA.

*Cell culture and transfection*

HEK293 cells were grown in Dulbecco's modified Eagle's medium (Bio Whittaker-Europe, Verviers, Belgium) containing 10% (v/v) fetal calf serum, 2 mM L-glutamine and 10 µg/ml ciproxin at 37°C in a humidity-controlled incubator with 5% (v/v) $CO_2$. The cells were transiently transfected with the respective constructs using Lipofectamine 2000 (Invitrogen-Life Technologies, Breda, The Netherlands), as described previously (15), and electrophysiological recordings were performed 16 to 36 hours post-transfection. Transfected cells were identified by their green fluorescence when illuminated at 480 nm. Non-transfected (GFP-negative) cells from the same batch were used as controls.

*Electrophysiology*

Patch-clamp experiments were performed in the tight-seal whole-cell configuration at room temperature (20-25°C) using an EPC-9 patch-clamp amplifier computer controlled by Pulse software (HEKA Electronik, Lambrecht, Germany). Patch pipettes had resistances between 2 and 4 MΩ after filling with the standard intracellular solution. Cells were held at 0 mV, and voltage ramps of 450 ms ranging from -100 to +100 mV were applied every 2 s. Cell capacitance and access resistance were continuously monitored using the automatic capacitance compensation of the Pulse software package. Extracting the current amplitudes at +80 and -80 mV from individual ramp current records assessed the temporal development of membrane currents. Current densities were obtained by normalizing the current amplitude to the cell membrane capacitance.

*Solutions*

The standard pipette solution contained (in mM): 150 NaCl, 10 EDTA, and 10 HEPES (pH 7.2 adjusted with NaOH). The extracellular solution contained (in mM): 150 NaCl and 10 HEPES (pH 7.4 adjusted with NaOH), supplemented with either 1 mM $CaCl_2$ (to assess the time-course for development of currents), 10 mM EDTA (divalent-free solutions, DVF), or the same

concentration of divalent cations (for the permeation profile determinations). The relative permeabilities ($P_X/P_{Na}$) of mono-, di-, tri-, and tetramethyl ammonium substituents and of *N*-methyl-*D*-glucamine (NMDG) were measured using solutions in which all $Na^+$ was substituted by the respective cations and calculated from the biionic reversal potentials (16). All potentials were corrected for possible liquid junction potentials, which were calculated according to Barry (17). In these permeation experiments, the standard pipette solution was used as intracellular solution. For the ammonium derivates, the following compounds diameters were used (in nm): 0.36, 0.46, 0.52, 0.58, and 0.68 for monomethylammonium ($MA^+$), dimethylammonium ($DMA^+$), trimethylammonium ($TriMA^+$), tetramethylammonium ($TetMA^+$), and for $NMDG^+$ respectively. To fit the points from the graph plotting permeability ratios of the different organic cations (X) *versus* their estimated diameters, the excluded volume considering friction of the permeating ion Equation 1 (18) was used:

$$P_X/P_{Na} = k(1 - a/d)^2/a$$

where *a* is the organic cation diameter, *k* is a constant factor and *d* the minimal pore diameter. The ammonium derivates were purchased from Sigma.

*Statistical Analysis*

Data analysis and graphs were prepared using IgorPro software (WaveMetrics, Lake Oswego, USA). Data are expressed as mean ± SEM. Overall statistical significance was determined by analysis of variance. In case of significance ($P < 0.05$), individual groups were compared using Student's *t* test.

## RESULTS

*Sequence analysis of the putative pore-forming region of TRPM6*

**Figure 1** shows a sequence alignment of the putative pore region of the TRPM subfamily. The structure of the loop between the 5$^{th}$ and the 6$^{th}$ transmembrane domains (TM5 and TM6) was modeled based on the $K^+$ channel KcsA crystal structure (19). In this region, TRPM6 shares the highest sequence homology with TRPM7, also known to conduct $Mg^{2+}$ when heterologously expressed in HEK293 cells (8,9,20). TRPM6 and TRPM7 contain two glutamate residues, $E^{1024}$ and $E^{1029}$ (*highlighted yellow* in **Figure 1**).

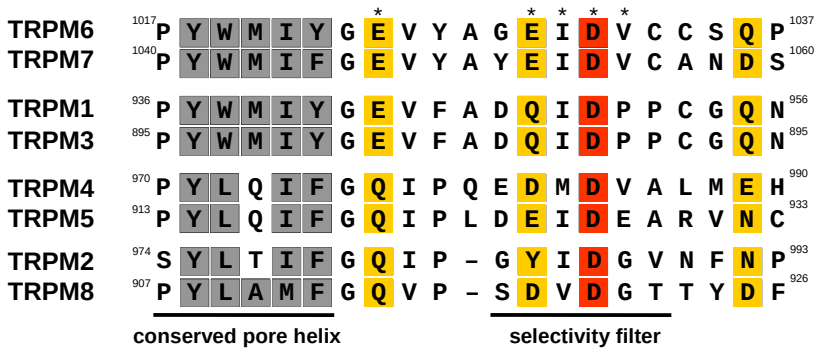


**Figure 1. The putative pore-forming region of TRPM6.** Alignment of the putative pore sequences of the TRPM subfamily on the rows, which represent the amino acid sequences from the respective human TRPM subfamily channels. The GenBank accession numbers are: NP_002411, AAY22174, NP_066003, NP_060106, NP_055370, NP_060132, NP_060142, and NP_076985 starting from TRPM1 to TRPM8. The highly conserved hydrophobic residues are highlighted in *grey*, the conserved aspartate is shown in *red*, and the conserved residues with polar or charged groups are shown in *yellow* (adapted from (24,35)). Asterisks denote the amino acid residues mutated in this study.

The $E^{1024}$ is conserved in TRPM1 and TRPM3. In addition, TRPM6 shares an aspartate residue $D^{1031}$ (*highlighted red* in **Figure 1**) with all the other members of the TRPM subfamily. To assess the contribution of these amino acid residues in the permeation properties of TRPM6, these residues were neutralized by alanine substitution (mutants $E^{1024}A$, $E^{1029}A$, and $D^{1031}A$). To delineate the role of the conserved aspartate residue ($D^{1031}$), adjacent amino acids were mutated. $I^{1030}$ was substituted by a methionine in order to mimic the pore properties of the monovalent selective channel TRPM4 (mutant $I^{1030}M$), and the $V^{1032}$ was substituted by an alanine (mutant $V^{1032}A$). The positions for the amino acid residues mutated for this study are marked with asterisks in **Figure 1**.

*Functional characterization of TRPM6 pore mutants*

To determine which amino acids in the pore region account for the permeation properties of TRPM6, the activation kinetics of wild-type channels were compared with those of the mutant proteins. The currents recorded from TRPM6-transfected cells reached a plateau level of 295 ± 40 pA/pF (n = 30 cells) within 100-200 s, while non-transfected (NT) cells (n = 10 cells) displayed only background current, probably endogenous TRPM7 (75 ± 27 pA/pF) that is activated over a longer period, as depicted in **Figure 2A**. When expressed in HEK293 cells, the

TRPM6 pore mutants showed three different phenotypes: $E^{1029}A$ displayed a time-course of activation and a current amplitude similar to wild-type TRPM6 (n = 10 cells) **(Figure 2B)**, $I^{1030}M$ and $V^{1032}A$ showed activation kinetics similar with TRPM6, while their current amplitudes were significantly reduced (178 ± 40 and 150 ± 45 pA/pF respectively *versus* 295 ± 40 pA/pF, $P < 0.05$, n = 10 cells for each mutant), as depicted in **Figure 2C** and **D**, and $E^{1024}A$ and $D^{1031}A$ showed no current (n = 5 cells) **(Figure 2E)**. Mutations in the pore region of TRPM6 did not change the current-voltage properties of the currents as summarized in **Figure 2F**.

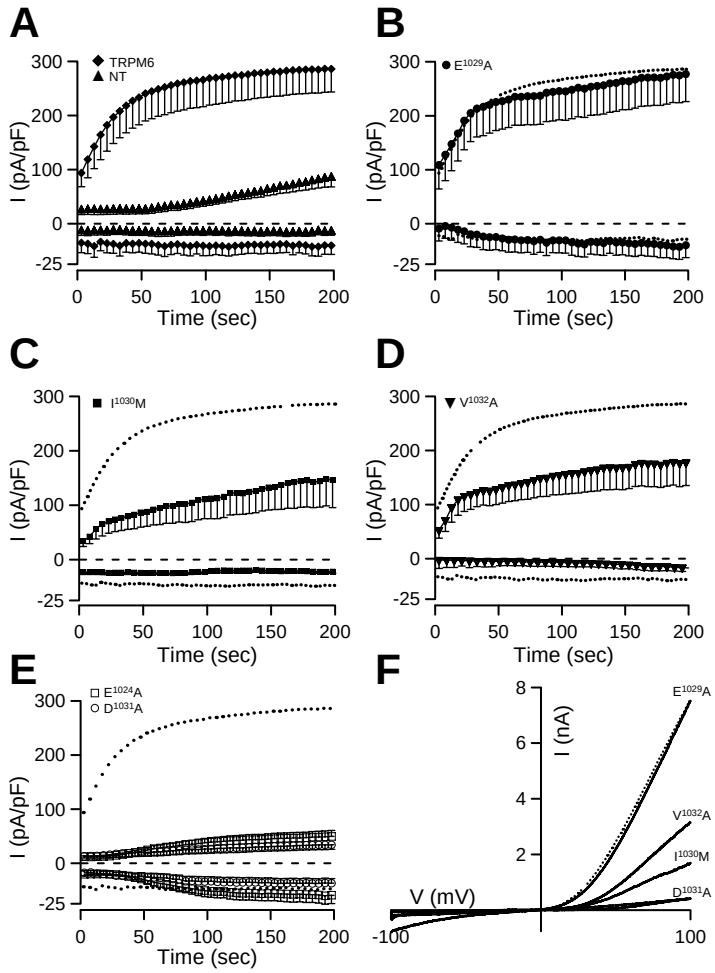


**Figure 2. Functional expression of wild-type TRPM6 and pore mutant proteins. (A)** Average time-course of inward (at -80 mV) and outward currents (at +80 mV) development from cells expressing wild-type TRPM6 (♦), and non-transfected cells (NT ▲). **(B-E)** Average time course of inward and outward currents development from cells expressing the mutant $E^{1029}A$ **(B)**, $I^{1030}M$ **(C)**, $V^{1032}A$ **(D)**, $E^{1024}A$ (□) and $D^{1031}A$ (○) **(E)**; the dotted line indicates the averaged time course for wild-type TRPM6. **(F)** Current-voltage relations from cells transfected with either TRPM6, or mutant proteins as indicated, obtained under experimental conditions as in other panels, measured 200 s after whole-cell establishment.

Interestingly, when co-expressed with wild-type TRPM6 in a 1:1 cDNA ratio, $D^{1031}A$ showed a dominant negative effect since the currents recorded from these cells (n = 8 cells) were identical in the time-course of development, current-voltage relation and amplitude with the currents from NT cells as shown in **Figure 3**. The dominant negative effect of $D^{1031}A$ suggests that assembly with wild-type TRPM6 is not disturbed. Channel complexes containing wild-type and mutant

proteins could be retained at the endoplasmic reticulum or reach the plasma membrane showing defective pore architecture.

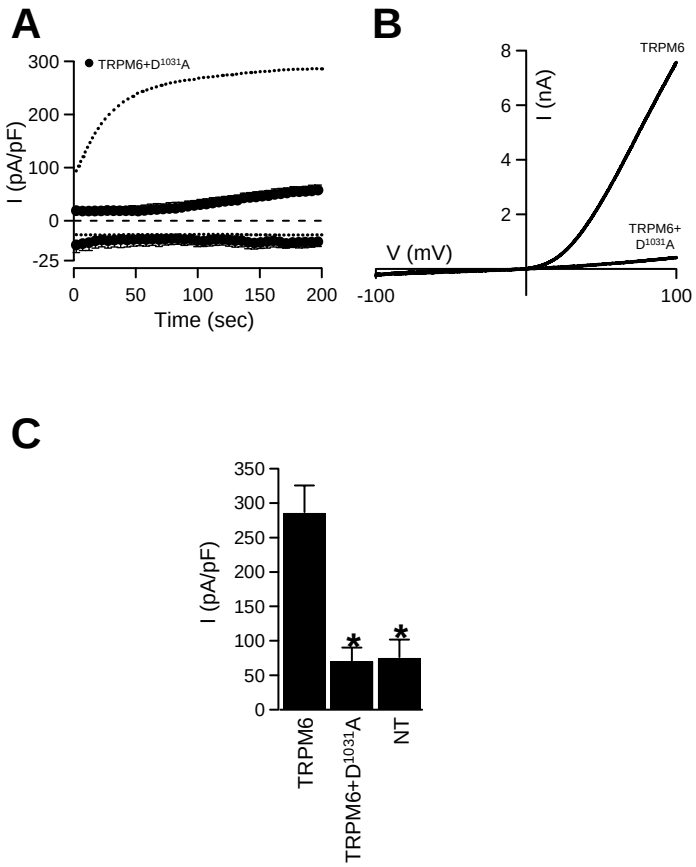


**Figure 3. Effect of co-expression of wild-type TRPM6 and the pore mutant $D^{1031}A$. (A)** Average time course of inward and outward currents development from cells expressing wild-type TRPM6 (dotted line) or TRPM6 with the pore mutant $D^{1031}A$. **(B)** Current-voltage relations from HEK293 cells transfected with either wild-type TRPM6, or TRPM6 with the pore mutant $D^{1031}A$, measured 200 s after whole-cell establishment. **(C)** Histogram summarizing the currents amplitudes measured 200s after whole-cell establishment at +80 mV from NT cells, cells transfected with wild-type TRPM6 and cells transfected with TRPM6 together with the pore mutant $D^{1031}A$, asterisk denotes $P < 0.05$ versus wild-type TRPM6.

Likewise, expression of $D^{1031}A$ alone could have the same outcome as the co-expression with wild-type TRPM6. Despite repetitive attempts, the low abundance of TRPM6 proteins at the plasma membrane did not allow us to determine whether these proteins are expressed at the cell surface.

*Conductance profile of TRPM6 pore mutants*

To establish the conductance properties of TRPM6, we determined the permeation profile of the wild-type channel and the functional pore mutants. The permeation rank order of divalent cations compared to $Ca^{2+}$ was assessed by the ratio of inward current at -80 mV, when $Ca^{2+}$ ions are equimolar substituted by other divalent cations. When normalized to the inward current amplitude in the presence of 10 mM $Ca^{2+}$, the following conductance profile for TRPM6 was obtained: $Ba^{2+}$ (1.66) > $Ni^{2+}$ (1.16) > $Mg^{2+}$ (1.08) > $Zn^{2+}$ (1.01) ≥ $Ca^{2+}$ (1.00) (n = 5-8 cells) **(Figure 4A)**. The permeation rank order obtained for the mutant $E^{1029}A$ was: $Ba^{2+}$ (2.34) > $Zn^{2+}$

(1.29) > $Ni^{2+}$ (1.14) > $Mg^{2+}$ (1.08) > $Ca^{2+}$ (1.00) **(Figure 4B)**. The $E^{1029}A$ displayed an increased conductance to $Ba^{2+}$ and $Zn^{2+}$ compared to TRPM6. For the permeation rank order of the mutant $I^{1030}M$, the following values were obtained: $Ba^{2+}$ (1.74) > $Mg^{2+}$ (1.01) ≥ $Ca^{2+}$ (1.00) ≥ $Zn^{2+}$ (0.99) > $Ni^{2+}$ (0.92), (n = 5 cells) **(Figure 4C)**. The $I^{1030}M$ mutant had a lower conductance for $Ni^{2+}$ compared to TRPM6. These data are summarized in **Figure 4D**.

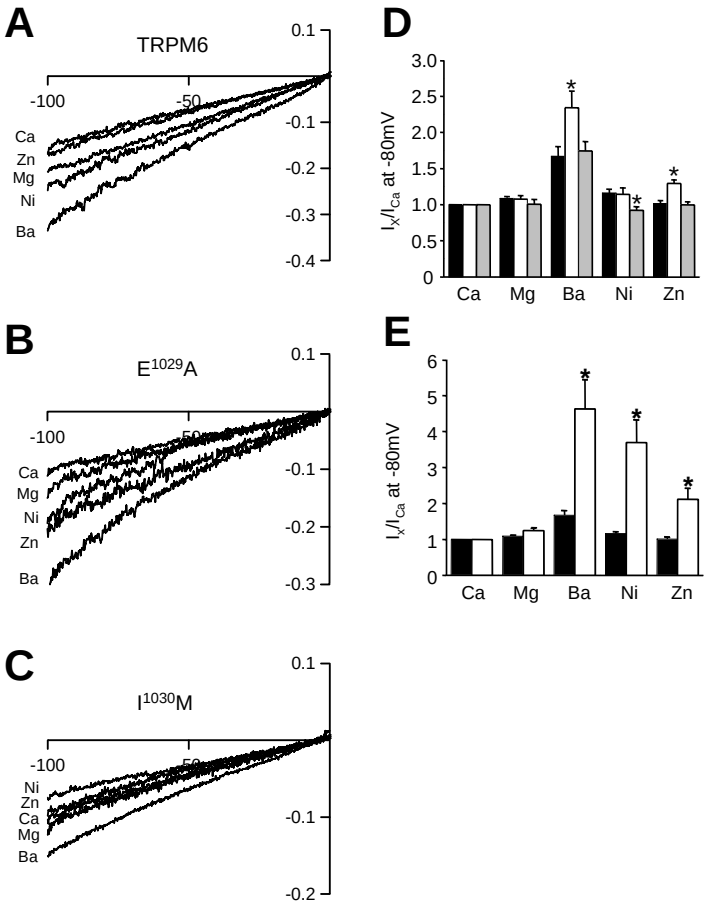


**Figure 4. Divalent permeation through wild-type TRPM6 and pore mutant proteins. (A-C)** Magnified views of the inward currents recorded with extracellular solutions containing 10 mM of the indicated divalent cations, from HEK293 cells expressing TRPM6 **(A)**, $E^{1029}A$ **(B)**, and $I^{1030}M$ **(C)**. **(D)** Histogram summarizing relative permeation rank order determined from the ratio of inward current for the indicated divalent cation, for TRPM6 (black bars) and pore mutants $E^{1029}A$ (white bars) and $I^{1030}M$ (grey bars), (asterisks represent $P < 0.05$ versus wild-type TRPM6). **(E)** Histogram summarizing the relative permeation profile for TRPM6 (black columns) and TRPM7 (white columns) determined from the ratio of inward current amplitude in the presence of the indicated divalent cation, and the inward current amplitude with $Ca^{2+}$ containing extracellular solution.

To further characterize the TRPM6 pore permeability, its permeation profile was compared with the homologous TRPM7 channel as previously described by Monteilh-Zoller *et al* (20). When normalized to the inward current amplitude in 10 mM $Ca^{2+}$, the following relative values were obtained for TRPM7: $Ba^{2+}$ (4.62) > $Ni^{2+}$ (3.69) > $Zn^{2+}$ (2.11) > $Mg^{2+}$ (1.24) > $Ca^{2+}$ (1.00) (n = 8 cells). This comparison, summarized in **Figure 4E**, revealed that TRPM6 and TRPM7 display different permeation rank orders in the way that TRPM6 has a higher conductance for $Mg^{2+}$ than TRPM7.

Next, the effect of micromolar concentrations of divalent cations ($Ca^{2+}$ and $Mg^{2+}$) present in the extracellular solutions on inward monovalent ($Na^{+}$) current was investigated. As shown in **Figure 5A,B** both $Mg^{2+}$ and $Ca^{2+}$ inhibited the TRPM6 current in the micromolar range. The concentration for half-maximal TRPM6 current inhibition ($IC_{50}$) was calculated from the dose-response curve for $Mg^{2+}$ (n = 5 cells for each point) **(Figure 5C)** and $Ca^{2+}$ (n = 5 cells for each point) **(Figure 5D)** and yielded values of 0.9 and 3.5 µM with Hill coefficients of 0.8 and 0.83 respectively.

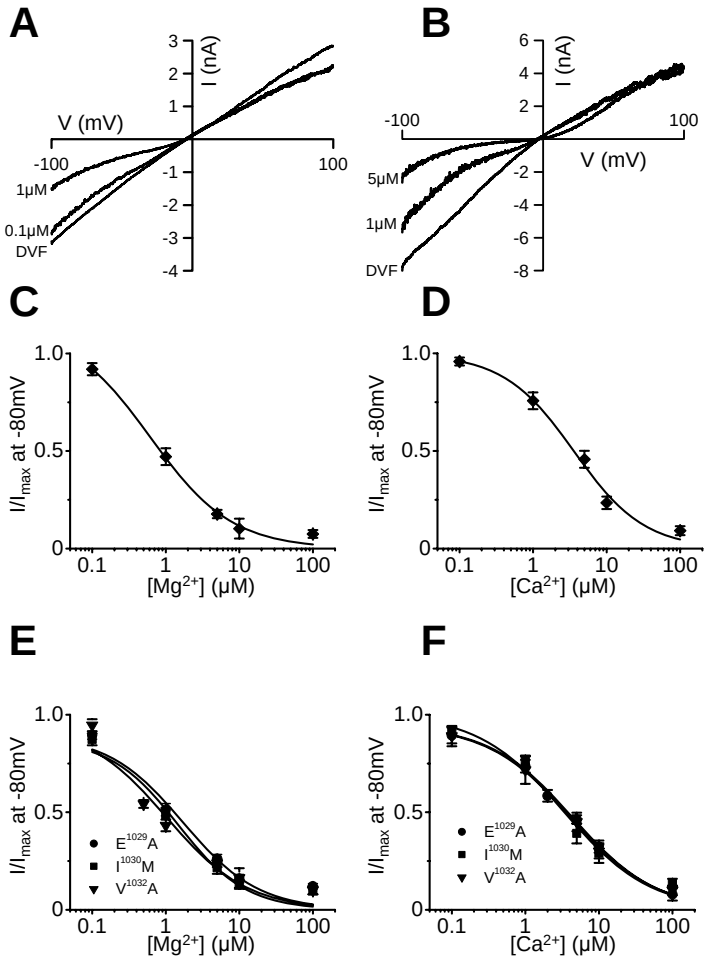


**Figure 5. $Mg^{2+}$ and $Ca^{2+}$ inhibit TRPM6-mediated inward monovalent currents. (A** and **B)** Current-voltage relations obtained from HEK293 cells expressing TRPM6 in divalent-free solution (DVF) and in the presence of 0.1 and 1 µM $Mg^{2+}$, or 1 and 5 µM $Ca^{2+}$. **(C)** Dose-response curve for the inhibition of inward monovalent current at -80 mV by $Mg^{2+}$. **(D)** Dose-response curve for the inhibition of inward monovalent current at -80 mV by $Ca^{2+}$. **(E** and **F)** Dose-response curves for the inhibition of inward monovalent current by $Mg^{2+}$ **(E)** and $Ca^{2+}$ **(F)** for the pore mutant proteins, $E^{1029}A$ (●), $I^{1030}M$ (■) and $V^{1032}A$ (▼).

These values were in concordance with the ones from our previous paper (6). For the pore mutants, the $IC_{50}$ for $Mg^{2+}$ sensitivity was (in µM): 1.1, 1.0, and 0.8, for $E^{1029}A$, $I^{1030}M$ and $V^{1032}A$, respectively **(Figure 5E)**, while the $IC_{50}$ for $Ca^{2+}$ sensitivity for the pore mutants was (in µM): 3.4, 3.6 and 3.4 for $E^{1029}A$, $I^{1030}M$ and $V^{1032}A$, respectively **(Figure 5F)**. No significant differences were observed between the pore mutants and wild-type TRPM6.

*Effect of pore mutations on TRPM6 ruthenium red sensitivity*

As previously demonstrated, TRPM6 can be blocked by the hexavalent cation ruthenium red (RR) in a voltage-dependent manner (6). As depicted in **Figure 6 A**-**D**, RR blocked specifically the inward monovalent currents carried by wild-type TRPM6 or the pore mutants. To determine which amino acid residues in the TRPM6 pore are involved in the inhibitory effect of RR, a dose-response curve was established for RR block of the inward TRPM6 and pore-mutant's monovalent currents (n = 5 cells for each point) **(Figure 6E)**. The following $IC_{50}$ for RR sensitivity were obtained (in µM): 15.3 for $E^{1029}A$ with the Hill coefficient of 0.92, 11.9 for $I^{1030}M$ with Hill coefficient of 0.77 and 4.8 for $V^{1032}A$ with a Hill coefficient of 0.84 compared to 5.3 for TRPM6 with a Hill coefficient of 0.90. $E^{1029}A$ and $I^{1030}M$ mutants showed a significantly ($P < 0.05$) reduced sensitivity to RR compared to wild-type channel.

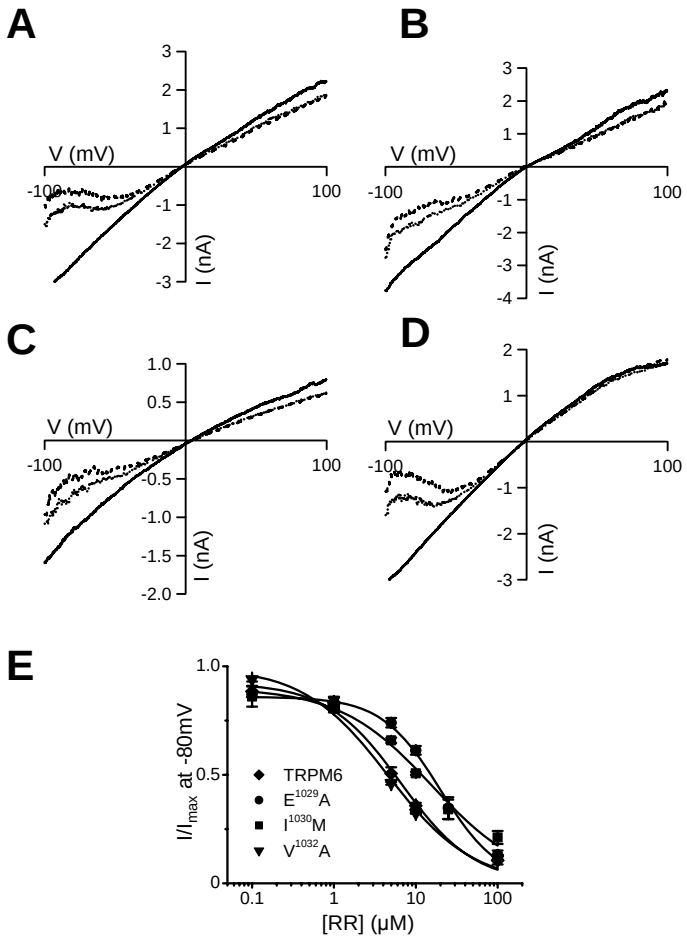


**Figure 6. The inhibitory effect of ruthenium red (RR) on TRPM6 pore mutants. (A**-**D)** Current-voltage relations of monovalent currents in absence (solid lines), or in the presence of RR either at 5 µM RR (dotted lines) or 10 µM RR (dashed lines) obtained from cells expressing wild-type TRPM6 **(A)**, and the pore mutants $E^{1029}A$ **(B)**, $I^{1031}M$ **(C)** and $V^{1032}A$ **(D)**. **(E)** Dose-response curves for the inhibition of the TRPM6-mediated inward monovalent current by RR (♦) and the pore mutant proteins: $E^{1029}A$ (●), $I^{1030}M$ (■) and $V^{1032}A$ (▼).

*Measurement of the pore diameter of TRPM6*

To estimate the TRPM6 pore diameter, the permeability ratios of currents carried by organic monovalent cations of increasing size relative to $Na^+$ current were measured. When $Na^+$ was used as the sole charge carrier, the current reverted close to 0 mV and had a slightly inward-rectifying shape **(Figure 7A)**. All $Na^+$ ions from the extracellular solution were substituted by methyl-ammonium or its di-, tri- and tetra methyl derivatives ($MA^+$, $DMA^+$, $TriMA^+$, $TetMA^+$), or by the larger organic cation *N*-methyl-*D*-glucamine ($NMDG^+$). All the tested cations were able to permeate wild-type TRPM6, $E^{1029}A$ and $I^{1030}M$ channels **(Figure 7A-C)**. The permeability ratios relative to $Na^+$ ($P_X/P_{Na}$) were calculated from the biionic reversal potentials (16): 0.827 ± 0.004, 0.483 ± 0.007, 0.360 ± 0.015, 0.262 ± 0.016, and 0.230 ± 0.015 for $MA^+$, $DMA^+$, $TriMA^+$, $TetMA^+$, and $NMDG^+$ respectively.

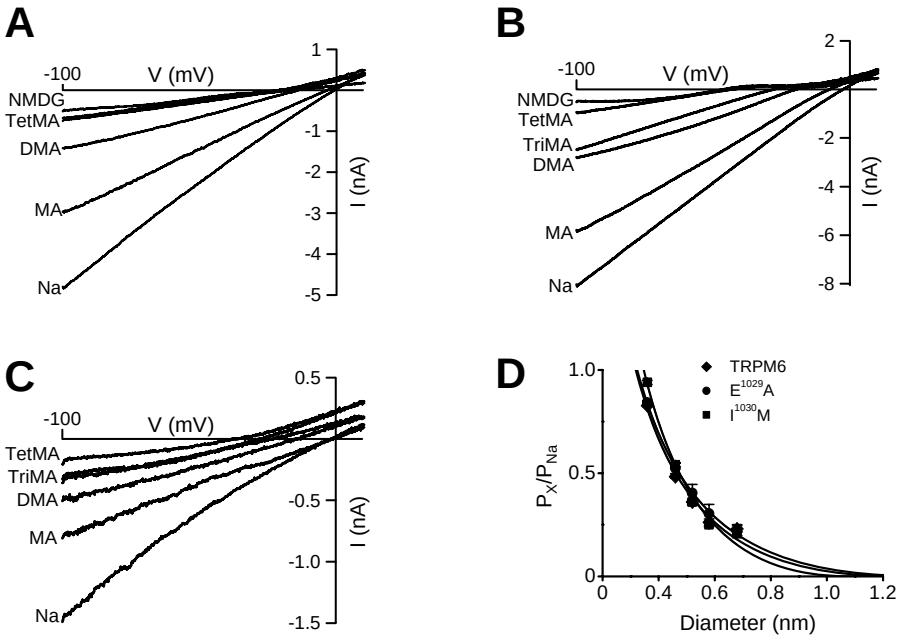


**Figure 7. Measurements of the TRPM6 pore diameter. (A-C)** Extracts of current-voltage relations obtained during voltage ramps in divalent-free (DVF) solutions containing $Na^+$, methylammonium ($MA^+$), dimethylammonium ($DMA^+$), trimethylammonium ($TriMA^+$), tetramethylammonium ($TetMA^+$), or *N*-methyl-D-glucamine ($NMDG^+$) as the sole extracellular cation, from cells expressing TRPM6 **(A)**, $E^{1029}A$ **(B)** and $I^{1030}M$ **(C)**. **(D)** The relative permeabilities ($P_X/P_{Na}$) of the different organic cations plotted as a function of the cation diameter for TRPM6 (♦) and pore mutants: E1029A (●) and $I^{1030}M$ (■). Data points were fitted according to Equation 1 (see *Experimental procedures* section for more details).

**Figure 7D** depicts the permeability ratios of the different cations *versus* their estimated diameter for TRPM6, $E^{1029}A$ and $I^{1030}M$ (n = 5 cells for each point). Data points were fitted using Eq. 1 (see *Experimental procedures* section for more details) resulting in significant differences ($P < 0.05$) in pore diameters of 1.15, 1.25 and 1.05 nm for TRPM6, $E^{1029}A$ and $I^{1030}M$, respectively.

To further delineate the selectivity filter of TRPM6, two chimeras were prepared in which the identified selectivity filters of TRPM4 or TRPV6 were inserted. To this respect an amino acid stretch from the TRPM6 pore $^{1028}$GEIDVC$^{1033}$ was replaced by the sequence $^{981}$EDMDVA$^{986}$ to

construct the TRPM6-TRPM4 selectivity filter chimera and by the sequence $^{539}$TIIDGP$^{544}$ to create the TRPM6-TRPV6 chimera. Both constructs resulted in non-functional channels when expressed in HEK293 cells (data not shown).

**DISCUSSION**

The $Mg^{2+}$-selective cation channel TRPM6 represents the first molecular key player of transcellular $Mg^{2+}$ (re)absorption in renal and intestinal epithelia. Mutations in TRPM6 described for HSH patients imply that TRPM6 indeed plays a crucial role as the gatekeeper of $Mg^{2+}$ (re)absorption. The present study indicates that a short amino acid stretch of the pore region, $^{1028}$GEIDVC$^{1033}$, determines the TRPM6 permeability properties and its sensitivity to the channel pore blocker, RR. Our conclusions are based on the following experimental observations. First, the mutant $E^{1029}$A shows different permeation properties compared to wild-type TRPM6. Second, the estimated pore diameter of TRPM6 increases when $E^{1029}$ is neutralized into an alanine and decreases when $I^{1030}$ is changed into a methionine. Third, the sensitivity of TRPM6 to RR block depends on the $E^{1029}$ and $I^{1030}$ residues in the pore forming region of the channel.

*TRPM6 pore localization*

Mutations that affect basic pore properties have been mainly described for the TRPV (vanilloid) subfamily, namely TRPV1, TRPV4, TRPV5 and TRPV6 (21-23), while the only characterized member of TRPM subfamily is TRPM4 (24). For TRPV5 and TRPV6, it has been shown that neutralization of an aspartate residue, $D^{542}$ in TRPV5, which corresponds to $D^{541}$ in TRPV6, abolishes the $Ca^{2+}$ permeation, $Ca^{2+}$-dependent current decay and block by extracellular $Mg^{2+}$, whereas permeation of monovalent cations remains basically intact (25).

Although the molecular determinants of TRPM6 $Mg^{2+}$ selectivity were not fully revealed with this study, we obtained essential evidences that the region between the residues $^{1028}$GEIDVC$^{1033}$ forms a part of the TRPM6 pore based on the fact that neutralizing the negatively charged residues in this region resulted in channels with different characteristics. Moreover, replacing the putative selectivity filter of TRPM6 with the previously identified pores of both TRPV6 and TRPM4 resulted in non-functional channels (data not shown). Similarly to TRPM4, neutralizing the negatively charged amino acid residues in this area has dramatic consequences on TRPM6 functionality. As demonstrated for TRPM4 (24), when mutating $D^{1030}$ into alanine, which is conserved throughout the entire TRPM subfamily, we obtained non-functional channels. This non-functional phenotype could be explained by a crucial role of $D^{1030}$ for the integrity of TRPM6 pore. In contrast to TRPM4, at positions 1028 and 1036, TRPM6 contains non-charged residues while TRPM4 possesses glutamates at these positions and therefore, the delineation of the TRPM6 selectivity filter sequence appears different. However, we showed by alteration of the pore diameter due to mutation of $E^{1029}$ and $I^{1030}$ that the region from 1029 to 1031 determines the narrowest area of the channel pore.

Traditionally, the minimal pore size of an ion channel can be estimated by the largest permeant ion that carries a measurable current (16,18). Recently, using this approach, the pore diameter of TRPV6 was estimated (26). Surprisingly, TRPM6-associated inward currents could be

measured with all organic cations including $NMDG^+$ whereas for TRPV6, $DMA^+$ was the largest cation that could permeate the channel pore (26). The remarkable inward current measured with $NMDG^+$ as the sole charge carrier could be blocked in the presence of RR (data not shown), proving clearly that $NMDG^+$ is able to permeate TRPM6 pore. $NMDG^+$ permeation has been already described for TRPV1 and purinergic receptors P2X (27,28). For estimation of the pore diameter of TRPM6, fitting of the relative permeation *versus* the cation diameter had to be extrapolated because we did not find any organic cation that does not permeate through TRPM6. Interestingly, the estimated diameter of the TRPM6 pore (1.15 nm) is significantly larger compared to other channels like TRPV6 (0.54 nm), voltage-gated $Ca^{2+}$ channels and estimations for $Ca^{2+}$ release activated currents (0.38 nm in Jurkat cells and 0.32-0.55 nm in rat basophilic leukemia cells (29-31). However, further studies are required to debate if molecular sieving is the main mechanism underlying the selectivity of $Mg^{2+}$ channels.

Recently, the selectivity filter of TRPM4 was revealed by Nilius *et al.* (24). They demonstrated that the pore properties of TRPM4 are determined by a subset of amino acid residues, in contrast to members of the TRPV subfamily in which a single amino acid residue accounts for the permeability properties of the pore. Our results support their observations and prove that members of the TRPM subfamily have a more complex pore structure compared to their close relatives of the TRPV subfamily.

*TRPM6 pore properties*

To investigate the key determinants of TRPM6 pore properties, two main directions were followed: first, the negatively charged residues of the putative pore region were neutralized, and second, the role of the conserved $D^{1031}$ and other amino acid residues in its close vicinity were investigated. Mutation of the three negatively charged residues in the putative TRPM6 selectivity filter ($E^{1024}$, $E^{1029}$ and $D^{1031}$) or in the conserved pore helix ($E^{1012}$, $E^{1016}$, data not shown) had important functional consequences since neutralization of these residues resulted in non-functional channels, except for $E^{1029}$. These data suggest that $E^{1012}$, $E^{1016}$, $E^{1024}$ and $D^{1031}$ play an important role in determining the pore properties of the channel. Neutralization of $E^{1029}$ did not alter the current amplitude, but significantly reduced the sensitivity to RR, and $Zn^{2+}$ and $Ba^{2+}$ conductance. Most likely, negative charge at the inner mouth of the channel pore provides a binding site for positively charged cations, inducing open channel block (32). These data are in line with the fact that the pore diameter of this mutant is increased. We suggest that $E^{1029}$ plays an important role in the TRPM6 pore architecture and takes part in the RR binding site of TRPM6. Second, alteration of the amino acid residues in close vicinity of the conserved $D^{1031}$ had relevant consequences as the mutation of $I^{1030}$ and $V^{1032}$ resulted in functional channels, but with different characteristics compared to wild-type TRPM6. Mutation of $I^{1030}$ resulted in a channel with a smaller pore size. For this latter mutant additional properties have been affected:

$I^{1030}M$ is less permeable to $Ni^{2+}$, but displays the same conductance for $Zn^{2+}$ and $Ca^{2+}$ with wild-type TRPM6 and is more sensitive to RR. Despite the fact that $Ni^{2+}$ has a smaller diameter than $Ca^{2+}$ and $Zn^{2+}$ and that $I^{1030}M$ forms channels with a reduced pore diameter, the altered conductance could be explained by differences in ion's hydration energy with water molecules and by structural changes in the selectivity filter encompassing the permeation of ions (33). Next, the $V^{1032}A$ mutant showed no change in RR block and pore diameter, but had decreased current amplitudes indicating that the molecular determinants of the TRPM6 gating parameters may lay up-stream in the TRPM6 sequence. None of these mutations ($E^{1029}$, $I^{1030}$, $V^{1032}$) affected the $Ca^{2+}$ and $Mg^{2+}$ sensitivity which is in line with the hypothesis that pore mutations are not expected to influence $Ca^{2+}$ binding to the activation site(s) (34).

We and other groups (6,13) are able to record TRPM6-associated currents in HEK293 cells without co-expressing TRPM7, whereas Gudermann and co-workers suggested that TRPM6 requires co-expression with TRPM7 to form functional channels at the plasma membrane (11). Moreover, Li *et al.* could demonstrate functional differences at the divalent ions permeation and single channel conductance between homomeric TRPM6 and TRPM7 and heteromeric TRPM6/TRPM7 channels (13). These apparent contradictions could be reconciled by the fact that we can detect low TRPM7-like endogenous currents in non-transfected HEK293 cells.

In conclusion, the molecular determinants of $Mg^{2+}$ selectivity and permeation of TRPM6 appear to be determined by changes in a stretch of amino acid residues from the pore region, $^{1028}$GEIDVC$^{1033}$, rather than by a single residue as demonstrated for the $Ca^{2+}$ selective TRPV5 and TRPV6 channels. Subsequent studies like crystallographic assays will be needed to investigate in more detail the pore structure of TRPM6.

**ACKNOWLEDGMENTS**

This work was supported by the Dutch Organization of Scientific Research (ZonMw 016.006.001), the Dutch Kidney Foundation (C03.6017), the European Molecular Biology Organization (long-term fellowship ALTF 727-2005), by the Human Frontiers Science Program (HFSP Research Grant Ref. RGP 32/2004), and in part by the Belgian Federal Government, the Flemish Government, the Onderzoeksraad KU Leuven (GOA 2004/07, F.W.O. G. 0136.00; F.W.O. G.0172.03, Interuniversity Poles of Attraction Program, Prime Minister's Office IUAP Nr.3P4/23, Excellentiefinanciering EF/95/010).

**REFERENCES**


1. Wolf, F. I., Torsello, A., Fasanella, S., and Cittadini, A. *Mol Aspects Med.* 24: 11-26, 2003
2. Tong, G. M., and Rude, R. K. *J Intensive Care Med.* 20: 3-17, 2005
3. Quamme, G. A., de Rouffignac ,C. *Front Biosci.* 5: 694-711, 2000
4. Schlingmann, K. P., Weber, S., Peters, M., Niemann Nejsum, L., Vitzthum, H., Klingel, K., Kratz, M., Haddad, E., Ristoff, E., Dinour, D., Syrrou, M., Nielsen, S., Sassen, M., Waldegger, S., Seyberth, H. W., and Konrad, M. *Nat Genet.* 31: 166-170, 2002
5. Walder, R. Y., Landau, D., Meyer, P., Shalev, H., Tsolia, M., Borochowitz, Z., Boettger, M. B., Beck, G. E., Englehardt, R. K., Carmi, R., and Sheffield, V. C. *Nat Genet.* 31: 171-174, 2002
6. Voets, T., Nilius, B., Hoefs, S., van der Kemp, A. W., Droogmans, G., Bindels, R. J., and Hoenderop, J. G. *J Biol Chem.* 279: 19-25, 2004
7. Groenestege, W. M., Hoenderop, J. G., van den Heuvel, L., Knoers, N., and Bindels, R. J. *J Am Soc Nephrol.* 17: 1035-1043, 2006
8. Nadler, M. J., Hermosura, M. C., Inabe, K., Perraud, A. L., Zhu, Q., Stokes, A. J., Kurosaki, T., Kinet, J. P., Penner, R., Scharenberg, A. M., and Fleig, A. *Nature.* 411: 590-595, 2001
9. Runnels, L. W., Yue, L., and Clapham, D. E. *Science.* 291: 1043-1047, 2001
10. Runnels, L. W., Yue, L., and Clapham, D. E. *Nat Cell Biol.* 4: 329-336, 2002
11. Chubanov, V., Waldegger, S., Mederos y Schnitzler, M., Vitzthum, H., Sassen, M. C., Seyberth, H. W., Konrad, M., and Gudermann, T. *Proc Natl Acad Sci U S A.* 101: 2894-2899, 2004
12. Ryazanova, L. V., Dorovkov, M. V., Ansari, A., and Ryazanov, A. G. *J Biol Chem.* 279: 3708-3716, 2004
13. Li, M., Jiang, J., and Yue, L. *J. Gen. Physiol.* 127: 525-537, 2006
14. Owsianik, G., Talavera, K., Voets, T., and Nilius, B. *Annu Rev Physiol.* 68: 685-717, 2006
15. Trouet, D., Nilius, B., Voets, T., Droogmans, G., and Eggermont, J. *Pflugers Arch.* 434: 632-638, 1997
16. Hille, B. (2001) *Ion Channels of Excitable Membranes*, 3rd Ed., Sinauer Associates Inc., Sunderland, MA
17. Barry, P. H. *J Neurosci Methods.* 51: 107-116, 1994
18. Dwyer, T. M., Adams, D. J., and Hille, B. *J. Gen. Physiol.* 75: 469-492, 1980
19. Doyle, D. A., Cabral, J., atilde, o, M., Pfuetzner, R. A., Kuo, A., Gulbis, J. M., Cohen, S. L., Chait, B. T., and MacKinnon, R. *Science.* 280: 69-77, 1998
20. Monteilh-Zoller, M. K., Hermosura, M. C., Nadler, M. J., Scharenberg, A. M., Penner, R., and Fleig, A. *J Gen Physiol.* 121: 49-60, 2003
21. Voets, T., Prenen, J., Vriens, J., Watanabe, H., Janssens, A., Wissenbach, U., Bodding, M., Droogmans, G., and Nilius, B. *J. Biol. Chem.* 277: 33704-33710, 2002
22. Nilius, B., Vennekens, R., Prenen, J., Hoenderop, J. G. J., Droogmans, G., and Bindels, R. J. M. *J. Biol. Chem.* 276: 1020-1025, 2001
23. Garcia-Martinez, C., Morenilla-Palao, C., Planells-Cases, R., Merino, J. M., and Ferrer-Montiel, A. *J. Biol. Chem.* 275: 32552-32558, 2000
24. Nilius, B., Prenen, J., Janssens, A., Owsianik, G., Wang, C., Zhu, M. X., and Voets, T. *J Biol Chem.* 280: 22899-22906, 2005
25. Nilius, B., Vennekens, R., Prenen, J., Hoenderop, J. G., Droogmans, G., and Bindels, R. J. *J Biol Chem.* 276: 1020-1025, 2001
26. Voets, T., Janssens, A., Droogmans, G., and Nilius, B. *J Biol Chem.* 279: 15223-15230, 2004
27. Hellwig, N., Plant, T. D., Janson, W., Schafer, M., Schultz, G., and Schaefer, M. *J Biol Chem.* 279: 34553-34561, 2004
28. Ma, W., Korngreen, A., Weil, S., Cohen, E. B., Priel, A., Kuzin, L., and Silberberg, S. D. *J Physiol.* 571: 503-517, 2006

29. Bakowski, D., and Parekh, A. *Pflügers Archiv European Journal of Physiology* 443: 892-902, 2002
30. Cataldi, M., Perez-Reyes, E., and Tsien, R. W. *J. Biol. Chem.* 277: 45969-45976, 2002
31. Prakriya, M., and Lewis, R. S. *Cell Calcium.* 33: 311-321, 2003
32. Kerschbaum, H. H., Kozak, J. A., and Cahalan, M. D. *Biophys J.* 84: 2293-2305, 2003
33. MacKinnon, R. *FEBS Lett.* 555: 62-65, 2003
34. Nilius, B., Prenen, J., Droogmans, G., Voets, T., Vennekens, R., Freichel, M., Wissenbach, U., and Flockerzi, V. *J Biol Chem.* 278: 30813-30820, 2003
35. Perraud, A. L., Schmitz, C., and Scharenberg, A. M. *Cell Calcium.* 33: 519-531, 2003

# ***Chapter 7***

## General discussion

Catalin N. Topala, Joost G. Hoenderop and René J. Bindels

Department of Physiology, Nijmegen Centre for Molecular Life Sciences, Radboud University Nijmegen Medical Centre, The Netherlands

Modified and updated after: *Curr Opin Nephrol Hypertens*. 16: 319-324, 2007

## INTRODUCTION

Many physiological functions rely on the precise maintenance of body $Ca^{2+}$ and $Mg^{2+}$ balance, which are tightly regulated by the concerted actions of intestinal absorption, renal reabsorption, and exchange with bone. The kidney plays a central role in the homeostasis of divalent ions. $Ca^{2+}$ and $Mg^{2+}$ reabsorption occurs mainly in the proximal tubules and the thick ascending limb (TAL) of Henle's loop via a passive paracellular pathway **(Figure 1A)**. At the level of the distal convoluted tubule (DCT) and the connecting tubule (CNT), $Ca^{2+}$ and $Mg^{2+}$ are reabsorbed via an active transcellular route **(Figure 1A)**. In these kidney segments, reabsorption of divalents is regulated in a $Ca^{2+}$ and $Mg^{2+}$-specific manner and it determines the final excretion in the urine.

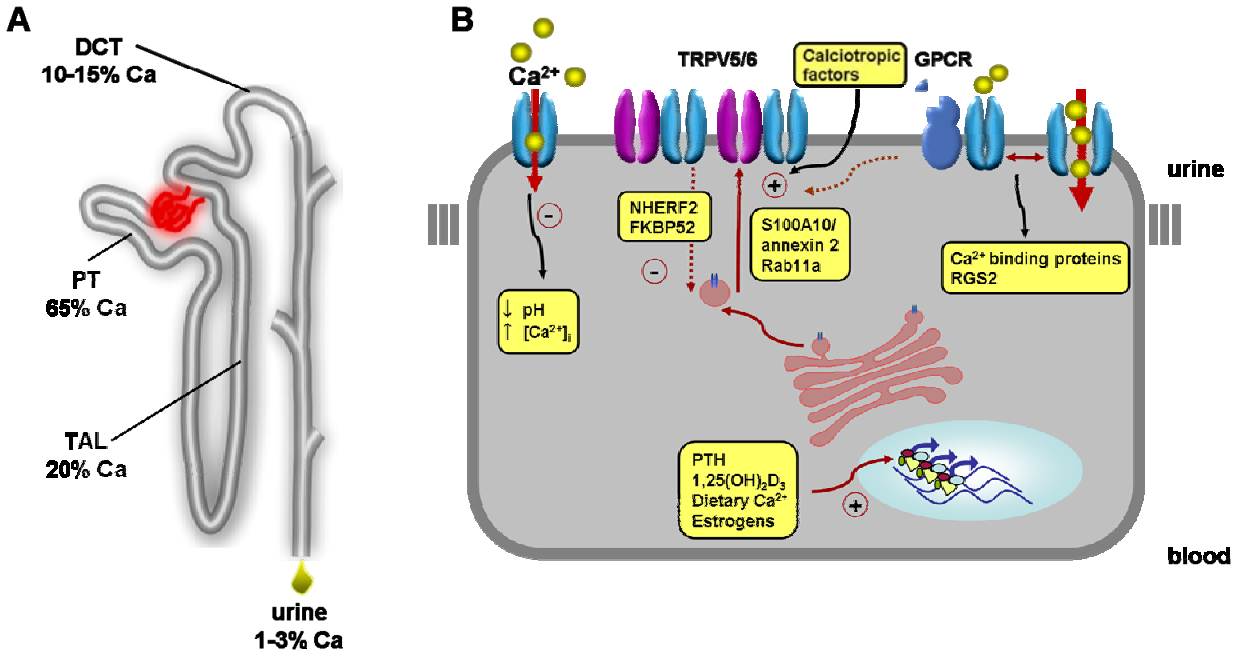


**Figure 1. Cellular regulation of epithelial $Ca^{2+}$ channels, the gatekeepers of renal $Ca^{2+}$ reabsorption. (A)** Overview of the $Ca^{2+}$ reabsorption process along the nephron consisting of the proximal tubule (PT), the thick ascending limb of Henle's loop (TAL) and the distal convoluted tubule (DCT). The reabsorbed proportions from the total filtered amount of $Ca^{2+}$ at the glomeruli are indicated in percentages. **(B)** Cartoon depicting: the long-term transcriptional/translational effect of hormones (PTH, $1,25(OH)_2D3$, dietary $Ca^{2+}$, 17β-estradiol); intracellular factors affection the biophysical properties of the channel (pH, $[Ca^{2+}]i$); the effect of accessory proteins indirectly affecting the trafficking of the channels to the plasma membrane (S100A10/annexin2, Rab11a, NHERF2, FKBP52) or directly affecting channel gating at the plasma membrane ($Ca^{2+}$ binding proteins, RGS2); the effect of new calciotropic factors from the pro-urine acting directly (klotho) or via GPCR (tissue kallikrein) to control the plasma membrane abundance of the channels.

By studying several mice models for $Ca^{2+}$-related disorders, the epithelial $Ca^{2+}$ channels, TRPV5 and TRPV6 have been demonstrated to act as physiological gatekeepers of active $Ca^{2+}$ transport (1-4). Therefore, a tight regulation of TRPV5 and TRPV6 is of particular importance since it determines the amount of $Ca^{2+}$ excreted and consequently affects $Ca^{2+}$ homeostasis. In this respect, the hormonal regulation of the epithelial $Ca^{2+}$ channels TRPV5 and TRPV6 has been extensively studied. It was demonstrated that activation of transcription/translation of TRPV5 and TRPV6 by the parathyroid hormone (PTH), 1,25-dihydroxyvitamin $D_3$ ($1,25(OH)_2D_3$), dietary $Ca^{2+}$ and 17β-estradiol (2,6-9) increased active $Ca^{2+}$ reabsorption **(Figure 1B)**. However,

dietary $Ca^{2+}$ and 17β-estradiol (2,6-9) increased active $Ca^{2+}$ reabsorption **(Figure 1B)**. However, the regulation of these ion channels is also governed *via* accessory proteins that control their activity (10), beside long-term effect of hormones affecting the transcription/translation of these proteins **(Figure 1B)**. We identified a number of auxiliary proteins as critical components modulating the activity of epithelial $Ca^{2+}$ channels (10). The characterization of these accessory proteins provided insights in important molecular pathways modulating $Ca^{2+}$ transport. This thesis describes the identification and characterization of auxiliary proteins regulating TRPV5 and/or TRPV6. Tissue kallikrein (TK) (**chapter 2**) and the extracellular $Ca^{2+}$-sensing receptor (CaSR) (**chapter 3**) were selected based on previous knowledge of their involvement in $Ca^{2+}$ homeostasis. FK506 binding protein (FKBP) was selected by a microarray assay (**chapter 4**), while RGS2 (**chapter 5**) was identified by yeast-two-hybrid screening for proteins binding the amino-terminal region of TRPV6. Moreover, the identification of the epithelial $Mg^{2+}$ channel TRPM6 as the gatekeeper of active $Mg^{2+}$ reabsorption provided new insights in our understanding of renal $Mg^{2+}$ wasting. In **chapter 6** of this thesis, the molecular determinants of cation permeation through TRPM6 are described together with the implications of channel function for overall $Mg^{2+}$ homeostasis.

**Extracellular factors control the epithelial $Ca^{2+}$ channels**

The studies included in this thesis proved the existence of calciotropic factors present in the pro-urine **(Figure 2)** that control the activity of TRPV5, the gatekeeper of active renal $Ca^{2+}$ reabsorption. Firstly, the anti-aging hormone klotho regulates TRPV5 activity *via* a novel mechanism modifying its glycosylation status, thereby entrapping the channel at the cell surface. Secondly, functional characterization of $TK^{-/-}$ mice revealed that these animals exhibit a pronounced hypercalciuria, analogous to the $Ca^{2+}$ leak observed in $TRPV5^{-/-}$ mice. The study described in **chapter 2** demonstrated that TK stimulates active $Ca^{2+}$ reabsorption via the bradykinin (BK) receptor type 2 pathway involving protein kinase C (PKC)-dependent activation of TRPV5. In addition, the study included in **chapter 3** implies that extracellular CaSR activation leads to increased TRPV5 activity. Furthermore, the extracellular pH appears to act as a dynamic switch controlling cell surface expression of TRPV5. In the following pages, the mechanisms for controlling TRPV5 activity by these novel calciotropic factors will be discussed.

*Klotho enhances TRPV5 activity*

In 1997, Kuro-o *et al*. (11) described a transgenic mice line with a single genomic insertion of a transgene, phenotypically resembling several age-related disorders. The affected gene was named klotho, after the Greek goddess who spins the thread of life. Besides a shortening of their lifespan, these infertile mice exhibit several characteristics frequently associated with human premature aging syndromes including arteriosclerosis, osteoporosis, skin atrophy and

ectopic calcification (14). Interestingly, overexpression of klotho in mice resulted in a significant extension of lifespan and suppression of aging related symptoms (12). Allelic variations of the klotho gene are related to life expectancy and coronary artery disease in humans (13-15). The klotho gene encodes a single-pass transmembrane protein with an amino terminal signal sequence, a putative extracellular domain with two internal repeats and a short intracellular domain at the carboxyl-terminus. Klotho is predominantly expressed in DCT/CNT of the kidney (16), and to a lesser extent in the choroid plexus of the brain (11), and the parathyroid glands (17). After cleavage, the amino-terminal domain of klotho is secreted into the urine, blood and cerebrospinal fluid (16,18). This secreted form exhibits β-glucuronidase activity (19).

Ample observations connect klotho to an important role in $Ca^{2+}$ homeostasis. Klotho deficient mice (klotho$^{-/-}$) show a mild hypercalcemia (11) associated with high levels of $1,25(OH)_2D_3$ caused by increased activity of renal 25-hydroxyvitamin D-1$\alpha$-hydroxylase (1$\alpha$-OHase), which is the rate-limiting enzyme in $1,25(OH)_2D_3$ synthesis (20). Dietary suppression of $1,25(OH)_2D_3$ levels reverted most of the klotho$^{-/-}$ mouse phenotype (no arteriosclerosis, osteoporosis and ectopic calcification), beside a prolongation of their life expectancy (24). Conversely, administration of $1,25(OH)_2D_3$ induced klotho expression in the kidney (21). Klotho$^{-/-}$ mice exhibit bone abnormalities, including osteoporosis, and have ~20% lower bone mineral density compared to wild-type littermates (11). In humans, several single-nucleotide polymorphisms in klotho gene have been associated with low mineral bone density in postmenopausal women (22,23). Recently, it was established that klotho is involved in the regulation of TRPV5 activity (19). First, microarray studies revealed that klotho expression is decreased in TRPV5 knockout (TRPV5$^{-/-}$) mice. Second, treatment of TRPV5-expressing human embryonic kidney (HEK293) cells with preconditioned culture medium from klotho-expressing cells strongly enhanced TRPV5-mediated $Ca^{2+}$ currents. Third, cell surface protein labeling experiments demonstrated a significant raise in plasma membrane expression of TRPV5 after overnight klotho treatment **(Figure 2)**. These effects could be mimicked by β-glucuronidase indicating that the enzymatic activity of klotho is responsible for enhanced TRPV5 activity **(Figure 2)**. Finally, deletion of the conserved N-glycosylation site of TRPV5 (N358Q) abolished the klotho-mediated activation of TRPV5, proving that klotho affects the extracellular glycosylation status of the channel.

Of interest, the molecular shift in protein size (~10-15 kDa) after glycosylation of TRPV5 suggests a complex N-glycan structure consisting of at least one hundred sugar residues attached at position N358. Consequent to the cleavage of the N-glycan, the epithelial $Ca^{2+}$ channels could be anchored at the plasma membrane. This effect may involve another plasma membrane protein(s) that could sense the glycosylation status of the channels and stabilize them at the cell surface. Another possible mechanism to increase plasma localization of these channels is to change the recycling rate of the proteins to the plasma membrane. This could be achieved by reducing protein degradation of the channels and stimulate their recycling towards

the plasma membrane. However, the actual molecular mechanism that determines the increased plasma membrane abundance of TRPV5 caused by klotho treatment remains to be discovered.

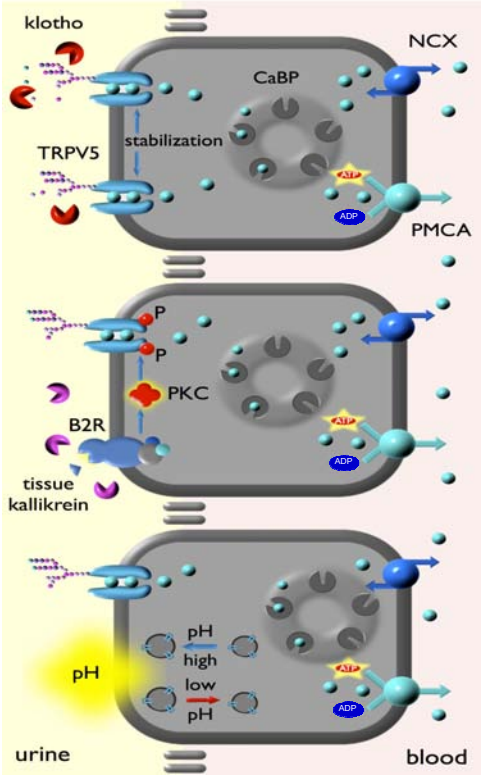


**Figure 2. Regulation of renal $Ca^{2+}$ reabsorption by new calciotropic factors.** Scheme depicting an epithelial cell from the distal convoluted tubule (DCT) showing the molecular effects of klotho, tissue kallikrein and extracellular pH on TRPV5 channel activity. $Ca^{2+}$ enters the cell from the pro-urine *via* TRPV5 and is sequestered by $Ca^{2+}$-binding protein ($CaBP_{28K}$). Next, bound $Ca^{2+}$ diffuses to the basolateral site of the cell where it is extruded into the blood compartment *via* NCX1 and/or PMCA1b. Klotho exerts its effect by hydrolysis of the N-glycosylated TRPV5 channel, thereby stabilizing the channel complex at the apical plasma membrane. This will enable prolonged transcellular $Ca^{2+}$ transport across the epithelium. Tissue kallikrein activates the bradykinin receptor 2 (B2R) resulting in protein kinase C (PKC) dependent phosphorylation of TRPV5 at the plasma membrane. Urinary pH controls trafficking of TRPV5 channels to and from the plasma membrane.

In line with these observations, other studies demonstrated that the activity of ion channels could be controlled *via* modifications of their glycosylation status. It was shown that N-glycosylation of TRPV4, a close relative of TRPV5, at position N651 influences channel expression at the plasma membrane (24). The glycosylation-defective mutant (N651Q) of TRPV4 displayed an increased cell surface abundance as demonstrated by expression and biotinylation experiments. In addition to TRP channels, the activity of voltage-gated potassium channels is also changed by the N-linked glycosylation status which determines the stability of the channel at the cell surface (25). Moreover, it was described that modifications in the N-linked glycans of voltage-gated sodium channel subunits affect the gating of these channels (21).

Interestingly, a recent study (26) postulated that klotho could influence $Ca^{2+}$ reabsorption by an alternative mechanism. In the choroid plexus, klotho increases the plasma membrane

localization of $Na^+$,$K^+$-adenosine triphosphatase ($Na^+$,$K^+$-ATPase). This effect of klotho might also occur in the kidney, where the $Na^+$ gradient created by increased $Na^+$,$K^+$-ATPase plasma membrane levels stimulates passive $Ca^{2+}$ reabsorption. In conclusion, klotho can directly increase the renal $Ca^{2+}$ entry pathway capacity (more TRPV5 channels in the plasma membrane) or indirectly stimulate passive renal $Ca^{2+}$ reabsorption *via* increased transepithelial driving force (by affecting $Na^+$,$K^+$-ATPase localization), for an efficient and integrated control of $Ca^{2+}$ balance (27).

The implications of these klotho-related studies are potentially far-reaching given the diversity and ubiquitous presence of ion channel glycosylation and add new dimensions to the potential mechanisms of channel regulation (28).

*Tissue kallikrein stimulates $Ca^{2+}$ reabsorption*

TK is the main kinin-forming enzyme in mammals (29) and is produced in the kidney (30), where it co-localizes with TRPV5 (3,31). Beside being one of the major proteins that is synthesized in the nephron and secreted into the tubular fluid, TK displays serine protease activity and converts kininogen to kinin, which then acts through kinin receptors such as the BK receptor type 2 (B2R) (32). Remarkably, TK can also directly activate the B2R independently of BK release by protease cleavage of the amino-terminal domain of B2R (33). Previous studies indicate that the kallikrein-kinin system plays an important role in blood pressure regulation, salt sensitivity, water balance and electrolyte excretion (34). Furthermore, it was demonstrated that TK knockout ($TK^{-/-}$) mice show a marked hypercalciuria as an effect of impaired renal tubular $Ca^{2+}$ reabsorption (31), a feature similar to the phenotype of $TRPV5^{-/-}$ mice (5). The striking increase in $Ca^{2+}$ excretion exhibited by $TK^{-/-}$ mice is not accompanied by changes in $Ca^{2+}$, PTH and 1,25-$(OH)_2D_3$ blood concentrations.

The molecular mechanisms by which TK influences renal $Ca^{2+}$ reabsorption are described in **chapter 3** (35). TK significantly enhanced transcellular $Ca^{2+}$ transport in primary cultures from rabbit CNT/cortical collecting duct (CCD) cells. This stimulation could be mimicked by application of BK and was prevented by a B2R antagonist demonstrating the involvement of the B2R in the stimulatory effect of TK **(Figure 2)**. An increase in TRPV5-mediated currents was observed after TK treatment, explaining the enhanced $Ca^{2+}$ transport. The role of phospholipase C (PLC) in TK-dependent increase of TRPV5 activity was investigated using PLC inhibitors. Inhibition of PLC prevented the stimulatory effect of TK. In accordance with previous observations, application of a cell permeable analog of diacylglycerol (DAG), oleyl-acetyl-glycerol (OAG), which activates PKC, also increased TRPV5 activity, suggesting the involvement of the PLC/DAG/PKC pathway **(Figure 2)**. Detailed sequence analysis of TRPV5 indicated that the channel contains six putative PKC phosphorylation sites. From these sites, only inactivation of serines at positions 299 and 654 into alanine rendered TRPV5 completely

insensitive to TK. Additionally, cell surface protein labeling experiments revealed that TK treatment significantly enhances expression of TRPV5 at the plasma membrane. Contrary, TK did not affect the cell surface abundance of the PKC phosphorylation-defective TRPV5 mutants S299A and S654A. Importantly, TK treatment did not affect TRPV5 closest homolog, TRPV6, since the serine at position 654 is not conserved in TRPV6. Therefore, it appears that both serine residues are critical for stimulation by TK. Pulse-chase assays demonstrated a slow internalization rate of TRPV5 from the plasma membrane after TK treatment pointing to a delayed retrieval of the channel complexes from the plasma membrane as possible mechanism. Interestingly, it was shown that a member of the Shaker family of potassium channels, the voltage-gated potassium channel Kv1.3, is regulated by changes in its phosphorylation status (36). Pulse-chase experiments showed an increased half-life residence time of the phosphorylated form of these channels at the cell surface.

Our study demonstrated a significant role of TK as a new calciotropic factor in the pro-urine. Beside its well described functions in the regulation of water-$Na^+$ balance and consequently in controlling blood pressure, TK secreted in the pro-urine is also involved in local regulation of active $Ca^{2+}$ reabsorption. This effect may be important in the spatial-temporal regulation of body $Ca^{2+}$ homeostasis, since it can lead to precise and rapid changes in the cell surface localization of the epithelial $Ca^{2+}$ channel TRPV5, the gatekeeper of active renal $Ca^{2+}$ transport. The autocrine and/or paracrine stimulation of TRPV5-mediated renal $Ca^{2+}$ reabsorption by TK represents a new mechanism efficiently controlling $Ca^{2+}$ excretion.

*Activation of the $Ca^{2+}$-sensing receptor stimulates TRPV5 activity*

Until the cloning of the extracellular CaSR, it was unclear how the body can sense the extracellular $Ca^{2+}$ concentration. The molecular cloning of CaSR, functioning as G protein-coupled receptor (GPCR) in bovine parathyroid gland, proved that extracellular $Ca^{2+}$ serves as extracellular first “messenger” in addition to its well-recognized functions as intracellular second messenger (38). Consequent to its molecular cloning, many subsequent studies addressed the function of CaSR in $Ca^{2+}$ homeostasis. In chief cells from the parathyroid glands, CaSR senses elevated blood $Ca^{2+}$ concentration and signals *via* $G\alpha_i$ and $G\alpha_q$ to regulate multiple second messengers. The result of CaSR activation and subsequent intracellular signaling is a reduction in PTH secretion from the parathyroid glands. Lower circulating PTH levels reduce renal $Ca^{2+}$ reabsorption resulting in lower blood $Ca^{2+}$ concentration. Beside its localization in the parathyroid glands, CaSR is expressed also in other tissues such as bone, intestine and kidney, all being important players in maintaining body $Ca^{2+}$ balance. In the kidney, CaSR is present at the luminal side of the proximal and DCT and basal lateral membranes of the thick ascending limb (41).

In TAL, CaSR functions to regulate $Ca^{2+}$ excretion and in the distal tubules, controls vasopressin mediated water flux. Although CaSR is co-expressed with TRPV5 at the apical membrane of the cells from DCT and CNT, the functional correlation between these two important proteins for $Ca^{2+}$ homeostasis was until now poorly investigated. The study in **chapter 4** describes for the first time a functional link between CaSR and TRPV5 **(Figure 1B)**. Consequent to CaSR stimulation, the down-stream signaling pathway is activated and TRPV5 activity is enhanced. The effect of CaSR stimulation with neomycin is specific for TRPV5 since the activity of its closest relative, TRPV6, was unaffected subsequent to CaSR activation. The molecular mechanism involved in this effect is dependent of the PLC/PKC signaling cascade. Using inactivating point mutations of the six putative PKC phosphorylation sites in TRPV5, we demonstrated that only two residues, S299 and S654 account for the increased channel activity consequent to CaSR stimulation. Furthermore, a pharmacological approach was used to down-regulate the PMA sensitive isoforms of PKC, demonstrating the one of these proteins is involved in the signaling pathway that connects CaSR activation to TRPV5 enhanced activity. The results are in concordance with our previous work, in which the same signaling cascade leads to increased TRPV5 activity upon activation of another GPCR, the B2R, by TK (36). Our study provided answers to the question concerning the role of CaSR in renal DCT/CNT. It is interesting that CaSR in DCT/CNT has an opposing effect on $Ca^{2+}$ reabsorption compared to its function in the parathyroid glands or the apical segments of the nephron. Moreover, in a previous study (37) it was postulated that activation of CaSR expressed at the basolateral membrane of Madin-Darby canine kidney (MDCK) cells inhibits $Ca^{2+}$ transport by inhibiting PMCA. However, our results show that, activation of the CaSR presumably expressed at the apical membrane of DCT/CNT cells, increase TRPV5-mediated $Ca^{2+}$ entry. These apparently contradicting findings could be conciliated by considering the expression site of the CaSR in these studies. Increased blood $Ca^{2+}$ concentrations could activate the CaSR expressed at the basolateral membranes determining reduction in $Ca^{2+}$ reabsorption. Alternatively, increased $Ca^{2+}$ concentrations in the pro-urine activate CaSR expressed at the apical membranes, which in turn stimulate $Ca^{2+}$ reabsorption. A balance of these two processes allows a precise control of urinary $Ca^{2+}$ excretion.

Since there is a clear correlation between high $Ca^{2+}$ levels in the urine and kidney stones formation, the body employs precise mechanisms to sense variations of $Ca^{2+}$ levels in the pro-urine. In addition, increased $Ca^{2+}$ concentration in the pro-urine is a sign for hypercalciuria besides being a sign of increased water reabsorption, and therefore, the organism is able to trigger compensatory mechanisms. Therefore, the expression of CaSR at the apical membrane of epithelial cells from DCT/CNT and its potential functional role unveiled in this study may represent a new pathway of a local feedback mechanism to rapidly control urinary $Ca^{2+}$

excretion. These results provide new clues in our understanding of the regulation of renal $Ca^{2+}$ reabsorption.

*Pro-urine pH dynamically controls TRPV5 activity*

Acid-base homeostasis is known to affect renal handling of $Ca^{2+}$ (38). In the past, the clinical effect of chronic metabolic acidosis and metabolic alkalosis on $Ca^{2+}$ reabsorption in the distal part of the nephron was intensively investigated. Urinary $Ca^{2+}$ excretion increases during metabolic and respiratory acidosis (39). This is attributed to direct effects of acidosis on active $Ca^{2+}$ reabsorption in the distal part of the nephron. Conversely, metabolic alkalosis in, for example, the milk-alkali syndrome, volume contraction, or treatment of nephrolithiasis by bicarbonate supplementation enhances $Ca^{2+}$ reabsorption (43). The effects of chronic acidosis and alkalosis on $Ca^{2+}$ reabsorption could be explained by variations in expression levels of the key proteins for this process such as TRPV5 and the calbindin-$D_{28K}$ (43). Beside the effects of chronic alterations in acid-base homeostasis on TRPV5 expression, pH changes could directly influence TRPV5 activity. In this aspect, it was shown that acidification of the apical medium inhibits transcellular $Ca^{2+}$ transport in primary cultures of rabbit CNT/CCD cells (40). Moreover, it was demonstrated that acidification of the extracellular medium reduces TRPV5-mediated currents, affecting the current kinetics, $Mg^{2+}$ blockage as well as the $Ca^{2+}$ affinity (41). Recently, there were indications that mutation of the glutamate at position 522 into glutamine (E522Q) in TRPV5, decreases inhibition of the channel by extracellular protons (42), suggesting that this amino acid residue controls conformational changes of the pore helix caused by extracellular acidification (43). However, a novel molecular mechanism was proposed (44) to explain the direct effects of pH on TRPV5 activity by showing that extracellular pH regulates the plasma membrane recruitment of TRPV5 **(Figure 2)**. Despite this apparent controversy, all observations show an important physiological role of extracellular pH in determining TRPV5 activity. Extracellular pH controls the TRPV5 activity at two levels: determines the levels of TRPV5 expression at the plasma membrane, and gates the channels at the cell surface. Extracellular acidification rapidly reduced, whereas alkalinization increased TRPV5-mediated currents. Total internal reflection fluorescence (TIRF) microscopy experiments revealed that alkalinization of the extracellular media determines the rapid recruitment of TRPV5-containing vesicles towards the plasma membrane, whereas acidification controls the retrieval of the same vesicles. Lambers and colleagues demonstrated that the effect of extracellular pH is specific for TRPV5 channels trafficking, since the movements of TRPM7-containing vesicles were unaffected by pH changes. However, extracellular pH affects directly the gating of other channels beside TRPV5, e.g. TRPM7 (45). Therefore, it is tempting to speculate that, in physiological conditions, extracellular pH controls TRPV5 activity mainly by affecting the trafficking of the channels towards the plasma membrane. Cell surface protein labeling assays further substantiated this

finding showing that increased extracellular pH triggers an increase in plasma membrane abundance of TRPV5 channels. This effect was additionally confirmed using methanethiosulfonate derivate (MTSET), a compound that irreversibly binds to a cysteine residue within the TRPV5 sequence inactivating the channels present in the plasma membrane (46). The functional recovery in TRPV5 activity after chemical inactivation with MTSET is enhanced by an alkaline pH. Altogether, these experiments provided evidence that changes in pH regulate TRPV5 activity by controlling its trafficking towards the cell surface. Although it was clearly demonstrated that extracellular pH controls the plasma membrane recruitment of TRPV5, the molecular machinery underlying this process needs to be clarified. It is still unclear how extracellular pH is sensed by the intracellular vesicles containing TRPV5. Variations in extracellular pH may affect the intracellular pH (40), which is shown to control the movement of intracellular trafficking vesicles to and from the plasma membrane. However, another potential mechanism is the existence of a plasma membrane proton sensor that translates extracellular pH changes into intracellular signals, leading to recruitment of TRPV5 containing vesicles towards the plasma membrane. Unraveling the molecular mechanisms by which pH affects TRPV5 activity increase our knowledge about the regulation renal $Ca^{2+}$ reabsorption, and contribute to the concept of the pH-dependent regulation of other ion transport proteins.

**Regulation of epithelial $Ca^{2+}$ channels by accessory proteins**

A number of regulatory proteins have recently been described that modify the biophysical, pharmacological, and expression properties of ion channels and transporters by direct protein-protein interactions. These newly identified associated proteins have facilitated the elucidation of important molecular pathways modulating ion transport. Similarly, identification of the molecular players that associate with TRPV5 and TRPV6 could be pivotal in our understanding of the regulation of these channels.

*The immunophilin FKBP52 inhibits TRPV5 activity*

FKBP was one of the genes determined by microarray assay to be regulated by dietary $Ca^{2+}$ supplementation of 1$\alpha$-OHase deficient mice (47). FKBP52 is a widely expressed cytosolic enzyme that belongs to the FKBP subfamily of immunophilin proteins (48-50). FKBP proteins are characterized by their peptidyl-prolyl cis-trans isomerase (PPIase) activity, as well as by their strong affinity to immunosuppressive drug FK506 (49). The PPIase has a chaperoning activity that often constitutes a rate-limiting step in protein folding and can be inhibited by FK506 (49). The immunosuppressive drug FK506 cause as common side-effect hypercalciuria. **Chapter 2** describes the co-localization of FKBP52 with TRPV5 in the DCT and CNT of the kidney and its putative role in regulating TRPV5 activity. To investigate the role of FKBP52 in TRPV5 regulation a small-interference (si)RNA approach was developed. Knocking-down

FKBP52 gene expression resulted in enhanced TRPV5-mediated $Ca^{2+}$ influx suggesting an inhibitory role for FKBP52 on TRPV5 activity **(Figure 1B)**. Consistent with our findings on the inhibitory effect of FKBP52 on TRPV5 activity, is a previous study that identified the FKBP52 *Drosophila melanogaster* homologue, FKBP59, as physiological regulator of TRPL channel activity (51). FKBP59 interacts directly with the highly conserved TRPL sequence $^{701}$LPPPFNVLP$^{709}$ and inhibits $Ca^{2+}$ influx. In *Drosophila melanogaster* (51) as well as in mammals (52) the proline residue of the first LP-motif, located next to mouth of the channel pore, plays a crucial role in this association. Conspicuously, TRPV5 contains such a LP motif next to the pore region at the amino acidic position 551-552, where the FKBP52 binding site is located. The FK506 drug has been shown to mimic the LP-dipeptide (53) and to disrupt the FKBP52 interaction with TRPCs (52). However, FK506 did not interrupt the FKBP52-TRPV5 association suggesting an alternative mechanism. This means that FK506 binds TRPV5 and modulates its activity without displacing the association of FKBP52, similar to the mechanism previously described for the regulation of the *Drosophila melanogaster* homologues FKBP59 and TRPL (51). The physiological relevance of the latter hypothesis needs further confirmation since it is based on *in vitro* experiments.

In addition, we demonstrated that ablation of FKBP52 PPIase activity either by FK506 administration or by mutation of the FKBP52 catalytic site resulted in the inhibition of TRPV5 channel. We hypothesized that FKBP52 affects TRPV5 activity by affecting trafficking of the channels to the cell surface **(Figure 1B)**. FKBP52 co-localizes with microtubules of the cytoskeleton and binds to cytoplasmic dynein (54,55), a motor protein responsible for the movement of vesicles along microtubules. Association of dynein to FKBP52 depends on the PPIase domain and defines the trafficking of steroid receptors to the cell nucleus (55,56). Similarly, FKBP52 could participate in the TRPV5 trafficking towards the plasma membrane through its PPIase activity by binding to microtubules of the cytoskeleton. In concordance with our hypothesis, a recent report demonstrated association of TRPV1 channels to the microtubules of the cytoskeleton, while TRPV1 activation resulted in the depolymerization of microtubules affecting the transmission of pain sensation (57). Functional studies with FK506 in primary cultures of DCT/CNT epithelial cells substantiated the physiological relevance of the co-localization of FKBP52 with TRPV5 in kidney. Submicromolar concentrations (10 nM) of FK506 stimulate active $Ca^{2+}$ reabsorption in these cells while higher concentrations have a toxic effect. This dose dependent effect could explain the nephrotoxicity observed in patients treated with this immunosuppressive drug FK506 (58,59). FK506-induced nephrotoxicity includes intratubular calcification and tubular basophilia in rats (61). In addition, long-term treatment (28 days) of rats with FK506 resulted in increased bone turnover with net bone resorption (62). Since TRPV5 is essential in bone turnover (60), FK506 could enhance osteoclastic bone resorption by increasing TRPV5-mediated active $Ca^{2+}$ transport. On the other hand, it has been

previously demonstrated that FK506 administration results in hypercalciuria (61). However, the doses and the duration of treatments cannot be compared between the experiments performed in rats and the primary cultures of DCT/CNT epithelial cells. The proposed molecular mechanism for the FK506-induced hypercalciuria is that FK506 down-regulates calbindin-$D_{28K}$ and TRPV5 expression. Altogether, given the complexity of the *in vivo* situation, the FK506-induced hypercalciuria awaits further investigation regarding the specificity of FK506 effect and, in particular, concerning the role of other FKBP's.

*RGS2 inhibits the epithelial $Ca^{2+}$ channel TRPV6*

RGS2 was identified as a novel binding partner of TRPV6 by a yeast two-hybrid screening for proteins that interact with the amino terminus of TRPV6. RGS2 is a member of the RGS family of proteins that terminate signaling of heterotrimeric GPCR, by enhancing the GTPase activity of active $G_\alpha$ subunits (62). To date, over twenty different RGS proteins have been identified, and their effector functions extend beyond negative regulation of GPCR signaling. RGS proteins can act as effector antagonists, binding to either the effector protein or the $G_\alpha$ subunit to prevent an operative physical interaction. It has also been demonstrated that RGS proteins can interact with a wide variety of auxiliary proteins, such as calmodulin, spinophilin (SPL) and the 14-3-3 protein, which can influence the subcellular localization, stability and function of RGS proteins (63). **Chapter 5** describes the interaction of the amino terminal domain of RGS2 with the amino terminus of TRPV6 in a $Ca^{2+}$-independent fashion, and the putative role of RGS2 in modulating TRPV6 functioning. To investigate the role of RGS2 in TRPV6 regulation, a combined approach including biochemical and functional assays was applied. Co-expression of TRPV6 with RGS2 determined an inhibition in both $Ca^{2+}$ and $Na^{+}$ TRPV6-mediated currents. Interestingly, the currents through TRPV5, the closest homologue of TRPV6, were not affected by RGS2 co-expression, demonstrating the specificity of the RGS effect on TRPV6. The physiological relevance of RGS2 binding to TRPV6 *via* its amino terminus was determined using a RGS2 mutant lacking the amino-terminal domain (delta-N RGS2). Co-expression of the delta-N RGS2 mutant with TRPV6 did not affect the current. To support our findings, the amino-terminal domain RGS2 has already been described as an important regulatory site for this protein. Together with the "RGS-box" domain, it is necessary for interactions with RGS2 effector proteins, GPCRs, and/or auxiliary proteins such as SPL. Since we showed that RGS2 does not affect the plasma membrane abundance of TRPV6 by biotinylation experiments, the inhibitory effect of RGS2 on TRPV6-mediated currents is mediated directly at the plasma membrane **(Figure 1B)**. Therefore, RGS2 needs to be recruited to the cell surface to affect the gating properties of TRPV6. In this aspect, it has been previously demonstrated that G-proteins recruit RGS proteins to the plasma membrane (64). However, the actual mechanism to explain the RGS2 inhibition of TRPV6 channels, still remains to be investigated. It is tempting to speculate

that RGS2 protein, upon binding to TRPV6, can determine conformational changes affecting the pore structure and altering the regular functioning of the channel. Future experiments, such as cysteine substitution of the amino acid residues in the TRPV6 pore, are needed to clarify this aspect. On the other hand, RGS2 may affect TRPV6 activity by closing either by blocking the channels at the plasma membrane. Given that TRPV6 forms constitutively active channels, measuring the single channel activity of TRPV6, may be the method of choice to study the actual mechanism of RGS2 inhibition on TRPV6 activity.

In addition, SPL has been shown to be involved in RGS protein recruitment to the plasma membrane (65). The inhibitory effect of RGS2 on TRPV6 activity is independently regulated of a GPCR and is mediated by a direct interaction between RGS2 and TRPV6. These findings suggest that the activity of TRP channels may be directly controlled by interacting proteins at the plasma membrane.

**TRPM6 channel, the gatekeeper of active $Mg^{2+}$ transport**

TRPM6 together with its closest relative, TRPM7, are the only channels from the TRPM family known to be permeable for $Mg^{2+}$. Unlike other members of the TRP family, TRPM6 and TRPM7 contain $\alpha$-kinase domains in their carboxyl-terminal tails (66). The identification of TRPM6 (67,68) as the gene mutated in patients suffering from hypomagnesemia with secondary hypocalcemia (HSH) represents the first case in which a human disorder has been attributed to a channel kinase. Correlated to its role in $Mg^{2+}$ homeostasis, TRPM6 protein is specifically localized along the apical membrane of the renal DCT, colon and the brush-border membrane of the small intestine, epithelia particularly associated with active $Mg^{2+}$ (re)absorption (66). When heterologously expressed, TRPM6 induces an $Mg^{2+}$ and $Ca^{2+}$ permeable cation channel with a 5-fold higher affinity for $Mg^{2+}$ than for $Ca^{2+}$, tightly regulated by intracellular $Mg^{2+}$ levels. Despite the initial functional characterization of TRPM6, the molecular determinants of its $Mg^{2+}$ permeability remained unknown. To date, limited understanding exists concerning the structure of TRP channels pores and lesser is known about TRPM pores. The study in **chapter 6** describes the role of amino acid residues from the putative selectivity filter of TRPM6 in the permeation properties of the channel. A short amino acid stretch from the pore region, $^{1028}$GEIDVC$^{1033}$ **(Figure 3A)**, determines the conductivity properties of the channel and the channel sensitivity to the channel pore blocker, the hexavalent cation ruthenium red. The structure of the loop between the fifth and the sixth transmembrane domains was modeled based on the crystal structure of the $K^+$ channel KcsA (69) **(Figure 3)**. In this region, TRPM6 shares two conserved amino acid residues, E1024 and E1029, with its closest homologue TRPM7. All members of the TRPM subfamily contain a conserved aspartate residue (D1031 in TRPM6), that could be and important structural component of their selectivity filters. Point mutations in the TRPM6 putative selectivity filter resulted in three different phenotypes: E1029A

with current amplitudes similar to wild-type TRPM6 channel, I1030M and V1032A with reduced current amplitudes, while the mutants E1024A and D1031A showed no measurable currents **(Figure 3A)**. This non-functional phenotype of D1031A could be explained by a crucial role of this residue in maintaining the integrity of the TRPM6 pore, as demonstrated for TRPM4 (70) or could be explained by the endoplasmic reticulum retaining of these mutant proteins. The ultimate prove to solve this dilemma will come from investigations of cell surface expression of these proteins.

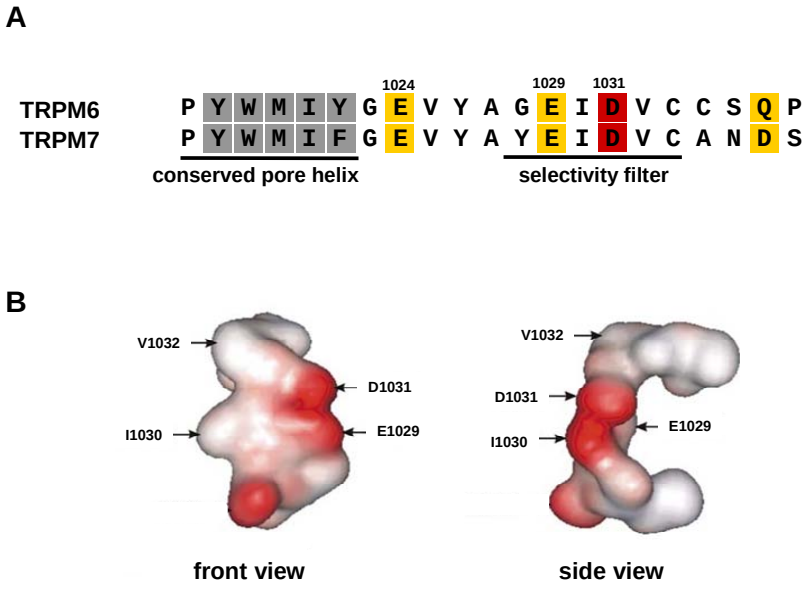


**Figure 3. Modeling of the selectivity filter of the epithelial $Mg^{2+}$ channel TRPM6 based on the pore structure of the KcsA channel. (A)** Sequence alignment of putative pore regions of TRPM6 and its closest relative TRPM7. **(B)** The amino acid residues lining the pore of TRPM6 channel are depicted in frontal as in lateral view. Localization of the key determinants of TRPM6 permeability is indicated by arrows. The 3-D modeling of the TRPM6 pore region was performed using Swiss Model software (5) using the pore structure of KcsA as template.

Recently, a study by Li and colleagues (71) implied that the stretch of amino acid residues from the position 1024 to 1029 are key determinants of the TRPM6 permeation properties. Moreover, this study showed that the negatively charged residues at positions E1024 and E1029 are involved in the pH sensitivity of TRPM6. These results, apparently contradicting our findings, could be reconciled by the hypothesis that the residues before the position E1024 are part of a putative α-helix actually sustaining the selectivity filter of the channel. Disrupting this α-helix structure may destabilize the channel pore leading to the formation of non-functional channels. It appears that the pore structure of TRPM channels is more complex than the pore structures of other TRP channels. In this respect, Oberwinkler and colleagues recently identified several TRPM3 spliced variants, TRPM3α1-5 (72). While the TRPM3α-2 displayed high permeability to $Ca^{2+}$ and $Mg^{2+}$, TRPM3α-1, which includes an additional stretch of 12 amino acids following the conserved aspartate, a residue equivalent to D1031 in TRPM6, exhibited a more than 10-fold

lower permeability for divalent cations (72). This can be explained by a possible re-arrangement of the pore structure caused by this stretch of additional twelve residues.

The increased estimated size of the TRPM6 pore diameter when E1029 is mutated and the decreased when I1030 is neutralized, demonstrated that the region from 1029 to 1031 determines the narrowest area of the channel pore **(Figure 3)**. E1029A showed an increased pore diameter, reduced ruthenium red sensitivity and conductance to $Zn^{2+}$ and $Ba^{2+}$ compared to wild-type TRPM6. Most likely, the negative charges at the inner mouth of the pore provide a binding site for positively charged cations, inducing open channel block (73). Our findings constitute the first evidence that permeation properties of $Mg^{2+}$ permeable channels are determined by a stretch of amino acid residues **(Figure 3)**, rather than single amino acid residues as for the $Ca^{2+}$-selective TRPV5 and TRPV6 channels (74,75).

**Conclusions and future perspectives**

Active $Ca^{2+}$ reabsorption in the kidney represents a key process in $Ca^{2+}$ homeostasis. Since TRPV5 is the rate-limiting step in $Ca^{2+}$ entry, tight control of its activity enables us to adjust $Ca^{2+}$ reabsorption to varying $Ca^{2+}$ demands of the body. The experimental data summarized in the first two studies from this thesis indicate the existence of novel calciotropic factors that act from the pro-urine to regulate active $Ca^{2+}$ reabsorption. The control of cell surface expression of the TRPV5 channel by its N-linked glycosylation status, its PKC-dependent phosphorylation and by extracellular pH describes new ways for an efficient control of the body $Ca^{2+}$ balance. Moreover, as described in the studies included in this thesis, associated proteins control from the intracellular compartment the activity of the epithelial $Ca^{2+}$ channels. In conclusion, the function of the epithelial $Ca^{2+}$ channels is controlled intracellular by accessory proteins and extracellular by novel calciotropic factors. The major challenges in the future are to completely understand how these mechanisms that functionally regulate the epithelial $Ca^{2+}$ channels are integrated in the complex machinery involved in maintaining body $Ca^{2+}$ balance. As discussed in the last study from this thesis, unraveling the molecular determinants of permeation through TRPM6 pore opens new lines in our understanding of general permeation characteristics of ion channels and particularly, $Mg^{2+}$ permeation. Future challenges lay ahead in correlating the molecular mechanisms controlling the epithelial $Ca^{2+}$ and $Mg^{2+}$ channels activity with their integrated role in wide physiological context.

**REFERENCES**


1. Dardenne, O., Prud'homme, J., Arabian, A., Glorieux, F. H., and St-Arnaud, R. *Endocrinology.* 142: 3135-3141, 2001
2. Hoenderop, J. G., Dardenne, O., Van Abel, M.*, et al. Faseb J.* 16: 1398-1406, 2002
3. Hoenderop, J. G., van Leeuwen, J. P., van der Eerden, B. C.*, et al. J Clin Invest.* 112: 1906-1914, 2003
4. Bianco, S. D., Peng, J. B., Takanaga, H.*, et al. J Bone Miner Res.* 22: 274-285, 2007
5. Schwede, T., Kopp, J., Guex, N., and Peitsch, M. C. *Nucl. Acids Res.* 31: 3381-3385, 2003
6. Renkema, K. Y., Nijenhuis, T., van der Eerden, B. C.*, et al. J Am Soc Nephrol.* 16: 3188-3195, 2005
7. van Abel, M., Hoenderop, J. G., Dardenne, O.*, et al. J Am Soc Nephrol.* 13: 2102-2109, 2002
8. van Abel, M., Hoenderop, J. G., van der Kemp, A. W., Friedlaender, M. M., van Leeuwen, J. P., and Bindels, R. J. *Kidney Int.* 68: 1708-1721, 2005
9. Walters, J. R. F., Balesaria, S., Khair, U., Sangha, S., Banks, L., and Berry, J. L. *The Journal of Steroid Biochemistry and Molecular Biology.* 103: 509-512, 2007
10. van de Graaf, S. F., Hoenderop, J. G., and Bindels, R. J. *Am J Physiol Renal Physiol.* 290: F1295-1302, 2006
11. Kuro-o, M., Matsumura, Y., Aizawa, H.*, et al. Nature.* 390: 45-51, 1997
12. Kurosu, H., Yamamoto, M., Clark, J. D.*, et al. Science.* 309: 1829-1833, 2005
13. Arking, D. E., Atzmon, G., Arking, A., Barzilai, N., and Dietz, H. C. *Circ Res.* 96: 412-418, 2005
14. Arking, D. E., Becker, D. M., Yanek, L. R.*, et al. Am J Hum Genet.* 72: 1154-1161, 2003
15. Arking, D. E., Krebsova, A., Macek, M., Sr.*, et al. Proc Natl Acad Sci U S A.* 99: 856-861, 2002
16. Chang, Q., Hoefs, S., van der Kemp, A. W., Topala, C. N., Bindels, R. J., and Hoenderop, J. G. *Science.* 310: 490-493, 2005
17. Nabeshima, Y. *Ageing Res Rev.* 1: 627-638, 2002
18. Imura, A., Iwano, A., Tohyama, O.*, et al. FEBS Lett.* 565: 143-147, 2004
19. Tohyama, O., Imura, A., Iwano, A.*, et al. J Biol Chem.* 279: 9777-9784, 2004
20. Yoshida, T., Fujimori, T., and Nabeshima, Y. *Endocrinology.* 143: 683-689, 2002
21. Tsujikawa, H., Kurotaki, Y., Fujimori, T., Fukuda, K., and Nabeshima, Y. *Mol Endocrinol.* 17: 2393-2403, 2003
22. Mullin, B. H., Wilson, S. G., Islam, F. M. A.*, et al. Calcified Tissue International.* V77: 145-151, 2005
23. Kawano, K., Ogata, N., Chiano, M.*, et al. J Bone Miner Res.* 17: 1744-1751, 2002
24. Xu, H., Fu, Y., Tian, W., and Cohen, D. M. *Am J Physiol Renal Physiol.* 290: F1103-1109, 2006
25. Watanabe, I., Zhu, J., Recio-Pinto, E., and Thornhill, W. B. *J Biol Chem.* 279: 8879-8885, 2004
26. Imura, A., Tsuji, Y., Murata, M.*, et al. Science.* 316: 1615-1618, 2007
27. Strewler, G. J. *Cell Metabolism.* 6: 93-95, 2007
28. Cohen, D. M. *Semin Cell Dev Biol.* 2006
29. Meneton, P., Bloch-Faure, M., Hagege, A. A.*, et al. Proc Natl Acad Sci U S A.* 98: 2634-2639, 2001
30. Figueroa, C. D., MacIver, A. G., Mackenzie, J. C., and Bhoola, K. D. *Histochemistry.* 89: 437-442, 1988
31. Picard, N., Van Abel, M., Campone, C.*, et al. J Am Soc Nephrol.* 16: 3602-3610, 2005
32. Bhoola, K. D., Figueroa, C. D., and Worthy, K. *Pharmacol Rev.* 44: 1-80, 1992
33. Hecquet, C., Tan, F., Marcic, B. M., and Erdos, E. G. *Mol Pharmacol.* 58: 828-836, 2000
34. Dendorfer, A., Wolfrum, S., and Dominiak, P. *Jpn J Pharmacol.* 79: 403-426, 1999
35. Gkika, D., Topala, C. N., Chang, Q.*, et al. Embo J.* 25: 4707-4716, 2006

36. Colley, B. S., Biju, K. C., Visegrady, A., Campbell, S., and Fadool, D. A. *Neuroscience.* 144: 531-546, 2007
37. Blankenship, K. A., Williams, J. J., Lawrence, M. S., McLeish, K. R., Dean, W. L., and Arthur, J. M. *Am J Physiol Renal Physiol.* 280: F815-822, 2001
38. Hoenderop, J. G., Nilius, B., and Bindels, R. J. *Physiol Rev.* 85: 373-422, 2005
39. Lemann, J., Jr., Bushinsky, D. A., and Hamm, L. L. *Am J Physiol Renal Physiol.* 285: F811-832, 2003
40. Bindels, R. J., Hartog, A., Abrahamse, S. L., and Van Os, C. H. *Am J Physiol.* 266: F620-627, 1994
41. Vennekens, R., Prenen, J., Hoenderop, J. G., Bindels, R. J., Droogmans, G., and Nilius, B. *Pflugers Arch.* 442: 237-242, 2001
42. Yeh, B. I., Sun, T. J., Lee, J. Z., Chen, H. H., and Huang, C. L. *J Biol Chem.* 278: 51044-51052, 2003
43. Yeh, B. I., Kim, Y. K., Jabbar, W., and Huang, C. L. *Embo J.* 24: 3224-3234, 2005
44. Lambers, T. T., Oancea, E., de Groot, T., Topala, C. N., Hoenderop, J. G., and Bindels, R. J. *Mol Cell Biol.* 2006
45. Jiang, J., Li, M., and Yue, L. *J. Gen. Physiol.* 126: 137-150, 2005
46. Dodier, Y., Banderali, U., Klein, H.*, et al. J. Biol. Chem.* 279: 6853-6862, 2004
47. Hoenderop, J. G., Chon, H., Gkika, D.*, et al. Kidney Int.* 65: 531-539, 2004
48. Gothel, S. F., and Marahiel, M. A. *Cell Mol Life Sci.* 55: 423-436, 1999
49. Ivery, M. T. *Med Res Rev.* 20: 452-484, 2000
50. Ruff, V. A., Yem, A. W., Munns, P. L.*, et al. J Biol Chem.* 267: 21285-21288, 1992
51. Goel, M., Garcia, R., Estacion, M., and Schilling, W. P. *J Biol Chem.* 276: 38762-38773, 2001
52. Sinkins, W. G., Goel, M., Estacion, M., and Schilling, W. P. *J Biol Chem.* 279: 34521-34529, 2004
53. Rosen, M. K., Standaert, R. F., Galat, A., Nakatsuka, M., and Schreiber, S. L. *Science.* 248: 863-866, 1990
54. Czar, M. J., Lyons, R. H., Welsh, M. J., Renoir, J. M., and Pratt, W. B. *Mol Endocrinol.* 9: 1549-1560, 1995
55. Silverstein, A. M., Galigniana, M. D., Kanelakis, K. C., Radanyi, C., Renoir, J. M., and Pratt, W. B. *J Biol Chem.* 274: 36980-36986, 1999
56. Galigniana, M. D., Radanyi, C., Renoir, J. M., Housley, P. R., and Pratt, W. B. *J Biol Chem.* 276: 14884-14889, 2001
57. Goswami, C., Dreger, M., Otto, H., Schwappach, B., and Hucho, F. *J Neurochem.* 96: 254-266, 2006
58. Andoh, T. F., Burdmann, E. A., Fransechini, N., Houghton, D. C., and Bennett, W. M. *Kidney Int.* 50: 1110-1117, 1996
59. Allison, A. C. *Ann N Y Acad Sci.* 696: xi-xx, 1993
60. van der Eerden, B. C., Hoenderop, J. G., de Vries, T. J.*, et al. Proc Natl Acad Sci U S A.* 102: 17507-17512, 2005
61. Nijenhuis, T., Hoenderop, J. G., and Bindels, R. J. *J Am Soc Nephrol.* 15: 549-557, 2004
62. De Vries, L., Zheng, B., Fischer, T., Elenko, E., and Farquhar, M. G. *Annu Rev Pharmacol Toxicol.* 40: 235-271, 2000
63. Abramow-Newerly, M., Roy, A. A., Nunn, C., and Chidiac, P. *Cell Signal.* 18: 579-591, 2006
64. Roy, A. A., Lemberg, K. E., and Chidiac, P. *Mol Pharmacol.* 64: 587-593, 2003
65. Wang, X., Zeng, W., Soyombo, A. A.*, et al. Nat Cell Biol.* 7: 405-411, 2005
66. Voets, T., Nilius, B., Hoefs, S.*, et al. J Biol Chem.* 279: 19-25, 2004
67. Walder, R. Y., Landau, D., Meyer, P.*, et al. Nat Genet.* 31: 171-174, 2002
68. Schlingmann, K. P., Weber, S., Peters, M.*, et al. Nat Genet.* 31: 166-170, 2002
69. Doyle, D. A., Morais Cabral, J., Pfuetzner, R. A.*, et al. Science.* 280: 69-77, 1998
70. Nilius, B., Prenen, J., Janssens, A.*, et al. J Biol Chem.* 280: 22899-22906, 2005
71. Li, M., Du, J., Jiang, J.*, et al. J Biol Chem.* 2007

72. Oberwinkler, J., Lis, A., Giehl, K. M., Flockerzi, V., and Philipp, S. E. *J Biol Chem.* 280: 22540-22548, 2005
73. Kerschbaum, H. H., Kozak, J. A., and Cahalan, M. D. *Biophys J.* 84: 2293-2305, 2003
74. Nilius, B., Vennekens, R., Prenen, J., Hoenderop, J. G., Droogmans, G., and Bindels, R. J. *J Biol Chem.* 276: 1020-1025, 2001
75. Voets, T., Janssens, A., Prenen, J., Droogmans, G., and Nilius, B. *J Gen Physiol.* 121: 245-260, 2003

# ***Chapter 8***

**Summary**

**Nederlandse samenvatting**

**Rezumat**

**SUMMARY**

**Introduction**

Ion channels are specialized proteins that span the plasma membrane of living cells allowing ion fluxes through this essentially impermeable barrier. Most ion channels show selectivity in that their pores are more permeable to some ions than to others. Based on their selective permeability, ion channels can be subdivided in: $Na^+$ selective channels, $K^+$ selective channels, $Ca^{2+}$ selective channels, $Cl^-$ selective channels, and non-selective channels that do not discriminate between their permeants. The development of the patch-clamp technique enabled the researcher for the first time to monitor in real-time the activity of ion channels in the plasma membrane. The TRP (Transient Receptor Potential) family consists of ion channels with structural similarities. TRP proteins are widely expressed in organisms and contribute to diverse functions and processes ranging from thermal, tactile or taste sense to transepithelial $Ca^{2+}$ and $Mg^{2+}$ transport. The epithelial $Ca^{2+}$ channels TRPV5 and TRPV6 represent two highly homologous members of the TRP family that are mainly expressed in $Ca^{2+}$-transporting epithelia. TRPV5 plays the role of gatekeeper for renal $Ca^{2+}$ reabsorption while TRPV6 forms the main $Ca^{2+}$ influx pathway in the small intestine. The epithelial $Mg^{2+}$ channel TRPM6 constitutes the $Mg^{2+}$ entry gate for transepithelial $Mg^{2+}$ transport. TRPM6 shares with its closest homologue, TRPM7, beside their exceptional $Mg^{2+}$ permeability, the presence of an atypical α-kinase in the carboxyl-terminal domain. A tight regulation of the epithelial $Ca^{2+}$ and $Mg^{2+}$ channels is of particular physiological importance for maintaining the body balance of these divalent ions. Therefore, the living organisms are equipped with an efficient feedback homeostatic system capable of maintaining the extracellular concentrations of these ions between narrow limits. The regulation of the epithelial $Ca^{2+}$ and $Mg^{2+}$ channels occurs at different levels and involves: (i) the long-term transcriptional and translational effects of hormones, (ii) the biophysical properties of the channels, and the effect of regulatory proteins acting (iii) on the trafficking of the channels to the plasma membrane or (iv) directly on its plasma membrane stabilization and activity. In recent years the electrophysiological properties of these ion channels were studied extensively, but particular aspects of the integration and control of their activity in a physiological context still remain to be studied. Therefore, the general goal of this thesis was to get further insight into the physiological and molecular regulation of epithelial $Ca^{2+}$ and $Mg^{2+}$ channels in order to ultimately understand the transcellular transport of these divalent cations.

**Tissue kallikrein stimulates TRPV5 activity**

Since it was recently demonstrated that mice lacking the serine protease tissue kallikrein (TK) exhibit robust hypercalciuria comparable to the $Ca^{2+}$ leak in TRPV5$^{-/-}$ mice, we delineated the molecular mechanisms connecting these two proteins. TK is excreted into urine in the CNT of

the kidney where it overlaps TRPV5 expression. First, using animal models, we demonstrated that TK expression correlates with the amount of $Ca^{2+}$ excreted. Furthermore, using *ex vivo* assays it was demonstrated that TK enhances transepithelial $Ca^{2+}$ transport. The stimulatory effect of TK was mimicked by bradykinin (BK) and could be reversed by application of an antagonist for the BK receptor type 2 (B2R). Using TRPV5 transiently transfected cells, it was shown that TK application stimulates TRPV5 activity. Then, the down-stream pathway consequent to B2R activation was investigated. Using a phospholipase C (PLC) inhibitor and a cell permeable analog of diacylglycerol (DAG) it was demonstrated that TK activates the PLC/DAG pathway. The DAG analog increased the TRPV5 activity *via* protein kinase C (PKC) phosphorylation of the channel since inactivation of the PKC phosphorylation sites S299 and S654 in TRPV5 prevented TK effect. Cell surface labeling with biotin revealed that TK enhances the amount of TRPV5 channels at the plasma membrane by delaying its retrieval. Summarizing, TK stimulates $Ca^{2+}$ reabsorption in the kidney *via* the BK activated PLC/DAG/PKC pathway and induces subsequently stabilization of the TRPV5 channels at the plasma membrane.

**$Ca^{2+}$-sensing receptor activation increases TRPV5 activity**

Although the involvement of the $Ca^{2+}$ sensing receptor (CaSR) in $Ca^{2+}$ homeostasis was comprehensively studied in the recent years, its role in the DCT and CNT of the kidney, where TRPV5 channels are expressed, remained elusive. Using combined functional and biochemical assays, we demonstrated that CaSR activation results in increased TRPV5 activity. CaSR can be activated, beside $Ca^{2+}$, by antibiotics and amino acids. We used neomycin and L-phenylalanine to specifically activate CaSR overexpressed in HEK293 cells. Activation of CaSR, co-expressed with TRPV5, determines an increase in TRPV5 activity via the PKC phosphorylation of the channel. Inactivation of the putative PKC phosphorylation sites at positions S299 and S654 in TRPV5 prevented the effect of CaSR activation, proving that these two amino acid residues are essential for the effect. Interestingly, the activity of TRPV5 closest homologue, TRPV6, was not affected upon CaSR activation. Cell surface protein labeling revealed that CaSR activation leads to increased plasma membrane localization of TRPV5 channels. In conclusion, we postulate a role for the CaSR in the apical compartment of the DCTs and CNTs in the kidney, where the CaSR is co-expressed together with TRPV5.

**FKBP52 inhibits TRPV5 activity**

FKBP52 is a ubiquitously expressed cytosolic enzyme characterized by the ability to catalyze the cis-trans isomerization of cis-peptidyl-propyl bonds, and by its strong binding to the immunosuppressive drug FK506. This protein was identified in a microarray screening for genes regulated by dietary $Ca^{2+}$ supplementation of 1α-OHase deficient mice. Our study demonstrated that FKBP52 specifically interact and co-localize with TRPV5 in the distal part of the nephron.

Moreover, by functional assays, we demonstrated that FKBP52 decreases TRPV5-mediated $Ca^{2+}$ influx. On the other hand, gene silencing of FKBP52 or administration of a FKBP52 blocker enhanced TRPV5 activity. The catalytic activity of FKBP52 is critical for this effect on TRPV5, since inactivation of its peptidyl-propyl cis-trans isomerase domain by mutagenesis prevented the effect. Furthermore, we demonstrated that submicromolar concentrations of FK506 stimulate $Ca^{2+}$ transport, while higher concentrations are toxic for the cells. This dose-response effect could explain the nephrotoxicity observed in patients treated with FK506. Certainly, given the complexity of the *in vivo* situation, the role of FK506 in hypercalciuria needs further investigations particularly concerning the putative role of other FKBP proteins.

**RGS2 inhibits TRPV6 activity**

RGS2 is a member of the RGS family of proteins that are able to terminate the signaling of heterotrimeric G-protein-coupled receptors (GPCR). This novel binding partner of TRPV6 was identified by yeast-two hybrid screening for regulatory proteins that interact with the amino-terminal domain of TRPV6. Using comprehensive biochemical assays, as the yeast-two hybrid screening and pulldown analysis, we confirmed that RGS2 interacts with TRPV6 in a $Ca^{2+}$-independent fashion. Functional assays demonstrated that RGS2 reduces both $Na^{+}$ and $Ca^{2+}$ TRPV6-mediated currents. The amino-terminal tail of RGS2 protein is critical for this effect, since deletion of this domain by mutagenesis prevented the reduction in TRPV6 currents. Interestingly, the currents of TRPV5, the closest relative of TRPV6, were not affected by RGS2. Furthermore, cell surface biotinylation indicated that the inhibitory effect of RGS2 on TRPV6 is not mediated by differences in trafficking or retrieval of TRPV6 to and from the plasma membrane. This effect is possibly accounted from the direct interaction between RGS2 and TRPV6, affecting the gating properties of the channel. Finally, we showed that spinophilin, a scaffolding protein known to recruit RGS2, does not affect the interaction between RGS2 and TRPV6, indicating a GPCR-independent mechanism of TRPV6 regulation by RGS2.

**Molecular determinants of TRPM6 permeation properties**

TRPM6 and its closest homologue TRPM7 are members of the TRPM subfamily of cation channels and are known to be $Mg^{2+}$ permeable. TRPM6 shares ~50% sequence homology at the amino acid level with its closest relative TRPM7, and atypically for other ion channels, both channels contain a serine/threonine protein kinase domain in their carboxyl-termini. Despite the initial functional characterization of TRPM6, the molecular determinants of its $Mg^{2+}$ permeability remained unknown. Using a sequence alignment of the putative TRPM6 pore with pore sequences of the other subfamily members, we located in the loop between the fifth and the sixth transmembrane domain, a stretch of six amino acid residues as the potential selectivity filter. By point mutations resulting in neutralization of the negatively charged residues, we found

two amino acid residues as important determinants of cation permeation through TRPM6. Neutralization of the glutamate at position 1029 and of the isoleucine at position 1030 resulted in channels with modified pore diameter and decreased ruthenium red block compared to wild-type TRPM6 channels. These findings suggest that the region between 1029 and 1031 determines the narrowest area of the TRPM6 channel pore. Our results demonstrate that subtle amino acid variation in the pore region accounts for TRPM6 permeation properties. Certainly, given the lack of crystallography data, subsequent studies are needed to investigate the actual three-dimensional structure of the TRPM6 pore in more detail.

**Conclusion and future perspectives**

The aim of this thesis was to get more insight into the physiological and molecular regulation of epithelial $Ca^{2+}$ and $Mg^{2+}$ channels. Indeed, the first five chapters of this thesis describe the molecular regulation of the epithelial $Ca^{2+}$ channels, TRPV5 and TRPV6, by accessory proteins. TK increased TRPV5 activity by affecting the PKC-dependent phosphorylation of TRPV5. Possibly, TK operates through a hormonal receptor, activating the PLC/DAG/PKC pathway that ultimately results in accumulation of TRPV5 channels at the plasma membrane by a decrease in their retrieval. CaSR activation increased TRPV5 activity, an effect initiated also from the extracellular compartment. FKBP52 inhibited the TRPV5 activity *via* its peptidyl-propyl cis-trans isomerase activity. RGS2 modulated TRPV6 activity affecting the channel gating by direct interaction at the plasma membrane. Finally, the study on TRPM6 permeation properties brought new light on the structure and function of amino acid residues from the pores of $Mg^{2+}$-permeable ion channels. Consequently, the functional characterization of accessory proteins controlling the function of epithelial $Ca^{2+}$ channels provided molecular insight into the regulatory mechanisms of ion channels activity. Further investigations, on the physiological relevance of the role of accessory proteins in regulating the epithelial $Ca^{2+}$ channels, may reveal the existence of new proteins networks and could elucidate the mechanisms of precise regulation and integration of $Ca^{2+}$ homeostasis to the body's varying demands.

## SAMENVATTING

### Inleiding

Ionkanalen zijn gespecialiseerde eiwitten in de plasmamembraan van levende cellen. Ze zorgen voor een ionenflux over de plasmamembraan die zelf in essentie impermeabel is voor ionen. De meeste ionkanalen vertonen selectiviteit, oftewel hun poriën zijn meer permeabel voor bepaalde ionen dan voor anderen. Op basis van hun selectieve permeabiliteit kunnen ionkanalen onderverdeeld worden in: $Na^+$ selectieve kanalen, $K^+$ selectieve kanalen, $Ca^{2+}$ selectieve kanalen, $Cl^-$ selectieve kanalen en non-selectieve kanalen die geen onderscheid maken tussen het soort ion. De ontwikkeling van de patch-clamp techniek maakte het voor het eerst mogelijk om de activiteit van ionkanalen aanwezig in de plasmamembraan rechtstreeks waar te nemen. De Transient Receptor Potential (TRP) familie van ionkanalen bestaat uit kanalen met structurele overeenkomsten. Deze TRP eiwitten komen tot expressie in verscheidene organismen en ze spelen een rol bij diverse functies en processen, van temperatuur-, gevoels- of tastzintuigen tot transepitheliaal $Ca^{2+}$ en $Mg^{2+}$ transport. Twee homologe leden van de TRPV subfamilie, TRPV5 en TRPV6, zijn $Ca^{2+}$ kanalen die voornamelijk tot expressie komen in $Ca^{2+}$-transporterende epitheelcellen. TRPV5 vervult de rol van poortwachter voor de $Ca^{2+}$ resorptie in de nier, terwijl TRPV6 betrokken is bij de $Ca^{2+}$ opname in de dunne darm. Het epitheliale $Mg^{2+}$ kanaal TRPM6 vormt de $Mg^{2+}$ toegangspoort bij transepitheliaal $Mg^{2+}$ transport. TRPM6 heeft, net als zijn homoloog TRPM7, een uitzonderlijke $Mg^{2+}$ permeabiliteit. Uniek voor deze kanalen is dat ze een α-kinase bevatten in het carboxyl terminus domein. Regulatie van de epitheliale $Ca^{2+}$ en $Mg^{2+}$ kanalen is van belang voor de ionenbalans in het lichaam. Daarom bevatten levende organismen een efficiënt feedback homeostase systeem dat de extracellulaire ionconcentraties begrenst. Er zijn diverse niveaus waarop de epitheliale $Ca^{2+}$ en $Mg^{2+}$ kanalen worden gereguleerd: via (i) de transcriptionele en translationele effecten van hormonen, (ii) de biofysische eigenschappen van kanalen, en door het effect van regulatoire eiwitten op (iii) het transport van de kanalen naar de plasmamembraan of (iv) direct op de stabiliteit en activiteit van de kanalen in de membraan. In de laatste jaren zijn de elektrofysiologische eigenschappen van deze ionkanalen intensief bestudeerd, waarbij echter bepaalde aspecten van de integratie en regulatie van kanaalactiviteit in een fysiologische context verder onderzoek vereisen. Dit proefschrift tracht meer inzicht te verschaffen in de fysiologische en moleculaire regulatie van epitheliale $Ca^{2+}$ en $Mg^{2+}$ kanalen om uiteindelijk het transcellulaire transport van deze divalente kationen beter te begrijpen.

### Kallikreine stimuleert de TRPV5 activiteit

Recent is aangetoond dat muizen zonder de serineprotease kallikreine (TK) een hypercalciurie vertonen, vergelijkbaar met het $Ca^{2+}$ lek in $TRPV5^{-/-}$ muizen. Deze studie beschrijft de moleculaire mechanismen die deze eiwitten verbinden. TK wordt uitgescheiden in de urine door

de verbindingsbuis van de nier, daar waar ook TRPV5 tot expressie komt. Door middel van een diermodel is aangetoond dat TK expressie correleert met de hoeveelheid $Ca^{2+}$ die uitgescheiden wordt. Verder laten *ex vivo* studies zien dat TK transepithelial $Ca^{2+}$ transport stimuleert. Het stimulerende effect van TK kan worden nagebootst door bradykinine (BK) en geblokkeerd worden door een antagonist van de BK receptor type 2 (B2R). Door gebruik te maken van TRPV5-getransfecteerde cellen is aangetoond dat toevoeging van TK de activiteit van TRPV5 stimuleert. Vervolgens is de navolgende route van B2R activering onderzocht. Het gebruik van een fosfolipase C (PLC) remmer en een celpermeabele analoog van diacylglycerol (DAG) heeft aangetoond dat TK de PLC/DAG route activeert. De DAG analoog verhoogt TRPV5 activiteit via proteïne kinase C (PKC) afhankelijke fosforylatie van het kanaal. Inactivatie van de PKC fosforylatieplaatsen S299 en S654 in TRPV5 verhinderde het TK effect. Door eiwitten op de plasmamembraan te labelen met biotine is aangetoond dat TK het aantal TRPV5 kanalen in de plasmamembraan verhoogt door de terugname van het kanaal uit de membraan te vertragen. Samengevat blijkt dat TK de $Ca^{2+}$ resorptie in de nier stimuleert via de BK geactiveerde PLC/DAG/PKC route en vervolgens de TRPV5 kanalen op de plasmamembraan stabiliseert.

**Activering van de calcium sensing receptor stimuleert de TRPV5 activiteit**

Hoewel de betrokkenheid van de $Ca^{2+}$ sensing receptor (CaSR) in de $Ca^{2+}$ homeostase intensief bestudeerd is in de afgelopen jaren, is er nog veel onbekend rondom haar rol in de distale en verbindingsbuizen van de nier, waar TRPV5 tot expressie komt. Door het gebruik van gecombineerde functionele en biochemische studies is aangetoond dat activering van de CaSR resulteert in een verhoogde TRPV5 activiteit. De CaSR kan naast activatie door $Ca^{2+}$ ook geactiveerd worden door bepaalde typen antibiotica en aminozuren. In een overexpressie celmodel is gebruik gemaakt van neomycine en L-fenylalanine om specifiek de CaSR te activeren. Co-expressie van TRPV5 en de CaSR, waarbij de CaSR geactiveerd wordt, leidt tot een verhoogde TRPV5 activiteit via PKC fosforylatie van het kanaal. Inactivatie van de mogelijke PKC fosforylatieplaatsen S299 en S654 in TRPV5 verhinderde het effect van CaSR activatie op het kanaal, dat aantoont dat deze twee aminozuren essentieel zijn voor het effect. Daarnaast bleek de activiteit van de TRPV5 homoloog, TRPV6, niet beïnvloed te worden door CaSR activatie. Het labelen van de plasmamembraan eiwitten toonde aan dat CaSR activatie leidt tot een verhoogd aantal TRPV5 kanalen in de plasmamembraan. Deze studie beschrijft voor het eerst een mogelijke rol van de CaSR aan de apicale zijde van de distale en verbindingsbuizen in de nier, waar de CaSR samen met TRPV5 tot expressie komt.

**FKBP52 remt TRPV5 activiteit**

FKBP52 is een cytosolisch enzym met een breed expressiepatroon. Het kan de cis-trans isomerisatie van cis-peptidyl-propyl verbinding katalyseren en het bindt aan de immunosuppressieve drug FK506. FKBP52 is geïdentificeerd door middel van een microarray screening naar genen die gereguleerd worden door $Ca^{2+}$-diëten in 1α-OHase knock-out muizen. Deze studie laat zien dat FKBP52 een specifieke interactie aangaat met TRPV5 en dat er sprake is van co-lokalisatie met TRPV5 in het distale deel van het nefron. Bovendien is door middel van functionele analyse aangetoond dat FKBP52 de TRPV5-afhankelijke $Ca^{2+}$ influx remt. Verder blijkt remming van FKBP52 gentranslatie, of door toevoeging van een FKBP52 remmer, de TRPV5 activiteit te stimuleren. De katalytische activiteit van FKBP52 is essentieel voor het effect op TRPV5, want inactivatie van het peptidyl-propyl cis-trans isomerase domein door mutagenese kon het effect voorkomen. Verder is aangetoond dat submicromolaire concentraties van FK506 $Ca^{2+}$ transport kan stimuleren, terwijl hogere concentraties toxisch zijn voor de cellen. Dit dosisafhankelijke effect kan de nefrotoxiciteit verklaren die voorkomt in patiënten die behandeld worden met FK506. Gezien de complexiteit in de *in vivo* situatie zal de rol van FK506 bij hypercalciurie verder onderzocht moeten worden, vooral de mogelijke rol van andere FKBP eiwitten.

**RGS2 remt de TRPV6 activiteit**

RGS2 is een lid van de RGS familie met eiwitten die de signalering van heterotrimere G-eiwit gekoppelde receptoren (GPCR) kunnen beëindigen. Deze nieuwe bindingspartner van TRPV6 is geïdentificeerd door middel van een yeast-two hybrid screening voor regulatoire eiwitten die binden aan het amino-terminale domein van TRPV6. Door het gebruik van biochemische assays zoals de yeast-two hybrid screening en een pulldown analyse is de $Ca^{2+}$-onafhankelijke interactie tussen RGS2 en TRPV6 bevestigd. Functionele studies toonden aan dat RGS2 de $Na^{+}$ en $Ca^{2+}$ stromen van TRPV6 kan remmen. Deletie van het amino-terminale domein van RGS2 door mutagenese kon de verminderde TRPV6 stromen verhinderen, waaruit blijkt dat dit domein essentieel is voor het effect op TRPV6. Daarnaast worden de stromen van TRPV5, die verwant is aan TRPV6, niet beïnvloed door RGS2. Labelen van eiwitten op de plasmamembraan met biotine heeft aangetoond dat het remmende effect van RGS2 op TRPV6 niet tot stand komt door veranderingen in transport van TRPV6 naar en uit de plasmamembraan. Het effect is mogelijk het resultaat van de directe interactie tussen RGS2 en TRPV6, dat de open status van het kanaal beïnvloed. Tot slot is er aangetoond dat spinophilin, een ankereiwit dat RGS2 rekruteert, niet de interactie tussen RGS2 en TRPV6 beïnvloedt. Dit duidt op een GPCR-onafhankelijk mechanisme van TRPV6 regulatie door RGS2.

**Moleculaire bepaling en eigenschappen van TRPM6 permeabiliteit**

TRPM6 en haar homoloog TRPM7 zijn leden van de TRPM subfamilie van kationkanalen en zijn permeabel voor $Mg^{2+}$. TRPM6 heeft op het niveau van aminozuurvolgorde een ~50% homologie met TRPM7. De kanalen zijn uniek in het feit dat ze een serine/threonine proteïne kinase domein bevatten in de carboxy terminus. Ondanks de eerdere functionele karakterisering van TRPM6 is er nog veel onbekend over de moleculaire aspecten van de $Mg^{2+}$ permeabiliteit. Door middel van sequentie vergelijking van de mogelijke TRPM6 porie met de porie sequenties van andere familieleden werd er tussen het vijfde en zesde transmembraan domein een regio gevonden van zes aminozuren die kan dienen als mogelijke selectiviteitsfilter. Door hier puntmutaties aan te brengen, die de negatief geladen residuen neutraliseren, zijn twee aminozuren gevonden die belangrijk zijn voor de doorgang van kationen in TRPM6. Neutralisatie van het glutaminezuur op positie 1029 en/of de isoleucine op positie 1030 resulteerde in kanalen met een veranderde poriediameter en een verlaagde remming van ruthenium rood vergeleken met normale TRPM6 kanalen. Deze bevindingen suggereren dat de regio tussen 1029 en 1031 het meest nauwe gedeelte van de porie in het kanaal bepaalt. De resultaten laten zien dat subtiele aminozuurveranderingen in de porie regio eigenschappen van de TRPM6 doorlaatbaarheid kan veranderen. Zeker vanwege het ontbreken van kristalstructuur gegevens zijn verder studies noodzakelijk om de driedimensionale structuur van de TRPM6 porie te onderzoeken.

**Conclusie en vooruitzichten**

Dit proefschrift tracht meer inzicht te verschaffen in de fysiologische en moleculaire regulatie van epitheliale $Ca^{2+}$ en $Mg^{2+}$ kanalen. De eerste vijf hoofdstukken van het proefschrift beschrijven de moleculaire regulatie van de epitheliale $Ca^{2+}$ kanalen TRPV5 en TRPV6 door geassocieerde eiwitten. TK verhoogt TRPV5 activiteit vanuit het extracellulaire compartiment, via een tot nu toe onbekende route om de activiteit van de ionkanalen te reguleren. TK activeert een hormonale receptor, dat zorgt voor activatie van de PLC/DAG/PKC route. Dit leidt uiteindelijk tot accumulatie van TRPV5 kanalen in de plasmamembraan door een verminderde terugname. Activering van de CaSR verhoogt de TRPV5 activiteit, een effect dat tevens vanuit het extracellulaire compartiment wordt geïnitieerd. FKBP52 remt de TRPV5 activiteit via peptidyl-propyl cis-trans isomerase activiteit. RGS2 moduleert de TRPV6 activiteit door de kanaal permeabiliteit te beïnvloeden via directe interactie aan de plasmamembraan. Daarnaast levert de studie naar de eigenschappen van TRPM6 iondoorlaatbaarheid nieuwe bevindingen in de structuur en functie van aminozuren in de porie van $Mg^{2+}$-permeabele ionkanalen. De functionele karakterisatie van geassocieerde eiwitten die epitheliale $Ca^{2+}$ kanalen reguleren geeft moleculair inzicht in de regulatiemechanismen van kanaalactiviteit. Verder onderzoek naar de fysiologische relevantie van de rol van deze eiwitten in de regulatie mechanismen zou het

bestaan van nieuwe eiwitnetwerken kunnen ontrafelen. Verder zou het de mechanismen achter de specifieke regulatie en intergratie van de $Ca^{2+}$ balans in het lichaam kunnen verhelderen.

## REZUMAT

### Introducere

Canalele ionice sunt proteine specializate integrate în membrana citoplasmatică a celulelor şi permit fluxul ionic prin această barieră impermeabilă. Majoritatea canalelor ionice prezintă selectivitate ionică, în faptul că porul lor este mai permeabil pentru anumiți ioni decât pentru alții. În funcție de selectivitatea lor, canalele ionice pot fi împărțite în: canale selective pentru $Na^+$, canale selective pentru $K^+$, canale selective pentru $Ca^{2+}$, canale selective pentru $Cl^-$, şi canale neselective care nu deosebesc ionii permeanți. Dezvoltarea tehnicii de patch-clamp a permis pentru prima dată monitorizarea în timp real a activității canalelor ionice din membrana citoplasmatică. Familia TRP de canale ionice este compusă din canale cu similarități structurale. Proteinele din această familie sunt exprimate în diverse țesuturi din organism şi contribuie la diverse funcții şi procese pornind de la senzații termice, tactile sau gustative până la transportul transepitelial al ionilor de $Ca^{2+}$ şi de $Mg^{2+}$. Canalele epiteliale de $Ca^{2+}$, TRPV5 şi TRPV6, reprezintă doi membri ai familiei TRP foarte asemănători din punct de vedere al secvenței de aminoacizi şi sunt exprimate în principal în epiteliile unde are loc transportul activ de $Ca^{2+}$. TRPV5 are rolul de controlor al reabsorbției renale de $Ca^{2+}$, în timp ce TRPV6 formează principala cale de absorbție a $Ca^{2+}$ în intestinul subțire. Canalul epitelial de $Mg^{2+}$ constituie calea de intrare a $Mg^{2+}$ în celule, în procesul de transport transepitelial al $Mg^{2+}$. Pe lângă excepționala permeabilitate pentru $Mg^{2+}$, TRPM6 are în comun cu cel mai apropiat omolog al său, TRPM7, prezența unei α-kinaze atipice în domeniul carboxyl terminal. Un strâns control al canalelor epiteliale de $Ca^{2+}$ şi de $Mg^{2+}$ are o importanță fiziologică deosebită pentru menținerea balanței organismului pentru aceşti ioni divalenți. De aceea, organismele sunt dotate cu un sistem homeostatic de feedback capabil să mențină în limite restrânse concentrația extracelulară a acestor ioni. Controlul canalelor epiteliale de $Ca^{2+}$ şi de $Mg^{2+}$ are loc la diferite niveluri: (i) la nivel transcripțional şi translațional pe termen lung al diferiților hormoni, (ii) la nivelul proprietăților biofizice ale canalelor determinate şi de efectul proteinelor reglatoare care acționează (iii) asupra translocației canalelor spre membrana citoplasmatică sau (iv) direct asupra activității canalelor din membrana citoplasmatică. În ultimii ani, proprietățile electrofiziologice ale acestor canale ionice au fost studiate pe larg, dar anumite aspecte ale integrării şi controlului activității lor într-un context fiziologic mai larg au rămas încă să fie investigate. De aceea, scopul general al acestei teze este să clarifice aspectele reglării la nivel fiziologic şi molecular a canalelor epiteliale de $Ca^{2+}$ şi de $Mg^{2+}$ pentru o mai bună înțelegere a transportului transepitelial al acestor cationi divalenți.

### Kalikreina stimulează activitatea canalului ionic TRPV5

Deoarece recent a fost demonstrat faptul că şoarecii lipsiți de kalikreină (TK) dezvoltă o extremă hipercalciurie comparabilă cu scurgerile de $Ca^{2+}$ ale şoarecilor fără TRPV5, am încercat să

descriem mecanismele moleculare care corelează aceste două proteine. TK este excretată în urină din segmentul tubular colector unde este exprimat şi TRPV5. Folosind modele animale, am demonstrat că nivelul de exprimare al TK este corelat cu cantitatea de $Ca^{2+}$ excretată. Apoi, folosind experimente *ex vivo* am demonstrat că TK stimulează transportul transepitelial de $Ca^{2+}$. Acest efect a fost inițiat şi de bradikinină (BK) şi a putut fi blocat prin aplicarea unui antagonist al receptorului pentru bradikinină subtipul 2 (B2R). Folosind celule transfectate temporar cu TRPV5 am arătat că TK stimulează activitatea canalului TRPV5. Apoi, a fost studiată cascada enzimatică care este activată după stimularea B2R. Folosind un inhibitor al fosfolipazei C (PLC) şi un analog permeabil al diacilglicerolului (DAG) am demonstrat că TK activează cascada PLC/DAG. Analogul DAG măreşte activitatea canalului TRPV5 prin fosforilarea canalului de către protein kinaza C (PKC), deoarece inactivarea situsurilor de fosforilare de către PKC din TRPV5 a împiedicat acest efect. Prin etichetarea proteinelor din membrana citoplasmatica cu biotină, am demonstrat că TK măreşte numărul de canale TRPV5 din membrana citoplasmatică prin încetinirea reciclării lor. În concluzie, TK stimulează reabsorbția renală a $Ca^{2+}$ prin activarea cascadei PLC/DAG/PKC de către BK şi induce stabilizarea canalelor TRPV5 în membrana citoplasmatică.

**Activarea receptorul pentru calciu determină creşterea activității canalului TRPV5**

Deşi implicarea receptorului pentru $Ca^{2+}$ (CaSR) în homeostazia $Ca^{2+}$ a fost studiată pe larg, rolul său în DCT şi CDT din rinichi, locul de maximă exprimare a canalului TRPV5, a rămas până acum necunoscut. Folosind experimente funcționale şi biochimice, am demonstrat că stimularea CaSR determină o activitate crescută a canalului TRPV5. CaSR poate fi activat prin aplicarea de antibiotice şi anumiți aminoacizi. Am folosit neomicina şi L-fenil-alanina pentru a activa CaSR în celule care exprimă acest receptor. Când este exprimat împreună cu TRPV5, activarea CaSR duce la o creştere în activitatea canalului TRPV5 prin intermediul fosforilării canalului de către PKC. Inactivarea în TRPV5 a posibilelor situsuri de fosforilare de către PKC, pozițiile S299 şi S654, a stopat efectul activării CaSR, demonstrând că aceşti doi aminoacizi sunt esențiali pentru acest efect. În mod surprinzător, activitatea celui mai apropiat omolog al canalului TRPV5, TRPV6, nu a fost influențată de activarea CaSR. Prin etichetarea proteinelor din membrana citoplasmatică cu biotină am demonstrat că după activarea CaSR creşte cantitatea de canale TRPV5 din membrana citoplasmatică. În concluzie, am demonstrat pentru primă oară un posibil rol al CaSR din compartimentul apical al DCT şi CNT din rinichi, acolo unde CaSR este exprimat împreună cu TRPV5.

**FKBP52 inhibă activitatea canalului TRPV5**

FKBP52 este o proteină citosolică exprimată în întreg organismul. Această proteină este caracterizată prin activitatea să enzimatică de cis-trans izomerază a legăturilor cis-peptidil-

isopropil şi prin afinitatea sa puternică față de compusul imunosupresiv FK506. Această proteină a fost identificată printr-un test pentru genele care sunt reglate prin suplimentarea cu $Ca^{2+}$ a dietei şoarecilor lipsiți de enzima 1αOHază. Studiul nostru a demonstrat că FKBP52 interacționează specific şi este co-exprimat împreună cu TRPV5 în partea distală a nefronului. Mai mult, prin experimente funcționale, am demonstrat că FKBP52 inactivează influxul de $Ca^{2+}$ mediat de către TRPV5. Pe de altă parte, inactivarea genei care codifică pentru FKBP52 sau administrarea unui blocant al FKBP52 au determinat o creştere a activității canalului TRPV5. Activitatea catalitică a FKBP52 este esențială pentru acest efect, deoarece inactivarea centrului catalitic activ al proteinei prin mutageneză a împiedicat efectul acesteia asupra canalului TRPV5. Apoi, am demonstrat că FK506 în concentrații submicromolare stimulează transportul de $Ca^{2+}$, pe când în concentrații mai mari FK506 manifestă un efect toxic asupra celulelor. Această caracteristică dependentă de doză ar putea explica efectul nefrotoxic observat la pacienții tratați cu FK506. Totuşi, ținând cont de complexitatea situației *in vivo*, rolul FK506 în hipercalciurie trebuie investigat în viitor, mai ales legat de rolul potențial al altor FKBP proteine în acest proces.

**RGS2 inhibă activitatea canalului TRPV6**

RGS2 este membră a familiei RGS, proteine capabile să întrerupă cascada de semnalizare a receptorilor cuplați cu proteinele G (GPCR). Acest nou partener al canalului TRPV6 a fost identificat printr-un studiu asupra proteinelor regulatoare care pot interacționa cu domeniul amino-terminal al TRPV6. Folosind experimente biochimice, am confirmat interacțiunea RGS2 cu domeniul amino-terminal al TRPV6 într-o manieră independenta de $Ca^{2+}$. Analize funcționale au demonstrat că RGS2 reduce curenții de $Na^{+}$ şi de $Ca^{2+}$ mediați de TRPV6. Domeniul amino-terminal al RGS2 este vital pentru acest efect deoarece un mutant al RGS2 lipsit de acest domeniu nu a mai putut reduce curenții prin TRPV6. Surprinzător, curenții prin TRPV5, cel mai apropiat omolog al canalului TRPV6, nu au fost afectați de RGS2. Apoi, etichetarea proteinelor din membrana citoplasmatică cu biotină a demonstrat că efectul RGS2 asupra canalului TRPV6 nu este determinat de diferențe în traficul canalului către şi de la membrana citoplasmatică. Este posibil ca acest efect să fie mediat prin interacțiunea directă dintre RGS2 şi TRPV6, care afectează proprietățile de deschidere-închidere a canalului. În final, am demonstrat că spinofilina, o proteină a scheletului celular cunoscută a media recrutarea RGS2 către membrana citoplasmatică, nu afectează interacțiunea RGS2 cu TRPV6. Acest fapt indică un mecanism independent de GPCR al reglării canalului TRPV6 de către RGS2.

**Determinanți moleculari ai permebilității canalului TRPM6**

TRPM6 şi cel mai apropiat omolog al său, TRPM7, sunt membri ai subfamiliei TRPM de canale ionice şi sunt printre puținele canale ionice permeabile pentru $Mg^{2+}$. TRPM6 are ~50% din

secvența de aminoacizi în comun cu TRPM7 şi ambele canale conțin o unitate enzimatică în domeniul carboxil terminal. Deşi recent a fost caracterizat funcțional, determinanții moleculari ai permeabilității canalul TRPM6 au rămas necunoscuți până în prezent. Folosind un aliniament al porului probabil al canalului TRPM6 cu porii altor canale din aceeaşi subfamilie, am localizat în bucla dintre segmentele transmembranare 5 şi 6 o scurtă secvență de aminoacizi care poate funcționa ca filtru de selectivitate. Folosind mutații singulare ale aminoacizilor încărcați cu sarcină negativă din această regiune am descoperit doi aminoacizi ca fiind determinanți importanți ai permeabilității canalului TRPM6 pentru cationi divalenți. Neutralizarea glutamatului de la poziția 1029 şi a izoleucinei de la poziția 1030 a avut ca rezultat formarea unor canale cu diametru al porului diferit şi cu sensibilitate la blocare cu ruthenium red scăzută în comparație cu canalele TRPM6. Aceste descoperiri sugerează faptul că regiunea cuprinsă între pozițiile 1029 şi 1031 formează cea mai îngustă parte a porului canalului TRPM6. Rezultatele noastre susțin ipoteza conform căreia variații subtile ale aminoacizilor din regiunea porului determină permeabilitatea canalului TRPM6. Totuşi, ținând cont de lipsa unor date concrete de cristalografie, studii viitoare sunt necesare pentru a clarifica în detaliu structura tridimensională a porului canalului TRPM6.

**Concluzii şi perspective**

Scopul acestei teze a fost să aducă noi detalii în reglarea fiziologica şi moleculară a canalelor epiteliale de $Ca^{2+}$ şi de $Mg^{2+}$. Primele cinci capitole ale tezei descriu reglarea la nivel molecular a canelelor epiteliale de $Ca^{2+}$, TRPV5 şi TRPV6, de către proteine accesorii. TK creşte activitatea canalului TRPV5, acționând din compartimentul extracelular, un nou mod de a controla activitatea canalelor ionice. TK acționează prin intermediul unui receptor pentru hormonul BK, activând cascada enzimatică PLC/DAG/PKC, care în final duce la acumularea canalelor TRPV5 în membrana citoplasmatică. Stimularea CaSR determină o creştere a activității canalului TRPV5, efect inițiat de asemenea din compartimentul extracelular. FKBP52 inhibă activitatea canalului TRPV5 prin intermediul activității enzimatice de peptidil-propil cis-trans izomerază. RGS2 modulează activitatea canalului TRPV6 modificând proprietățile de deschidere-închidere ale canalului prin interacțiunea directă cu TRPV6 în membrana citoplasmatică. În final, studiul despre proprietățile de permeabilitate ale canalului TRPM6 aruncă o noua lumină asupra structurii şi funcției aminoacizilor din porurile canalelor permeabile pentru $Mg^{2+}$. În consecință, caracterizarea funcțională a proteinelor reglatoare ale activității canalelor epiteliale de $Ca^{2+}$ aduce noi cunoştințe despre mecanismele pentru controlul activității canalelor ionice. Studii viitoare, despre însemnătatea fiziologică a acestor proteine accesorii în reglarea canalelor epiteliale de $Ca^{2+}$, vor putea demonstra existența unor noi rețele de proteine şi vor ajuta la clarificarea mecanismelor de reglare şi integrare specifică şi precisă a homeostaziei $Ca^{2+}$ la nevoile variate ale organismului.

**Acknowledgments**

Finally, the last and, by far, most difficult and at the same time most fun part of this thesis needs to be written. Looking back at the four years spent as PhD student, I realized that all the hard work was not a lonely journey, but the scientific cooperation with all my colleagues made this thesis possible. Therefore, I would like to thank to all people which helped me throughout the whole process, from graduate student to a Doctorate degree.

First, after all the working and writing are done, I would like to take the opportunity to thank my supervisor, Prof. Dr. René Bindels. Dear René, from the first time we met each other, at the interview in Nijmegen, February 2004, I admired your very organized and efficient way of working. It gave me always a feeling of high standard science and professional atmosphere around our lab. I suppose we have to be always “pro-active” to meet these standards.

And every time when René was not there or was too busy, Joost came and take care of every possible problem encountered on the lab. Dear Joost, with your highly competitive and hyperactive way of being, I had always challenges and the everyday lab routine was spiced up. Even drinking coffee with you, during the short brakes you took, it was energizing and at times hard to keep the pace with you.

Alex, vreau sa iti multumesc pentru increderea acordata in timpul ultimului an de facultate in care am avut primul contact cu stiinta adevarata din subsolul Facultatii de Biologie din Bucuresti. In fiecare dimineata, cafeaua avea savoare stiintifica in timp de discutam despre patch-clamp si TRPV1.

Dear Bernd, I am very grateful to you for giving me the opportunity to learn the patch-clamp technique in your lab. I was just starting with my scientific adventure and it was great to have you as mentor and supervisor. Learning patch-clamp gets easier being in one of the leading labs from the entire world together with all the Belgian colleagues and celebrating every now and then with the best beer in the world, Duvel!

Beste Jenny, het is een plezier dat jij naast mij kunt staan tijdens mijn promotie. Het was altijd leuk om met jouw Nederlands te praten en jouw correcties hielp mij om mij taal vaardigeden te verbeteren. Bedankt voor al de gezelligheid van de patch ruimte. Keep on patching! Beste Joost, jij was altijd een steun als ik problemen met iets in het lab had. Ook voor jouw hulp met de vertaling in het Nederlands van mijn samenvatting wil ik graag jouw bedanken. Het is een echte ere om jouw als paranimf te hebben.

All the colleagues from the Physiology Department helped creating a nice and friendly working atmosphere on the 7-th floor of NCMLS. Stan, Qing, Wouter, Kirsten, Monique, Tim, Dennis, Rob, Gang, Tom, Sylvie, Theun, Peng, Bob, Sjoerd, Kyupil, it was always fun to work together with all of you. I found all the time an advice on learning Dutch and the Dutch way from all of you. But not only work was fun, we had great time during the barbecues and lab days-out. Dear

Freek, it was a pleasure to learn from you the ins and outs of our patch-clamp set-up. Arjen, my first neighbour and friend from Nijmegen, you were very helpful with the two strangers knocking on your door in their first morning in Boeckstaetehof. Beste Susan, bedankt voor onze poes, Hopy. Elke dag met haar “miauw” voorkomt alle zorgen. Beste Annemiete, je bent echt aardig en behulpzaam ziel van de afdeling. Dear Sandor, your openness and friendliness really helped me a lot during the hard days of thesis writing on the eight floor.

Dr. Levison and Dr. Van Rees van de Hematologie Afdeling Universitair Medisch Centrum St Radboud, wil ik aan jullie bedanken, ook aan de verpleegkundigen van de deze Afdeling, voor al de care and support tijdens de hardste maanden van mijn leven. Dank jullie allemaal wel!

Calin, ai fost primul meu prieten roman din Nijmegen, si este o adevarata placere ca te-am intalnit si iti multumesc pentru tot sprijinul tau in timpul terapiei. Acele luni au trecut parca mai usor cu toate intalnirile si dicustiile nostre interesante. Mihai, iti sunt recunoscator pentru toate sfaturile medicale si mai ales morale intr-o perioada nefasta a vietii mele. Ai facut ca totul sa para mai usor si mai ales vindecarea realizabila. Toti prietenii mei romani din Muzenplaats, Lucian, Angelica, Dan si Miha, Lucian si Alice au creat intotdeauna o atmosfera adevat romaneasca la gratare, discutii aprinse si jocuri „de-a mafia”. Parca eram in Romania si nu in Olanda in spatele caminului studentesc Muzenplaats. Nicu si Roberta, va multumesc pentru toate sfaturile bune si incurajarile primite in toti acesti ani Ski-ul cu voi in Germania sau Austria a fost mereu reconfortant si distractia maxima. Mirto et Céline, je vous remercie pour votre amitié. C’était vraiment des très belle temps avec vous dans notre jardin de Muzenplaats. Apprendre du skier dans les Alpes a été très facile avec vous et cette vacance a été fabuleux. Il faut que nous allons ensemble encore une fois dans les Alpes françaises pour faire du ski et surtout pour l’après-ski.

Dan, iti multumesc pentru inspiratia data in realizarea copertei pentru teza. Esti o pata de culoare in peisajul cateodata monoton al Olandei si a mai ales al imprejurimilor Amersfoort-ului, ceea ce ma face sa ma simt mai aproape de locurile natale.

Mama si tata, vreau sa va multumesc pentru tot ce ati facut pentru mine in acesti ani si mai ales pentru increderea acordata si incurajarea de a mi urma chemarea si de a cauta drumul propriu departe de voi aici in Olanda. Stiu ca nu va este usor sa fiu asa departe de voi, dar sper ca sunteti mandri de realizarile mele si ca va bucurati de ale alaturi de mine. Domnica si Ruse (undeva acolo sus) va multumesc pentru ca m-ati privit de la inceput ca pe un copil de-al vostru si ca m-ati acceptat cu bratele deschise.

Ana, puiut, tu esti toata viata mea si nu exista destule cuvinte sa iti multumesc pentru ca imi esti alaturi si ca ma iubesti. Tu ma ajuti sa imi indrept toate greselile, sa fac altele si mai ales imi dai mereu incredere si speranta. In noi gasesc mereu bucurie de viata si motivatie sa continui ce am inceput. „Daca dragoste nu e, nimic nu e!”

**List of abbreviations**

| | |
|---|---|
| $1,25(OH)_2D_3$ | 1,25-dihydroxy-vitamin $D_3$ |
| $[Ca^{2+}]_i$ | intracellular $Ca^{2+}$ concentration |
| 1α-OHase | 25-hydroxyvitamin $D_3$-1α-hydroxylase |
| 2-APB | 2-aminoethoxydiphenyl borate |
| ADP | adenosine diphosphate |
| ANOVA | analysis of variance |
| ATP | adenosine 5'-triphosphate |
| B2R | bradykinin 2 receptor |
| BAPTA | 1,2-bis(2-aminophenoxy)ethane-N,N,N',N'-tetraacetic acid |
| BK | bradykinin |
| bp | base pairs |
| BSA | bovine serum albumin |
| BSPRY | B-box and SPRY-domain containing protein |
| CaM | calmodulin |
| CaBP | $Ca^{2+}$-binding protein |
| cAMP | cyclic adenosine monophosphate |
| CaSR | $Ca^{2+}$-sensing receptor |
| CCD | cortical collecting duct |
| cDNA | complementary deoxyribonucleic acid |
| cGMP | cyclic guanosine monophosphate |
| CNT | connecting tubules |
| CTRL | control |
| DAG | diacylglycerol |
| DCT | distal convoluted tubules |
| DMA | dimethylammonium |
| DMEM | Dulbecco modified Eagle's minimal essential medium |
| DRG | dorsal root ganglion |
| DTT | dithiothreitol |
| DVF | divalent free |
| ECaC | epithelial $Ca^{2+}$ channel |
| EDTA | ethylene diamine tetra acetic acid |
| eEF-2 | elongation factor 2 |
| EGTA | ethylene glycol-bis(b-aminoethyl ether)-N,N,N',N'-tetra acetic acid |
| ENaC | epithelial $Na^+$ channel |
| ER | endoplasmic reticulum |
| FACS | fluorescence-activated cell sorting |
| FKBP52 | FK506-binding protein 52 |
| GFP | green fluorescent protein |
| GPCR | G protein-coupled receptor |
| GST | glutathione S-transferase |
| GTP | guanosine triphophate |
| HEK 293 | human embryonic kidney 293 |
| HEPES | 4-(2-hydroxyethyl)-1-piperazineethanesulfonic acid |

| | |
|---|---|
| HSH | hypomagnesemia with secondary hypocalcemia |
| i | single channel current |
| I | whole cell current |
| $IC_{50}$ | half maximal inhibitory concentration |
| $IP_3$ | inositol triphoshpate |
| I-V | current-voltage |
| L-Phe | L-phenylalanine |
| MA | monomethylammonium |
| MDCK | Madin-Darby Canine Kidney |
| mRNA | messenger ribonucleic acid |
| MTSET | [2-(trimethylammonium)-ethyl]-methanethiosulfonate |
| NCX1 | $Na^+$-$Ca^{2+}$-exchanger 1 |
| NHE | $Na^+$-$H^+$ exchanger |
| NHERF4 | NHE regulating factor 4 |
| NKCC2 | $Na^+$,$K^+$,$2Cl^-$-co-transporter subtype 2 |
| NMDG | N-methyl-D-glucamine |
| OAG | 1-oleoyl-acetyl-sn-glycerol |
| P2X | purinergic receptors |
| PAGE | polyacrylamide electrophoresis gel |
| PBS | phosphate buffered saline |
| PCR | polymerase chain reaction |
| PDZ | PS095/DLG/Z0-1 |
| $PIP_2$ | phosphatidylinositol-4,5-biphosphate |
| PKA | protein kinase A |
| PKC | protein kinase C |
| PLC | phospholipase C |
| PMA | phorbol 12-myristate 13-acetate |
| PMCA1b | $Ca^{2+}$-ATPase 1b |
| $P_o$ | open probability |
| PPIase | peptidyl-propyl cis-trans isomerase |
| PTH | parathyroid hormone |
| $P_x$ | permeability for cation x |
| RGS2 | regulator of G protein signaling 2 |
| ROC | receptor operated channel |
| ROMK | renal outer medullary $K^+$ channel |
| RR | ruthenium red |
| SCAM | substituted cysteine accessibility method |
| SDS | sodium dodecyl sulphate |
| SEM | standard error of the mean |
| siRNA | small interference ribonucleic acid |
| SMOC | second messenger operated channel |
| SNARE | soluble N-ethylmaleimide-sensitive-factor attachment |
| SPL | spinophilin |
| TAL | thick ascending limbs of the Henle’s loop |

| | |
|---|---|
| TBS | tris buffered saline |
| TCA | trichloroacetic acid |
| TetMA | tetramethylammonium |
| TIRF | Total Internal Reflection Fluorescence |
| TG | trigeminal ganglion |
| TK | tissue kallikrein |
| $TK^{-/-}$ | TK knockout |
| TM | transmembrane domain |
| TriMA | trimethylammonium |
| Tris | tris(hydroxyl-methyl)aminomethane |
| TRP | transient receptor potential |
| TRPA | anchorin-repeat containing TRP |
| TRPC | TRP canonical |
| TRPL | TRP like |
| TRPM | TRP melastatin |
| TRPML | mucolipins TRP |
| TRPP | TRP polycistyns |
| TRPV | TRP vanilloid |
| $TRPV5^{-/-}$ | TRPV5 knockout |
| VOC | voltage operated channel |
| WNK4 | “with no lysine” kinase 4 |

**List of publications related to this thesis**

Els den Dekker, Joost P. Schoeber, **Catalin N. Topala**, Stan F. van de Graaf, Joost G. Hoenderop and René J. Bindels.
Characterization of a Madin-Darby canine kidney cell line stably expressing TRPV5.
*Pflügers Arch*. 450: 236-244, 2005

Qing Chang, Susan Hoefs, Annemiete W. van der Kemp, **Catalin N. Topala**, René J. Bindels and Joost G. Hoenderop.
The beta-glucuronidase klotho hydrolyzes and activates the TRPV5 channel.
*Science* 310: 490-493, 2005

Dimitra Gkika, **Catalin N. Topala**, Joost G. Hoenderop and René J. Bindels.
The immunophilin FKBP52 inhibits the activity of the epithelial $Ca^{2+}$ channel TRPV5.
*Am J Physiol Renal Physiol*. 290: F1253-F1259, 2006

Joost P. Schoeber, **Catalin N. Topala**, Xinhua Wang, Shmuel Muallem, Robin J. Diepens, Tim T. Lambers, Joost G. Hoenderop and René J. Bindels.
RGS2 inhibits the epithelial $Ca^{2+}$ channel TRPV6.
*J Biol Chem*. 281: 29669-29674, 2006

*Dimitra Gkika, ***Catalin N. Topala**, Qing Chang, Stéphanie Thébault, Nicolas Picard, Pascal Houillier, Joost G. Hoenderop and René J. Bindels.
Tissue kallikrein stimulates $Ca^{2+}$ reabsorption *via* PKC-dependent plasma membrane accumulation of TRPV5.
*Contributed equally to this work.
*Embo J*. 25: 4707-4716, 2006

**Catalin N. Topala**, Wouter Tiel Groenestege, Stéphanie Thebault, Dennis van den Berg, Bernd Nilius, Joost G. Hoenderop and René J. Bindels.
Molecular determinants of permeation through the cation channel TRPM6.
*Cell Calcium* 41: 513-523, 2007

Tim T. Lambers , Elena Oancea, Theun de Groot, **Catalin N. Topala**, Joost G. Hoenderop and René J. Bindels.
Extracellular pH dynamically controls cell surface delivery of functional TRPV5 channels.
*Mol Cell Biol*. 27:1486-1494, 2007

**Catalin N. Topala**, René J. Bindels and Joost G. Hoenderop.
Regulation of the epithelial calcium channel TRPV5 by extracellular factors.
*Curr Opin Nephrol Hypertens*. 16:319-324, 2007

Joost P. Schoeber, **Catalin N. Topala**, Tim T. Lambers, Guenola Ricard, Martijn A. Huynen, Joost G. Hoenderop and René J. Bindels.
Identification of Nipsnap1 as a novel auxiliary protein inhibiting TRPV6 activity.
*Pflügers Arch.* in press, 2008

**Catalin N. Topala**, Joost P. Schoeber, Daniela Riccardi, Joost G. Hoenderop and René J. Bindels.
The calcium-sensing receptor stimulates TRPV5 activity.
*Manuscript in preparation*, 2008

**Curriculum Vitae**

Catalin Topala was born on July 6th 1978 in Giurgiu, Romania. He received basic and intermediate education in his home town Giurgiu and graduated high school (Baccalaureate) with the highest grades from his year. In 2002, he completed his studies with a Bachelor Degree in Biochemistry at University of Bucharest, Romania. After obtaining the Bachelor Degree, he started a Master in Neurobiology at the University of Bucharest. During his first year as a Master student he received a European Union Erasmus fellowship to visit the laboratory of Prof. Dr. Bernd Nilius at the Catholic University Leuven in Belgium. Growing interests in scientific research encouraged him to start working in August 2003 as a junior researcher (Ph.D. student) at the department of Physiology, Radboud University Nijmegen Medical Centre, the Netherlands. He received scientific supervision from Prof. Dr. R.J.M. Bindels and Dr. J.G.J. Hoenderop on a project to study the functional regulation of the epithelial calcium and magnesium channels. He participated in various teaching programs including coordinating internships of the first-year students from Biomedical Sciences at Radboud University Nijmegen. He is currently working as postdoctoral fellow within the department of Animal Physiology and Cognitive Neuroscience, Swammerdam Institute for Life Sciences at the University of Amsterdam (UvA).